Geometric Design of Independent Suspension Linkages

by

David E. Kline

A dissertation submitted in partial fulfillment
of the requirements for the degree of
Doctor of Philosophy
(Mechanical Engineering)
in the University of Michigan
2018

Doctoral Committee:

Professor Gregory M. Hulbert, Chair
Assistant Professor Evgueni Filipov
Associate Professor C. David Remy
Professor Kazuhiro Saitou

David E. Kline

delkline@umich.edu

ORCID iD: 0000-0001-5194-1837

Table of Contents

List of Tables

List of Figures

Abstract

The independent suspension allows each wheel of an automobile to move approximately vertically relative to the vehicle body without affecting the motion of the other wheels. Independent suspensions are designed when an existing vehicle is in need of improved performance or when an all-new vehicle is developed. The limitations of the modern suspension design approach are particularly apparent in the kinematics stage, where the linkage allowing the approximately-vertical wheel motion is selected and dimensioned. Selection is guided by experience, while dimensioning occurs by iterating a draft geometry. This is an expensive process, especially if the selected linkage is conceptually incapable of the desired motion. The desire to improve this kinematic design process resulted in four main contributions to the geometric design of independent suspension linkages.

The first contribution is the formulation of a mathematically-complete description of wheel motion. This description allows suspension designers to state a desired wheel trajectory before choosing any particular linkage, and to better understand the compromises inherent in stating the trajectory itself. The approach is to treat the wheel as a spatial rigid body, and place meaningful coordinates on $SE(3)$, the group of spatial rigid body motions. These coordinates either are suspension characteristics of interest or may be easily mapped to such characteristics. A curve in $SE(3)$ can then be defined based on the desired wheel kinematics, representing the desired wheel trajectory in a mathematically-coherent way.

The second contribution is a practical enumeration of spatial independent suspension linkages. This enumeration is systematic, generating potential linkage types from a set of practical body-wheel connections and basic assumptions on how these can

be assembled into suspension linkages. The body-wheel connections considered are the revolute joint, spherical-spherical link, cylindrical joint, spherical joint, revolute-spherical link, revolute-revolute link, and spherical-cylindrical link. The underlying approach is extensible to other connection types and rules of construction. Such an enumeration is essential when wanting to consider all practical design possibilities.

The third contribution is dimensional synthesis methods for each of the considered body-wheel connections. These methods ensure each body-wheel connection can be dimensioned to its maximum practical capability. In general, these methods convert wheel position and/or velocity requirements into algebraic equations where the variables are the coordinates of the joint or link. This algebraic approach allows a large number of geometries to be generated rapidly. In general, the algebraic design equations are systems of polynomial equations, but, where possible, these are simplified into linear systems or closed form expressions.

The fourth contribution is a systematic approach for filtering and assembling individual connections into the enumerated linkages. Suspensions are required to satisfy application-specific non-kinematic design requirements, such as fitting within an allotted space or accommodating a steering system. The methods developed in this dissertation allow the numerous link solutions that achieve the kinematic requirements to be pruned and assembled into linkages according to these non-kinematic requirements, following a set-based design process.

Altogether, this dissertation presents a set of mathematical tools useful for specifying mathematically-complete wheel trajectories, enumerating possible suspension linkages, solving for linkage geometry, and satisfying non-kinematic requirements. Examples that demonstrate the efficacy of the methods are provided, including a complete synthesis example for each of the considered body-wheel connections. Examples include the semi-trailing arm, five link, double wishbone, control blade, and MacPherson strut architectures.

Chapter 1

Introduction

An independent suspension consists primarily of a linkage connecting the wheel carrier to the vehicle body, a coil spring, and a shock absorber, Figure 1.1. The left and right suspensions of an axle are mirror images of each other. With strut-type suspensions, the shock absorber also functions as part of the linkage, notably reducing the number of necessary components. In general, independent suspensions allow the wheel to move approximately vertically in response to road disturbances. The spring and shock absorber serve as control devices with competing functions: reducing vehicle body acceleration, improving *ride*, and maintaining tire-ground contact, improving *handling*. Further influencing ride and handling are wheel position and attitude with wheel travel, and how the suspension reacts cornering, braking, driving, and impact loads. Additionally, for road vehicles, at least the front wheels are steered, so the suspension must allow one of the links to be actuated by a steering mechanism, typically a rack-and-pinion, Figure 1.2. Remaining links in the steered suspension must be arranged to allow rotation of the wheel about the desired steer axis. Link connections are typically cylindrical rubber bushings, Figure 1.3, where isolation from the road is desired, or metal ball joints, Figure 1.4, where well-defined motion is necessary, such as the connections allowing a steered wheel to rotate. Independent suspensions are not the only option for road vehicles; however, their superior performance has led to their eventual adoption in most segments of the market. Next, after a brief aside to handle some basic terminology, this history is outlined.

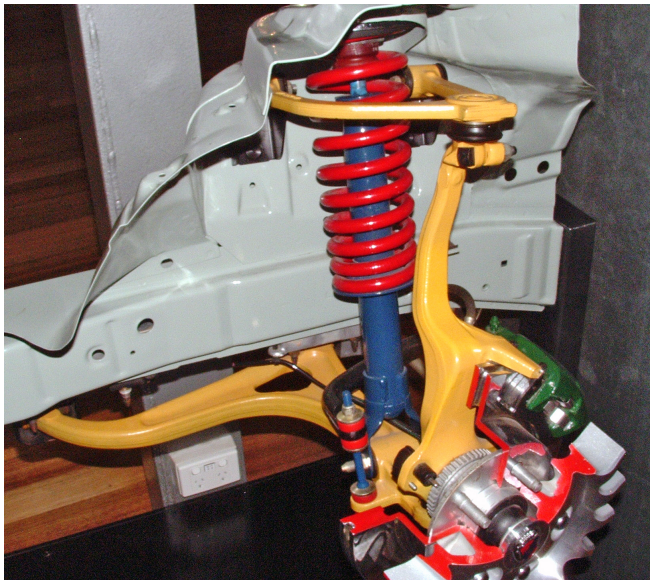

Figure 1.1. A double wishbone independent suspension [59].

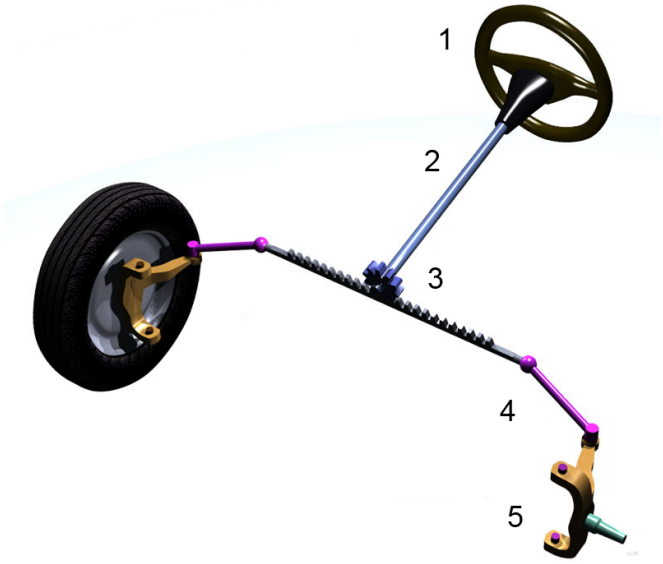

Figure 1.2. Rack and pinion steering mechanism, where (1) steering wheel, (2) steering column, (3) rack and pinion, (4) actuated suspension link (tie rod), (5) wheel carrier [58].

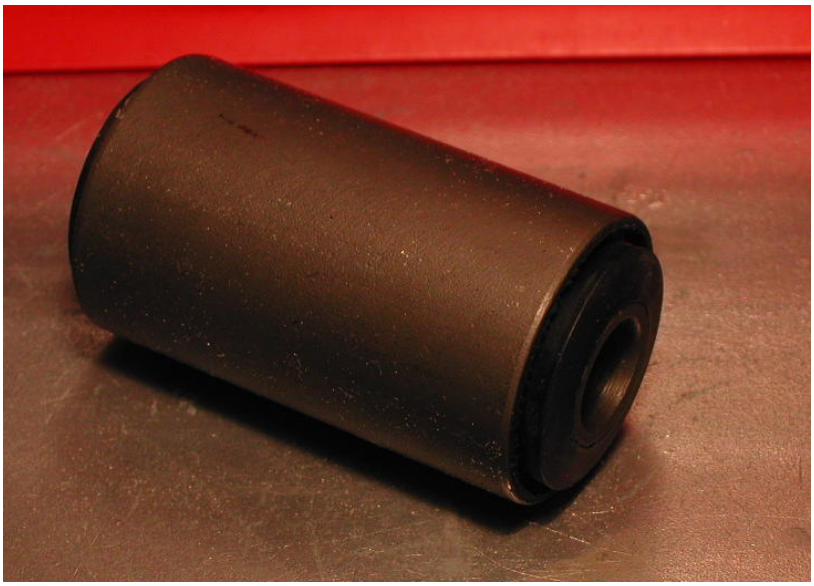

Figure 1.3. Cylindrical rubber bushing [56], typically pressed into suspension link and attached to vehicle body in double shear.

Figure 1.4. Ball joint [60], typically pressed into suspension link, with wheel carrier attached in single shear.

1.1 Basic Terms

Terms are defined with the vehicle stationary. Some terms vary with the load the vehicle is carrying. Usually, terms are given at the vehicle's *design load*, which includes, for the category of vehicle, what is considered a reasonable amount of fuel, occupants, and luggage.

- The *wheel plane* is the plane through the wheel center that is normal to the wheel's spin axis.
- The *tire contact point* is the center of the tire contact *patch*, which is the region of the tire that is in contact with the road surface (Figure 1.5).
- The *static loaded radius* of the wheel is the distance between the tire contact point and the wheel center, measured along the wheel plane.
- The *camber angle* of the wheel is the angle between the wheel plane and the vertical. It is positive when the top of the wheel leans away from the vehicle; negative when it leans into the vehicle. See Figure 1.6.
- The *toe angle* of a wheel is the angle between a longitudinal axis of the vehicle and the line of intersection of the wheel plane and the road surface. It is positive when the front of the wheel aims toward the vehicle (*toe-in*) and negative when the front of the wheel aims away from the vehicle (*toe-out*). See Figure 1.7.
- *Track* is the lateral distance between the tire contact points of an axle, measured along the ground. See Figure 1.8.
- *Wheelbase* is the longitudinal distance between the front and rear tire contact points of one side of the vehicle, measured along the ground. See Figure 1.8.

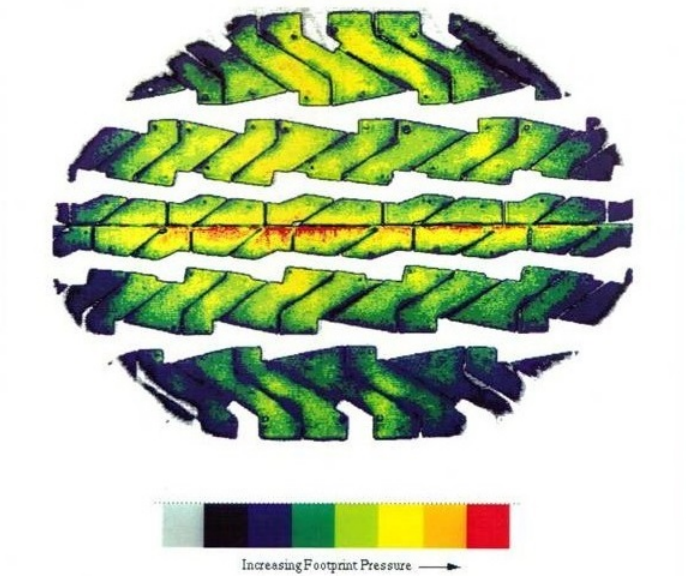

Figure 1.5. Contact patch with pressure distribution [54].

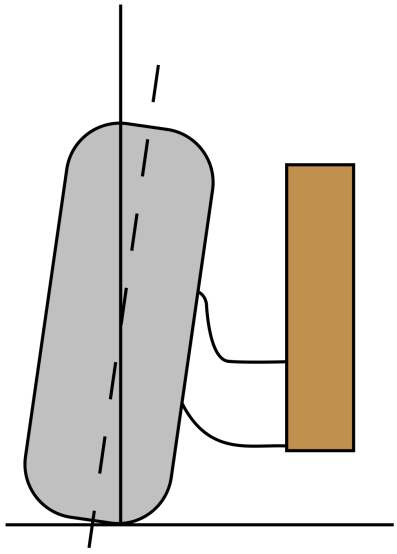

Figure 1.6. Camber angle illustrated in a front view; negative shown [57].

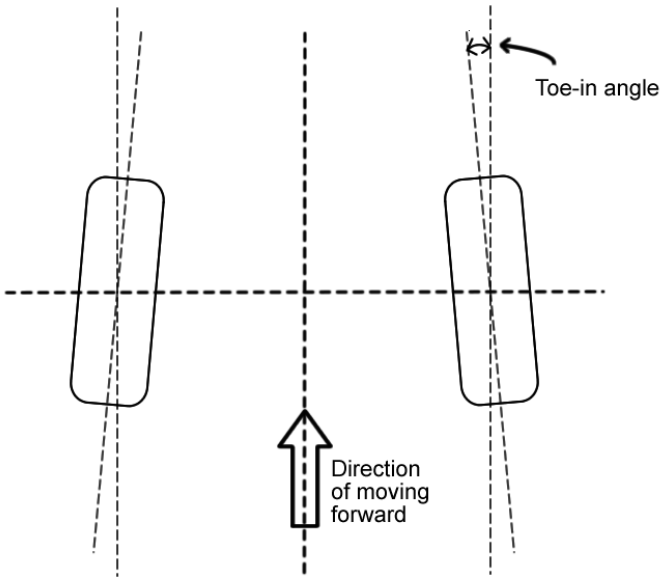

Figure 1.7. Toe angle illustrated in a top view; positive (toe-in) shown [61].

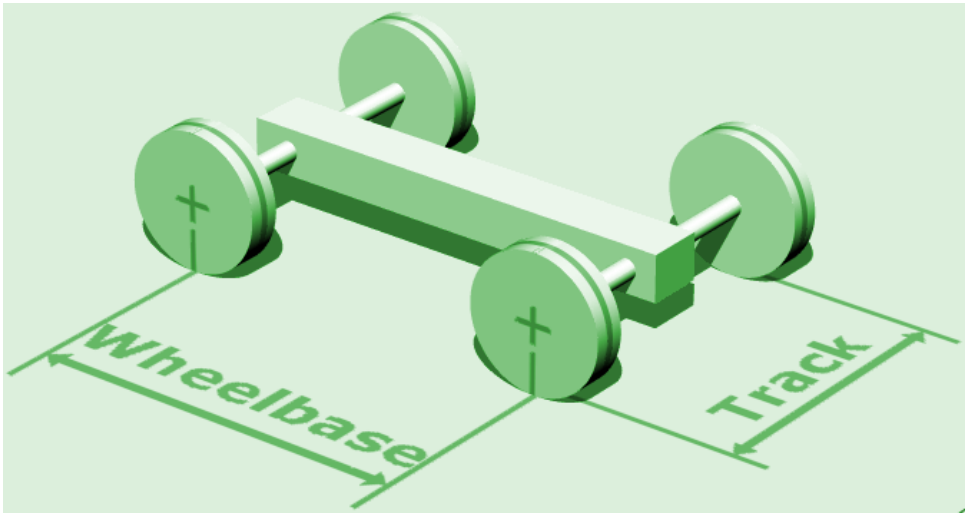

Figure 1.8. Wheelbase and track illustrated [63].

1.2 History of the Suspension

Early, animal-drawn, four-wheeled vehicles consisted of a platform mounted on two axles, with a wheel at each end of the axles. At the center of the front axle was a flat plate with a pin, which fit into a hole in a plate on the platform. This allowed the front axle to turn relative to the platform. The animals' harness was attached to the front axle, so when the animals pulled the vehicle it could steer accordingly. If the vehicle was intended to carry passengers, it was common to *suspend* the platform from the axles with chains or leather straps, making journeys more comfortable. By the early nineteenth century, leaf springs were used for this purpose. Friction between the leaves provided some amount of oscillation control. Steering by rotation of the whole front axle proved problematic. There was significant longitudinal movement of the wheels, which limited the turning radius and the size of the platform near the front axle. Another issue was that turning both front wheels the same amount meant that they did not track a common turn center, so the wheels had to slip for the vehicle to turn in a circle. This could cause wear on the wheels, as well as damage to the road — in those days, loose gravel or dirt. These concerns lessened with the introduction of a new type of steering arrangement. The innovation, patented in 1817 by Rudolf Ackermann, was to eliminate the center pivot, and instead have a pivot on each end of the front axle. This was accomplished by having a pin mounted at the end of axle, called a *kingpin*, about which a *wheel carrier* could turn. The wheel was then mounted, appropriately, to the wheel carrier. The carriers on the axle were connected by a link, which in turn was connected to a link that animals could be hitched to, Figure 1.9. The geometry of the mechanism was selected such that the packaging and slip issues described previously were mitigated.

Automobiles, as known today, began appearing towards the end of the nineteenth century, and were little more than carriages with their own power source. The steering linkage was revised so that the front wheels could be steered by hand, initially using a tiller. As internal combustion engines became increasingly powerful, the higher achievable speeds inspired further improvements in suspension and steering design.

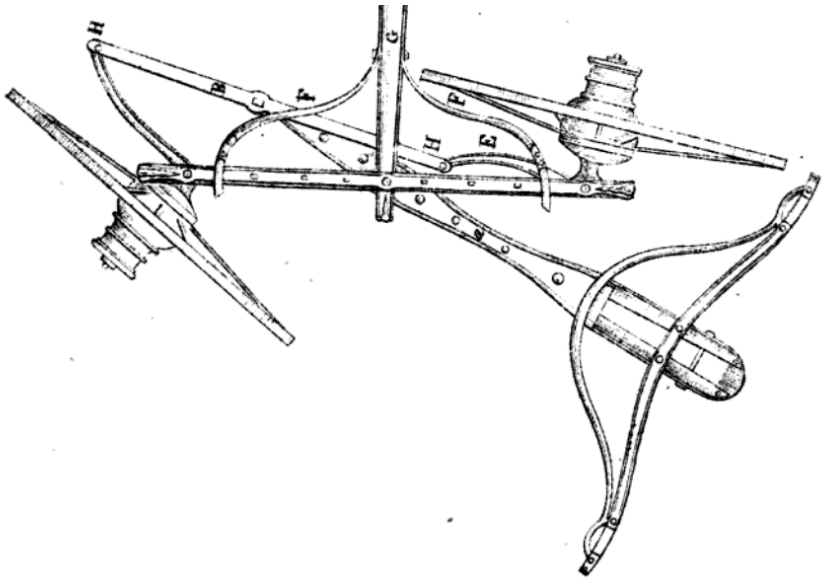

Figure 1.9. Ackermann's steering mechanism [1].

For example, the steering wheel ultimately replaced the tiller. A typical steering system used a gearbox that converted rotation of the steering wheel into rotation of a Pitman arm, which was then connected to the wheels by a linkage, Figure 1.10. Further efforts in the early twentieth century included the application of shock absorbers, which damp oscillations of the passenger compartment independently of the leaf springs. Shock absorbers in this period were mostly the friction disk and block-and-belt snubber types, both relying on dry friction, while hydraulic shock absorbers became common after World War II [9]. The most ubiquitous car of the early twentieth century was the Ford Model T, with 16.5 million produced between 1908 and 1927. The Model T was suspended from two axles using transverse leaf springs and employed Ackermann-style steering using a steering wheel. It included no separate shock absorbers, but these were available from the aftermarket. (Curiously, a 1915 owner's manual says that shock absorbers are "...not only unnecessary on Ford cars, but they are *dangerous*," [8]. Emphasis not added.)

By the 1920s, *shimmy* of the front axle had become a serious problem. Here is General Motors (GM) engineer Maurice Olley's description [29]:

> "On a smooth road with front wheels carefully balanced, the car might be traveling at 60 or 70 mph. Suddenly, for no apparent reason (perhaps

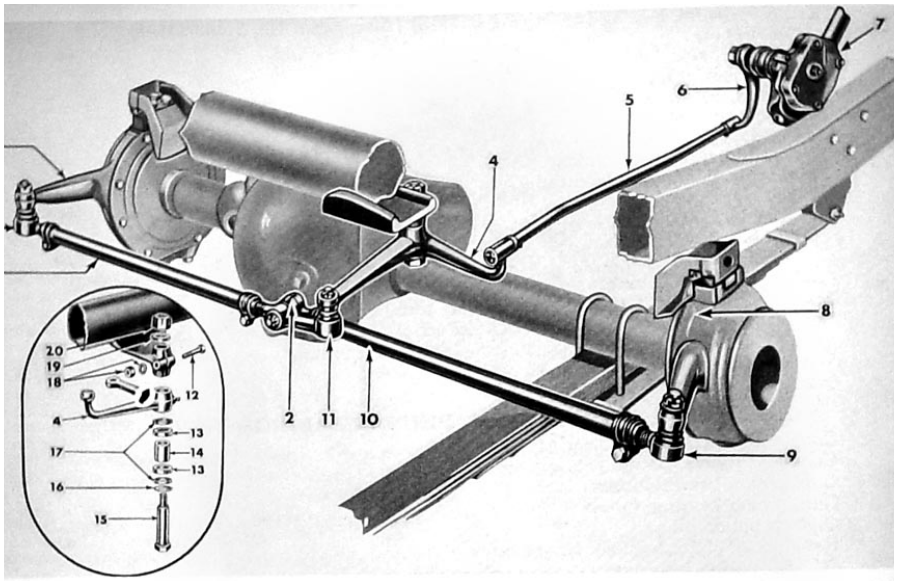

Figure 1.10. Gearbox steering system from a Willys CJ-3B [40].

> a small dip or pothole passing under one front wheel), the steering wheel would be wrenched out of the driver's hands, and would start oscillating violently, while each front wheel would leap along the road in giant ten foot jumps. The front axle would be tramping at 550–600 cpm [cycles per minute], each front wheel jumping three inches into the air."

Olley and his colleagues at GM determined that a solution to the shimmy problem was the switch to the independent front suspension (IFS), which "suppresses shimmy by connecting the mountings of the two wheels through the entire sprung mass of the front of the car". The IFS also had the advantage of allowing for softer front spring rates, which decreased how much the car would pitch over bumps — this *flat ride* proved pleasant. Further, the IFS allowed the engine to be moved forward relative to the front wheels and placed lower, between the wheels. This repackaging allowed stylists to produce the low, wide cars of today.

Independent suspensions are conceptually different from leaf spring axle suspensions. With leaf springs, the axle is both located and sprung by the leaf spring. This is a compliant mechanism, which relies on the spring's deformation to produce the desired vertical motion of the wheel. In contrast, an independent suspension is designed to have a vertical degree-of-freedom (DOF), upon which separate springs and dampers may act. Independent suspensions had actually been around for a number

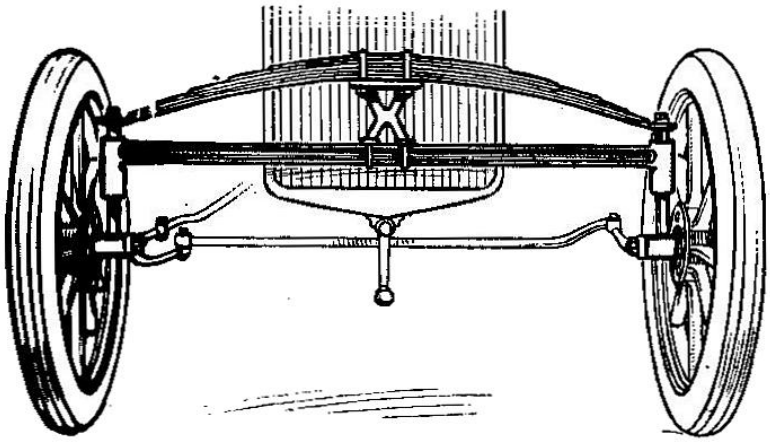

Figure 1.11. Sliding pillar IFS of an early Sizaire-Naudin car [2].

of years prior to GM's realization of their merits in the 1930s. The first production car to have an IFS was the Decauville, circa 1898, which used a sliding pillar IFS. A drawing of this type is seen in Figure 1.11. Another early independent suspension approach was the swing axle. This amounted to allowing each "half" of the axle to swing independently, Figure 1.12. Some designs of this type were even employed as rear suspensions, and used the drive axle as one of the arms. The design favored by GM was the *double wishbone*, also known as the short-long-arm (SLA), seen in Figure 1.13. In addition to leaf springs and coil springs, torsion springs were also in use. An example can be seen in Figure 1.14. In this figure, there is also a hydraulic shock absorber.

As the century went along, the MacPherson strut suspension, Figure 1.15, introduced in the late 1940s, became an increasingly popular IFS. This was due to its relatively few number of components, especially when the spring is placed over the strut, and its ability to provide a steer DOF. The rack and pinion steering system, seen in Figure 1.2, in use in Europe by the 1930s, found its way to American cars in the 1970s. While the shimmy problem and styling demands led to the almost total extinction of the traditional front axle in favor of the double wishbone and MacPherson suspensions, there was no similarly urgent reason to discard the rear axle. That

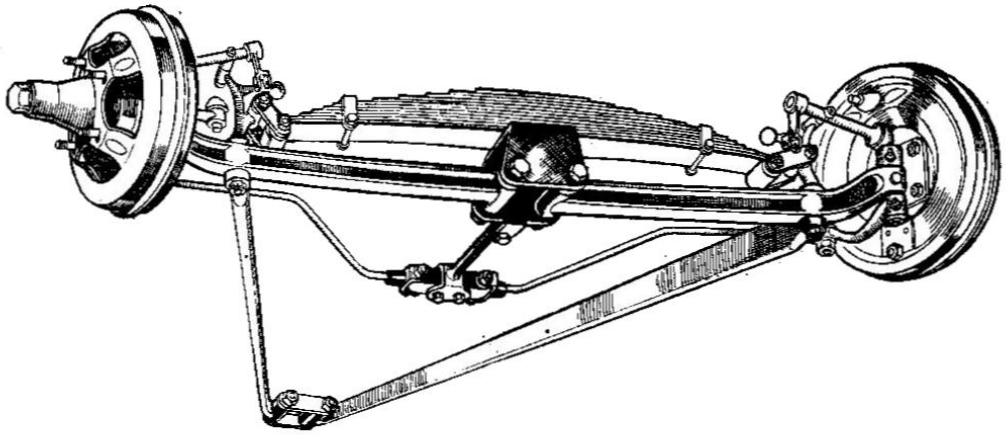

Figure 1.12. Ballamy swing axle IFS [2].

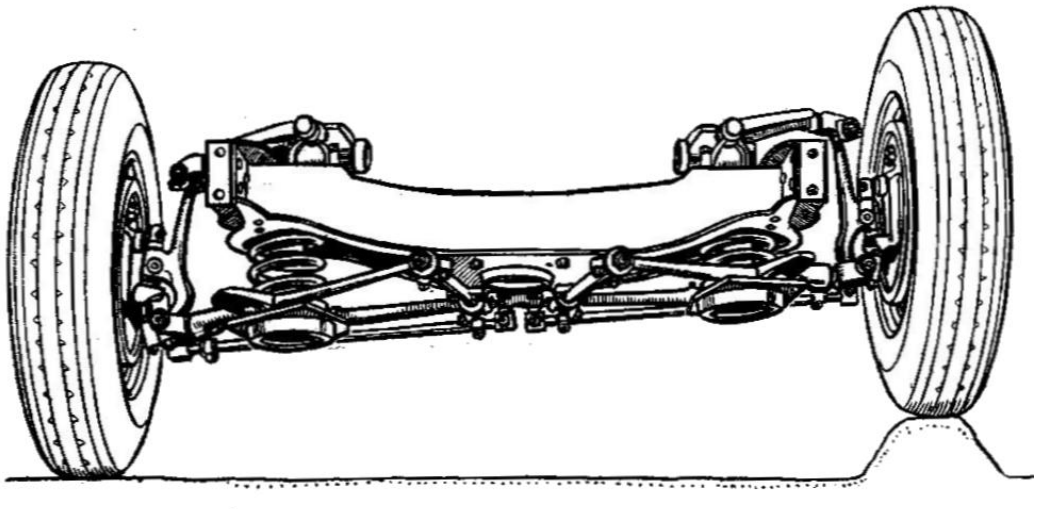

Figure 1.13. Oldsmobile SLA IFS [2].

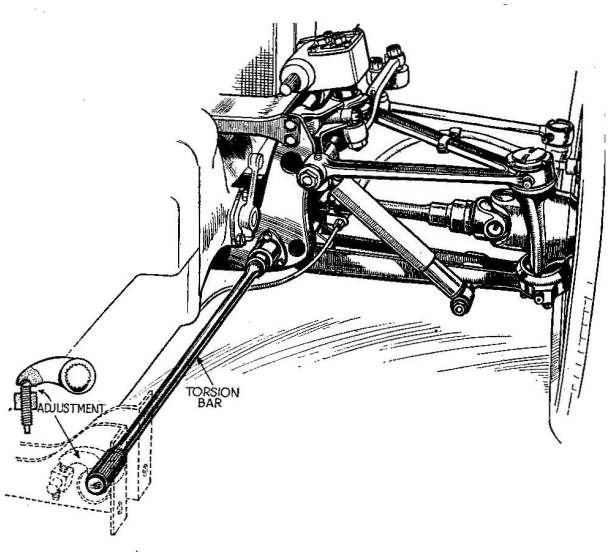

Figure 1.14. Citroen IFS, using a torsion spring and a hydraulic shock absorber [2].

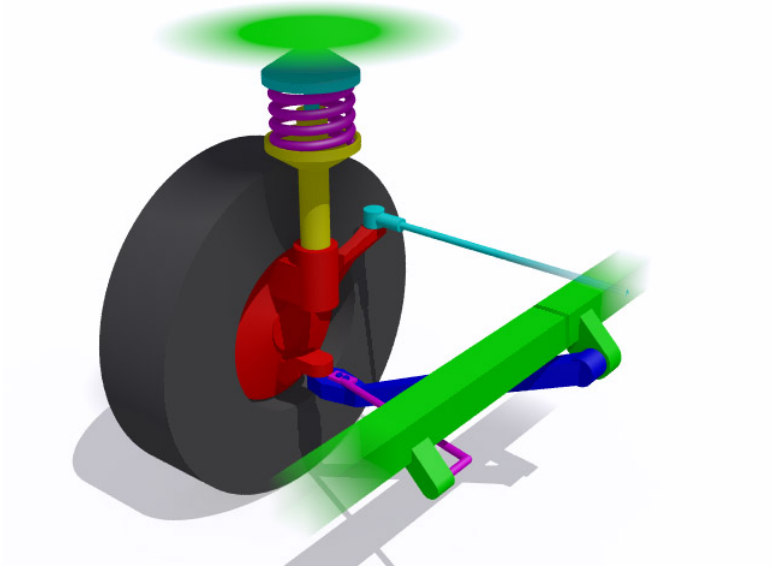

Figure 1.15. MacPherson strut IFS [55].

is not to say that the advantages of the independent suspension are unique to a front application. Indeed, even on rear axles, the independent suspension has the following advantages [18, p. 395]:

- Reduced unsprung mass;
- Reduced opportunity for a disturbance of one wheel to affect the other;
- Increased capability to specify the kinematic and compliant behavior;
- Ease of managing noise, vibration, and harshness.

The disadvantages of the independent suspension versus the rigid axle are

- Wheel travel and ground clearance are limited;
- An anti-roll bar is often needed, which prevents truly independent wheel motion;
- A less robust design.

The ground clearance and robustness aspects are not relevant for passenger cars. If one is curious how far designers have taken the independent suspension with respect to ground clearance and robustness, consider that the military Humvee features independent front suspensions front and rear, Figure 1.16.

One way to provide some measure of independent rear wheel motion economically is to allow the axle itself to deform, thus requiring the further classification of an axle as *rigid* or *semi-rigid*. The primary realization of the semi-rigid axle is the twist beam, introduced in 1974 by Volkswagen. An example of the type is shown in Figure 1.17. This design allows the axle to swing relative to the vehicle body, while independent wheel motion is a result of torsional deformation of the axle itself. On the other hand, more expensive cars did begin to use independent rear suspensions (IRS) shortly after the mid-century mark. Multilink designs, such as Mercedes-Benz's five link IRS, seen in Figure 1.18, provide the designer with considerable choice over how to guide the wheel's vertical motion. Recently, even cheaper, compact cars have adopted the IRS. This transition was initiated by the original Ford Focus, introduced to European

Figure 1.16. AM General Humvee featuring robust double wishbone suspensions front and rear with excellent ground clearance [28].

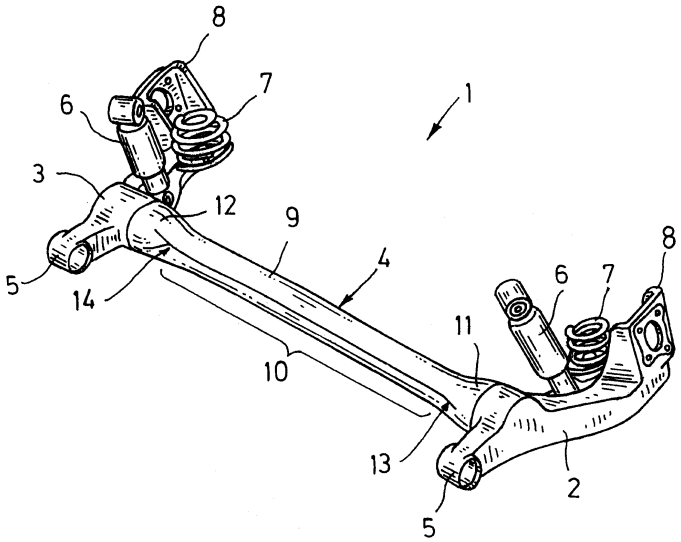

Figure 1.17. Twist beam semi-rigid rear axle [14].

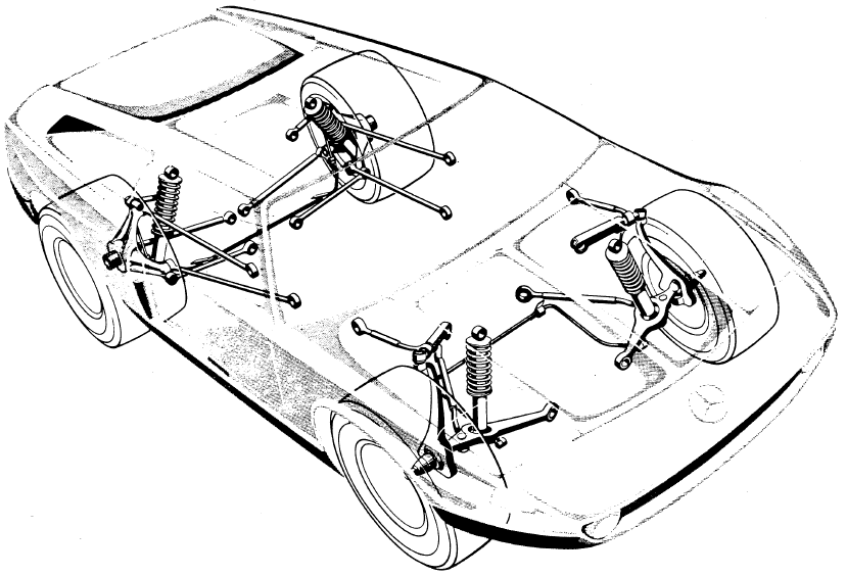

Figure 1.18. Mercedes C111, circa 1969, using a five link IRS and a double wishbone IFS [62].

markets in 1999 with its multi-link *control blade* suspension [18, p. 391]. Later versions of the car continued with this successful design, Figure 1.19. The improved ride and handling due to the independent rear suspension led other automakers to redesign their compact cars — Volkswagen went as far as hiring ex-Ford engineers to replace the twist beam axle of the Golf with a Focus-style multi-link IRS [48]!

Where do these developments leave matters in recent times? In 2010, 97% of vehicles produced had independent front suspensions, dominated by the MacPherson type, Table 1.1. In the same year, 45% of vehicles produced used an independent rear suspension, Table 1.2. Can IRS market share be expected to rise? The vehicles using rigid rear axles are essentially pickups and pickup-based sport-utility vehicles and vans. These vehicles have reduced ride/handling expectations and increased towing/hauling expectations, so it is unlikely the status quo will change. (This is not to say an IRS is not technically possible if the market demands it; one only has to look as far as the Humvee.) On the other hand, semi-rigid axles, realized as the various twist beam types, continue to target subcompact cars where cost is their main advantage. There has already been a transition to IRS in the similar compact market once an economical-enough design was introduced.

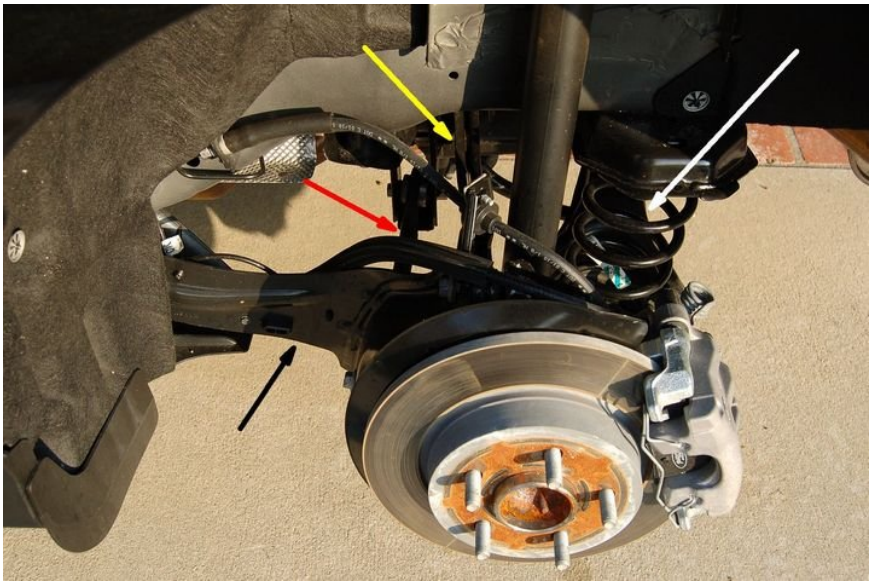

Figure 1.19. 2012 Ford Focus control blade IRS; arrows indicate the control blade and three lateral links [10].

Table 1.1. Market share of the front axles used by vehicles produced in 2010 [18, p. 418]; the twist beam is used in just one vehicle model.

Front Axle/Suspension	Classification	Market Share
MacPherson	Independent	76.5%
Double Wishbone	Independent	19.8%
Rigid Axle	Rigid	2.7%
Multi-Link	Independent	0.7%
Twist Beam	Semi-Rigid	0.3%

Table 1.2. Market share of the rear axles used by vehicles produced in 2010 [18, p. 418]; the De Dion axle is used in one vehicle model.

Rear Axle/Suspension	Classification	Market Share
Twist Beam	Semi-Rigid	24.9%
Rigid Axle	Rigid	24.3%
Multi-Link	Independent	24.2%
Double Wishbone	Independent	7.1%
Trailing Arm	Independent	8.1%
Twist Beam, Torsion-Type	Semi-Rigid	5.4%
Semi-Trailing	Independent	2.7%
Five-Link	Independent	1.7%
Trapezoidal	Independent	1.3%
De Dion	Rigid	0.3%

Another opportunity for future independent suspension development is presented by electric hub motors, which integrate an electric drive unit into the wheel and hub assembly. Should these become viable, new suspensions will need to be developed, even if only to suit the differing space requirements. Hub motors will almost certainly reduce the amount of space available on the wheel side for the linkage, and it is likely that designers will push for less space on the body side, as they no longer have to accommodate a final drive or internal combustion engine. Consumers will ultimately expect the same or better ride/handling performance, which will prove challenging with less space available, not to mention the unsprung weight of the hub motor.

The two opportunities discussed above, in the subcompact market and the electric vehicle market, exemplify two general reasons why independent suspension development will continue:

1. Occasionally, new versions of existing vehicles will need a new suspension design. This happens when the current design is incapable, even with optimization, of meeting revised ride and handling targets.

2. Vehicles with no predecessors will continue to be designed. This happens when an automaker enters a new market segment and is unable to adapt an existing suspension design.

With the need for continued development of the independent suspension established, it is time to review the modern design process.

1.3 Suspension Design

The product development process (PDP) for the modern automobile in general follows a V-pattern, Figure 1.20: the product is defined at the vehicle-level, and requirements are flowed down to the system-level, subsystem-level, and eventually the component-level. The components are then assembled into subsystems, subsystems assembled into systems, and systems assembled into the vehicle, allowing requirements to be validated along the way. The design process is iterative, by way of simulations early

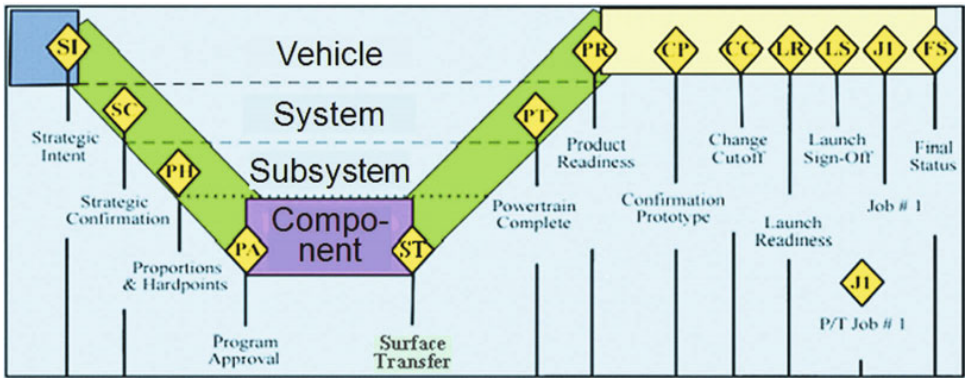

Figure 1.20. Schematic of Ford's product development process as of 1998 [18, p. 451].

on, and eventually with hardware tuning (minimal, if all goes to plan). The rest of the PDP focuses on getting the vehicle ready for mass production. Here the interest is the suspensions. The vehicle-level requirements for these are the starting point.

1.3.1 Ride & Handling Targets

The first task when designing a suspension is to establish *vehicle-level* ride and handling targets. These specify the intended performance of the completed vehicle without assuming any particular design solution for the suspensions. There are hundreds of possible metrics engineers can measure or derive from vehicle testing. Ultimately, the goal is to come up with a minimal set of metrics that establish the "fundamental handling character of the vehicle" [43]. For the 1997–2004 Chevrolet Corvette (C5), the engineers settled on 23 metrics spread across four categories, Table 1.3. As one can see, there are fewer objective metrics for ride than for handling. The *control* aspect of ride, regarding the rigid body motion of the sprung and unsprung masses, is fairly well understood — designers can talk about natural frequencies, damping ratios, accelerations of the sprung and unsprung masses. The *isolation* aspect, concerned with higher frequency noise and vibration, is difficult to reduce to simple metrics, with development ongoing. The reliance on subjective metrics is not ideal for synthesizing a design in an analytical setting, as these are best suited for vehicle-to-vehicle comparisons in a controlled environment.

After deciding on the ride and handling metrics of interest, each is assigned a

Table 1.3. C5 ride and handling metrics with associated units [43].

Category	Metric	Units
Linear Handling	Understeer Gradient	deg/g
	Steering Sensitivity	g/(100 deg)
	Steering Sensitivity Linear Range	g
	Lateral Acceleration Response Time	s
	Roll Gradient	deg/g
	Roll Damping	–
	Yaw Velocity Damping	–
	Pitch Gradient, Acceleration & Braking	deg/g
Non-Linear Handling	Maximum Lateral Acceleration	g
	Dropped Throttle Stability	g
	Single Bump Roadholding	deg
On-Center Handling	Minimum Steering Sensitivity	g/(100 deg)
	Steering Sensitivity Ratio	–
	Steering Hysteresis	deg
	Lateral Acceleration at Zero Torque	g
	Steering Torque Gradient Ratio	–
	Steering Work Sensitivity	g^2/(100 N·m)
	Static Steering Effort	N
	Curb-to-Curb Turning Circle	m
Ride	Front Ride Frequency	Hz
	Ride Frequency Ratio (Rear/Front)	–
	Impact Harshness	Subjective Rating
	Vertical Damping	Subjective Rating

number or interval. Engineers rely on customer input, benchmarking, and experience to make these decisions. For C5, existing Corvette owners were queried at clinics across the country and through JD Power surveys. Customer wishes were correlated to the ride and handling metrics, with each desire being assigned a strong, medium, or weak correlation to a metric. Benchmarking of 45 peer vehicles and 22 existing Corvettes allowed the engineers to understand the current landscape. Several metrics were set to be best-in-class due to their perceived importance. All metrics were scrutinized with analytical methods to ensure they were realistic and did not conflict with others.

Several vehicle-level characteristics that are outside the direct control of the suspension development team are nevertheless important for ride and handling. Part of establishing achievable ride and handling targets is properly communicating needs to the rest of the vehicle's development team. In the C5 example, the suspension designers recommended an increased wheelbase, wider tracks, more equal front-to-rear weight distribution, and reduced yaw and pitch moment of inertias. There is only so much the suspension itself can do!

1.3.2 Architecture

Suspension design proper starts with the selection of the front and rear suspension architectures. For the independent front suspension, MacPherson, double wishbone, and multi-link architectures are commonly used (Table 1.1). For the independent rear suspension, Table 1.2, there is more variety: multi-link, double wishbone, trailing arm, semi-trailing arm, five link, and trapezoidal. In new versions of existing vehicles, the suspension architectures are typically carried over, except in cases where the old architecture is seen as incapable of meeting improved vehicle-level targets. For example, the rear multi-link of the 1984–1996 Chevrolet Corvette (C4) was replaced with a double wishbone architecture for the C5. An impetus for this change was the desire for improved camber angle and roll center height behavior with wheel travel [11], both having positive effects on vehicle-level performance.

In the case of an all-new vehicle, various architectures may be prototyped to assess

performance. For the compact Mercedes Model W201 [33], engineers wanted the ride and handling performance characteristic of their larger, heavier cars. For the front, they designed and tested the

- Double control arm (aka double wishbone),
- Spring strut (aka MacPherson), and
- Damper strut (MacPherson, but with spring separated from strut).

The damper strut axle was chosen; strongly in its favor was its ability to be compactly configured. With no upper control arm, there was plenty of room laterally for the powertrain. By separating the damper and spring, the hood height could be lowered beyond what was possible with the strut-mounted spring, important for styling. For the rear of the Model W201, Mercedes investigated the

- De Dion axle (the lone non-independent),
- Extended swing axle (uses the half-shaft as part of the linkage; virtually nonexistent in modern cars due to poor toe and camber changes with wheel travel),
- Semi-trailing arm,
- Triple control arm (double wishbone with lower arm split into two links),
- Spring strut,
- Damper strut,
- Double control arm, and
- Multi-link (aka five link).

The engineers designed 77 variations of these architectures, with over half being built and tested physically. It should be clear that Mercedes spared no expense during the development of its first compact car! The five link design was selected because it was capable of being optimized to meet both ride and handling objectives. The noted

downside was that such optimization required "intensive efforts of the departments handling design, computer application, testing, and manufacturing".

There is a wide range of possible behavior for a given architecture — consider that both the Humvee and the Corvette successfully employ double wishbone suspensions. Meeting vehicle-level targets requires that the chosen architecture be configured precisely for its purpose. The first consideration is kinematics.

1.3.3 Kinematics

In the kinematics stage, designers are interested in locating the geometric centers of the various bushings and ball joints of the chosen architecture. These points establish

- The volume occupied by the suspension;
- How the wheel moves as it travels vertically;
- How the wheel's vertical travel is related to shock absorber and spring compression/extension;
- The steering axis, if the wheel is to be steered.

In the case of suspensions carried over from an existing vehicle, linkage geometry is well-defined and may require only slight adjustment. Designers essentially go straight to an analysis and optimization stage. On the other hand, if a new vehicle is being designed, geometry must be selected from scratch.

The first consideration is packaging — how much room is available? *Package drawings* define the basic vehicle dimensions and how people and major components fit within them. Example packaging drawings are available as a result of the Ultra Light Steel Auto Body (ULSAB) project; Figures 1.21, 1.22, 1.23, 1.24 show the side, front, rear, and plan views, respectively. The suspension must package around the occupants, powertrain, steering rack, fuel tank, etc.

Gerrard shows how initial linkage geometry is synthesized in [12]. The desired wheel motion is specified as its velocity when the wheel is in the *design position* (position relative to the vehicle body at the vehicle's design weight). In particular,

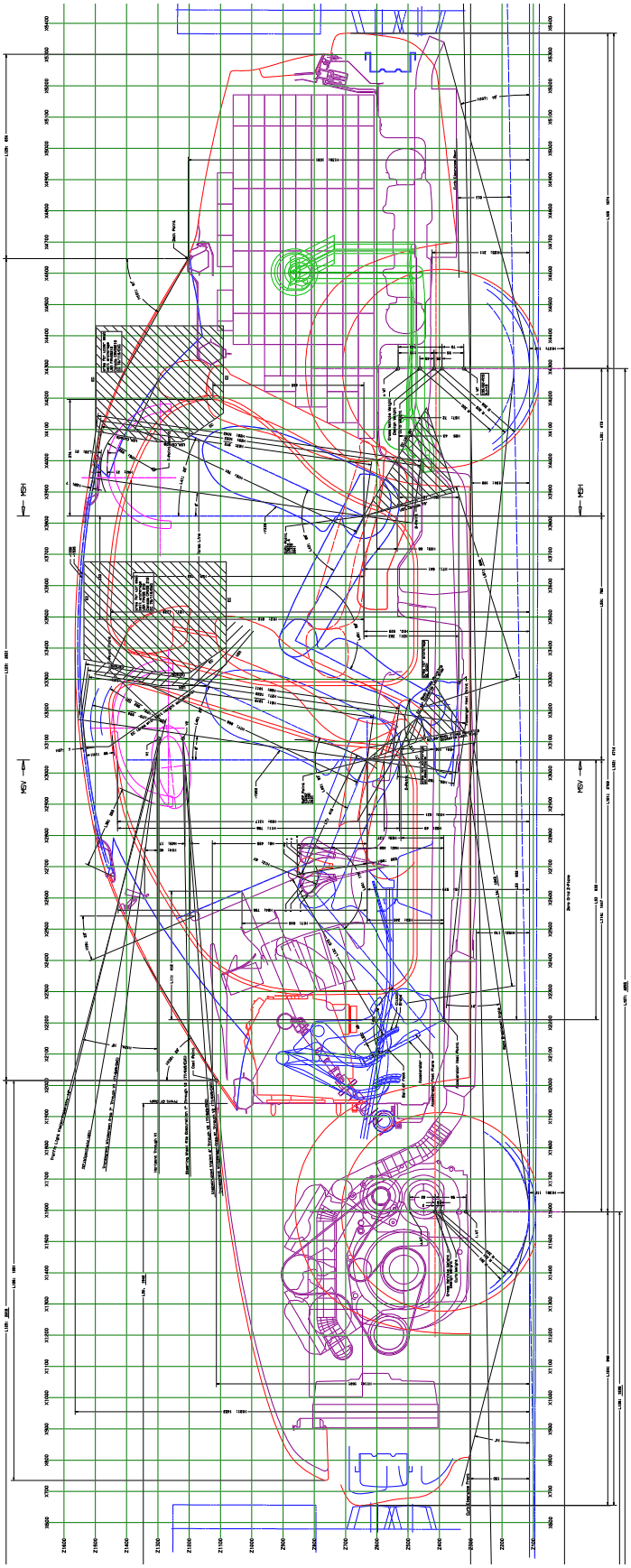

Figure 1.21. ULSAB side view package drawing [46].

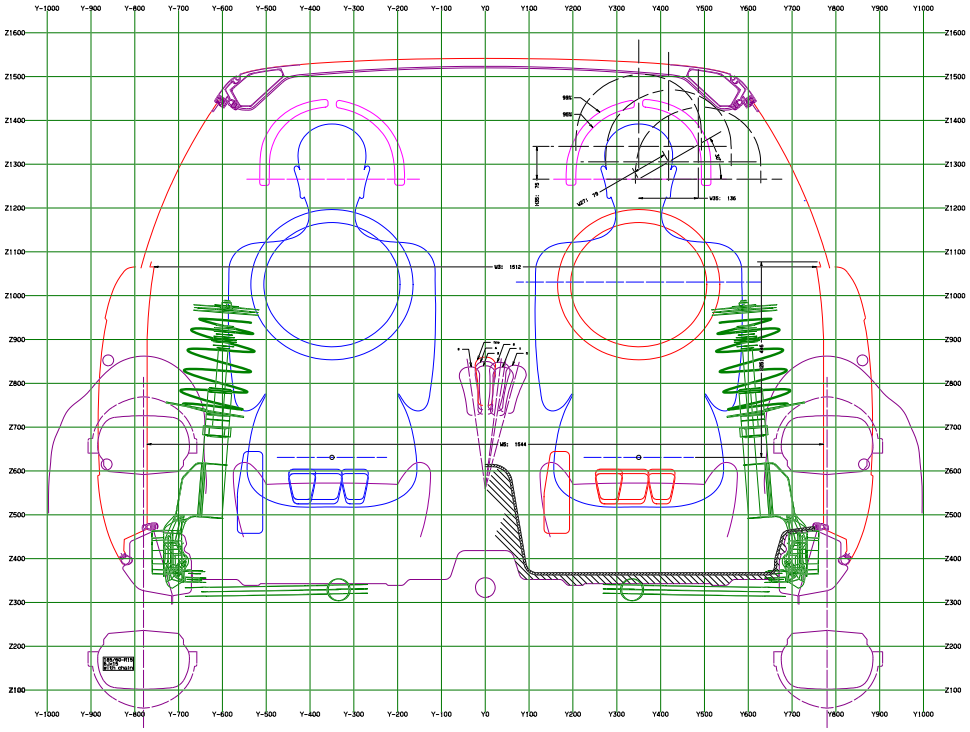

Figure 1.22. ULSAB front view package drawing [46].

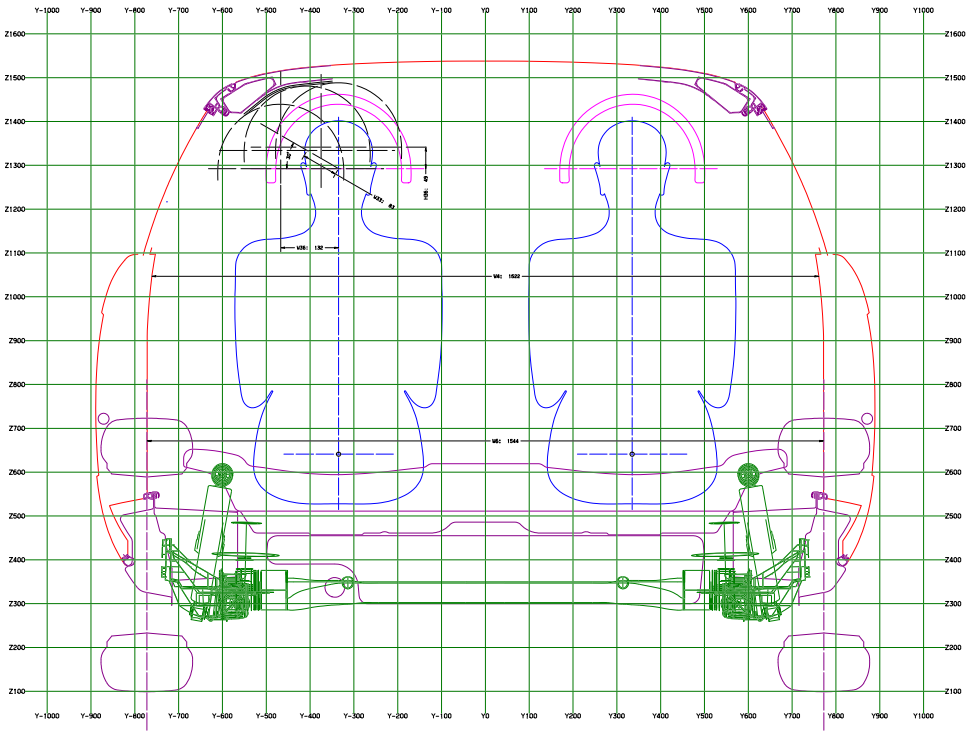

Figure 1.23. ULSAB rear view package drawing [46].

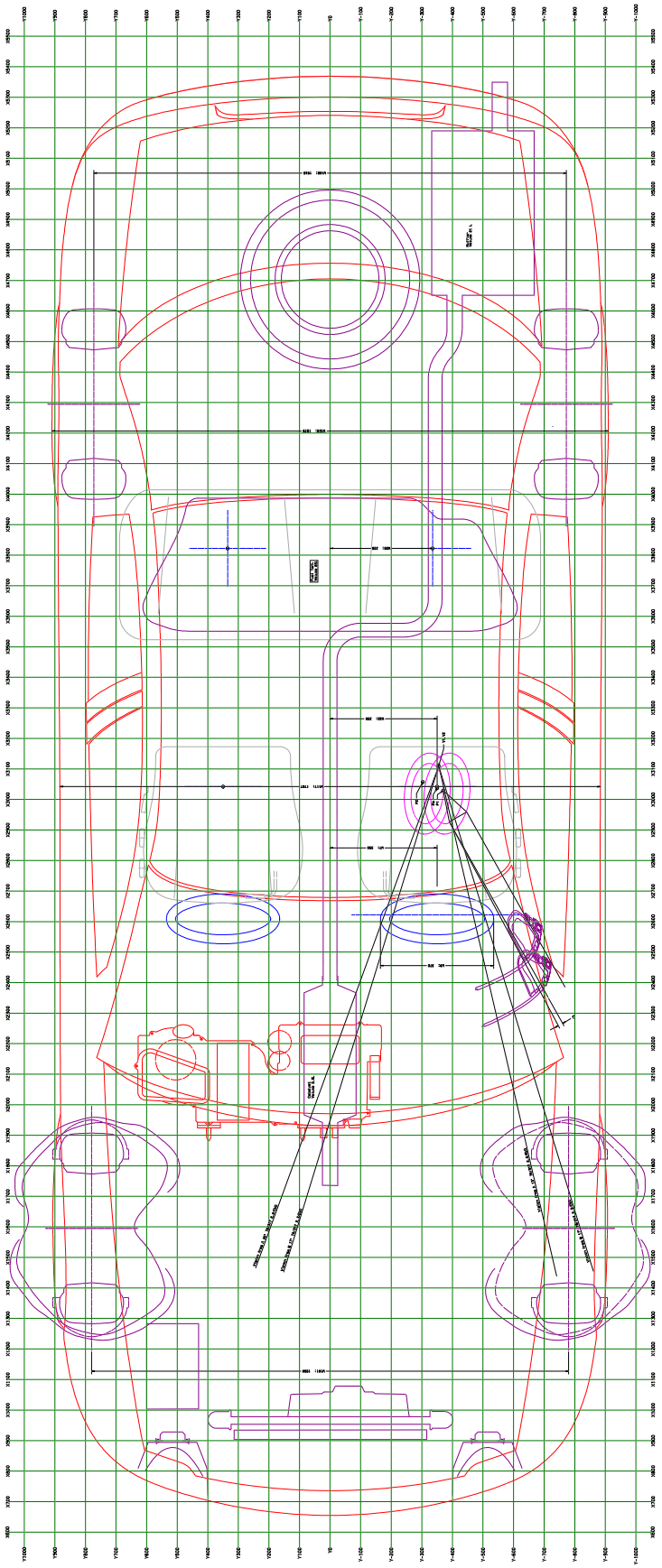

Figure 1.24. ULSAB plan view package drawing [46].

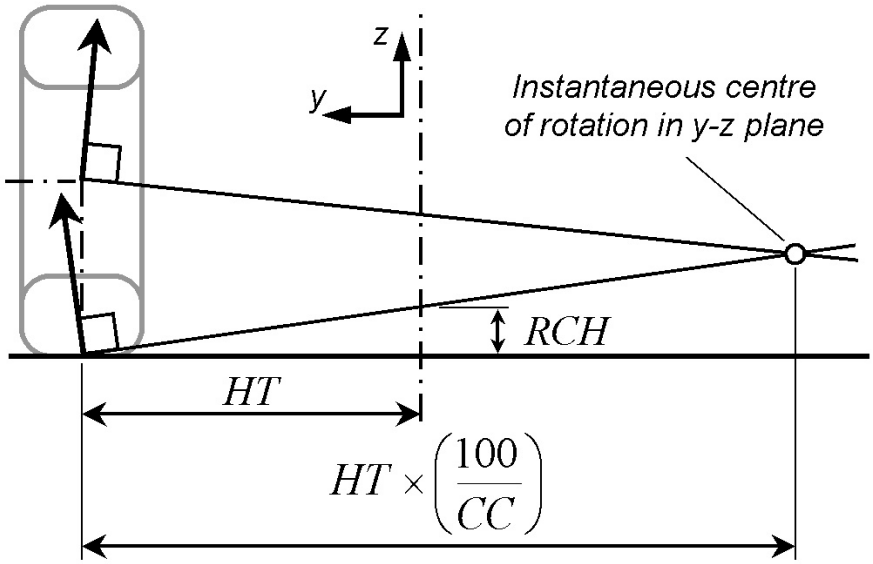

Figure 1.25. Front view instant center definition [12].

the velocity is given by way of front and side view instant centers. Assuming a unit vertical velocity of a point on the wheel, the front view instant center gives the lateral velocity of that point and the angular velocity of the wheel about a longitudinal axis. In the side view, the same unit velocity gives the longitudinal velocity of the chosen point and the angular velocity of the wheel about a lateral axis. A plan view instant center is not considered; instead, angular velocity of the wheel about a vertical axis is given directly to complete the velocity specification.

In practice, the instant centers are themselves given in various ways. Gerrard, for example, locates the front view instant center with *roll center height* (RCH, millimeters) and a parameter associated with camber angle change, *camber compensation* (CC, percent). *Half of the track width* (HT, millimeters), a vehicle-level specification, completes the location, Figure 1.25. Gerrard gives the side view instant center with two angles: the *wheel center trajectory* (WCT, radians) and the *contact point trajectory* (CPT, also in radians). A vehicle-level specification, *static loaded radius* (SLR, millimeters) of the tire, completes the picture, Figure 1.26. The vertical component of the wheel angular velocity is given directly as the parameter *kinematic toe change* (KTC, radians per millimeter), Figure 1.27. All of these wheel-motion characteristics correlate to the vehicle-level targets.

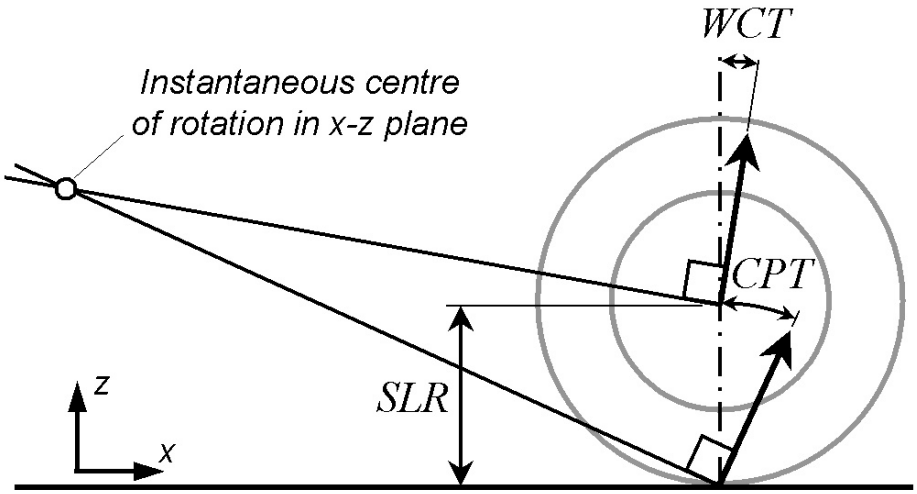

Figure 1.26. Side view instant center definition [12].

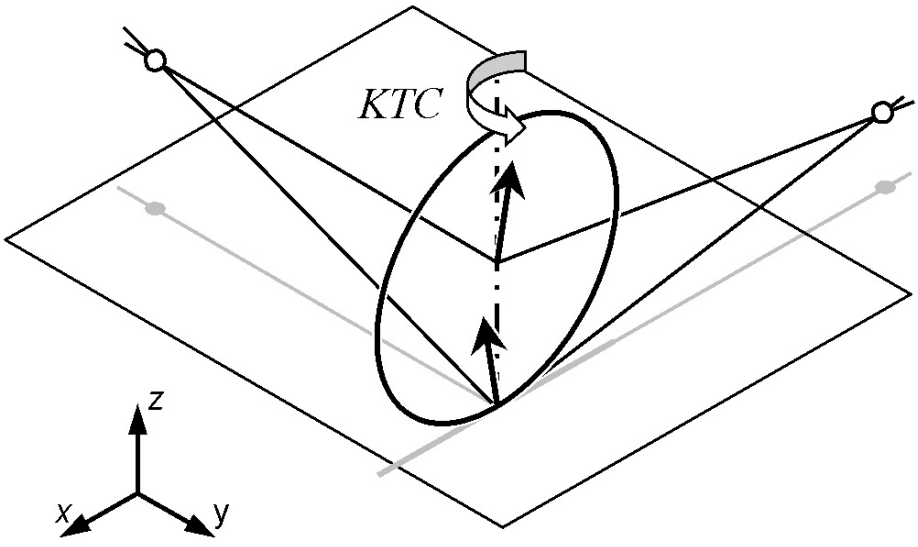

Figure 1.27. Definition of the vertical component of the angular velocity [12].

Gerrard considers two cases of the velocity specification. In the first case, the velocity of the chosen point is perpendicular to the angular velocity. Consequently, the motion can be considered as the result of instantaneous rotation about an axis. Gerrard shows how to orient links and locate joints to achieve this velocity specification. For example, a trailing link suspension is shown in Figure 1.28. In the second velocity specification case, the velocity is a general rigid body velocity, which is often interpreted as the result of instantaneous rotation about a screw axis. In this second case, Gerrard finds it more useful to consider this velocity as the result of two instantaneous rotation axes that are interrelated by a *gear link*. Gerrard shows how to compute the two axes from the velocity specification and locate the gear link. The designer is able to select one of the axes at will, allowing it to be used as a steering axis, for example, and there is considerable flexibility in locating the gear link, making it suitable for use as the tie rod of a steering system, for example. Gerrard gives rules for orienting the non-gear links so that they provide the two instantaneous axes of rotation. For example, a double wishbone is shown in Figure 1.29. To be clear, Gerrard's method does not fully define the link geometry. The designer selects some of the link geometry (one ball joint of a wishbone, for example) and the synthesis method computes the rest. This allows the designer to package the suspension into the available space while still satisfying the basic velocity specification.

After the preliminary geometry is synthesized, often in a CAD environment, a multi-body model is built that allows the wheel motion to be analyzed. Designers iterate the linkage geometry — for example, changing the length of a link — to ensure wheel motion is acceptable throughout the full range of wheel travel. For non-MacPherson designs, the spring and shock absorber locations must be determined. A typical goal is to have *installation ratio(s)* of one; that is, a unit of vertical wheel travel correspond to a unit of shock absorber or spring travel. Also of importance is making sure there are appropriate clearances, so that the linkage does not interfere with itself. Of course, the wheel must also stay within its allotted space as it articulates. The geometry at this point is not final, since components have yet to be designed and the suspension has not been assessed under load. It will continue to be revised as

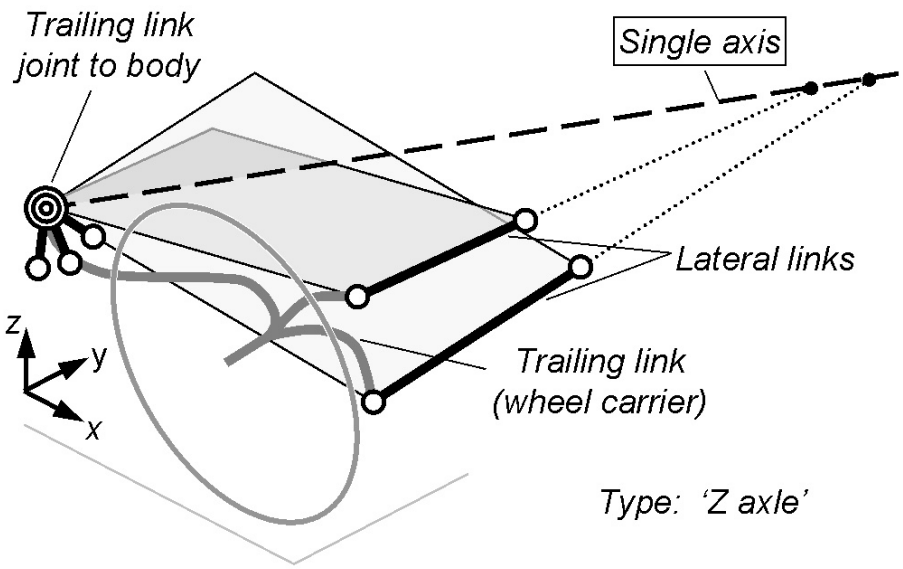

Figure 1.28. Layout of a trailing link suspension to achieve one-axis velocity specification [12].

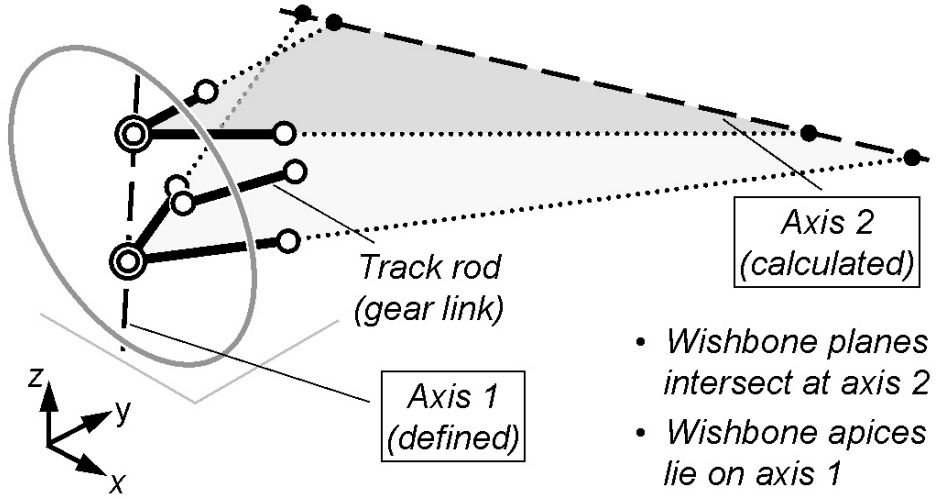

Figure 1.29. Layout of a double wishbone suspension to achieve a two-axis velocity specification [12].

necessary.

1.3.4 Elastokinematics

For comfort, passenger vehicles require the wheel to move longitudinally a considerable amount, around 25 mm, when subject to impact. This motion must occur without otherwise disturbing the vehicle by, for example, steering the wheel. In this stage of suspension design, these kinds of considerations come into play, as the focus is on how the wheel moves under load when the elasticity of the suspension is considered — the wheel's so-called *elastokinematics*. Here are some typical elastokinematic requirements [18, p. 32]:

- Longitudinal compliance under braking (mm/kN)
- Longitudinal compliance under impact (mm/kN)
- Toe change under braking (deg/kN)
- Wheel lateral stiffness (mm/kN)
- Toe and camber change under lateral loading (mm/kN).

These requirements are set so that they help achieve the vehicle-level ride and handling targets. The set of kinematic and elastokinematic targets for a suspension are sometimes called its *static design factors* (SDFs). In [11], GM states that the "... modeling, measuring, and balancing of suspension SDFs is key to arriving at a vehicle which delivers capable, pleasible dynamic performance".

Working with the MBS model, designers replace some or all of the kinematic joints with bushings. This potentially requires locating bushings along an axis — for example, in the kinematic stage, a wishbone is equivalent to a revolute-spherical link, so the location of the wishbone legs along the axis does not affect wheel motion. However, the location of the two bushings along the revolute axis in the elastokinematic stage is meaningful. In addition to the bushing rates, the stiffness of the spring is added. From here, loads can be applied to the wheel in a quasi-static fashion and wheel

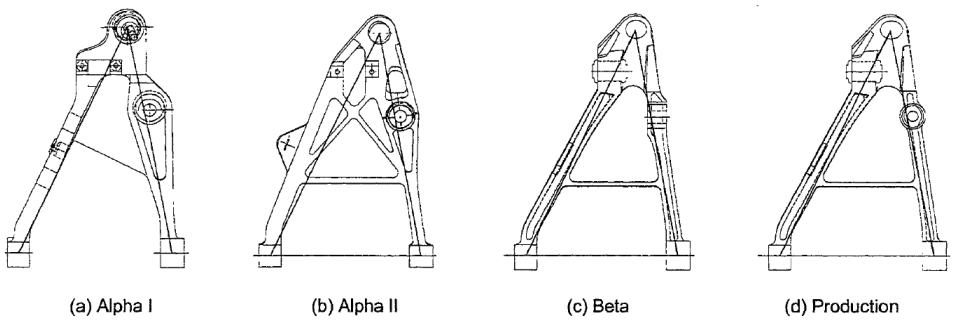

Figure 1.30. Design evolution of the C5 rear lower control arm [45].

movement assessed. Loads are determined early on from vehicle-level acceleration targets — for example, a lateral force at the tire contact point based on 2 g lateral acceleration. Bushing rates are optimized. In some cases link geometry is refined; in the C5 example, plan view tie rod angle was adjusted to improve toe change under braking [11].

The load analyses also give a starting point for loads on the suspension components and reaction loads on the vehicle body. These results allow structural design of these parts to proceed. An account of how the control arms for the C5 were developed is available in [45]. For the rear lower control arm, a basic design, *Alpha I*, was created that was functionally acceptable but not optimal. Finite element analysis led to *Alpha II*. Issues with mass, suitability for production, and the durability of the shock absorber mount led to a new *Beta* design. Further testing and refinement resulted in the *Production* design. Drawings of these four design stages are shown in Figure 1.30. When ready, compliance of the suspension components and vehicle body itself, from finite element analysis, can be added into the MBS model and the elastokinematics re-assessed. Eventually, the design is complete enough to consider the vehicle as a whole.

1.3.5 Vehicle Dynamics

In the last stage, the completed vehicle design is assessed to see if it meets the original ride and handling targets. Early on, whole-vehicle simulations are used. This allows changes to be made to the design before committing to hardware. Once the

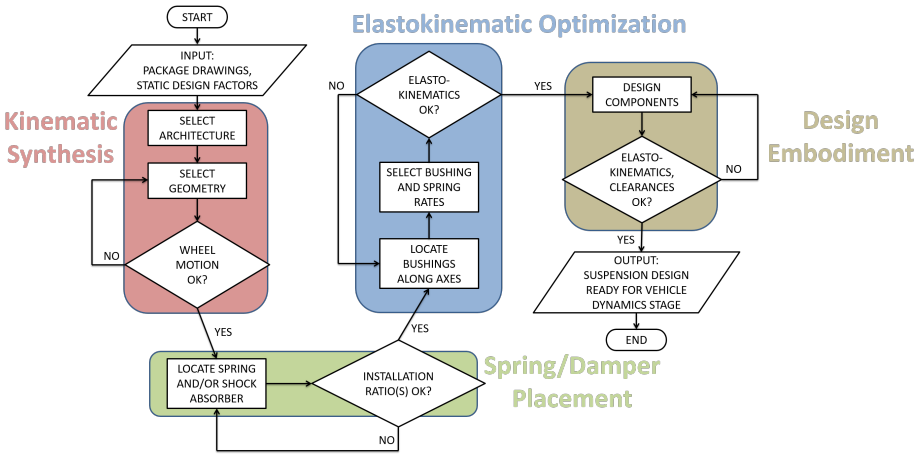

Figure 1.31. Summarized suspension design process.

design is ready, it is constructed and tested. Ride and handling engineers further tune the springs, bushings, and dampers to result in a product that satisfies both objectively and subjectively. General Motors discusses this process for the C5 Corvette extensively in [31].

1.3.6 Discussion

In Figure 1.31, the suspension design process described in the previous sections is depicted as a flowchart, presuming that vehicle-level specifications have already been mapped to the static design factors. Characteristic of the design process is its reliance on analysis, visualized as the feedback loops in the flowchart. Designers come up with an initial design through experience or incomplete synthesis methods, then iterate the design with an analysis tool until performance is satisfactory. Raghavan of GM gives a good example: determining the location of a tie rod [37]. Designers often wish for the toe angle to vary linearly with vertical wheel travel. As mentioned previously, the initial linkage geometry is based on a velocity specification, so there is no guarantee that the toe angle will vary as desired. Designers modify the tie rod endpoints and analyze the wheel motion, repeating this process at least two dozen times, each iteration taking around ten minutes. Raghavan points out that this is entirely unnecessary, since the problem can be formulated with a closed-form solution. Raghavan suspects that designers have not adopted synthesis methods for

two reasons: the tradition of machines being experimentally verified, and a reluctance to use advanced mathematical tools.

Aside from the fact that design by repeated analysis is time-consuming, there is another problem, which motivated Gerrard to develop his synthesis process [12]: trial-and-error design does not promote an understanding of what is possible. Without this understanding, there is no confidence that an optimal result has been achieved. Additionally, the initial design may not be capable of ever matching the requirements within the desired tolerance. A proper synthesis process forces the designer to state exactly what they want, and if no practical solutions exist, restate their requirements, making the necessary compromises clear. Of course, it must be noted that Gerrard's synthesis method for linkage geometry is itself incomplete, in the sense that it guarantees velocity but designers care about more than that. The point remains that Gerrard's methodology leads to a better conceptual understanding than guesswork!

Much of architecture selection has to do with package space and wheel motion requirements. If designers can directly synthesize all possible architectures from a complete wheel motion specification, they can compare how they package and potentially come up with the simplest architecture that meets the space and motion requirements in less time. This balancing of architecture, package space, and wheel motion is, arguably, the essential suspension design problem. The shock absorber placement, bushing rates, and component design all require this geometric foundation to proceed, and any geometry changes as a result of these later suspension design stages must be compatible with the foundational package space and wheel motion requirements. In cases where the package space and wheel motion requirements do not fully define linkage geometry, a parameterized family of solutions could be output, which would give well-defined geometric knobs to turn when, for example, trying to improve elastokinematic performance. With this discussion in mind, the research objectives can be articulated clearly.

1.4 Research Objectives

1. Develop a mathematically-complete wheel motion specification that is compatible with the existing velocity specification. This amounts to putting a set of coordinates on $SE(3)$, the group of spatial rigid body motions, that either are suspension characteristics of interest or are easily-mapped to such characteristics. The desired wheel motion can then be described in general as a curve in $SE(3)$, with the traditional motion specification being simply the tangent of that curve at the identity. This development enables a true conceptual understanding of wheel motion, preventing conflicting design requirements, and is necessary if synthesis methods using more than design position velocity are to be created.

2. Enumerate all possible independent suspension architectures. Rather than relying on a historical survey or the genius of invention, modern design methods for suspensions should be able to generate potential suspension architectures from a first-principles process given a basic set of assumptions. This allows all possibilities for that set of assumptions to be considered equally, facilitating a set-based design process where no potential architecture is eliminated until proven incapable of meeting the design requirements.

3. Formulate methods allowing all possible architectures to be dimensioned according to the motion specification. These methods should be easy to automate, so that a large number of potential geometries may be generated readily, rather than constructed one at a time as done with traditional graphical methods. These new methods will allow more design possibilities to be considered in less time.

4. Develop methods to filter suspension geometry solutions according to non-kinematic design requirements such as allotted space or desired kingpin geometry. These methods should follow the set-based design process, where linkage solutions are systematically pruned until the desired result is achieved. This

approach is necessary to the overall goal of developing true synthesis methods, where the designers achieve what they want or realize what they want is not possible.

1.5 Dissertation Format

In Chapter 2, progress by other researchers toward the specific research objectives is assessed via summary of a comprehensive literature review. This effort brings the reader up to speed on some of the finer details as well as further justifying the choice of research objectives. The body of this dissertation begins proper with the development of a wheel motion formalism in Chapter 3. The approach to *wheel motion* is to consider a position parameterization of the wheel's motion, which can then be, loosely-speaking, differentiated so that velocity characteristics can be defined as well. Next, in Chapter 4, *number synthesis* is performed, producing a basic, yet practical, enumeration of spatial independent suspension linkages. In Chapters 5–12, methods for *dimensional synthesis* and *solution pruning* are developed and demonstrated for each body-wheel connection, each with a corresponding chapter:

Chapter 5: The R Joint

Chapter 6: The S-S Link

Chapter 7: The C Joint

Chapter 8: The S Joint

Chapter 9: The R-S Link

Chapter 10: The S-R Link

Chapter 11: The R-R Link

Chapter 12: The S-C Link.

Methods that are useful for subsequent chapters are not necessarily repeated in detail in those subsequent chapters, so these body-wheel connection chapters should be read in order for maximum clarity. In each chapter, an example architecture that is considered representative of that connection is fully synthesized. These examples demonstrate the efficacy of the methods developed; here are the architectures considered:

Chapter 5: Semi-Trailing Arm

Chapter 6: Five Link

Chapter 7: Sliding Semi-Trailing Arm with Gear Link

Chapter 8: Trailing Link

Chapter 9: Double Wishbone

Chapter 10: Control Blade

Chapter 11: Trapezoidal Link

Chapter 12: MacPherson Strut.

This dissertation concludes in Chapter 13 by comparing the various connections and architectures, summarizing the methods developed, and offering guidance on future work.

Chapter 2

Literature Review

2.1 Wheel Motion Specification

In the kinematics stage, the wheel carrier is treated as a rigid body that moves with respect to a fixed, rigid vehicle body, as described by experienced suspension designer Gerrard [12]. The simplest motion specification is that the wheel carrier translates vertically, with no longitudinal position, lateral position, or orientation changes throughout its travel. Zhao et al. take this approach, stating that "any changes in the wheel orientation and position parameters ... will surely bring undesirable dynamic phenomena" [67]. Simionescu and Beale arrive at the same motion specification [47]. Unfortunately, the desired wheel motion is usually not so simple, even in the pure translation case. For example, a suspension designer may wish to reduce how much the nose of the vehicle dives under braking. When designing the suspension of an outboard-braked front wheel, designers establish this brake dive behavior by choosing the *anti-dive coefficient* [30]

$$\%\text{ anti-dive} = (\%\text{ front braking})(\tan\phi_F)(\ell/h),$$

where ϕ_F is the inclination of the design position tire contact point velocity vector in a side view, positive if leaning forward (called contact point trajectory, CPT, by Gerrard), ℓ is the vehicle wheelbase, and h is the vehicle CG height. Zero percent

anti-dive means no reduction in brake dive, 100% means a complete reduction in brake dive, and an intermediate value reflects a partial reduction. Clearly, if vertical wheel motion is specified, contact point trajectory ϕ_F is zero, and there is no reduction in brake dive.

Barak accounts for vehicle pitch control under both braking and accelerating, stating for ideal suspensions "one would like no camber, caster, and toe angle changes, no lateral scrub of tires" as well as "100% anti-dive and anti-squat coefficients" [3]. The former quote means that the wheel should not change orientation or displace laterally with vertical travel. Regarding the latter quote, Barak speaks in the context of a rear wheel drive vehicle, so he is saying 100% anti-dive for front suspensions and 100% anti-squat for rear suspensions. (Anti-*squat* reduces how much the rear of a rear drive vehicle squats under acceleration. Anti-*lift* reduces how much the front of a front drive vehicle lifts under acceleration. Anti-*rise* reduces how much the rear of an outboard-braked vehicle rises under braking. These are all analogous to anti-dive, being associated with a side view angle and a coefficient.) For example, Barak's ideal front wheel motion specification is a pure translation, where the wheel moves forward as it moves upward. In this way, Barak's approach is more complete than Zhao and the others, but all of these translation-only specifications ignore the fact that practicing designers are interested in having the orientation of the wheel change as the wheel moves up and down with respect to the vehicle body. For instance, according to Reimpell et al., "manufacturers tend to design the suspension on passenger cars such that the wheels go into negative camber as they travel in bump [aka jounce] and into positive camber as they rebound" [41]. The former case is shown in the illustration reproduced from Reimpell's book, Figure 2.1. The intent here is to keep the tire contact patch in better contact with the road during cornering.

If the wheel is considered to rotate, orientation changes such as camber can be specified. The simplest such case is to assume that the wheel moves on a plane normal to the forward direction of the car, as in Figure 2.1. Raghavan gives such a motion specification in [36]. In particular, the tire contact point is located relative to its initial position by Cartesian coordinates (x, y) — positive x-direction to driver's left,

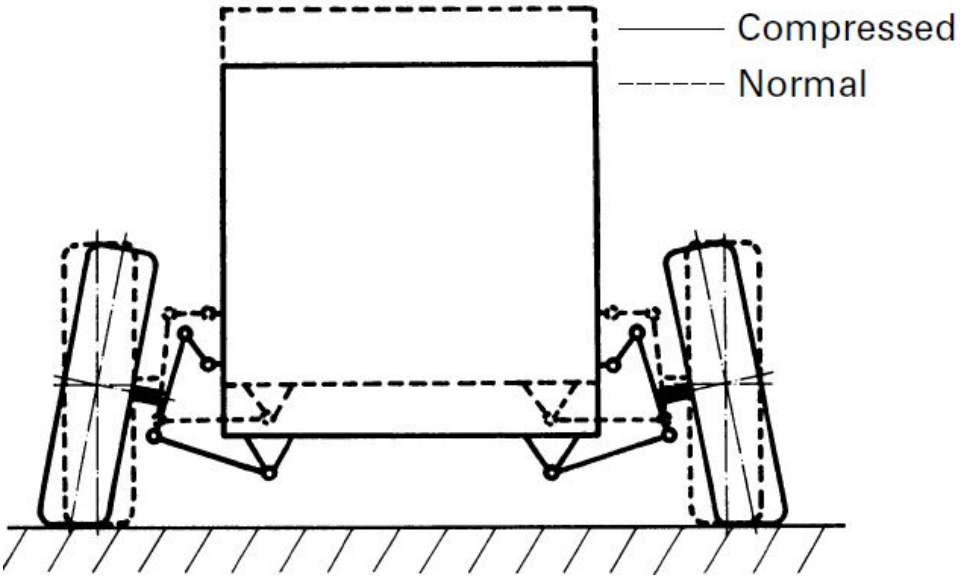

Figure 2.1. Example of desirable camber angle change [41].

positive y-direction up — and the wheel angular displacement is given by angle θ, positive counterclockwise. The three parameters x, y, and θ are sufficient to describe any position of the rigid, planar wheel relative to its design position. The parameter y gives the vertical displacement of the wheel, while x represents lateral displacement and θ is negative the camber angle, since Raghavan considers a left-hand wheel. Raghavan specifies $-95 \text{ mm} \leq y \leq 80 \text{ mm}$, with constant lateral displacement

$$x(y) = 0,$$

and linear camber change

$$\theta(y) = \frac{3^\circ}{80 \text{ mm}} y.$$

This specification is indeed a true rigid body trajectory, albeit planar, completely specifying the desired motion of the wheel. Missing, however, is the ability to specify roll center height.

Raghavan addressed roll center height in a subsequent paper [38]; unfortunately, his method to achieve desired roll center height is specific to SLA suspensions. In particular, Raghavan takes inspiration from Olley [29, Ch. 7], considering the planar geometry of Figure 2.2. In particular, the lateral displacement of the tire contact

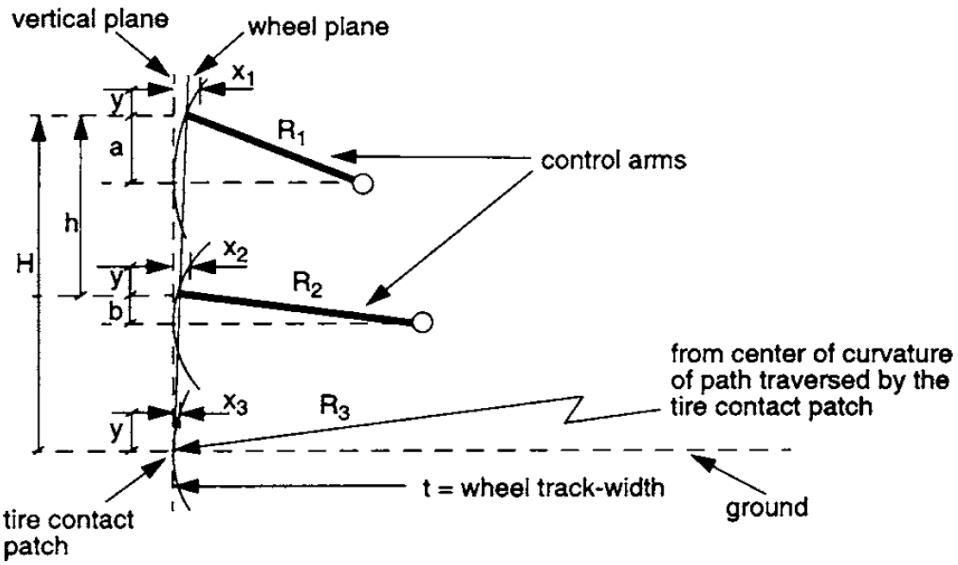

Figure 2.2. SLA geometry considered by Raghavan for roll center synthesis [38].

point, x_3, is related to x_1 and x_2 since the wheel–control-arm connection points and tire contact points are collinear:

$$x_3 = \frac{Hx_2}{h} - \frac{(H-h)}{h}x_1.$$

Raghavan, following Olley, approximates x_1 and x_2 using a parabolic approximation for the circular arcs; in particular,

$$x_1 \approx \frac{y^2}{2R_1} + \frac{ya}{R_1},$$
$$x_2 \approx \frac{y^2}{2R_2} + \frac{yb}{R_1}.$$

The derivation of this approximation is somewhat tedious, involving use of the implicit equation defining a circle, the quadratic formula, and the binomial series. For details see Olley's book.

Roll center height, to give its proper technical definition, is the signed distance from the ground to the point where the perpendicular of the contact point velocity (when projected onto a front-view plane) intersects the centerline of the vehicle body, as shown in [15, p. 319]. It is positive when the perpendicular to the contact

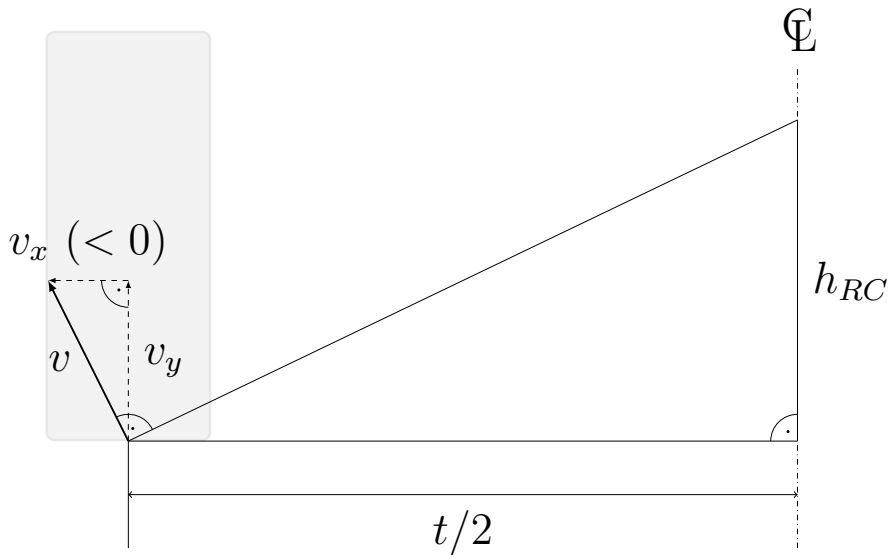

Figure 2.3. Roll center height h_{RC} graphical definition.

point velocity crosses the vehicle centerline above the ground plane. See Figure 2.3. Consequently,

$$h_{RC} = \frac{t}{2}\left(\frac{-v_x}{v_y}\right).$$

The parameter t is the track width of the vehicle. Track width changes with wheel travel, but Raghavan treats it as constant, since $t \gg x_3$. The tire contact point has coordinates (x_3, y); its velocity vector, as driven by parameter y, is $(dx_3/dy, 1)$, so that

$$h_{RC} = -\frac{t}{2}\frac{dx_3}{dy}.$$

Raghavan wishes to specify roll center height so that it decreases/increases n times as much as the tire contact point moves up/down. For example, if $n = 1$, and the tire contact point moves up 20 mm, the roll center height should decrease by 20 mm. In this case, roll center height defines a point of the vehicle body that does not move with wheel travel — a desirable case, as detailed by Raghavan. Presuming constant track width, roll center height changes with wheel travel according to

$$\frac{dh_{RC}}{dy} = -\frac{t}{2}\frac{d^2x_3}{dy^2}.$$

When $dh_{RC}/dy = -n$, roll center height behaves as desired. Plugging in the approximations for x_1 and x_2 into the expression for x_3 and evaluating derivatives results in Raghavan's design formula:

$$\frac{t}{2h}\left(\frac{H}{R_2} - \frac{H-h}{R_1}\right) = n.$$

This design formula is valid for planar SLA suspensions with the geometry of Figure 2.2, and approximately so for spatial ones where the wishbone axes are close to normal to the forward-view plane. Raghavan shows how this design formula can be used with such a spatial linkage to choose control arm geometry such that the desired roll center height behavior is achieved. Unfortunately, there are not similar results for other suspension architectures. The other oversight is not showing how to compute roll center height in terms of the position parameters of his earlier paper — if done, this would allow the designer to give lateral coordinate x indirectly, by specifying the desired roll center height curve. Of course, Raghavan's design formula is reliant on two mathematical assumptions: (1) the circular arc approximations are sufficiently accurate, and (2) track width is, as near as makes no difference, constant.

Gerrard's method [12], discussed initially in §1.3.3 as an example of the typical spatial approach, considers wheel velocity as its motion specification. Gerrard works with a right-hand-side wheel, with a coordinate system having x-rearward, y-rightward, z-upward. In particular, let v be the velocity vector of the tire contact point in the wheel's design position, and let ω be the angular velocity vector of the wheel in the same position. Gerrard specifies these in column vector form as

$$v = \begin{bmatrix} \tan(\mathrm{CPT}) \\ \mathrm{RCH}/\mathrm{HT} \\ 1 \end{bmatrix}$$

and

$$\omega = \begin{bmatrix} (\mathrm{CC}/100)/\mathrm{HT} \\ [\tan(\mathrm{WCT}) - \tan(\mathrm{CPT})]\,/\mathrm{SLR} \\ \mathrm{KTC} \end{bmatrix},$$

where

- CPT (contact point trajectory) is the angle contributing to reduced dive or rise during braking (effect dependent on outboard brakes and whether specified for a front or rear wheel);
- RCH is roll center height;
- HT is half of the track width;
- CC (camber compensation) is the ratio (in percent) of camber change with respect to vehicle roll angle;
- WCT (wheel center trajectory) is the angle contributing to reduced lift or squat during acceleration (effect dependent on the particular wheel being driven);
- SLR is static loaded radius;
- KTC (kinematic toe change) is toe change per unit of wheel travel.

Two vehicle-level characteristics — HT and SLR — are required, together with five wheel-motion characteristics: CPT, RCH, CC, WCT, and KTC. Of the five wheel-motion characteristics, two concern changes in wheel position — CC and KTC, while three are purely velocity concerns: CPT, WCT, and RCH. Gerrard recognizes that his five wheel-motion characteristics may not be capable of being specified independently for certain types of suspensions links. (Five is the maximum number of kinematic characteristics that can be defined at each position for a spatial rigid body constrained by a linkage to have one DOF.) For example, attaching the wheel carrier to the vehicle body with a revolute or spherical joint requires that $v \cdot \omega = 0$; only four of the characteristics can be set independently.

Gerrard, by specifying only design position wheel velocity, guarantees the desired behavior is achieved only at an instant from the design position. The problem of stating a full, spatial wheel trajectory with analogous behavior is left open. This is not a problem of not knowing how the wheel-motion characteristics should behave across the full range of wheel travel — there is plenty of discussion on that in sources like [30, 41]:

- Rearward wheel travel in jounce (reduces harshness when impacting bumps).
- Minimal change in the lateral position of the contact point (improves directional stability).
- Minimal change in orientation of the wheel carrier in the side view — anti-lock braking and traction-control systems rely on wheel speed sensors that measure the angular velocity of the wheel with respect to the carrier. Excessive side view rotation of the wheel carrier during jounce/rebound can interfere with these wheel speed measurements.
- Progressive, negative camber function in jounce; camber goes positive in rebound (keeps tires at favorable angle to road during cornering).
- Zero toe change, to make handling more predictable. Occasionally, for a rear wheel, a linear toe function that gives a roll understeer effect is desired. This would be toe-in with jounce for a right-hand wheel.
- For a driven front wheel, anti-lift behavior that does not diminish in rebound. For a driven rear wheel, anti-squat behavior that does not diminish in jounce.
- For an outboard-braked front wheel, anti-dive behavior that does not diminish in jounce. For an outboard-braked rear wheel, anti-rise behavior that does not diminish in rebound.
- Positive roll center height in the design position that decreases by n times the amount the ground plane moves up, and increases by n times the amount the

ground plane moves down. This is the aforementioned requirement of Raghavan [38].

The problem is that these numerous, potentially conflicting requirements — after all, a single-DOF suspension only lets up to five wheel motion characteristics be defined at each point of travel — have yet to be converted into one coherent mathematical framework. For the planar treatment of the problem, Raghavan got close, but unfortunately did not address the mixed position/velocity specification in one go, handling roll center height separately and specifically for one type of linkage.

Suh provided a more mathematically complete, spatial wheel motion specification than Gerrard in [50]. Suh specifies an initial velocity of the wheel, a wheel displacement, and the velocity of the wheel at its displaced position. The values are not derived from desired behavior in terms of suspension characteristics like roll center height and camber angle, but instead copied from the analysis of a preexisting, spatial double wishbone suspension. In this way, Suh is able to demonstrate his numerical methods without getting too far afield. It is a shame, then, that no one seems to have built a wheel motion formalism that can take the desires of suspension designers, concerned with both wheel position and velocity characteristics, and translate them into a mathematically complete motion specification, suitable for methods like Suh's.

2.2 Enumeration of Suspension Architectures

Despite the market now being dominated by only a handful of suspension architectures (see discussion at the end of §1.2), there remains interest in systematically enumerating possible architectures from first principles — has the historical development of the independent suspension, led by numerous individual inventors, missed anything? This enumeration is a problem in *kinematic synthesis*, defined by Hartenberg and Denavit [16] as the determination of mechanisms that are to fulfill certain motion specifications. According to these authors, the general problem of mechanism synthesis is approached in three phases:

1. *Type synthesis*, establishing the basic building blocks (links, gears, cams, belts,

etc.). These choices depend on how the mechanism will be used, what materials and manufacturing processes are available, and other considerations not necessarily having to do with kinematics.

2. *Number synthesis*, establishing the number of links and connecting elements. This process is based on achieving the desired mobility, or degree-of-freedom, of the mechanism, by applying extensions of *Grübler's criterion*. For example, planar rigid bodies have 3 DOFs, so a system of n planar bodies has, before constraint, $3n$ DOFs. If one body is fixed as a base link, $3(n-1)$ DOFs remain. Suppose, to produce a mechanism, the bodies are constrained to each other with j revolute joints, each of which removes 2 DOFs. Consequently, the degree of freedom F, or *mobility*, of such a mechanism is estimated by

$$F = 3(n-1) - 2j.$$

   To find mechanisms with mobility $F = 1$, n links and j revolutes are established according to $2j - 3n + 4 = 0$, the classic Grübler criterion. For example, $n = 4$ bodies yields $j = 4$ revolutes, the classic four bar linkage. This criterion can of course be extended for spatial cases and other connecting elements. Mechanism mobility is in fact affected by mechanism geometry — consider the Sarrus linkage — and consequently, Grübler-like criterion can only estimate mobility.

3. *Dimensional synthesis*, establishing the dimensions of the mechanism. For example, determining the geometry of a four bar linkage that guides one of the coupler points along a certain path. Dimensional synthesis is discussed in the next section.

The suspension architecture enumeration problem can be answered by performing type and number synthesis. It is possible to enumerate *all possible* suspension architectures, at least within the context of a chosen type of mechanism and a Grübler-like criterion. Raghavan has such a treatment [35].

Regarding mechanism type, Raghavan considers linkages where the wheel carrier

is connected to the vehicle body indirectly by at least two in-parallel links having a joint on each end. He notes that in-parallel linkages are better suited to withstand the applied forces and moments than in-series linkages, since stiffnesses add in parallel while compliances add in series. Both planar and spatial linkages of the type are considered. Raghavan considers the following joints to be useful for suspensions:

- Revolute, removing two DOFs (planar) or five DOFs (spatial), symbolized by R;
- Prismatic, removing two DOFs (planar) or five DOFs (spatial), symbolized by P;
- Cylindric, removing four DOFs (spatial only), symbolized by C;
- Pin-in-sphere, removing four DOFs (spatial only), symbolized by K;
- Spherical, removing three DOFs (spatial only), symbolized by S.

By *pin-in-sphere*, Raghavan means a joint equivalent to two in-series revolute joints having intersecting axes — also realizable as a universal joint.

Raghavan uses the format X-Y to describe a link, where X is a joint connecting between the vehicle body and the link and Y is a joint connecting between the link and the wheel carrier. For the selected joints, one can construct 2^2-many planar links and 5^2-many spatial links — consider words of length n from an alphabet of k letters; there are k^n-many words. For each of the enumerated links, Raghavan computes its mobility, defined as the number of freedoms introduced by the link (3 for planar, 6 for spatial) minus the total number of freedoms taken away by the two joints. For example, a planar R-R link has mobility $3 - 2 - 2 = -1$. The four planar links and their mobility are shown in Table 2.1, while the 25 spatial links and mobilities are shown in Table 2.2. Raghavan points out that the P-P link is incapable of allowing wheel orientation changes such as camber, so it is discarded. The S-S link has a superfluous DOF, that of the link rotating about the axis between the two spherical joints. Because it is functionally equivalent to the K-S and S-K joints, it is also discarded by Raghavan.

Table 2.1. Planar links enumerated by Raghavan [35], together with their mobility.

R-R (−1)	P-R (−1)
R-P (−1)	P-P (−1)

Table 2.2. Spatial links enumerated by Raghavan [35], together with their mobility.

R-R (−4)	P-R (−4)	C-R (−3)	K-R (−3)	S-R (−2)
R-P (−4)	P-P (−4)	C-P (−3)	K-P (−3)	S-P (−2)
R-C (−3)	P-C (−3)	C-C (−2)	K-C (−2)	S-C (−1)
R-K (−3)	P-K (−3)	C-K (−2)	K-K (−2)	S-K (−1)
R-S (−2)	P-S (−2)	C-S (−1)	K-S (−1)	S-S (0)

Single-DOF architectures are then synthesized by Raghavan according to the Grübler-like criterion

$$1 = (3 \text{ or } 6) + \sum_{i=1}^{m} n_i,$$

where 3 or 6 is planar or spatial, m is the number of in-parallel links between the vehicle body and wheel carrier, and n_i is the mobility (as defined above) of the ith link. To start, Raghavan finds $n_1, \ldots, n_m$ that add to -2, corresponding to the planar case. The only possibility is $m = 2$, where $(n_1, n_2) = (-1, -1)$. The planar suspension architectures can then be found by choosing two links from the three possible links R-R, R-P, P-R, repetition allowed, resulting in 6 planar architectures: {R-R, R-R}, {R-R, R-P}, {R-R, P-R}, {R-P, R-P}, {R-P, P-R}, and {P-R, P-R}. The same general process can be done for spatial cases, where instead $n_1, \ldots, n_m$ should add to -5. Raghavan found 76 two-link spatial architectures, 224 three-link spatial architectures, 160 four-link spatial architectures, and 56 five-link spatial architectures. The desired overall mobility could not be achieved with more than five links.

Matschinsky [26] presents a smaller set of joints and links suitable for independent suspensions than Raghavan, perhaps guided by practical experience during his time at BMW. He also focuses only on the spatial case. Regarding joints, Matschinsky presents those of Figure 2.4, where f is the degree-of-freedom of the joint. The *ball joint*, Figure 2.4a, called the spherical joint by Raghavan, has $f = 3$, and can often be replaced by the *rubber joint*, Figure 2.4b, which, according to Matschinsky, has

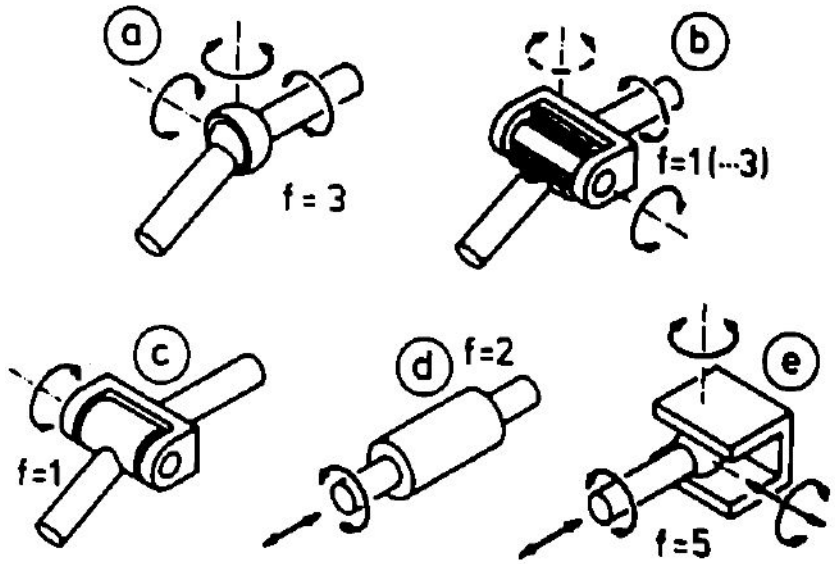

Figure 2.4. Joint types, reproduced from [26].

"...good resistance against transient overload, freedom from maintenance, better noise isolation and lower cost." This substitution is possible when only one axis of rotation is primarily used by a ball joint, allowing the two orthogonal rotations to occur via bushing compliance. The *turning joint*, Figure 2.4c, also known as the revolute joint, is another possibility, as is the *turning-and-sliding* joint, Figure 2.4d, also known as the cylindric joint. Matschinsky notes that the turning joint is often implemented practically with two rubber joints, while the turning-and-sliding joint takes the form of a telescopic damper; see Figure 2.5. Finally, he mentions the *ball-and-surface* joint, Figure 2.4e, but says it is very rarely found in independent suspensions, discussing it further only in the context of rigid axle suspension linkages.

Matschinsky does not construct links combinatorially like Raghavan, instead directly stating the most important types, Figure 2.6. The *rod link*, Figure 2.6a, has a ball joint (or equivalent rubber joint) at each end. It comes with a superfluous rotation r, which does not affect the wheel carrier motion. The *triangular link*, also known as the A-arm or wishbone, Figure 2.6b, has a ball joint at one end and a turning joint at the other. The turning-joint side is typically at the vehicle body, but the reverse is also possible. The *trapezoidal link*, also known as the H-arm, Figure 2.6c, has turning joints at each end. The *turning-and-sliding link*, Figure 2.6d, has a ball joint at one

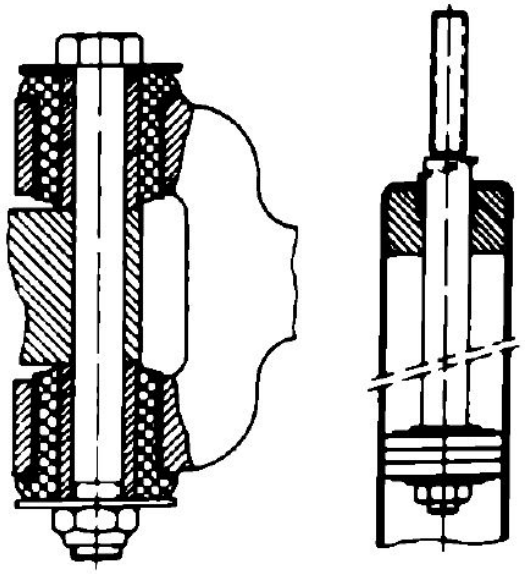

Figure 2.5. Practical implementations of the turning joint with two rubber bushings (left), and the turning-and-sliding joint as a telescopic damper (right), reproduced from [26].

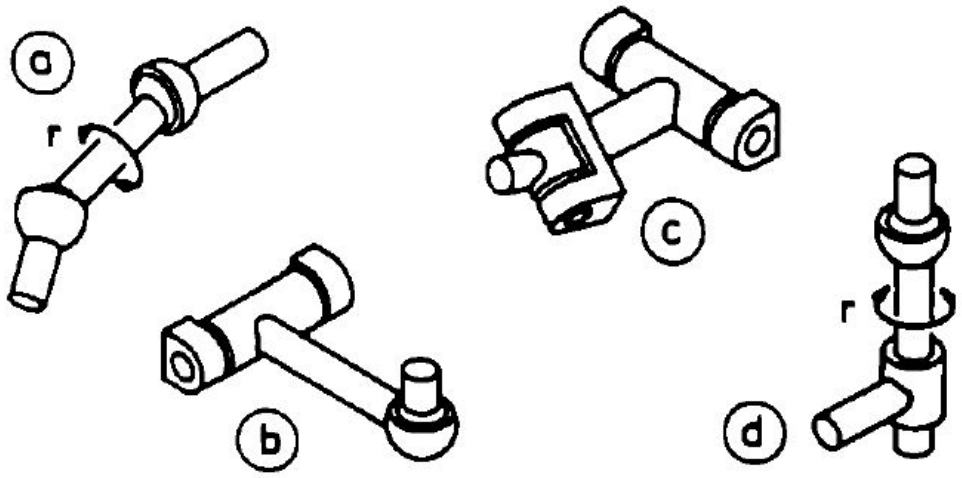

Figure 2.6. Link types important for suspensions, reproduced from [26].

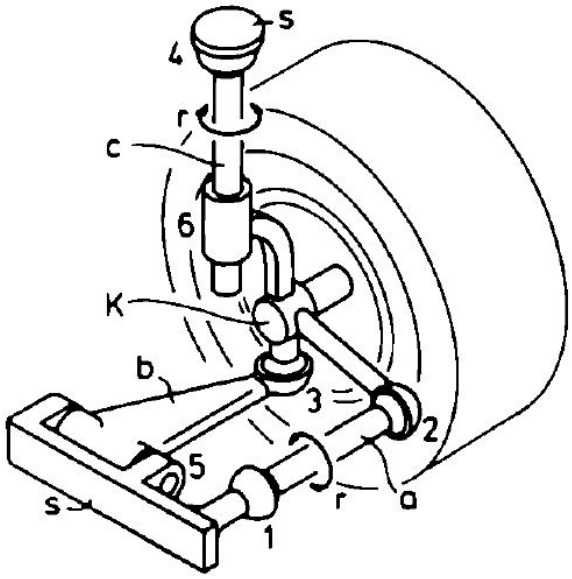

Figure 2.7. MacPherson independent suspension, reproduced from [26].

end and a turning-and-sliding joint at the other, with the turning-and-sliding joint axis passing through the ball joint. Like the rod link, it has a superfluous rotation r that does not affect wheel carrier motion. In practice, the ball joint end of the turning-and-sliding link is at the vehicle body.

Matschinsky provides the following mobility formula for suspensions:

$$F = 6(k + l - g) - r + \sum_{i=1}^{g} f_i,$$

where F is mobility, k is the number of wheel carriers ($k = 1$ for independent suspensions), l is the number of links, g is the number of joints, r is the number of superfluous link rotations, and f_i is the degree-of-freedom of the ith joint. For example, the MacPherson suspension of Figure 2.7 has one wheel carrier K ($k = 1$); three links a, b, and c ($l = 3$); six joints labeled one through six ($g = 6$); two superfluous link rotations ($r = 2$); and $(f_1, \ldots, f_6) = (3, 3, 3, 3, 1, 2)$. Consequently, $F = 1$. Unfortunately, Matschinsky does not use his mobility formula as the basis of a systematic enumeration, instead presenting various architectures of interest and showing how they conform to the formula. He does however, consider rigid axle suspensions and the extremely rare *compound* suspensions, which guide multiple wheel

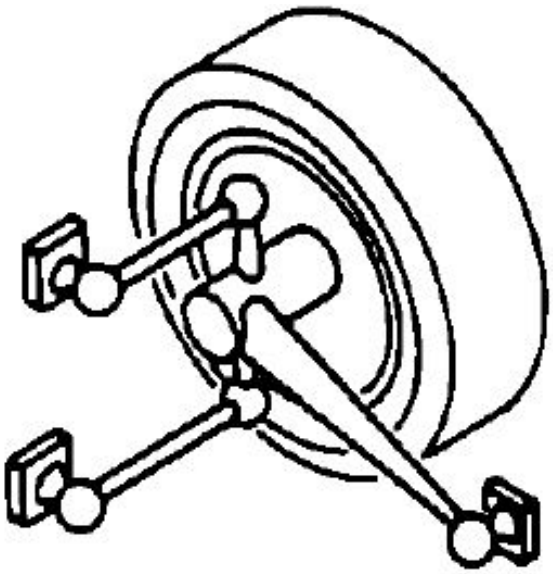

Figure 2.8. An independent suspension employing a ball joint and two rod links, reproduced from [26].

carriers, showing the generality of his approach. The generality also allows for independent suspensions like Figure 2.8 to be considered, with the wheel carrier both directly (with the ball joint) and indirectly (with the rod links) connected to the vehicle body. Raghavan's approach excludes mechanisms of this type. The downside of allowing other types is the potentially infinite number of possible architectures. Indeed, this is why Matschinsky chooses not to perform an enumeration, rather favoring a survey of historically important architectures. It is interesting then, that Raghavan considers a large number of joints and links and only one linkage type, while Matschinsky considers a small number of joints and links and a large number of linkage types. Perhaps a highly useful enumeration would result from considering the practical joints and links of Matschinsky, and body-wheel connections beyond the joint-link-joint type of Raghavan.

2.3 Linkage Dimensioning

Given a wheel motion specification and a suspension architecture, how is the geometry of the linkage determined? As stated in the previous section, this is the problem

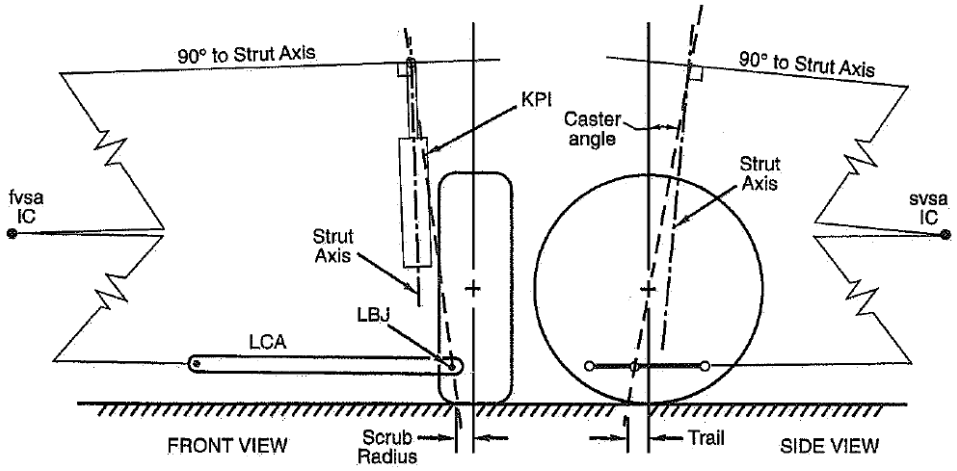

Figure 2.9. Graphical synthesis of the lower control arm (LCA) and strut of a MacPherson architecture, reproduced from [30].

of *dimensional synthesis*. Gerrard [12] exemplifies the traditional approach, where graphical rules are provided for placing joints and links to achieve a velocity specification. Matschinsky [26] also gives a method involving graphical solution from a velocity specification. Milliken and Milliken [30] provide an in-depth, step-by-step treatment for both the SLA and MacPherson architectures, again using a velocity specification. For example, the Millikens show how to orient the lower control arm (triangular link) and strut (turning-and-sliding link) of a MacPherson architecture in Figure 2.9. Graphical methods are best suited for an interactive design process, on the drawing board or in CAD, where a designer can sketch out a potential architecture and assess its suitability for achieving the motion specification. These methods are cumbersome if the task at hand is automated dimensional synthesis of tens, if not hundreds, of architectures.

Fortunately, there is another approach that enables the direct computation of linkage geometry. It also allows for more than one rigid body position to be specified. It is the approach of, amongst others, Suh and Radcliffe, 1978, [51, Ch. 6], which numerically solves for the geometry of a chosen link. The process is summarized as

1. Specify several positions of the moving rigid body. (The maximum number of specifiable positions depends on the link being considered.)

2. Convert the body positions into *displacement matrices*, by designating one of

the positions as a reference position. (Displacement matrices transform body coordinates from one pose to another.)

3. Formulate *geometric constraint equations* for each of the specified positions, based on the link being synthesized.

4. Use the displacement matrices to rewrite the geometric constraint equations so that the only unknowns are the link coordinates in the reference position.

5. Solve these nonlinear *design equations* using the Newton-Raphson method.

Suh and Radcliffe state that the initial guesses for the Newton-Raphson method may be generated randomly in cases where such estimates are difficult to come up with. In cases where there are free variables, these are treated as parameters that are incremented to result in a family of solutions. The dimensional synthesis process is repeated for each type of link considered, using the same motion specification (the number of positions that can be specified is limited to that of the link with the fewest maximum specifiable positions). These link solutions can then be assembled into a final linkage, which can be analyzed to see how well it guides the rigid body along the intended trajectory.

Motion specifications are application-specific, and it is beyond the scope of Suh-and-Radcliffe's book to consider beyond the most basic examples. On the other hand, they recognize that linkages typically rely on only a handful of link types, and so provide the geometric constraint equations for these. For example, for the spatial rigid body guidance problem, they provide constraint equations for the spherical-spherical (S-S) link, revolute-spherical (R-S) link, revolute-revolute (R-R) link, revolute-cylindrical (R-C), and cylindrical-cylindrical (C-C) links. They also provide considerable guidance on how to use a computer to solve the resulting design equations. A later work by Suh [50] dimensions an R-S link for an independent suspension. An subsequent paper by Kang [20], with Suh as co-author, provides constraint equations for the spherical-cylindrical (S-C) link, and also dimensions it and the R-S, and S-S links, resulting in a MacPherson independent suspension. Raghavan uses the same process

to dimension his planar suspension architectures in 1996 [36]. These works demonstrate the numerical synthesis process for suspensions; but, as previously discussed, the motion specifications themselves could be improved. Other than using a better motion specification, is there another opportunity to improve the dimensional synthesis process for independent suspensions?

The Newton-Raphson method used in the past to solve the nonlinear design equations has limitations: it depends on a good estimate for the solution, it does not find all solutions, and it not finding a solution does not mean that there are no solutions. On the other hand, Wampler et al. recognize that, in most cases, the nonlinear design equations are in fact *systems of polynomial equations* [65]. Taking advantage of this fact, they demonstrate *numerical continuation methods* that can compute *all* solutions to polynomial systems of moderate size. They point out that, "When applied to mechanism synthesis, such a method would provide the engineer all choices that meet the motion specifications." They give two rigid body guidance examples: the planar four-bar and the spatial seven-bar, which are generalized versions of the planar SLA suspension and the spatial five-link suspension, respectively. Wampler et al. refer to numerical continuation methods for polynomial systems as *polynomial continuation* methods for short. According to them, polynomial continuation was first applied to mechanism problems in 1985, by Tsai and Morgan [52], to solve the inverse kinematics problem for six-revolute robots. The Tsai-Morgan paper inspired further improvements of the polynomial continuation method; the aforementioned Wampler et al. paper being an effort in 1990 to summarize these developments and communicate them to the broader community of kinematicians. Raghavan, with Roth, 1995, also recognized that many mechanism problems lead to polynomial systems, and included polynomial continuation as one possible solution method [39].

By 1996, Sommese and Wampler had named their field of numerically solving and manipulating polynomial systems *numerical algebraic geometry*. Their ongoing efforts led to a book published in 2005, summarizing the field as applied to applications in engineering and science [49]. An article by these authors in 2011 focused on the application of numerical algebraic geometry to kinematics [66]. Currently,

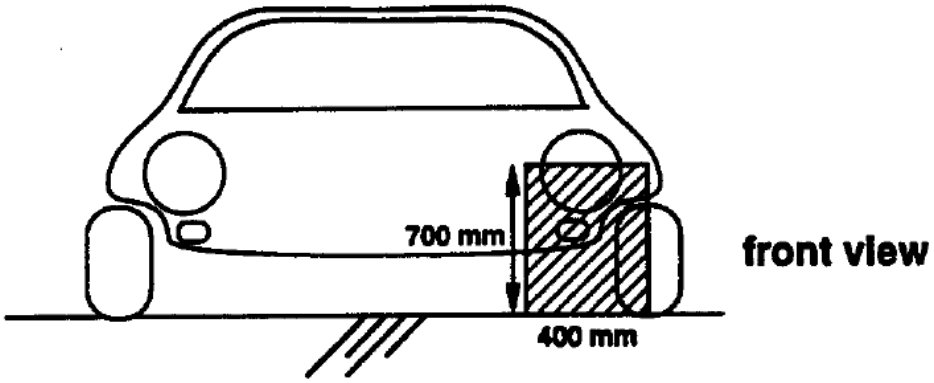

Figure 2.10. Package space considered by Raghavan for the planar suspension [36].

there are four numerical algebraic geometry software packages under ongoing development [17]: Bertini [5], Hom4PS [25], NAG4M2 [23], and PHCpack [64]. Bertini, by Bates, Hauenstein, Sommese, and Wampler, is well-documented by their accompanying book [6], and a MATLAB interface, BertiniLab, is available [4]. The availability of "black box" solvers like Bertini, which require no special knowledge to operate, together with improvements in the speed of personal computers and the efficiency of the solvers themselves, means that polynomial continuation is now ready for broader use. Indeed, in 2014, Bertini was applied to a design a planar, six-bar linkage suitable for use as a suspension [34]. The application of polynomial continuation to the more general suspension design problem, involving the numerous possible spatial architectures, is overdue.

2.4 Filtering Solutions

It is not enough to dimension a given architecture — package space requirements for suspensions are severe, as these mechanisms must compete for space with the occupants, engine, transmission, batteries, fuel tank, luggage space, spare tire, steering gear, body structure, etc. Consequently, solutions for linkage geometry must be pruned according to the space allotted. Other non-kinematic requirements such as providing a steering axis must also be handled when necessary. Raghavan, in his planar suspension synthesis [36], considered a simple package space, Figure 2.10. Each

of his planar chains, the R-R, R-P, P-R, and R, was synthesized for the maximum number of specifiable wheel positions. He found that none fit in the desired area. Consequently, he considered fewer specified wheel positions, freeing up some of the variables in the design equations, allowing these to be set according to the available area. Eventually, he was able to synthesize all five chains: the R-R and R-P for two wheel positions (out of four possible), the P-R for three wheel positions (out of four possible), and the R for one wheel position (out of two possible). (The last case is actually not much of a solution, since guaranteeing one wheel position does not guarantee anything about how the wheel moves!)

There is not an analogous treatment for spatial suspensions, where a subset of space is identified and links that fit inside it are systematically synthesized. In an optimization setting, Simionescu and Beale [47] searched for joint coordinates within intervals around the coordinates of an existing Mercedes five-link geometry. Sancibrian et al. similarly considered a range of acceptable coordinates around a baseline geometry, that of a double-wishbone front suspension for a bus [44]. This is a nice strategy, if the goal is to optimize an existing design. Raghavan, in his toe-link synthesis [37], had the engineer pick one ball joint location as desired, computing the other ball joint location. This other ball joint must have packaged acceptably, as no further commentary was provided. Suh [50], Kang [20], and Zhao [67], while synthesizing spatial suspension links, do not state any package space considerations explicitly.

Characteristic of the suspension problem is sacrificing wheel positions to meet package space requirements. Indeed, the traditional wheel motion specification is just the velocity of the wheel at one point of the wheel's travel. On the other hand, general treatments of the synthesis problem, like Suh-and-Radcliffe's, focus mostly on solving the design equations for the maximum number of specifiable body positions. McCarthy and Soh, in their 2011 book [27], state the same focus, but recognize that fewer specified positions can provide flexibility for other aspects of the design. They note that, "This feature of spatial linkage design has yet to be exploited in a systematic way." One way to handle these underspecified problems for suspensions is to come up with methods to filter solutions according to non-kinematic requirements.

2.5 Summary

- The traditional wheel motion specification is a velocity specification, where some of the specified velocity components have to do with the rate of change of position parameters (e.g., toe change), and others are true velocity concerns (e.g., roll center height). Existing wheel motion specifications beyond a single velocity are overly simplified (e.g., vertical translation) or presented without justification (e.g., copied from analysis of an existing mechanism). A mathematically-complete, spatial wheel motion formalism allowing precise specification of both wheel position and velocity characteristics has yet to be developed.

- Number synthesis has been demonstrated, but only exhaustively for one type of suspension linkage, consisting of at least two in-parallel joint-link-joint chains. Even a smaller, more practical set of joints and links than previously considered for number synthesis, together with more variety in how they can be assembled, may prove highly useful.

- There is a well-known dimensional synthesis process, suited to automated computation and capable of meeting a motion specification as close as theoretically possible for a link or joint, which has been successfully applied to the suspension problem. Polynomial continuation is the current state of the art for solving these types of problems, allowing the mechanism designer to explore all possible solutions to a design problem. Its application to the spatial suspension design problem, to truly explore the solution space, is overdue.

- Characteristic of the suspension problem is trading off wheel kinematics for other design requirements. This involves relaxing the number of specified wheel positions to free up design variables. This approach to spatial linkage design has yet to be given a systematic treatment; instead, the focus is on synthesizing each link for the maximum number of specifiable body positions without regard to other aspects.

Chapter 3

Wheel Kinematics

3.1 Mathematical Preliminaries

This section mostly follows the terminology of Roe [42]. Vectors in Euclidean space are identified with $\mathbf{R}^3$ in the usual way, writing their components with respect to a right-handed, orthonormal basis. These are written down as *column vectors* (3×1 matrices). An origin of Euclidean space is also fixed, so points can be identified with their position vectors, and, ultimately, their column vectors, which are called *coordinate vectors* in this context. An *isometry* of Euclidean space is a function from the space to itself that preserves the distance between points. An isometry is said to be *direct* if it preserves the handedness of coordinate systems and *indirect* if it does not. Direct isometries are a useful model of the physical motion of a body from one pose to another, provided the body is sufficiently rigid; the restriction to direct isometries prevents physically impossible motions such as mapping a right hand to a left hand. In terms of coordinate vectors, an isometry is a function $\mathbf{R}^3 \to \mathbf{R}^3$ given by

$$\boldsymbol{x} \mapsto \boldsymbol{A}\boldsymbol{x} + \boldsymbol{b},$$

where $\boldsymbol{A}$ is an orthogonal matrix — that is, $\boldsymbol{A}^T\boldsymbol{A} = \boldsymbol{A}\boldsymbol{A}^T = \boldsymbol{I}$, where $\boldsymbol{I}$ is the 3×3 identity matrix — and $\boldsymbol{b}$ is a column vector. A direct isometry has $\det \boldsymbol{A} = +1$, while an indirect isometry has $\det \boldsymbol{A} = -1$. Orthogonal matrices with determinant $+1$ are

called *special orthogonal* matrices.

Examples of direct isometries include rotations and translations. Translations are straightforward: points are moved the direction and distance given by a vector. In terms of coordinate vectors, the *translation by a (column) vector* $\boldsymbol{v}$ is the function $\mathbf{R}^3 \to \mathbf{R}^3$ given by $\boldsymbol{x} \mapsto \boldsymbol{x}+\boldsymbol{v}$. Rotations are trickier. In this context, a rotation is one about an axis through the origin. In particular, let θ be an angle and $\boldsymbol{u} = (u_1, u_2, u_3)^T$ a column vector of unit length giving the direction of the axis, which gives the direction of the rotation by the right-hand rule. In terms of coordinate vectors, the *rotation through angle θ with axis through the origin in direction $\boldsymbol{u}$* is the function $\mathbf{R}^3 \to \mathbf{R}^3$ defined by $\boldsymbol{x} \mapsto \boldsymbol{R}_{\boldsymbol{u},\theta}\boldsymbol{x}$, where

$$\boldsymbol{R}_{\boldsymbol{u},\theta} = \boldsymbol{I} + \sin\theta\tilde{\boldsymbol{u}} + (1-\cos\theta)\tilde{\boldsymbol{u}}^2, \tag{3.1}$$

where $\tilde{\boldsymbol{u}}$ is the skew-symmetric matrix

$$\tilde{\boldsymbol{u}} = \begin{pmatrix} 0 & -u_3 & u_2 \\ u_3 & 0 & -u_1 \\ -u_2 & u_1 & 0 \end{pmatrix}.$$

These matrices arise from writing the cross product of two vectors as a matrix-vector product; in particular, given $\boldsymbol{u} \in \mathbf{R}^3$, for all $\boldsymbol{v} \in \mathbf{R}^3$

$$\boldsymbol{u} \times \boldsymbol{v} = \tilde{\boldsymbol{u}}\boldsymbol{v}.$$

The rotation matrix (3.1) follows from converting Rodrigues' rotation formula to matrix form using the matrix-vector form of the cross product.

The *trajectory*, or *continuous motion* of a rigid body can be modeled with a time-varying family of direct isometries, with the isometry at a particular instant being the one that takes the body from the original position to the current position. (As such, the identity isometry given by orthogonal matrix $\boldsymbol{I}$ and column vector $\boldsymbol{0}$ must be included.) Suppose there is such a family of direct isometries, where $\boldsymbol{A}(t)$ and $\boldsymbol{b}(t)$

are the orthogonal matrix and the column vector, respectively, of the direct isometry at time t. A point on the body with coordinate vector $\boldsymbol{x}_0$ in the body's original position has coordinate vector

$$\boldsymbol{x}(t) = \boldsymbol{A}(t)\boldsymbol{x}_0 + \boldsymbol{b}(t)$$

at time t. The velocity of the point on the body with coordinate vector $\boldsymbol{x}(t)$ is

$$\boldsymbol{v}_{\boldsymbol{x}}(t) = \boldsymbol{\omega}(t) \times \boldsymbol{x}(t) + \boldsymbol{v}(t),$$

where $\boldsymbol{\omega}(t)$ is the angular velocity of the body, given by

$$\tilde{\boldsymbol{\omega}}(t) = \dot{\boldsymbol{A}}(t)(\boldsymbol{A}(t))^T,$$

and $\boldsymbol{v}(t)$ is the velocity of the point on the body that is currently passing through the origin, given by

$$\boldsymbol{v}(t) = \dot{\boldsymbol{b}}(t) - \boldsymbol{\omega}(t) \times \boldsymbol{b}(t).$$

3.2 Wheel Motion

The desire is to model the wheel of a passenger car as a body that moves with respect to a fixed vehicle body. Both of these bodies are assumed to be rigid. By *wheel*, the combined wheel and wheel carrier assembly is meant, ignoring the possibility of relative rotation between these two. To this end, the vehicle body is identified with Euclidean space. The origin is defined as the intended location of the center of a right-hand side wheel when the vehicle is at its design load, and the standard basis vectors $\boldsymbol{i} = (1,0,0)^T$, $\boldsymbol{j} = (0,1,0)^T$, and $\boldsymbol{k} = (0,0,1)^T$ have the following meaning: $\boldsymbol{i}$ aims in the driving direction, $\boldsymbol{j}$ aims to the driver's left-hand side, and $\boldsymbol{k}$ aims upward. The wheel is modeled as a disk with radius r, the wheel's *static loaded radius*, and it is in the *design position* when its center is at the origin and it is normal to the vector $\boldsymbol{j}$. The ground is modeled as a $\boldsymbol{k}$-normal plane that translates

vertically so that it always contains the lowest-hanging point of the wheel. This lowest-hanging point is considered to model the physical wheel's tire contact point, which was previously defined as the center of the physical contact patch. In the design position, the circumference of the wheel can be given by

$$\{(r\sin\psi, 0, -r\cos\psi)^T : -\pi < \psi \leq \pi\}. \tag{3.2}$$

The lowest-hanging point is given by $\psi = 0$, corresponding to coordinate vector $(0, 0, -r)^T$.

The goal is to give a convenient form of general wheel motion from the design position. Since the wheel is assumed to be rigid, in general its motion is described by direct isometries. So what is desired is a convenient parameterization of these.

Proposition. *For any direct isometry, there exists angles ϕ, γ, δ and column vector $(x, y, z)^T$ such that this isometry is equivalent to the result of the following sequence of direct isometries:*

1. *Rotation by ϕ about an axis through the origin with direction $\boldsymbol{j}$.*
2. *Rotation by γ about an axis through the origin with direction $\boldsymbol{i}$.*
3. *Rotation by δ about an axis through the origin with direction $\boldsymbol{k}$.*
4. *Translation by $(x, y, z)^T$.*

Proof. Recall that a direct isometry acts on coordinate vectors as $\boldsymbol{x} \mapsto \boldsymbol{A}\boldsymbol{x} + \boldsymbol{b}$, where $\boldsymbol{A}$ is a special orthogonal matrix and $\boldsymbol{b}$ is a column vector. The sequence of direct isometries stated in the proposition acts on coordinate vectors as

$$\boldsymbol{x} \mapsto \boldsymbol{R}_{\boldsymbol{k},\delta}\boldsymbol{R}_{\boldsymbol{i},\gamma}\boldsymbol{R}_{\boldsymbol{j},\phi}\boldsymbol{x} + (x, y, z)^T.$$

Clearly, $(x, y, z)^T = \boldsymbol{b}$; the nontrivial part is finding angles ϕ, γ, and δ. By direct

computation,

$$\boldsymbol{R}_{\boldsymbol{k},\delta}\boldsymbol{R}_{\boldsymbol{i},\gamma}\boldsymbol{R}_{\boldsymbol{j},\phi} = \begin{pmatrix} c_\delta c_\phi - s_\delta s_\gamma s_\phi & -c_\gamma s_\delta & c_\delta s_\phi + c_\phi s_\delta s_\gamma \\ c_\phi s_\delta + c_\delta s_\gamma s_\phi & c_\delta c_\gamma & s_\delta s_\phi - c_\delta c_\phi s_\gamma \\ -c_\gamma s_\phi & s_\gamma & c_\gamma c_\phi \end{pmatrix},$$

where $c_* = \cos *$, $s_* = \sin *$, and this is a special orthogonal matrix. Now consider the following notation for the columns of a general special orthogonal matrix $\boldsymbol{A}$:

$$\boldsymbol{A} = \begin{pmatrix} \boldsymbol{f} & \boldsymbol{g} & \boldsymbol{h} \end{pmatrix}.$$

Notice that because $\boldsymbol{f} = \boldsymbol{A}\boldsymbol{i}$, $\boldsymbol{g} = \boldsymbol{A}\boldsymbol{j}$, and $\boldsymbol{h} = \boldsymbol{A}\boldsymbol{k}$, the vectors $\boldsymbol{f}, \boldsymbol{g}, \boldsymbol{h}$ form a right-handed, orthonormal basis. To proceed, equate $\boldsymbol{g} = (g_1, g_2, g_3)^T$ with the second column of $\boldsymbol{R}_{\boldsymbol{k},\delta}\boldsymbol{R}_{\boldsymbol{i},\gamma}\boldsymbol{R}_{\boldsymbol{j},\phi}$:

$$\begin{pmatrix} g_1 \\ g_2 \\ g_3 \end{pmatrix} = \begin{pmatrix} -\cos\gamma \sin\delta \\ \cos\delta\cos\gamma \\ \sin\gamma \end{pmatrix}.$$

Any unit vector can be given in the form on the right-hand side; this is an azimuth-elevation description. To solve for γ, use the arcsine function, which gives $-\pi/2 \leq \gamma \leq \pi/2$:

$$\gamma = \arcsin g_3.$$

Next, find δ. For now, assume that $\gamma \neq \pm\pi/2$. This means that $\cos\gamma \neq 0$, and

$$\frac{-g_1}{\cos\gamma} = \sin\delta$$
$$\frac{g_2}{\cos\gamma} = \cos\delta.$$

Hence, δ can be found using the two-argument arctangent function, which gives $-\pi < \delta \leq \pi$:

$$\delta = \operatorname{atan2}(-g_1/\cos\gamma, g_2/\cos\gamma).$$

Consider the equations formed from the first and third columns of $\boldsymbol{A}$ and $\boldsymbol{R}_{\boldsymbol{k},\delta}\boldsymbol{R}_{\boldsymbol{i},\gamma}\boldsymbol{R}_{\boldsymbol{j},\phi}$.

Using a convenient factorization on the right-hand side,

$$\begin{pmatrix} f_1 \\ f_2 \\ f_3 \end{pmatrix} = \cos\phi \begin{pmatrix} \cos\delta \\ \sin\delta \\ 0 \end{pmatrix} - \sin\phi \begin{pmatrix} \sin\delta\sin\gamma \\ -\cos\delta\sin\gamma \\ \cos\gamma \end{pmatrix}, \tag{3.3}$$

and

$$\begin{pmatrix} h_1 \\ h_2 \\ h_3 \end{pmatrix} = \sin\phi \begin{pmatrix} \cos\delta \\ \sin\delta \\ 0 \end{pmatrix} + \cos\phi \begin{pmatrix} \sin\delta\sin\gamma \\ -\cos\delta\sin\gamma \\ \cos\gamma \end{pmatrix}. \tag{3.4}$$

In fact,

$$\begin{pmatrix} \cos\delta \\ \sin\delta \\ 0 \end{pmatrix}, \begin{pmatrix} -\cos\gamma\sin\delta \\ \cos\delta\cos\gamma \\ \sin\gamma \end{pmatrix}, \begin{pmatrix} \sin\delta\sin\gamma \\ -\cos\delta\sin\gamma \\ \cos\gamma \end{pmatrix} \tag{3.5}$$

is a right-handed, orthonormal basis. Because $\boldsymbol{g}$ is equal to the second basis vector of (3.5), $\boldsymbol{f}$ and $\boldsymbol{h}$ must be in the same plane as the first and third vectors in the basis (3.5). Because both bases are right-handed, one can be rotated to match the other. Hence, it makes sense that one can give $\boldsymbol{f}$ and $\boldsymbol{h}$ in the forms seen in (3.3) and (3.4). For a relevant picture, see Figure 3.1.

To solve for ϕ, continue to assume that $\gamma \neq \pm\pi/2$, so that

$$\begin{aligned} \frac{-f_3}{\cos\gamma} &= \sin\phi \\ \frac{h_3}{\cos\gamma} &= \cos\phi, \end{aligned}$$

meaning that

$$\phi = \operatorname{atan2}(-f_3/\cos\gamma, h_3/\cos\gamma),$$

which gives $-\pi < \phi \leq \pi$.

Now suppose that $\gamma = \pi/2$. This means that $\boldsymbol{g} = \boldsymbol{k}$; it follows that $\boldsymbol{f}$ and $\boldsymbol{h}$ are

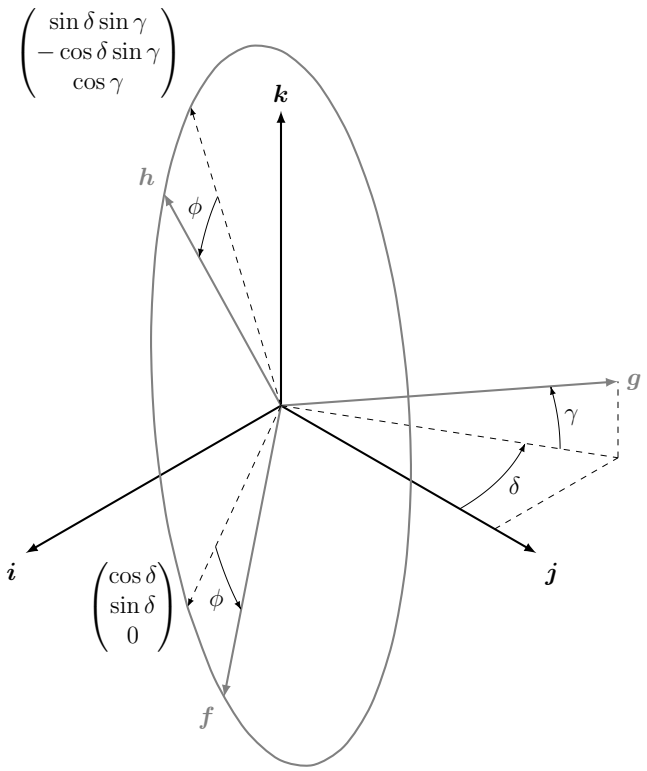

Figure 3.1. Identifying a special orthogonal matrix $(\boldsymbol{f}, \boldsymbol{g}, \boldsymbol{h})$ with the angles ϕ, γ, δ.

in the plane spanned by $\boldsymbol{i}$ and $\boldsymbol{j}$. Hence

$$\begin{pmatrix} f_1 & 0 & h_1 \\ f_2 & 0 & h_2 \\ 0 & 1 & 0 \end{pmatrix} = \begin{pmatrix} \cos(\delta+\phi) & 0 & \sin(\delta+\phi) \\ \sin(\delta+\phi) & 0 & -\cos(\delta+\phi) \\ 0 & 1 & 0 \end{pmatrix}.$$

When $\gamma = \pi/2$, one cannot distinguish between δ and ϕ. There is thus no unique solution, but the sum can be solved for:

$$\delta + \phi = \operatorname{atan2}(h_1, f_1).$$

From there one could pick a value for one of the unknowns and solve for the other.

When $\gamma = -\pi/2$, there is a similar result:

$$\begin{pmatrix} f_1 & 0 & h_1 \\ f_2 & 0 & h_2 \\ 0 & -1 & 0 \end{pmatrix} = \begin{pmatrix} \cos(\delta - \phi) & 0 & -\sin(\delta - \phi) \\ \sin(\delta - \phi) & 0 & \cos(\delta - \phi) \\ 0 & -1 & 0 \end{pmatrix},$$

leading to

$$\delta - \phi = \operatorname{atan2}(-h_1, f_1). \qquad \square$$

The preceding parameterization of direct isometries is convenient because the parameters $\phi, \gamma, \delta, x, y, z$ have meaning in an automotive engineering context:

- The angle ϕ is the *spin angle* of the wheel. It is is positive when the wheel (and carrier fixed to it!) rotates as if it rolled forward.

- The angle γ is the *camber angle* of the wheel. It is positive when the top of the wheel rotates away from the vehicle body and negative when the top of the wheel rotates toward the vehicle body. As seen in the proof, the parameterization is not unique when the camber angle is $\pm\pi/2$, because it cannot distinguish between δ and ϕ. (One would never expect a wheel to get anywhere near a camber angle of $\pm\pi/2$.)

- The angle δ is the *toe angle* of the wheel. It is positive when the front of the wheel rotates toward the vehicle body (*toe-in*) and negative when the front of the wheel rotates away from the vehicle body (*toe-out*).

For the other parameters, recall that in the design position, the wheel center coincides with the origin. The parametrized isometry maps this to the point with coordinate vector $(x, y, z)^T$. Hence

- The coordinate x is the *longitudinal displacement* of the wheel center. It is positive when the wheel moves toward the front of the vehicle.

- The component y is the *lateral displacement* of the wheel center. It is positive when the wheel moves to the left side of the vehicle.

- The component z is the *vertical displacement* of the wheel center. It is positive when the wheel moves up. When $z > 0$ the wheel is said to be in *jounce* and when $z < 0$ the wheel is said to be in *rebound*.

Of interest is the location of the ground plane after the wheel moves. Recall the parametric form of a point on the circumference of the wheel in the design position, (3.2). The wheel isometry maps this to

$$\begin{pmatrix} x - r\sin(\phi-\psi)\cos\delta - r\cos(\phi-\psi)\sin\delta\sin\gamma \\ y - r\sin(\phi-\psi)\sin\delta + r\cos(\phi-\psi)\cos\delta\sin\gamma \\ z - r\cos(\phi-\psi)\cos\gamma \end{pmatrix},$$

where some trigonometric identities have been used. In order to have a unique lowest-hanging point, assume that $-\pi/2 < \gamma < \pi/2$. Then find ψ such that $\cos(\phi-\psi) = 1$. The obvious solution here is just $\psi = \phi$. Thus, the lowest-hanging point on the wheel after a wheel motion is

$$\begin{pmatrix} x - r\sin\delta\sin\gamma \\ y + r\cos\delta\sin\gamma \\ z - r\cos\gamma \end{pmatrix}. \tag{3.6}$$

3.3 Wheel Trajectory

In general, all six parameters — spin angle ϕ, camber angle γ, toe angle δ, longitudinal displacement x, lateral displacement y, and vertical displacement z — are required to locate the wheel in space relative to the design position. However, this is assuming that the wheel has the full six degrees of freedom of a rigid body in space. In reality, the wheel must be connected to the vehicle body, and this necessarily constrains the wheel's motion. A typical independent suspension linkage is designed to constrain the wheel so that there is only one degree of freedom. Assume that wheel center vertical displacement z drives the other five. In particular, let z take values in the interval I_z, which is assumed to contain zero. Then, assume that $\phi : I_z \to (-\pi, \pi]$, $\gamma : I_z \to [-\pi/2, \pi/2]$, $\delta : I_z \to (-\pi, \pi]$, $x : I_z \to \mathbf{R}$, $y : I_z \to \mathbf{R}$ are differentiable

functions that satisfy

$$\phi(0) = \gamma(0) = \delta(0) = x(0) = y(0) = 0.$$

The trajectory of the wheel is thus described by the z-varying family of direct isometries with special orthogonal matrix

$$\boldsymbol{A}(z) = \boldsymbol{R}_{\boldsymbol{k},\delta(z)}\boldsymbol{R}_{\boldsymbol{i},\gamma(z)}\boldsymbol{R}_{\boldsymbol{j},\phi(z)}$$

and column vector

$$\boldsymbol{b}(z) = (x(z), y(z), z)^T.$$

Notice that the original, design position of the wheel corresponds to $z = 0$.

The angular velocity of the wheel at vertical displacement z is given by

$$\tilde{\boldsymbol{\omega}}(z) = \boldsymbol{A}'(z)(\boldsymbol{A}(z))^T;$$

in particular, omitting dependencies on z for brevity,

$$\boldsymbol{\omega} = \begin{pmatrix} \gamma' \cos\delta - \phi' \cos\gamma \sin\delta \\ \gamma' \sin\delta + \phi' \cos\delta \cos\gamma \\ \delta' + \phi' \sin\gamma \end{pmatrix}.$$

The velocity of the point on the wheel that is passing through the origin at vertical displacement z is given by

$$\boldsymbol{v}(z) = \boldsymbol{b}'(z) - \boldsymbol{\omega}(z) \times \boldsymbol{b}(z).$$

Again omitting dependencies on z, $\boldsymbol{v}$ is equal to

$$\begin{pmatrix} x' + \delta' y - \gamma' z \sin\delta + \phi'(y \sin\gamma - z \cos\delta \cos\gamma) \\ y' - \delta' x + \gamma' z \cos\delta - \phi'(x \sin\gamma + z \sin\delta \cos\gamma) \\ \gamma'(x \sin\delta - y \cos\delta) + \phi' \cos\gamma(x \cos\delta + y \sin\delta) + 1 \end{pmatrix}.$$

Several suspension characteristics are defined from the wheel's velocity. In particular, these come from the wheel center velocity and the contact point velocity. Dependencies on z continue to be omitted in this section. At vertical displacement z, the wheel center has coordinate vector

$$\boldsymbol{b} = (x, y, z)^T.$$

The velocity of the point on the wheel with that coordinate vector is

$$\begin{aligned}\boldsymbol{v_b} &= \boldsymbol{\omega} \times \boldsymbol{b} + \boldsymbol{v} \\ &= \boldsymbol{\omega} \times \boldsymbol{b} + \boldsymbol{b}' - \boldsymbol{\omega} \times \boldsymbol{b} \\ &= \boldsymbol{b}' \\ &= (x', y', 1)^T.\end{aligned}$$

Referring to (3.6), at vertical displacement z, the contact point, or lowest-hanging point of the wheel, has coordinate vector

$$\boldsymbol{c} := \begin{pmatrix} x - r\sin\delta\sin\gamma \\ y + r\cos\delta\sin\gamma \\ z - r\cos\gamma \end{pmatrix}.$$

The velocity of the point on the wheel with coordinate vector $\boldsymbol{c}$ is

$$\begin{aligned}\boldsymbol{v_c} &= \boldsymbol{\omega} \times \boldsymbol{c} + \boldsymbol{v} \\ &= \begin{pmatrix} x' - \phi' r\cos\delta - \delta' r\cos\delta\sin\gamma - \gamma' r\cos\gamma\sin\delta \\ y' - \phi' r\sin\delta + \gamma' r\cos\delta\cos\gamma - \delta' r\sin\delta\sin\gamma \\ \gamma' r\sin\gamma + 1 \end{pmatrix}.\end{aligned}$$

The vector $\boldsymbol{v}_c$ is the velocity of the particular point on the wheel that happens to be the contact point for that value of z, not the tangent vector of $\boldsymbol{c}$ at z; that is, $\boldsymbol{v}_c \neq \boldsymbol{c}'$. This is because the contact point is not a unique point of the wheel; it instead moves

around the circumference in order to hang the lowest.

Two suspension characteristics are defined from the velocities $\boldsymbol{v_b}$ and $\boldsymbol{v_c}$ when considering a side ($\boldsymbol{j}$-normal) view of the wheel; see Figure 3.2. The first is *wheel-travel angle* ε, which is the inclination of $\boldsymbol{v_b}$ to the vertical in this side view. In particular,

$$\tan\varepsilon = \frac{v_{b_1}}{v_{b_3}} = x'. \tag{3.7}$$

For a driven front wheel, positive values of ε give an anti-lift effect; for a driven rear wheel, negative values of ε give an anti-squat effect. Notice that ε is entirely dependent on wheel center longitudinal displacement x.

The second characteristic from $\boldsymbol{v_b}$ in the side view is *support angle* ε^*, which is the inclination of $\boldsymbol{v_c}$ to the vertical in this side view; in particular,

$$\tan\varepsilon^* = \frac{v_{c_1}}{v_{c_3}} = \frac{x' - \phi' r\cos\delta - \delta' r\cos\delta\sin\gamma - \gamma' r\cos\gamma\sin\delta}{\gamma' r\sin\gamma + 1}. \tag{3.8}$$

For an outboard-braked front wheel, positive values of ε^* give an anti-dive effect. For an outboard-braked rear wheel, negative values of ε^* give an anti-rise effect. In the design position, support angle ε^* is given by the spin angle ϕ and wheel center longitudinal displacement x. (The names "wheel-travel angle" and "support angle" follow Matschinsky [26].)

One suspension characteristic, *roll center height*, denoted by h, is defined from the velocity $\boldsymbol{v_c}$ when considering a front ($\boldsymbol{i}$-normal) view of the wheel; see Figure 3.3. The roll center height is the signed distance from the ground plane to the point where the perpendicular of the front view projection of $\boldsymbol{v_c}$ intersects the centerline of the vehicle body. Letting s denote the design position track width of the axle,

$$\frac{h}{s/2 - c_2} = \frac{-v_{c_2}}{v_{c_3}}.$$

In particular,

$$h = \frac{-(y' - \phi' r\sin\delta + \gamma' r\cos\delta\cos\gamma - \delta' r\sin\delta\sin\gamma)}{\gamma' r\sin\gamma + 1} \times (s/2 - (y + r\cos\delta\sin\gamma)) \tag{3.9}$$

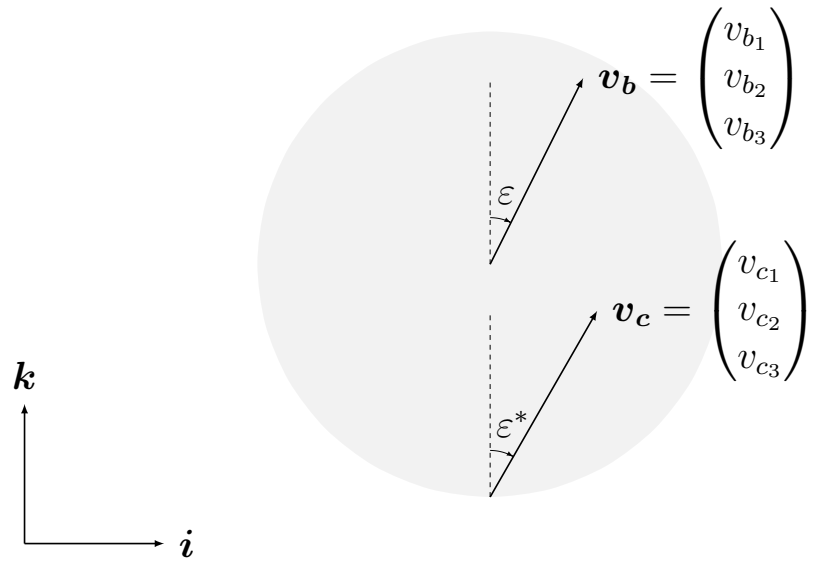

Figure 3.2. Suspension characteristic definitions in the side view.

Notice that roll center height h in the design position is given by wheel center lateral displacement y and camber angle γ.

3.4 Example Trajectory

Consider a driven, outboard-braked rear wheel. Here, the γ, δ, ε, ε^*, and h curves are chosen, meaning the remaining curves x, y and ϕ may be deduced from there. Throughout, length units are millimeters and angle units are radians. First, let

$$I_z = \{z \in \mathbf{R} : -99 \leq z \leq 99\},$$

wheel radius $r = 300$, and design position track width $s = 1400$. The camber function is defined by

$$\gamma(z) = (-1.5 \times 10^{-6})z^2 + \left(\frac{-0.5}{25.4}\frac{\pi}{180}\right)z.$$

The coefficient of z is the camber change rate from the design position, while the coefficient of z^2 controls whether the graph of γ is concave up or down and how sharply curved it is. The z-coefficient gives a design position camber change rate of negative half a degree per inch of jounce. The chosen value for the z^2-coefficient produces

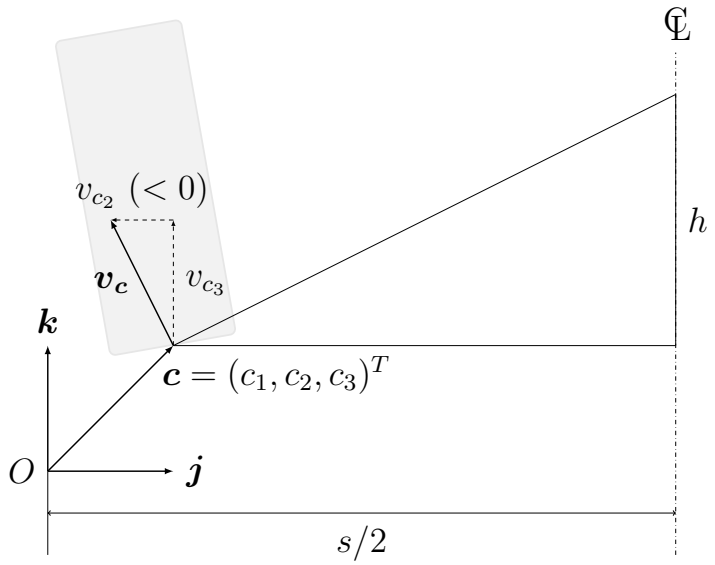

Figure 3.3. Roll center height definition in the front view, with velocity component v_{c_2} drawn negative to result in a positive roll center height h.

reasonable-looking values for maximum positive and negative camber. Camber angle is plotted in Figure 3.4; the convention of wheel center vertical displacement z on the vertical axis is adopted.

The toe function is defined by

$$\delta(z) = \left(0.005 \times \frac{\pi}{180}\right) z,$$

which gives a very slight roll understeer effect. See Figure 3.5 for a plot.

For a driven rear wheel, anti-squat behavior is wanted; consequently, there must be negative values for the wheel-travel angle ε. Let

$$\varepsilon(z) = -6 \times \frac{\pi}{180}.$$

For a driven rear wheel in the design position,

$$\%\text{ anti-squat} = \frac{\tan|\varepsilon|}{(\text{CG height})/\text{wheelbase}} \times 100;$$

assuming a ratio in the denominator of around 0.2, this gives approximately 50% anti-

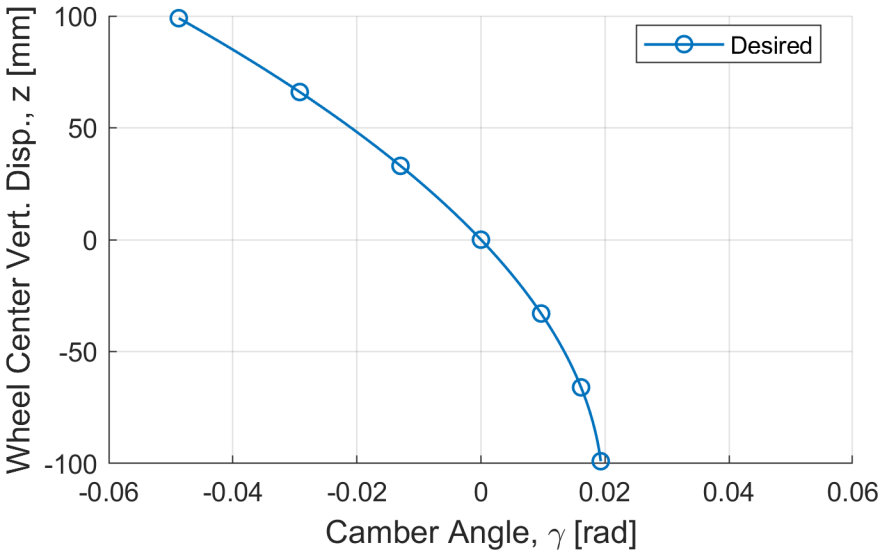

Figure 3.4. Camber angle specification.

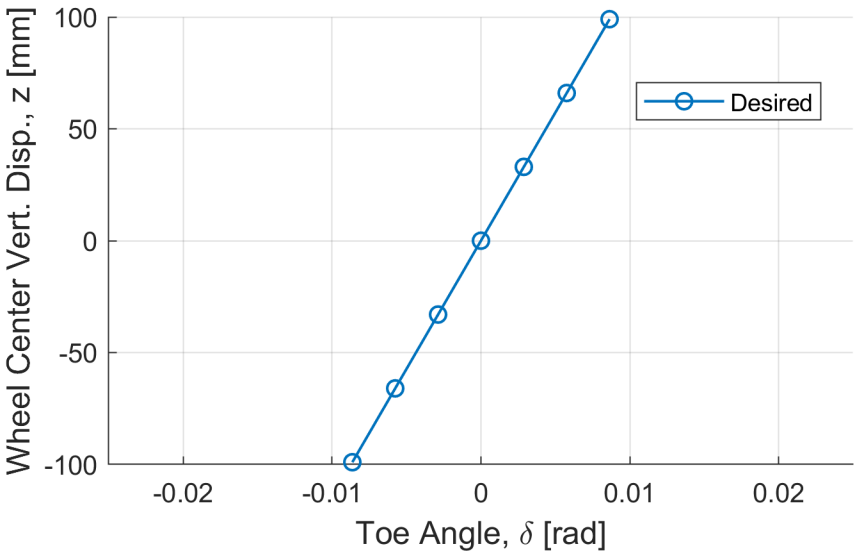

Figure 3.5. Toe angle specification.

squat. A constant wheel-travel angle doesn't imply a constant percent anti-squat, but the wheelbase tends to lengthen as the CG height decreases, so this isn't far off.

Similarly, for an outboard-braked rear wheel, anti-rise behavior is desired, and thus negative values for support angle ε^*. Let

$$\varepsilon^*(z) = -15 \times \frac{\pi}{180}.$$

For an outboard-braked rear wheel in the design position,

$$\%\text{ anti-rise} = \frac{(\%\text{ rear braking}) \tan|\varepsilon^*|}{(\text{CG height})/\text{wheelbase}}.$$

Assuming 40% rear braking, and the same CG height to wheelbase ratio of 0.2, -15 degrees of support angle gives approximately 50% anti-rise.

The roll center height is defined by

$$h(z) = 100 - (1)(z - r\cos\gamma(z) - (-r)),$$

which gives an initial roll center height of 100 mm, which decreases/increases by one times the amount the ground plane moves up/down.

Determining the remaining x, y, and ϕ curves amounts to solving a few first order differential equations. The x curve, Figure 3.6, is found by solving (3.7) with initial condition $x(0) = 0$. Next, the ϕ curve, Figure 3.7, is found by solving (3.8) with initial condition $\phi(0) = 0$. Finally, the y curve, Figure 3.8, is found by solving (3.9) with initial condition $y(0)$. These three differential equations can be solved numerically, with, in this case, MATLAB. In the end, the mixed position/velocity requirements have been converted into five position-parameter curves. This shows how suitable choices of suspension characteristics of interest can be converted into a mathematically-coherent wheel trajectory.

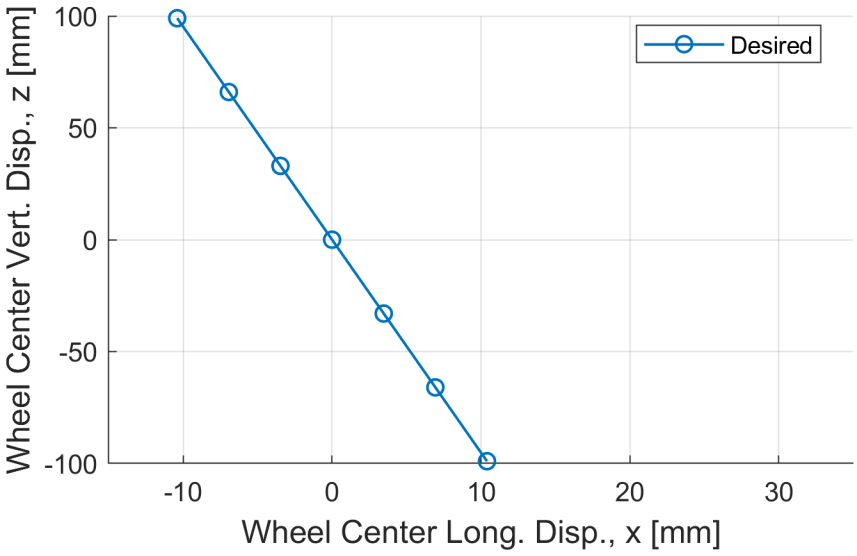

Figure 3.6. Wheel center longitudinal displacement specification.

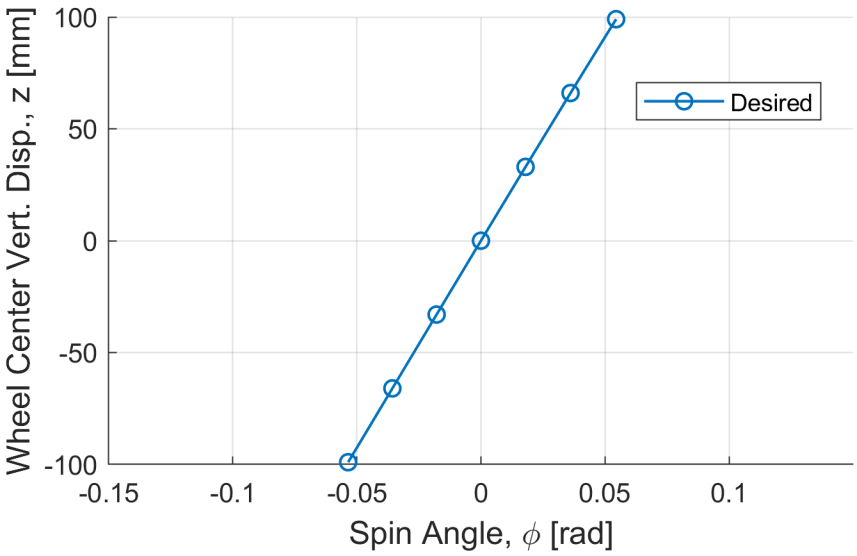

Figure 3.7. Spin angle specification.

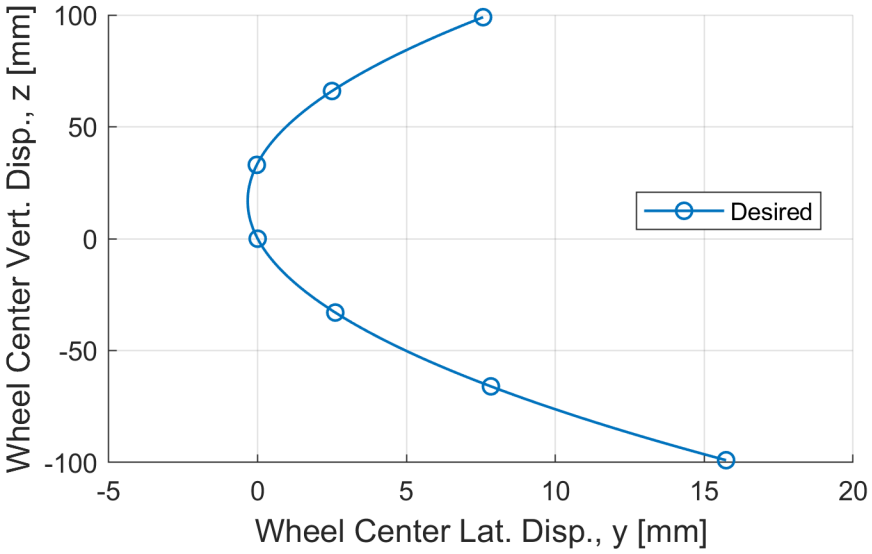

Figure 3.8. Wheel center lateral displacement specification.

Chapter 4

Number Synthesis

The focus is on two types of vehicle-body–wheel-carrier connections:

- *Joints*, which directly connect the wheel carrier to the vehicle body.
- *Links*, which have a joint on each end and indirectly connect the wheel carrier to the vehicle body.

Recall, from the literature review, that Matschinsky [26] identifies, for independent suspensions, three practical joints and four practical links. Matschinsky's joints are the spherical (S), revolute (R), and cylindrical (C) joints, which he calls the ball, turning, and turning-and-sliding joints, respectively. The links he identifies are the rod (S-S), triangular (R-S), trapezoidal (R-R), and turning-and-sliding (S-C, with S joint located along C joint axis). If the ordering of the joints in X-Y is taken to be significant; namely, X being the joint that connects the link to the vehicle body and Y being the joint that connects the link to the wheel carrier, then the ordering as written represents the most common cases. The reversed triangular link (S-R) is encountered much more frequently than the reversed turning-and-sliding link (C-S). In fact, there is no evidence of a C-S link being used on any vehicle.

The freedom f of a joint is the number of parameters it takes to describe the position of one body with respect to another when they are connected by the joint in question. The R joint requires one angle ($f = 1$). The S joint requires three angles ($f = 3$). The C joint requires an angle and a displacement ($f = 2$). Key to the

Table 4.1. The body-wheel connections.

Connection	g	$\sum_{i=1}^{g} f_i$	r_{sf}	c	Remark
S	1	3	0	3	Often implemented with rubber bushing.
R	1	1	0	5	Often implemented with two rubber bushings.
C	1	2	0	4	Often implemented with telescopic damper.
S-S	2	6	1	1	–
R-S	2	4	0	2	Reversible.
R-R	2	2	0	4	–
S-C	2	5	1	2	S joint lies on C joint axis; reversible.

number synthesis is the number of DOFs each connection removes from the wheel, denoted by c;

$$c = 6 - \left(\sum_{i=1}^{g} f_i - r_{sf} \right),$$

where g is the number of joints in the connection, f_i is the freedom of the ith joint, and r_{sf} is the number of superfluous rotations associated with the connection. The results for each connection are shown in Table 4.1.

A necessary (but not sufficient) condition is that an independent suspension linkage removes five DOFs from the wheel. Assuming that each body-wheel connection provides a unique set of constraints, one can determine all combinations of connections (repetition allowed) that leave one DOF. These are mere candidates because a linkage with one DOF is not necessarily capable of the desired wheel motion.

A *partition* of a positive integer is a way of writing it as a sum of positive integers, where the order of the summands does not matter. There are seven partitions of five: 5, $4+1$, $3+2$, $3+1+1$, $2+2+1$, $2+1+1+1$, and $1+1+1+1+1$. These partitions suggest possible suspension architectures.

Partition 5**.** The only body-wheel connection to remove five DOFs directly is the R joint. This is the (semi-)trailing arm rear suspension.

Partition $4 + 1$**.** The C joint and the R-R link remove four DOFs each. The only connection removing a single DOF is the S-S link. Consequently, there are two potential architectures here. A potential architecture is written as the multiset (or

bag) of its connections. Here, {C, S-S} and {R-R, S-S}. An example of the former is the classical sliding pillar front suspension, while the latter is the trapezoidal link rear suspension.

Partition $3+2$**.** The only connection that removes three DOFs is the S joint. There are two connections that remove two: R-S and S-C, each of which is reversible. There are thus four potential architectures here: {S, R-S}, {S, S-R}, {S, S-C}, and {S, C-S}.

Partition $3+1+1$**.** The only possibility here is {S, S-S, S-S}. This is a type of trailing link rear suspension.

Partition $2+2+1$**.** Including reversals, there are four connections that remove two DOFs: R-S, S-R, S-C, and C-S. How many ways are there to choose two of these, repetition allowed? Ten: {R-S, R-S}, {R-S, S-R}, {R-S, S-C}, {R-S, C-S}, {S-R, S-R}, {S-R, S-C}, {S-R, C-S}, {S-C, S-C}, {S-C, C-S}, and {C-S, C-S}. These, with the addition of an S-S link, form another ten possible suspension architectures. These possibilities include the venerable double wishbone {R-S, R-S, S-S} and MacPherson {R-S, S-C, S-S} architectures.

Partition $2+1+1+1$**.** There are four possibilities: {R-S, S-S, S-S, S-S}, {S-R, S-S, S-S, S-S}, {S-C, S-S, S-S, S-S}, and {C-S, S-S, S-S, S-S}.

Partition $1+1+1+1+1$**.** One potential architecture: {S-S, S-S, S-S, S-S, S-S} — the five-link suspension made popular by Mercedes-Benz.

Since each of the C, S-C, and C-S connections is bound to be practically realized with a telescopic damper, there is not a strong argument for architectures having more than one of these of these connection types. Consider cost, weight, and package space required. Consequently, it does not seem unreasonable at some stage to eliminate such architectures from consideration. Additionally, having seen no evidence that the C-S link is practical, it is not unreasonable to eliminate it from further con-

Table 4.2. Potential independent suspension architectures, organized by number of connections. Types identified as impractical are crossed out.

Connections	Architectures
1	{R}
2	{C, S-S}, {R-R, S-S}, {S, R-S}, {S, S-R}, {S, S-C}, ~~{S, C-S}~~
3	{S, S-S, S-S}, {R-S, R-S, S-S}, {R-S, S-R, S-S}, {R-S, S-C, S-S}, ~~{R-S, C-S, S-S}~~, {S-R, S-R, S-S}, {S-R, S-C, S-S}, ~~{S-R, C-S, S-S}~~, ~~{S-C, S-C, S-S}~~, ~~{S-C, C-S, S-S}~~, ~~{C-S, C-S, S-S}~~
4	{R-S, S-S, S-S, S-S}, {S-R, S-S, S-S, S-S}, {S-C, S-S, S-S, S-S}, ~~{C-S, S-S, S-S, S-S}~~
5	{S-S, S-S, S-S, S-S, S-S}

sideration. In any case, the techniques soon presented for the more common S-C link are easily extended to its reversal if necessary. The 23 enumerated architectures in total are summarized in Table 4.2, organized by number of connections. The three "dual damper" architectures are marked with an X as are any having a C-S link. It is interesting that of the 23 total architectures, nearly half (11) come from the 3-connection family, with the number of architectures dropping down to one on both sides of "3".

Occasionally, when the standard multiset notation is too cumbersome, multisets are written as the "product" of their unique elements, with each unique element having a superscript indicating its multiplicity (when said multiplicity is greater than one). For example, the multiset $\{a, a, b\}$ will be written as a^2b.

Chapter 5

The R Joint

5.1 Synthesis

The revolute (R) joint directly connects the wheel carrier to the vehicle body. The R joint's geometry in the design position can be described by a column vector $\boldsymbol{u}_0 \in \mathbf{R}^3$, giving the direction of the joint axis, and a coordinate vector $\boldsymbol{x}_0 \in \mathbf{R}^3$, giving the coordinates of a point on the joint axis. See Figure 5.1 for a picture; the R joint is achieved with two legs having point-connections on each end, as is common practice. As the wheel carrier moves from the design position to the position given by some $\boldsymbol{A} \in SO(3)$ and some $\boldsymbol{b} \in \mathbf{R}^3$, the axis remains invariant:

$$\boldsymbol{A}\boldsymbol{u}_0 = \boldsymbol{u}_0 \tag{5.1}$$

$$\boldsymbol{A}\boldsymbol{x}_0 + \boldsymbol{b} = \boldsymbol{x}_0. \tag{5.2}$$

With, at most, six independent variables to work with, and these six design equations, no more than two wheel positions are possible when working with the R joint. Further, it is not yet known for sure if the design equations are solvable for the two wheel positions.

Rather than one additional wheel position beyond design, one can also consider specifying design position wheel velocity; this approach would be more in line with the traditional wheel motion specification. The velocity-based design equations can

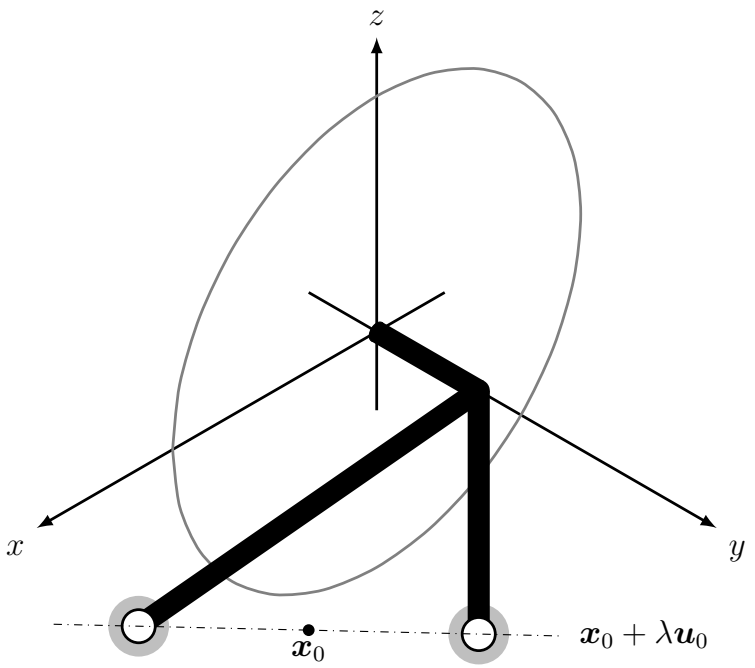

Figure 5.1. Depiction of an R joint.

be derived by differentiating the standard design equations with respect to wheel center vertical displacement z. Beginning with Equation (5.1), let the prime mark be the shorthand for the derivative with respect to z:

$$\frac{d}{dz}\left(\boldsymbol{A}\boldsymbol{u}_0\right) = \frac{d\boldsymbol{u}_0}{dz} \tag{5.3}$$

$$\boldsymbol{A}'\boldsymbol{u}_0 = \boldsymbol{0} \tag{5.4}$$

$$\boldsymbol{A}'\boldsymbol{A}^T\boldsymbol{u}_0 = \boldsymbol{0} \tag{5.5}$$

$$\boldsymbol{\omega} \times \boldsymbol{u}_0 = \boldsymbol{0}. \tag{5.6}$$

The last equation, (5.6), simply says that the R joint axis must be parallel to the intended angular velocity vector $\boldsymbol{\omega}$. Consequently, one solution for R joint direction is the unit vector

$$\boldsymbol{u}_0 = \boldsymbol{\omega}/|\boldsymbol{\omega}|. \tag{5.7}$$

The second R joint design equation, (5.2), can be similarly differentiated:

$$\boldsymbol{A}\boldsymbol{x}_0 + \boldsymbol{b} = \boldsymbol{x}_0 \tag{5.8}$$

$$\boldsymbol{A}'\boldsymbol{x}_0 + \boldsymbol{b}' = \boldsymbol{0} \tag{5.9}$$

$$\boldsymbol{A}'\left(\boldsymbol{A}^T(\boldsymbol{x}_0 - \boldsymbol{b})\right) + \boldsymbol{b}' = \boldsymbol{0} \tag{5.10}$$

$$\boldsymbol{A}'\boldsymbol{A}^T\boldsymbol{x}_0 + \boldsymbol{b}' - \boldsymbol{A}'\boldsymbol{A}^T\boldsymbol{b} = \boldsymbol{0} \tag{5.11}$$

$$\boldsymbol{\omega} \times \boldsymbol{x}_0 + \boldsymbol{b}' - \boldsymbol{\omega} \times \boldsymbol{b} = \boldsymbol{0} \tag{5.12}$$

$$\boldsymbol{\omega} \times \boldsymbol{x}_0 + \boldsymbol{v} = \boldsymbol{0} \tag{5.13}$$

$$\boldsymbol{\omega} \times \boldsymbol{x}_0 = -\boldsymbol{v}. \tag{5.14}$$

Since the left-hand side of (5.14) is perpendicular to $\boldsymbol{\omega}$, the right-hand side must be as well. Consequently, when specifying wheel velocity for an R joint, it is required that

$$\boldsymbol{\omega} \cdot \boldsymbol{v} = 0. \tag{5.15}$$

To solve for $\boldsymbol{x}_0$ in (5.14),both sides can be crossed with $\boldsymbol{\omega}$ as follows:

$$\boldsymbol{\omega} \times (\boldsymbol{\omega} \times \boldsymbol{x}_0) = -\boldsymbol{\omega} \times \boldsymbol{v} \tag{5.16}$$

$$(\boldsymbol{\omega} \cdot \boldsymbol{x}_0)\boldsymbol{\omega} - (\boldsymbol{\omega} \cdot \boldsymbol{\omega})\boldsymbol{x}_0 = -\boldsymbol{\omega} \times \boldsymbol{v}. \tag{5.17}$$

If it is assumed that $\boldsymbol{x}_0$ is perpendicular to $\boldsymbol{\omega}$, there is the unique solution

$$\boldsymbol{x}_0 = \frac{\boldsymbol{\omega} \times \boldsymbol{v}}{\boldsymbol{\omega} \cdot \boldsymbol{\omega}}. \tag{5.18}$$

This is the unique point on the axis that is closest to the origin (an application of Roe's Corollary 4.2.4 [42]).

It is time to give attention to the R joint motion specification in terms of the suspension characteristics of interest rather than the general $\boldsymbol{\omega}$ and $\boldsymbol{v}$. Recall the general expressions for wheel angular velocity $\boldsymbol{\omega}(z)$ and the velocity $\boldsymbol{v}(z)$ of the point

on the wheel passing through the origin:

$$\boldsymbol{\omega}(z) = \begin{pmatrix} \gamma' \cos\delta - \phi' \cos\gamma \sin\delta \\ \gamma' \sin\delta + \phi' \cos\delta \cos\gamma \\ \delta' + \phi' \sin\gamma \end{pmatrix},$$

$$\boldsymbol{v}(z) = \begin{pmatrix} x' + \delta' y - \gamma' z \sin\delta + \phi'(y \sin\gamma - z \cos\delta \cos\gamma) \\ y' - \delta' x + \gamma' z \cos\delta - \phi'(x \sin\gamma + z \sin\delta \cos\gamma) \\ \gamma'(x \sin\delta - y \cos\delta) + \phi' \cos\gamma(x \cos\delta + y \sin\delta) + 1 \end{pmatrix}.$$

Here, the desire is to specify $\boldsymbol{\omega}(0)$ and $\boldsymbol{v}(0)$, these velocity terms at the design position ($z = 0$). These terms are much simpler than the general ones, with

$$\boldsymbol{\omega}(0) = \begin{pmatrix} \gamma'(0) \\ \phi'(0) \\ \delta'(0) \end{pmatrix},$$

and

$$\boldsymbol{v}(0) = \begin{pmatrix} x'(0) \\ y'(0) \\ 1 \end{pmatrix}.$$

Typically, suspension designers want to be able to specify wheel-travel angle ε, support angle ε^*, and roll center height h. In this case, the appropriate substitutions into the wheel velocity terms can be made. For wheel-travel angle, $\tan\varepsilon(0) = x'(0)$. The other two are more involved. Recall that

$$\tan\varepsilon^* = \frac{x' - \phi' r \cos\delta - \delta' r \cos\delta \sin\gamma - \gamma' r \cos\gamma \sin\delta}{\gamma' r \sin\gamma + 1}.$$

In the design position,

$$\tan\varepsilon^*(0) = x'(0) - \phi'(0) r.$$

Consequently, $\phi'(0) = (\tan\varepsilon(0) - \tan\varepsilon^*(0))/r$. Regarding roll center height, recall

that

$$h = \frac{-(y' - \phi' r \sin\delta + \gamma' r \cos\delta \cos\gamma - \delta' r \sin\delta \sin\gamma)}{\gamma' r \sin\gamma + 1} \times (s/2 - (y + r\cos\delta\sin\gamma)) \,.$$

In the design position, roll center height is

$$h(0) = -(y'(0) + \gamma'(0)r)(s/2).$$

Consequently,

$$y'(0) = \frac{-h(0)}{s/2} - \gamma'(0)r.$$

Now substitute the expressions for $x'(0)$, $\phi'(0)$, and $y'(0)$ into the design position velocity terms, yielding

$$\boldsymbol{\omega}(0) = \begin{pmatrix} \gamma'(0) \\ (\tan\varepsilon(0) - \tan\varepsilon^*(0))/r \\ \delta'(0) \end{pmatrix},$$

and

$$\boldsymbol{v}(0) = \begin{pmatrix} \tan\varepsilon(0) \\ -2h(0)/s - \gamma'(0)r \\ 1 \end{pmatrix}.$$

This motion specification is analogous to Gerrard's kinematic velocity vector [12], but derived from the general position parameterization rather than defined directly.

However, for the R joint, one cannot pick all five of $\gamma'(0)$, $\varepsilon(0)$, $\varepsilon^*(0)$, $\delta'(0)$, and $h(0)$ independently. One must be dictated by the condition (5.15). Which of the five should be first to go? The R joint is, on its own, capable of serving as an independent suspension linkage. There is no means to provide a steer axis; as such, the R joint is only suitable for non-steered axles, such as the rear axle of a typical passenger car. In this context,

- $\gamma'(0)$ is camber change rate at design;

- $\varepsilon(0)$ is wheel-travel angle at design, establishing anti-squat behavior if the rear wheel is driven;
- $\varepsilon^*(0)$ is the support angle at design, establishing anti-rise behavior if the rear wheel has outboard brakes;
- $\delta'(0)$ is toe change rate at design;
- $h(0)$ is roll center height at design.

The most likely of these five to not be needed is $\varepsilon(0)$, since most cars do not drive the rear wheels but do have outboard brakes. So wheel-travel angle $\varepsilon(0)$ may be eliminated from the motion specification. This amounts to solving for $\tan\varepsilon(0)$ in the equation $\boldsymbol{\omega}(0) \cdot \boldsymbol{v}(0) = 0$. Consequently,

$$\tan\varepsilon(0) = \left(\left(\frac{rs}{2}\right)\frac{\gamma'(0)}{h(0)} + 1\right)\tan\varepsilon^*(0) + \left(\frac{rs}{2}\right)\frac{\delta'(0)}{h(0)}. \tag{5.19}$$

5.2 Synthesis Example

Recall the rear wheel trajectory given by

- Wheel center vertical displacement $z \in [-99, 99]$ [mm];
- Wheel radius $r = 300$ [mm];
- Design position track width $s = 1400$ [mm];
- Camber curve $\gamma(z) = (-1.5 \times 10^{-6})z^2 + (-0.5/25.4)(\pi/180)z$ [rad];
- Toe curve $\delta(z) = 0.005(\pi/180)z$ [rad];
- Wheel-travel angle curve $\varepsilon(z) = -6\pi/180$ [rad];
- Support angle curve $\varepsilon^*(z) = -15\pi/180$ [rad];
- Roll center height curve $h(z) = 100 - (z - r\cos(\gamma(z)) + r)$ [mm].

This wheel trajectory can be converted into the following R joint motion specification:

- Camber change rate at design $\gamma'(0) = (-0.5/25.4)(\pi/180)$ [rad/mm];
- Toe change rate at design $\delta'(0) = 0.005(\pi/180)$ [rad/mm];
- Support angle at design $\varepsilon^*(0) = -15\pi/180$ [rad];
- Roll center height at design $h(0) = 100$ [mm].

The resultant wheel-travel angle, per (5.19), is approximately 6.2°, which gives a pro-squat effect (if the rear wheel is driven). This effect is opposite the originally-intended anti-squat effect given by the original wheel-travel angle of −6°! However, this difference in wheel-travel angle is of no concern (at least for squat) if the rear wheels are not driven. After computing $\boldsymbol{\omega}(0)$ and $\boldsymbol{v}(0)$ from the R joint motion specification, joint direction $\boldsymbol{u}_0$ can be solved for with (5.7) and joint location $\boldsymbol{x}_0$ with (5.18). To three significant figures,

$$\boldsymbol{u}_0 = \begin{pmatrix} -0.263 \\ 0.962 \\ 0.0669 \end{pmatrix} \text{ [mm]},$$

and

$$\boldsymbol{x}_0 = \begin{pmatrix} 740 \\ 208 \\ -72.1 \end{pmatrix} \text{ [mm]}.$$

These values result in an R joint that is nearly in an xy plane and is forward of the wheel center, Figure 5.2. The axis is visualized with a line segment of length 400 mm, centered on the point $\boldsymbol{x}_0$.

5.3 Analysis

The equations (5.1) and (5.2) can also be used to analyze an R joint suspension after it has been synthesized. In this case, the unknowns are not the joint coordinates, but the wheel motion parameters for a given value of wheel center vertical displacement

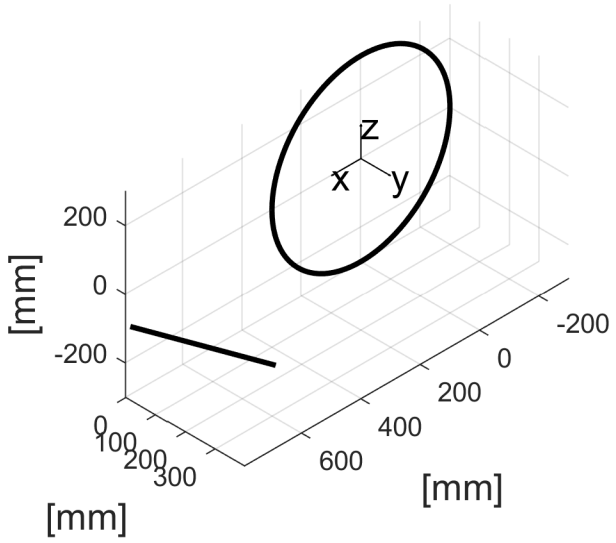

Figure 5.2. Solution for R joint from design position velocity specification.

.

z. First consider solving for wheel position parameters ϕ, γ, δ, x, and y, given z. A straightforward strategy is to use Newton's method to solve the equations numerically, but there are five variables in six equations. Consider replacing the R joint direction equation $\boldsymbol{A}\boldsymbol{u}_0 = \boldsymbol{u}_0$ with

$$\boldsymbol{A}\boldsymbol{u}_1 \cdot \boldsymbol{u}_0 = 0 \tag{5.20}$$

$$\boldsymbol{A}\boldsymbol{u}_2 \cdot \boldsymbol{u}_0 = 0, \tag{5.21}$$

where $\{\boldsymbol{u}_0, \boldsymbol{u}_1, \boldsymbol{u}_2\}$ is a right-handed, orthonormal basis. Such a basis is easily constructed given $\boldsymbol{u}_0$. Do equations (5.20) and (5.21) imply the original direction equation (5.1)? On one hand,

$$\boldsymbol{A}\boldsymbol{u}_1 \times \boldsymbol{A}\boldsymbol{u}_2 = \boldsymbol{A}(\boldsymbol{u}_1 \times \boldsymbol{u}_2) = \boldsymbol{A}\boldsymbol{u}_0.$$

On the other hand,

$$\boldsymbol{A}\boldsymbol{u}_1 \times \boldsymbol{A}\boldsymbol{u}_2 = |\boldsymbol{A}\boldsymbol{u}_1||\boldsymbol{A}\boldsymbol{u}_2| \sin\left(\frac{\pi}{2}\right) \boldsymbol{n} = \boldsymbol{n},$$

where $\boldsymbol{n}$ is the unit vector that is perpendicular to both $\boldsymbol{A}\boldsymbol{u}_1$ and $\boldsymbol{A}\boldsymbol{u}_2$, with orientation given by the right-hand rule. Assuming (5.20) and (5.21) are true, $\boldsymbol{u}_0$ is perpendicular to both $\boldsymbol{A}\boldsymbol{u}_1$ and $\boldsymbol{A}\boldsymbol{u}_2$. In $\mathbf{R}^3$, there are only two choices for the unit vector that is perpendicular to two independent vectors — the right-handed or the left-handed. Consequently, it must be that $\boldsymbol{n} = \pm\boldsymbol{u}_0$. So (5.20) and (5.21) are equivalent to the statement

$$\boldsymbol{A}\boldsymbol{u}_0 = \pm\boldsymbol{u}_0.$$

In the minus case, -1 is an eigenvalue of $\boldsymbol{A}$. For $\boldsymbol{A} \in SO(3)$ this is possible (think about a rotation by π about either of $\boldsymbol{u}_1$ or $\boldsymbol{u}_2$), but not true in general. On the other hand, in the plus case, $+1$ is an eigenvalue of $\boldsymbol{A}$. A matrix $\boldsymbol{A} \in SO(3)$ always has $+1$ as an eigenvalue. Consider, for any $\boldsymbol{A} \in SO(3)$,

$$\begin{aligned}
\det(\boldsymbol{A} - \boldsymbol{I}) &= \det(\boldsymbol{A} - \boldsymbol{A}\boldsymbol{A}^T) \\
&= \det(\boldsymbol{A}(\boldsymbol{I} - \boldsymbol{A}^T)) \\
&= \det \boldsymbol{A} \det(\boldsymbol{I} - \boldsymbol{A}^T) \\
&= \det(\boldsymbol{I} - \boldsymbol{A}^T) \\
&= \det(\boldsymbol{I} - \boldsymbol{A}) \\
&= (-1)^3 \det(\boldsymbol{A} - \boldsymbol{I}) \\
&= -\det(\boldsymbol{A} - \boldsymbol{I}).
\end{aligned}$$

Consequently, $\det(\boldsymbol{A} - \boldsymbol{I}) = 0$ in general, and (5.20) and (5.21) imply the original direction equation (5.1). Any solutions of (5.20) and (5.21) found where -1 is an eigenvalue, meaning $\det(\boldsymbol{A} + \boldsymbol{I}) = 0$, do not imply the R joint geometry and must be discarded.

With the preceding discussion in mind, wheel position analysis of the R joint

amounts to solving $\boldsymbol{f}(\boldsymbol{q}) = \boldsymbol{0}$ for a given value of z, where $\boldsymbol{q} := (\phi, \gamma, \delta, x, y)^T$ and

$$\boldsymbol{f}(\boldsymbol{q}) := \begin{pmatrix} \boldsymbol{A}\boldsymbol{u}_1 \cdot \boldsymbol{u}_0 \\ \boldsymbol{A}\boldsymbol{u}_2 \cdot \boldsymbol{u}_0 \\ \boldsymbol{A}\boldsymbol{x}_0 + \boldsymbol{b} - \boldsymbol{x}_0 \end{pmatrix}.$$

Recall that $\boldsymbol{A} = \boldsymbol{R}_{\boldsymbol{k},\delta}\boldsymbol{R}_{\boldsymbol{i},\gamma}\boldsymbol{R}_{\boldsymbol{j},\phi}$ and $\boldsymbol{b} = (x, y, z)^T$. Given a value for z and an estimated solution $\boldsymbol{q}_0$ for that value of z, a hopefully-better estimate of the solution is

$$\boldsymbol{q}_1 = \boldsymbol{q}_0 - (\boldsymbol{J}(\boldsymbol{q}_0))^{-1} \boldsymbol{f}(\boldsymbol{q}_0),$$

where $\boldsymbol{J}$ is the *Jacobian of* $\boldsymbol{f}$; in particular,

$$\boldsymbol{J} = \begin{pmatrix} \frac{\partial \boldsymbol{f}}{\partial \phi} & \frac{\partial \boldsymbol{f}}{\partial \gamma} & \frac{\partial \boldsymbol{f}}{\partial \delta} & \frac{\partial \boldsymbol{f}}{\partial x} & \frac{\partial \boldsymbol{f}}{\partial y} \end{pmatrix}.$$

Newton's method is to repeat this process until the estimated solution is sufficiently accurate:

$$\boldsymbol{q}_{n+1} = \boldsymbol{q}_n - (\boldsymbol{J}(\boldsymbol{q}_n))^{-1} \boldsymbol{f}(\boldsymbol{q}_n).$$

Obviously, the Jacobian at each step must be nonsingular for this simple root-finding algorithm to work. In practice, it is expensive and unnecessary to invert the Jacobian; rather, Gaussian elimination can be used to solve

$$(\boldsymbol{J}(\boldsymbol{q}_n))\,(\boldsymbol{q}_{n+1} - \boldsymbol{q}_n) = -\boldsymbol{f}(\boldsymbol{q}_n)$$

for the unknown $\boldsymbol{q}_{n+1} - \boldsymbol{q}_n$.

Convergence of Newton's method is, in general, not guaranteed, but is likely provided the initial estimate $\boldsymbol{q}_0$ is good. Here, it makes physical sense to start at the design position and work out to the maximum positive z-value, using the prior z-value's solution as the initial guess for the current z-value's solution. The same process can then be repeated, but instead working out to the most negative z-value from the design position. There is the related issue of the parameterization of $SO(3)$

breaking down — the case where $\gamma = \pm\pi/2$, where there is no difference between spin ϕ and toe δ. In this case, the Jacobian is singular and Newton's method fails. Fortunately, such extreme camber angles are physically unlikely, and the strategy of working outwards from the design position should prevent the estimated solutions for γ from ever approaching $\pm\pi/2$.

Velocity analysis is straightforward. After a solution for wheel position is found for a given value of z, the goal is to solve $\boldsymbol{f}'(\boldsymbol{q}) = \boldsymbol{0}$ for $\boldsymbol{q}'$. Using the chain rule,

$$\boldsymbol{f}'(\boldsymbol{q}) = \frac{\partial \boldsymbol{f}}{\partial \phi}\phi' + \frac{\partial \boldsymbol{f}}{\partial \gamma}\gamma' + \frac{\partial \boldsymbol{f}}{\partial \delta}\delta' + \frac{\partial \boldsymbol{f}}{\partial x}x' + \frac{\partial \boldsymbol{f}}{\partial y}y' + \frac{\partial \boldsymbol{f}}{\partial z} = \boldsymbol{J}\boldsymbol{q}' + \frac{\partial \boldsymbol{f}}{\partial z},$$

so one can simply solve for $\boldsymbol{q}'$ in

$$\boldsymbol{J}\boldsymbol{q}' = -\frac{\partial \boldsymbol{f}}{\partial z},$$

where $\boldsymbol{J}$ and $\partial \boldsymbol{f}/\partial z$ are evaluated at the current wheel position. In fact, the latter term is constant, being equal to $(0, 0, 0, 0, 1)^T$. With a complete set of values $\boldsymbol{q}$ and $\boldsymbol{q}'$ for a given z-value, the velocity characteristics of interest, namely, wheel-travel angle ε, support angle ε^*, and roll center height h, are easily computed.

5.4 Analysis Example

Consider the R joint synthesized earlier. Here, the resultant camber, toe, wheel-travel angle, support angle, and roll center height curves are compared to those desired initially.

Camber results are shown in Figure 5.3. The R joint motion specification guarantees the slope at $z = 0$ but nothing else. The camber angle does go negative with jounce and positive with rebound, but is more linear than quadratic. The progressive increase of negative camber with jounce is not achieved.

Toe results, Figure 5.4, show that the toe change rate at design is indeed achieved. Rather than the linear toe curve specified, which gives a predictable roll understeer effect, the R joint provides increasing toe change with jounce/rebound.

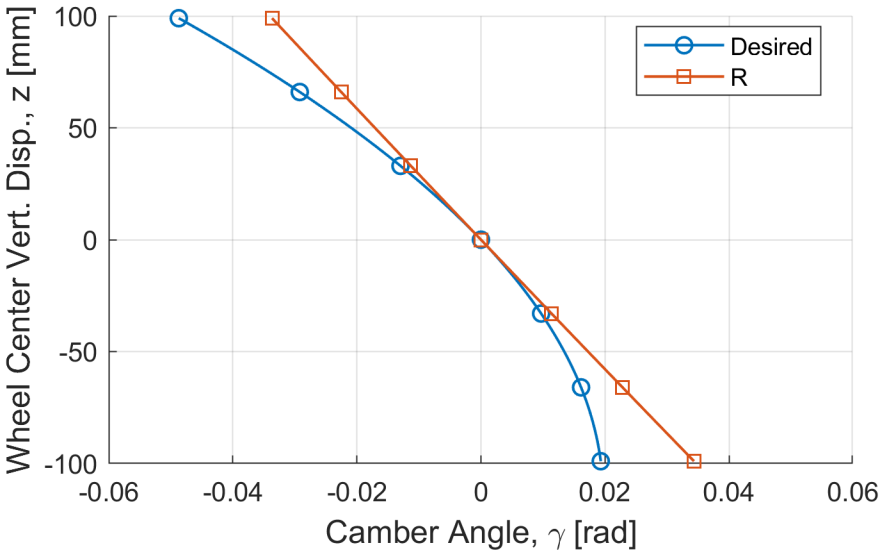

Figure 5.3. Camber curve for the synthesized R joint suspension.

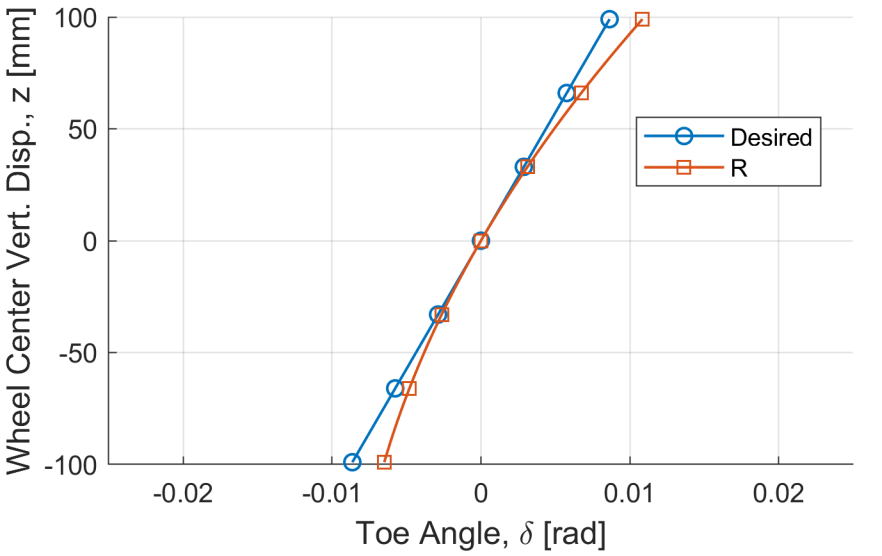

Figure 5.4. Toe curve for the synthesized R joint suspension.

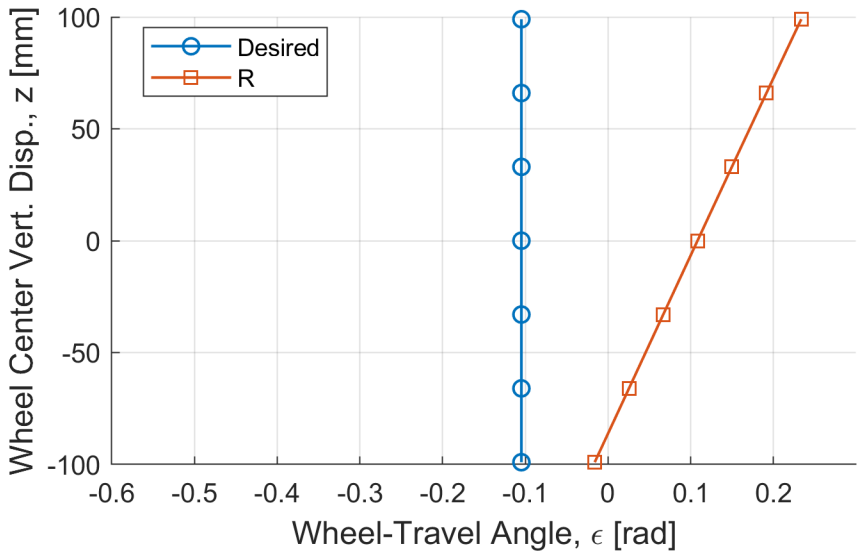

Figure 5.5. Wheel-travel angle curve for the synthesized R joint suspension.

Wheel-travel angle, Figure 5.5, is what had to be sacrificed to adapt the desired wheel trajectory to the geometry of the R joint. Consequently, the desired anti-squat behavior is completely lost, with a pro-squat behavior (positive wheel-travel angle) that increases with jounce. This would be a poor suspension to use for a rear wheel drive vehicle. If the rear wheels are not driven, there is no anti- or pro-squat effect. What a designer may worry about then is the fact that the wheel moves forward as it moves upward. This is bad for ride quality.

Support angle, Figure 5.6, is achieved at the design position. The effect here is anti-rise during braking. Support angle becomes increasingly negative with downward wheel travel; there is actually increasing anti-rise behavior with braking. This is not as specified but not necessarily bad.

For roll center height results, see Figure 5.7. The design position roll center height is achieved, as intended. Roll center height variation is qualitatively what it needs to be, decreasing with jounce and increasing with rebound; but, quantitatively, less roll center height variation is achieved than desired.

A different design-position velocity specification could be considered, but for a given choice, the packaging and kinematics of the R joint suspension are completely determined. There are no knobs to turn to make this suspension fit better or perform

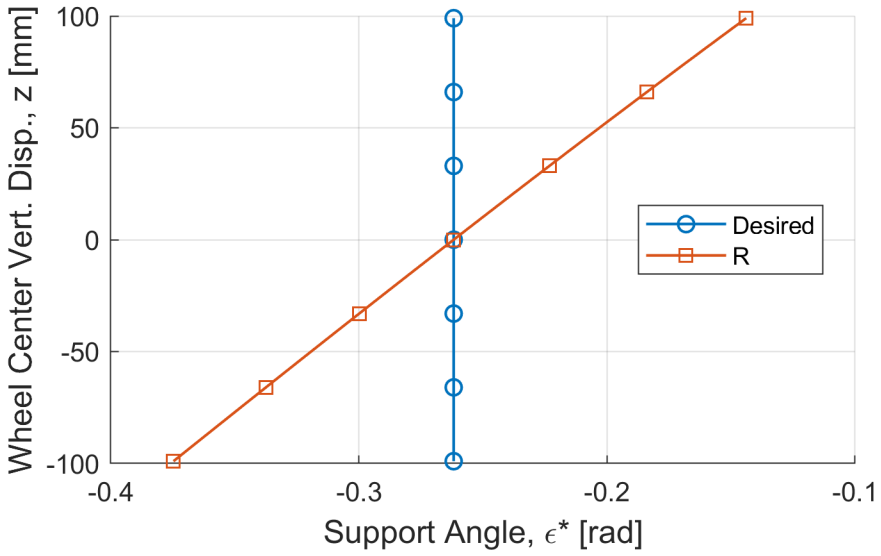

Figure 5.6. Support angle curve for the synthesized R joint suspension.

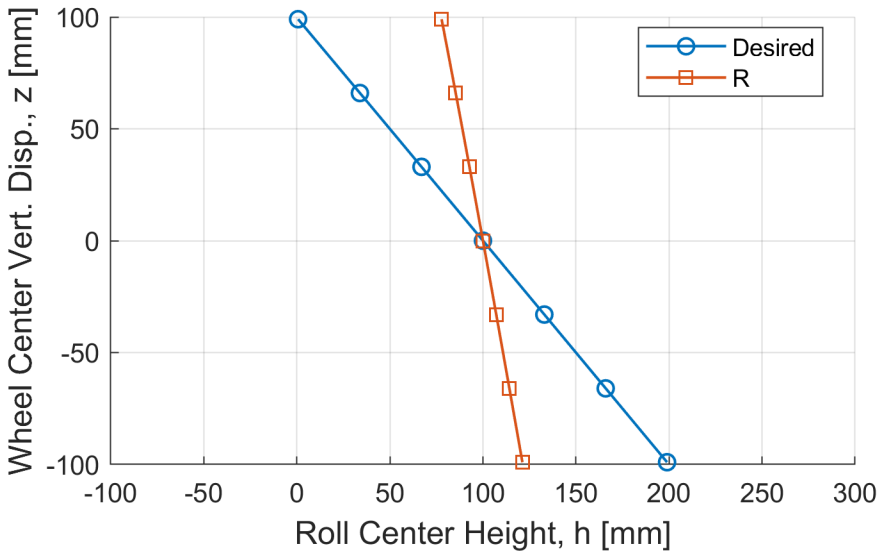

Figure 5.7. Roll center height curve for the synthesized R joint suspension.

better. The motion specification itself is already severely compromised, in that one can only guarantee camber change, toe change, support angle, and roll center height at design. Relaxing the motion specification any further makes little sense. Nevertheless, the R joint independent rear suspension is appealing in its simplicity and has had success in the marketplace; notably, it found a long-term home in the 1963 to 1993 Porsche 911. The market for these then, and now, does not seem to mind the design's compromised ride and handling!

Chapter 6

The S-S Link

6.1 Design Equations

The spherical-spherical (S-S) link indirectly connects the wheel carrier to the vehicle body. In the design position, the body-side S joint is to be located at $\boldsymbol{x}_0 \in \mathbf{R}^3$, while the wheel-side S joint is to be located at $\boldsymbol{x}_1 \in \mathbf{R}^3$. For a picture, see Figure 6.1. For a wheel motion from Position 1 (the design position) to Position i given by $\boldsymbol{A}_i \in SO(3)$ and $\boldsymbol{b}_i \in \mathbf{R}^3$, the distance between the wheel-side point $\boldsymbol{x}_i := \boldsymbol{A}_i\boldsymbol{x}_1 + \boldsymbol{b}_i$ and the fixed body-side point $\boldsymbol{x}_0$ must remain constant; equivalently,

$$(\boldsymbol{x}_i - \boldsymbol{x}_0) \cdot (\boldsymbol{x}_i - \boldsymbol{x}_0) = (\boldsymbol{x}_1 - \boldsymbol{x}_0) \cdot (\boldsymbol{x}_1 - \boldsymbol{x}_0).$$

Algebraic manipulation results in the equivalent and useful equation

$$\boldsymbol{x}_1^T(\boldsymbol{I} - \boldsymbol{A}_i^T)\boldsymbol{x}_0 + \boldsymbol{b}_i^T\boldsymbol{A}_i\boldsymbol{x}_1 - \boldsymbol{b}_i^T\boldsymbol{x}_0 + \boldsymbol{b}_i^T\boldsymbol{b}_i/2 = 0.$$

For $i = 2, 3, \ldots, 7$, there are six equations in six variables; up to seven wheel positions (includes the design position) can be specified for the S-S link. If the interest is in specifying wheel velocity, differentiating either form of the position equations results in

$$(\boldsymbol{\omega}_i \times (\boldsymbol{A}_i\boldsymbol{x}_1 + \boldsymbol{b}_i) + \boldsymbol{v}_i) \cdot (\boldsymbol{A}_i\boldsymbol{x}_1 + \boldsymbol{b}_i - \boldsymbol{x}_0) = 0,$$

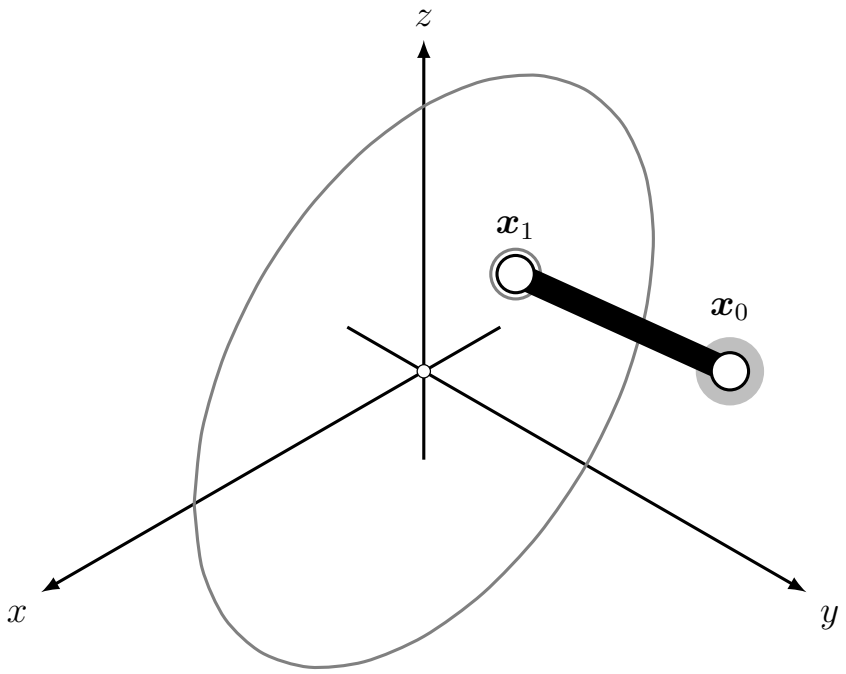

Figure 6.1. Depiction of an S-S link.

which just says that the velocity vector of $\boldsymbol{x}_i$ should be perpendicular to the link, which has direction $\boldsymbol{x}_i - \boldsymbol{x}_0$. To specify a velocity, an associated position must be specified. The design position is "free", so to specify the maximum number of velocities the following six design equations can be used: Velocity at Position 1, Position 2, Velocity at Position 2, Position 3, Velocity at Position 3, and Position 4. With the R joint synthesis, there was little flexibility. For the S-S link, as seen above, up to six equations can be written, ensuring whatever choice of various wheel positions and velocities. In general, specifying less than six equations allows a potentially-infinite number of compatible link geometries to be created. Consequently, there is no single representative synthesis example for the S-S link, like there was for the R joint. In this chapter, the focus is on S-S synthesis in the context of a five S-S link independent rear suspension. Examples in later chapters will include S-S link synthesis in other contexts.

A particularly attractive choice of design equations, especially for the five S-S link suspension, is the result of choosing design position velocity (Velocity at 1), a jounce position (Position 2), and a rebound position (Position 3). That is, $\boldsymbol{x}_0$ and $\boldsymbol{x}_1$ are

sought such that

$$(\boldsymbol{\omega}_1 \times \boldsymbol{x}_1 + \boldsymbol{v}_1) \cdot (\boldsymbol{x}_1 - \boldsymbol{x}_0) = 0$$
$$\boldsymbol{x}_1^T(\boldsymbol{I} - \boldsymbol{A}_i^T)\boldsymbol{x}_0 + \boldsymbol{b}_i^T\boldsymbol{A}_i\boldsymbol{x}_1 - \boldsymbol{b}_i^T\boldsymbol{x}_0 + \boldsymbol{b}_i^T\boldsymbol{b}_i/2 = 0;\ i = 2, 3.$$

An equivalent form of these equations is

$$\begin{pmatrix} (\boldsymbol{\omega}_1 \times \boldsymbol{x}_1 + \boldsymbol{v}_1)^T \\ (\boldsymbol{b}_2 - (\boldsymbol{I} - \boldsymbol{A}_2)\boldsymbol{x}_1)^T \\ (\boldsymbol{b}_3 - (\boldsymbol{I} - \boldsymbol{A}_3)\boldsymbol{x}_1)^T \end{pmatrix} \boldsymbol{x}_0 = \begin{pmatrix} (\boldsymbol{\omega}_1 \times \boldsymbol{x}_1 + \boldsymbol{v}_1)^T \boldsymbol{x}_1 \\ \boldsymbol{b}_2^T(\boldsymbol{A}_2\boldsymbol{x}_1 + \boldsymbol{b}_2/2) \\ \boldsymbol{b}_3^T(\boldsymbol{A}_3\boldsymbol{x}_1 + \boldsymbol{b}_3/2) \end{pmatrix}.$$

Consequently, for a choice of wheel-side S joint coordinate $\boldsymbol{x}_1$, body-side S joint coordinate $\boldsymbol{x}_0$ can be found by solving a system of linear equations. The attractiveness of this form of the S-S link design equations is due to this fact — in general, the design equations are systems of polynomial equations. More of the wheel's trajectory is specified than is traditional, which would only guarantee the design position velocity. The ability to have the specified wheel position z-values be symmetric about the design position is also attractive.

6.2 Synthesis Example

Here, the previously-defined rear wheel trajectory is used with the linear form of the design equations. Positions 2 and 3 are chosen as those of $z = \pm 25$ mm, respectively. To three significant figures,

$$\boldsymbol{\omega}_1 = \begin{pmatrix} -0.344 \\ 0.543 \\ 0.0873 \end{pmatrix} \times 10^{-3}\ [\text{mm}^{-1}] \text{ and } \boldsymbol{v}_1 = \begin{pmatrix} -0.105 \\ -0.0398 \\ 1.00 \end{pmatrix}.$$

The second wheel position has, to three significant figures,

$$\begin{pmatrix} \phi \\ \gamma \\ \delta \end{pmatrix} = \begin{pmatrix} 0.0136 \\ -0.00953 \\ 0.00218 \end{pmatrix} \text{ and } \boldsymbol{b}_2 = \begin{pmatrix} -2.63 \\ -0.257 \\ 25.0 \end{pmatrix} \text{ [mm]},$$

while the third wheel position has, again to three significant figures,

$$\begin{pmatrix} \phi \\ \gamma \\ \delta \end{pmatrix} = \begin{pmatrix} -0.0135 \\ 0.00765 \\ -0.00218 \end{pmatrix} \text{ and } \boldsymbol{b}_3 = \begin{pmatrix} 2.63 \\ 1.74 \\ -25.0 \end{pmatrix} \text{ [mm]}.$$

In order to use the linear form of the design equations, wheel-side S joint $\boldsymbol{x}_1$ must be specified. The strategy here is to establish a package space, discretize it, and solve for $\boldsymbol{x}_0$ for every discretized point in the space. The solutions for $\boldsymbol{x}_0$ that do not fit inside the space can then be discarded, leaving the solutions that satisfy both the design equations and the package space requirement. Here, the package space is chosen as the coordinate vectors

$$\{(x, y, z)^T \in \mathbf{R}^3 : -300 \leq x \leq 300, 0 \leq y \leq 600, -150 \leq z \leq 450\}.$$

This is a cube with dimension 600 mm, equal to the tire's diameter, as seen in Figure 6.2. The cube is easily discretized by considering 1 mm increments along each dimension, giving 601^3 or approximately 217 million grid points. The linear design equations can be solved for these grid points in parallel, reducing run times. Package spaces more interesting than a cube could of course be considered without much difficulty, but a cube suffices here. As for the choice of a 1 mm step size? According to Matschinsky, "...suspension design is in reality simply a hunt for millimetres..." [26].

Solving was done in MATLAB R2017b. The parallel for-loop *parfor* is handy when using MATLAB. The only case where the design equations had a singular matrix was when $\boldsymbol{x}_1 = \mathbf{0}$; consequently, $601^3 - 1$ link solutions were found. Of these, 4011018,

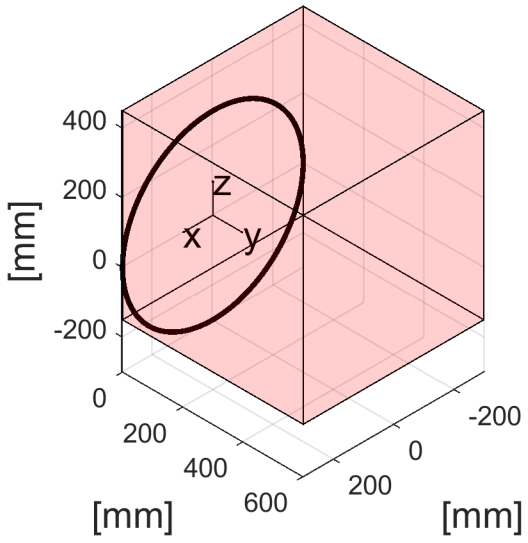

Figure 6.2. Package space allotted for the S-S link synthesis example.

or about 1.8%, fit inside the box. This set of packageable solutions is denoted by S. The solve process, including filtering based on package space, took about half an hour running in parallel on a 2014-model 2.20 GHz quad-core notebook PC.

It is hardly practical to visualize or work directly with S, due to its cardinality (four million plus!). Instead, it is helpful to think of S as a rich family of solutions that can be increasingly filtered until only what is preferred remains. In the next section, this *set-based design* approach is used to produce a viable five S-S link suspension.

Why not specify more of the wheel trajectory and produce a smaller family of solutions? Experience has shown that it is improbable that a "better" motion specification produces links that are packageable. For automobile suspension linkages, it seems the relevant advantage of the S-S link is not its ability to match more points and/or tangents of a wheel trajectory, but its ability to offer a uniquely large number of packageable solutions (compared to the other body-wheel connection types). These packageable solutions can then be pruned by concerns other than wheel kinematics, as seen in the next section.

6.3 Set-Based Design of the Five S-S Link Suspension

6.3.1 Links Packaging Inside a Wheel

Suppose the outer S joint is to lie within the rim of the wheel. This space, at its simplest, can be modeled as that inside a cylinder; for example,

$$\{(x, y, z)^T \in \mathbf{R}^3 : x^2 + z^2 < r_w^2, y_{\min} < y < y_{\max}\},$$

where r_w is the wheel's (inner) radius and $y_{\min}$ and $y_{\max}$ establish the depth of the available space inside the rim. For example, let $r_w = 150$ mm, $y_{\min} = 0$ mm, and $y_{\max} = 100$ mm. Searching the solutions S results in a set denoted by S_w, $|S_w| = 135873$.

6.3.2 Links Achieving a Certain Kingpin

To establish a steering axis, or *kingpin*, in the design position, designers may be interested in having the line through $\boldsymbol{x}_0$ and $\boldsymbol{x}_1$ intersect the kingpin. If a line ℓ_1 has equation $\boldsymbol{r} \times \boldsymbol{a}_1 = \boldsymbol{b}_1$ and a line ℓ_2 has equation $\boldsymbol{r} \times \boldsymbol{a}_2 = \boldsymbol{b}_2$, and the two lines are not parallel, then the least distance between them is equal to [42, §8.5, #9]

$$\pm \frac{\boldsymbol{b}_1 \cdot \boldsymbol{a}_2 + \boldsymbol{a}_1 \cdot \boldsymbol{b}_2}{|\boldsymbol{a}_1 \times \boldsymbol{a}_2|}. \tag{6.1}$$

What one can do is compute the least distance between each link and the desired kingpin. If the distance is zero, there is a true intersection; if the distance is within some tolerance (say, 0.1 mm), then there is a *de facto* intersection — good enough for present purposes, considering link geometry that guaranteed any particular kingpin was not solved for. (Of course, the kingpin requirement could have been included in the synthesis. It amounts to another design position velocity specification. But either the linearity of the design equations or a wheel position are lost.)

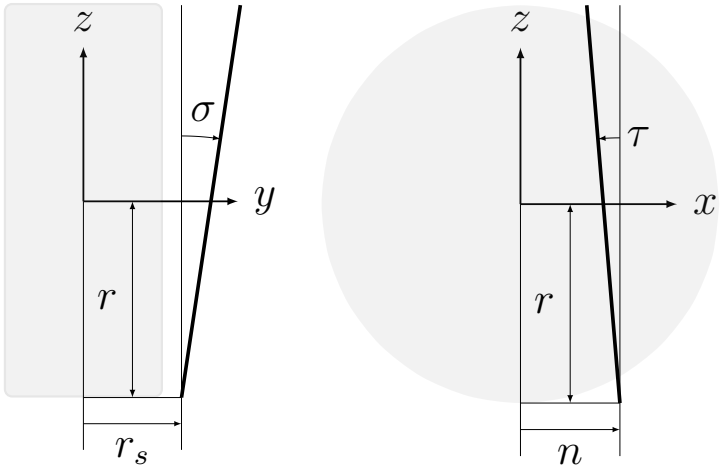

Figure 6.3. Kingpin geometry definition.

Equation (6.1) may now be translated into suspension geometry terminology. If ℓ_1 is the line through a link solution $\boldsymbol{x}_0$ and $\boldsymbol{x}_1$, then a choice for $\boldsymbol{a}_1$, its direction vector, is $\boldsymbol{x}_1 - \boldsymbol{x}_0$. The vector $\boldsymbol{b}_1$ is the *moment vector* of the line ℓ_1, found by crossing any point on the line with the chosen direction vector. Hence, let $\boldsymbol{b}_1 = \boldsymbol{x_1} \times (\boldsymbol{x}_1 - \boldsymbol{x}_0) = \boldsymbol{x}_0 \times \boldsymbol{x}_1$. For the kingpin, which will be line ℓ_2, consider the geometry of Figure 6.3. The kingpin is given by four parameters: kingpin inclination angle σ, positive when the kingpin leans toward the vehicle body; scrub radius r_s, positive when the kingpin/ground intersection is inboard of the wheel center; caster angle τ, positive when the kingpin leans rearward; and caster offset n, positive when the kingpin/ground intersection is ahead of the tire contact point. Consequently, a choice of direction vector for ℓ_2 is

$$\boldsymbol{a}_2 = \begin{pmatrix} -\tan\tau \\ \tan\sigma \\ 1 \end{pmatrix}.$$

A point on the kingpin is $(n, r_s, -r)^T$; the corresponding moment vector of ℓ_2 is

$$\boldsymbol{b}_2 = \begin{pmatrix} r\tan\sigma + r_s \\ r\tan\tau - n \\ r_s\tan\tau + n\tan\sigma \end{pmatrix}.$$

As an example, one can find link solutions with the simple kingpin geometry given by $\sigma = 0$, $r_s = 0$, $\tau = 0$, and $n = 0$. Consequently, $\boldsymbol{a}_2 = \boldsymbol{k}$ and $\boldsymbol{b}_2 = \boldsymbol{0}$. Searching the set S yields a set denoted by S_k with cardinality 1284. The de facto intersection tolerance was set to 0.1 mm.

6.3.3 Links Achieving the Desired Plan View Angle

Designers may have an interest in specifying the *plan view angle*, which is the angle between the S-S link and the lateral ($\boldsymbol{j}$) direction when the link is projected onto a plan view ($\boldsymbol{k}$-normal) plane. The plan view angle is considered positive when the body-side point $\boldsymbol{x}_0$ is ahead of the wheel-side point $\boldsymbol{x}_1$ in the plan view. The plan view angle, denoted by α, can be computed as

$$\alpha = \arctan \frac{(\boldsymbol{x}_0 - \boldsymbol{x}_1) \cdot \boldsymbol{i}}{(\boldsymbol{x}_0 - \boldsymbol{x}_1) \cdot \boldsymbol{j}}.$$

For example, suppose the desire is plan view angle α_1, where $-5^\circ \leq \alpha_1 \leq 0^\circ$. Searching S results in the set denoted by S_{α_1}, $|S_{\alpha_1}| = 174759$. For the five S-S link suspension, there may be several plan view angles of interest. For α_2, $25^\circ \leq \alpha_2 \leq 30^\circ$, there is S_{α_2}, with size 146320; whereas for α_3, $0^\circ \leq \alpha_3 \leq 5^\circ$, there is S_{α_3}, $|S_{\alpha_3}| = 170668$.

6.3.4 Links at a Certain Coordinate

Of course, one can search for link solutions that match all or part of the desired coordinates of the S joints. For example, suppose solutions that have $x_1 \geq 100$ and $z_1 = 0$ are wanted, where $\boldsymbol{x}_1 = (x_1, y_1, z_1)^T$. Searching S for this condition results in the set denoted by S_c, with $|S_c| = 2140$.

6.3.5 Link Types Based on Set Intersections

A typical five S-S link independent suspension linkage is constructed with a pair of upper links, a pair of lower links, and a separate fifth link [18]. Each of the upper and

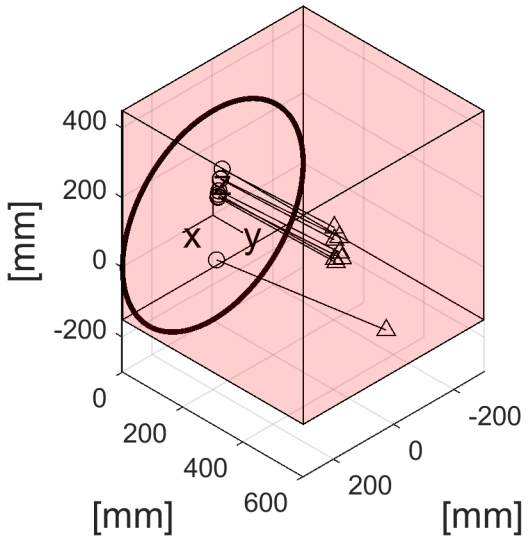

Figure 6.4. Plot of the back links S_b.

lower pairs aims towards the intended kingpin, with the links angling toward each other in the plan view. The fifth link, also called the toe link, is at the height of the wheel center; it can be either ahead or behind the wheel center. Here, define *back links* as

$$S_b := S_w \cap S_k \cap S_{\alpha_1},$$

front links as

$$S_f := S_w \cap S_k \cap S_{\alpha_2},$$

and *toe links* as

$$S_t := S_w \cap S_{\alpha_3} \cap S_c.$$

There are 8 back links (Figure 6.4), 12 front links (Figure 6.5), and 14 toe links (Figure 6.6). The fixed, body-side point is plotted with the triangular marker.

6.3.6 Choosing Five Links by Minimizing Reaction Loads

To get down to the final five links, the strategy is to choose five such that the reaction forces in the linkage are minimized. After all, lower loads mean less material and less mass. This means choosing two from S_b, two from S_f, and one from S_t. Consequently,

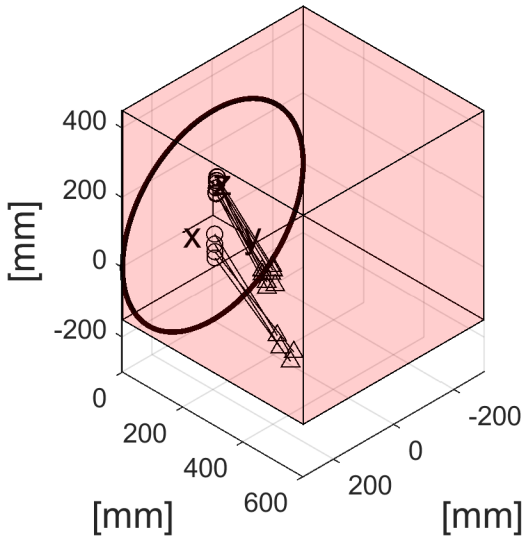

Figure 6.5. Plot of the front links S_f.

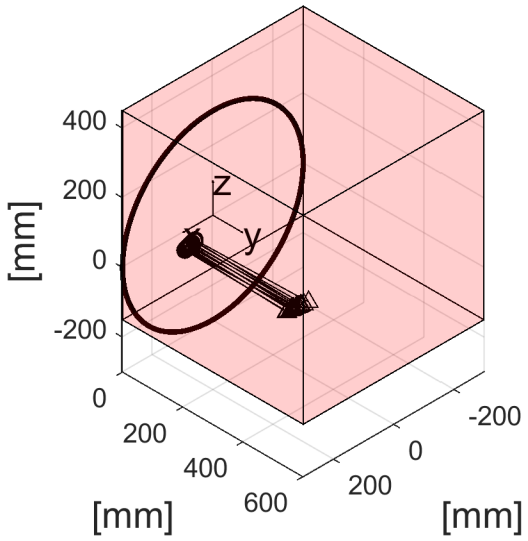

Figure 6.6. Plot of the toe links S_t.

there are

$$(|S_b| \text{ choose } 2) \times (|S_f| \text{ choose } 2) \times |S_t| = 28 \times 66 \times 14 = 25872$$

possible five link suspensions here. For each of these, the link reaction loads from a force at the tire contact point can be determined as follows.

Let $\boldsymbol{F} = (F_x, F_y, F_z)^T$ be the force at the design position tire contact point, which has coordinates $\boldsymbol{c}(0) = (0, 0, -r)^T$. The components F_x and F_y are specifiable, whereas F_z is an unknown. This is because the wheel is wanted to be in static equilibrium, when it would otherwise accelerate vertically because it has that degree-of-freedom. So F_z that ensures static equilibrium can be solved for. The reaction force of the ith link ($i = 1, 2, \ldots, 5$) is

$$\lambda_i(\boldsymbol{x}_1^{(i)} - \boldsymbol{x}_0^{(i)}),$$

where λ_i is unknown. Consequently, the magnitude of the reaction force is $\lambda_i|\boldsymbol{x}_1^{(i)} - \boldsymbol{x}_0^{(i)}|$. Conditions for static equilibrium of the wheel are that the net moment about the tire contact point is zero and that the net force is zero. The first of these conditions gives

$$\sum_{i=1}^{5}(\boldsymbol{x}_1^{(i)} - \boldsymbol{c}(0)) \times \lambda_i(\boldsymbol{x}_1^{(i)} - \boldsymbol{x}_0^{(i)}) = \boldsymbol{0},$$

while the second static equilibrium condition gives

$$\boldsymbol{F} + \sum_{i=1}^{5} \lambda_i(\boldsymbol{x}_1^{(i)} - \boldsymbol{x}_0^{(i)}) = \boldsymbol{0}.$$

All together, this is a system of six linear equations with six unknowns $\lambda_1, \ldots, \lambda_5$ and F_z. After solving, the *cost* is computed, defined as

$$\sum_{i=1}^{5}(\lambda_i|\boldsymbol{x}_1^{(i)} - \boldsymbol{x}_0^{(i)}|)^2.$$

That is, the sum of the squares of the reaction force magnitudes. Once the cost for

Table 6.1. Coordinates of the five S-S link example (three significant figures).

	Back Lower	Back Upper	Front Lower	Front Upper	Toe
x_0	-46.0	-25.0	261	214	170
y_0	530	378	519	378	415
z_0	-88.1	142	-29.6	138	14.2
x_1	-1.00	-2.00	7.00	17.0	143
y_1	11.0	29.0	14.0	30.0	53.0
z_1	-123	146	-112	134	0.00

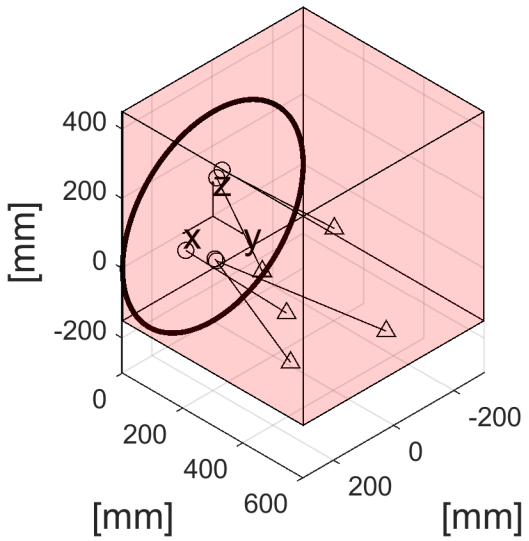

Figure 6.7. Plot of the assembled five S-S link suspension.

each of the possible choices of five links is known, the one with minimum cost can be chosen.

Here, values $F_x = -1000$ N and $F_y = 1000$ N are selected; that is, the linkage is optimized for a combined braking and cornering load. The coordinates of the linkage are given in Table 6.1; the linkage is plotted in Figure 6.7.

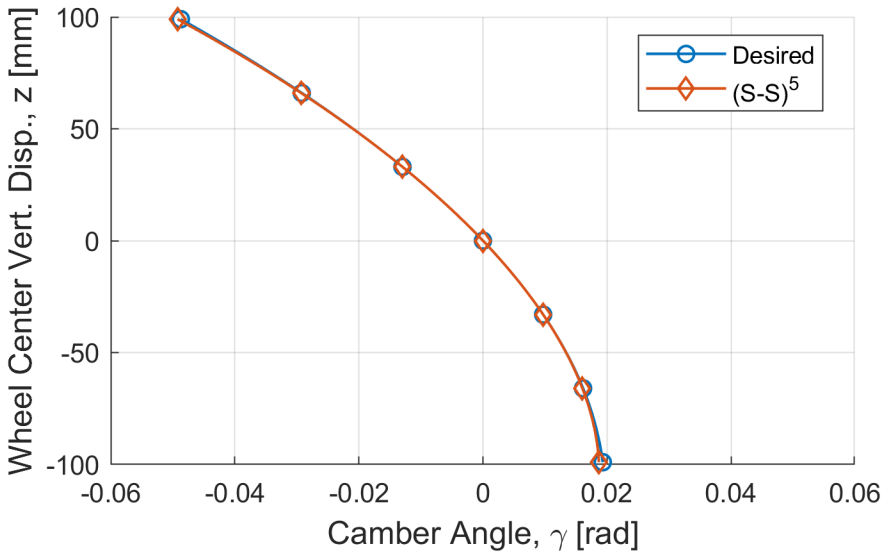

Figure 6.8. Camber curve for the synthesized five link suspension.

6.4 Analysis of the Five S-S Link Suspension

The same approach used for analyzing the R joint suspension can be used for the five link suspension. Here,

$$\boldsymbol{f}(\boldsymbol{q}) = \begin{pmatrix} \left(\boldsymbol{x}_1^{(1)}\right)^T (\boldsymbol{I} - \boldsymbol{A}^T)\boldsymbol{x}_0^{(1)} + \boldsymbol{b}^T\boldsymbol{A}\boldsymbol{x}_1^{(1)} - \boldsymbol{b}^T\boldsymbol{x}_0^{(1)} + \boldsymbol{b}^T\boldsymbol{b}/2 \\ \left(\boldsymbol{x}_1^{(2)}\right)^T (\boldsymbol{I} - \boldsymbol{A}^T)\boldsymbol{x}_0^{(2)} + \boldsymbol{b}^T\boldsymbol{A}\boldsymbol{x}_1^{(2)} - \boldsymbol{b}^T\boldsymbol{x}_0^{(2)} + \boldsymbol{b}^T\boldsymbol{b}/2 \\ \vdots \\ \left(\boldsymbol{x}_1^{(5)}\right)^T (\boldsymbol{I} - \boldsymbol{A}^T)\boldsymbol{x}_0^{(5)} + \boldsymbol{b}^T\boldsymbol{A}\boldsymbol{x}_1^{(5)} - \boldsymbol{b}^T\boldsymbol{x}_0^{(5)} + \boldsymbol{b}^T\boldsymbol{b}/2 \end{pmatrix}.$$

Despite only specifying design position velocity and the two positions of $z = \pm 25$, the synthesized suspension produces wheel motion very close to desired — it is difficult to tell the actual versus desired curves apart in the plots. Camber results are shown in Figure 6.8. Toe results, Figure 6.9. For wheel-travel angle, see Figure 6.10. Support angle is shown in Figure 6.11. For roll center height results, see Figure 6.12. The five link suspension offers excellent kinematic performance and considerable flexibility in its packaging. Mercedes-Benz pioneered the five link suspension for production cars, as discussed in the introduction.

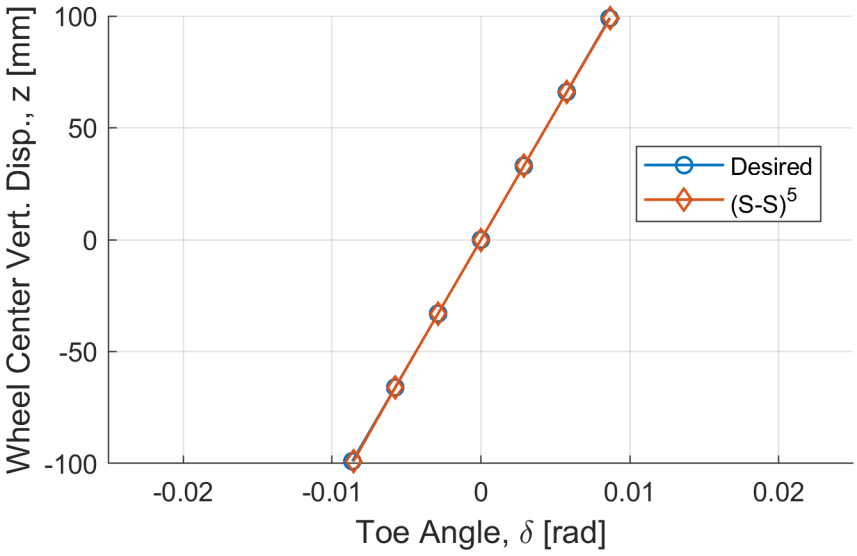

Figure 6.9. Toe curve for the synthesized five link suspension.

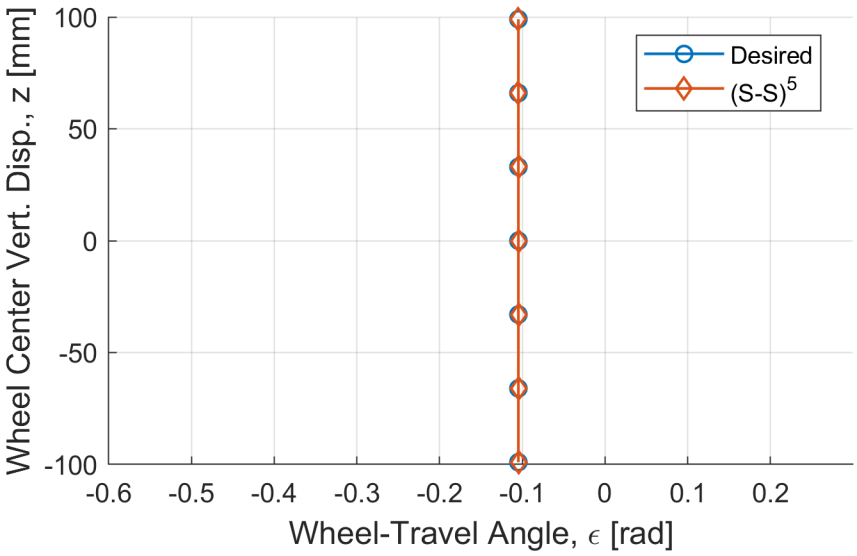

Figure 6.10. Wheel-travel angle curve for the synthesized five link suspension.

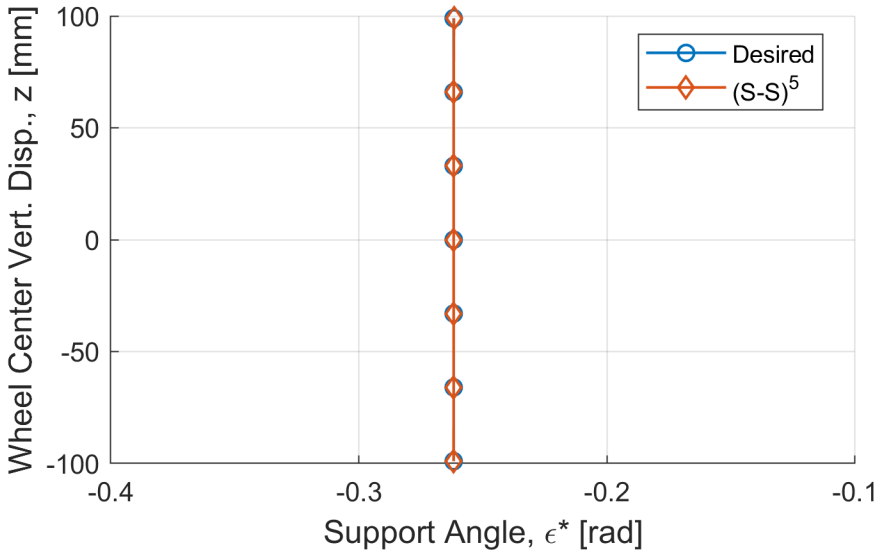

Figure 6.11. Support angle curve for the synthesized five link suspension.

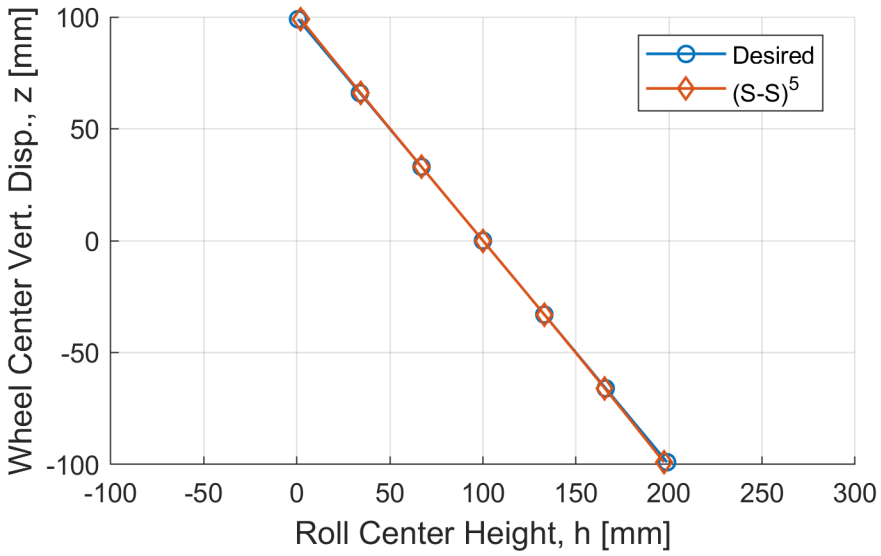

Figure 6.12. Roll center height curve for the synthesized five link suspension.

Chapter 7

The C Joint

7.1 Synthesis

The cylindrical (C) joint directly connects the wheel carrier to the vehicle body. A stylized drawing is shown in Figure 7.1. The C joint allows both translation along and rotation about an axis. Here the search is for $\boldsymbol{u}_0 \in \mathbf{R}^3$, giving the axis's direction, and $\boldsymbol{x}_0 \in \mathbf{R}^3$, giving a point on the axis. For a wheel motion given by $\boldsymbol{A} \in SO(3)$ and $\boldsymbol{b} \in \mathbf{R}^3$, it is required that $\boldsymbol{u}_0$ is invariant:

$$\boldsymbol{A}\boldsymbol{u}_0 = \boldsymbol{u}_0,$$

and that the vector between $\boldsymbol{x}_0$ and its displaced position remains parallel to the C joint axis:

$$(\boldsymbol{A}\boldsymbol{x}_0 + \boldsymbol{b} - \boldsymbol{x}_0) \times \boldsymbol{u}_0 = \mathbf{0}.$$

Only one wheel motion can be prescribed (one wheel position other than design); there are four independent design equations and four independent design variables. Of course, velocity can be specified instead, with angular velocity $\boldsymbol{\omega} \in \mathbf{R}^3$ and velocity $\boldsymbol{v} \in \mathbf{R}^3$ of the wheel at its point passing through the origin. Differentiation of the position equations results in

$$\boldsymbol{\omega} \times \boldsymbol{A}\boldsymbol{u}_0 = \mathbf{0}$$

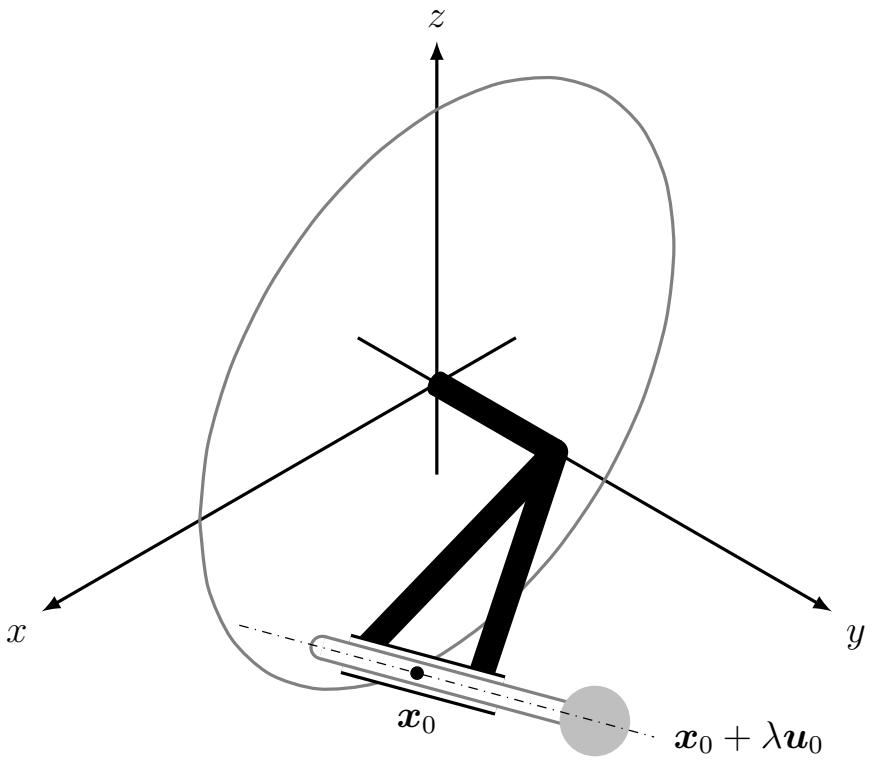

Figure 7.1. Stylized drawing of a C joint.

and

$$(\boldsymbol{\omega} \times (\boldsymbol{A}\boldsymbol{x}_0 + \boldsymbol{b}) + \boldsymbol{v}) \times \boldsymbol{u}_0 = \boldsymbol{0}.$$

The first velocity equation requires that the angular velocity vector of the wheel be parallel to the C joint axis. The second velocity equation requires that the velocity of the point $\boldsymbol{A}\boldsymbol{x}_0 + \boldsymbol{b}$ be parallel to the C joint axis. In the design position, $\boldsymbol{A} = \boldsymbol{I}$ and $\boldsymbol{b} = \boldsymbol{0}$, so that a solution for the vector $\boldsymbol{u}_0$ is

$$\boldsymbol{u}_0 = \boldsymbol{\omega}/|\boldsymbol{\omega}|.$$

A solution for $\boldsymbol{x}_0$ is found by substituting this result into the second velocity equation as follows:

$$\begin{aligned}(\boldsymbol{\omega} \times \boldsymbol{x}_0 + \boldsymbol{v}) \times \boldsymbol{\omega}/|\boldsymbol{\omega}| &= \mathbf{0} \\ (\boldsymbol{\omega} \times \boldsymbol{x}_0) \times \boldsymbol{\omega} + \boldsymbol{v} \times \boldsymbol{\omega} &= \mathbf{0} \\ -(\boldsymbol{\omega} \cdot \boldsymbol{x}_0)\boldsymbol{\omega} + (\boldsymbol{\omega} \cdot \boldsymbol{\omega})\boldsymbol{x}_0 + \boldsymbol{v} \times \boldsymbol{\omega} &= \mathbf{0}.\end{aligned}$$

If $\boldsymbol{x}_0$ is assumed to be the point on the axis closest to the origin, then $\boldsymbol{\omega} \cdot \boldsymbol{x}_0 = 0$ and

$$\boldsymbol{x}_0 = \frac{\boldsymbol{\omega} \times \boldsymbol{v}}{\boldsymbol{\omega} \cdot \boldsymbol{\omega}}.$$

Notice that the solutions for $\boldsymbol{u}_0$ and $\boldsymbol{x}_0$ are the same as for the R joint. However, there is a key difference: the C joint does not require that $\boldsymbol{\omega} \cdot \boldsymbol{v} = 0$. This is because the C joint allows a general rigid body, or screw, motion. The R joint cannot translate as it rotates. As such, the C joint can use the full design position velocity specification, making it better-suited for driven axles.

7.2 Synthesis Example

The design position wheel velocity is specified from the same trajectory used throughout. In particular, to three significant figures, the angular velocity is

$$\boldsymbol{\omega}(0) = \begin{pmatrix} -0.344 \\ 0.543 \\ 0.0873 \end{pmatrix} \times 10^{-3} \text{ [mm}^{-1}\text{]},$$

and the velocity of the wheel center (which is the point on the wheel at the origin) is, to three significant figures,

$$\boldsymbol{v}(0) = \begin{pmatrix} -0.105 \\ -0.0398 \\ 1.00 \end{pmatrix}.$$

These result in the following solutions for $\boldsymbol{u}_0$ and $\boldsymbol{x}_0$, again to three significant figures:

$$\boldsymbol{u}_0 = \begin{pmatrix} -0.530 \\ 0.837 \\ 0.135 \end{pmatrix} \text{ [mm]},$$

$$\boldsymbol{x}_0 = \begin{pmatrix} 1300 \\ 796 \\ 168 \end{pmatrix} \text{ [mm]}.$$

The C joint axis is in the "semi-trailing" position, Figure 7.2, mostly in an xy plane and well ahead of the wheel center. This positioning makes the implementation of this joint with a telescopic damper unlikely, as large changes in jounce/rebound will cause only small changes in the wheel's position along the joint axis. Here, the need for a separate, vertically-placed damper as on the R joint suspension reduces the appeal of the C joint. Historically, C joints were used in the *sliding pillar* front suspension, where the C joint *was* oriented vertically, allowing both jounce/rebound travel and serving as the steering axis. It is impossible to specify the full design position velocity and the steering axis at the same time, so extreme compromise is necessary if this arrangement is intended. As such, the C joint is near irrelevant for steered axles, mostly appealing nowadays as a rear suspension offering improved wheel kinematics over the R joint. Unlike the R joint, the C joint needs another wheel-body connection to form a complete suspension — the C joint has two DOFs, after all. As enumerated in the number synthesis chapter, the necessary additional connection is the S-S link. Next, methods for dimensioning such a link are shown.

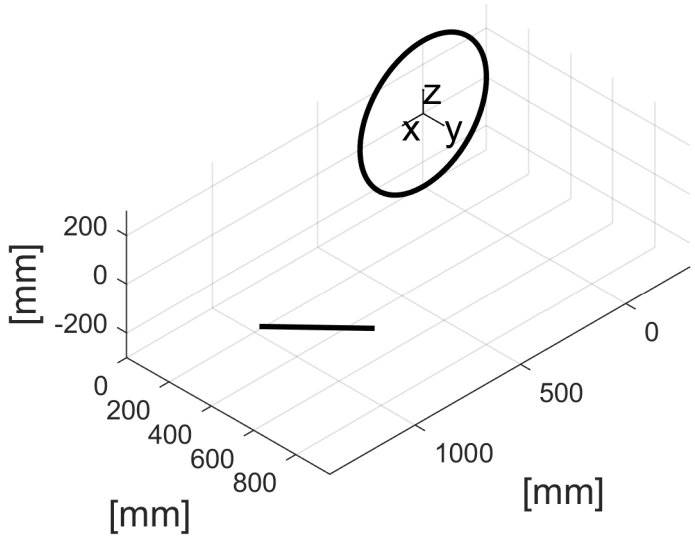

Figure 7.2. Synthesized example of a C joint.

7.3 An S-S Link for the C Joint

At the very least, one could synthesize an S-S link that guarantees the desired design position velocity. If $\boldsymbol{x}_1 \in \mathbf{R}^3$ locates the wheel-side S joint and $\boldsymbol{x}_0^{(2)} \in \mathbf{R}^3$ locates the body-side S joint, then then the design position velocity given by $\boldsymbol{\omega} \in \mathbf{R}^3$ and $\boldsymbol{v} \in \mathbf{R}^3$ is ensured if

$$(\boldsymbol{\omega} \times \boldsymbol{x}_1 + \boldsymbol{v}) \cdot (\boldsymbol{x}_1 - \boldsymbol{x}_0^{(2)}) = 0.$$

Unfortunately, this approach leaves the S-S link quite underdetermined, since it has six design variables and this is but one design equation. Can one somehow specify more of the wheel's trajectory, while maintaining compatibility with the C joint geometry?

A point $\boldsymbol{q} \in \mathbf{R}^3$ on the wheel is mapped by C joint motion to

$$\boldsymbol{R}_{\boldsymbol{u}_0,\theta}(\boldsymbol{q} - \boldsymbol{x}_0) + \boldsymbol{x}_0 + d\boldsymbol{u}_0,$$

where θ is the angle of rotation about the C joint and d is the displacement along the joint. This means that the special orthogonal part of the C joint motion is $\boldsymbol{R}_{\boldsymbol{u}_0,\theta}$, while the translation part is $(\boldsymbol{I} - \boldsymbol{R}_{\boldsymbol{u}_0,\theta})\boldsymbol{x}_0 + d\boldsymbol{u}_0$. Can θ and d be found that result in

a C joint motion close to a desired motion? In particular, suppose there is a desired wheel motion given by $\boldsymbol{A} \in SO(3)$ and $\boldsymbol{b} \in \mathbf{R}^3$. In general, there are not solutions for θ and d that make $\boldsymbol{A} = \boldsymbol{R}_{\boldsymbol{u}_0,\theta}$ and $\boldsymbol{b} = (\boldsymbol{I} - \boldsymbol{R}_{\boldsymbol{u}_0,\theta})\boldsymbol{x}_0 + d\boldsymbol{u}_0$. However, what about θ and d that result in a wheel motion that is *as close as possible* to the desired?

Begin with θ such that the difference between $\boldsymbol{R}_{\boldsymbol{u}_0,\theta}$ and $\boldsymbol{A}$ is as small as possible. A suitable distance metric on $SO(3)$ is, for $\boldsymbol{A}_1, \boldsymbol{A}_2 \in SO(3)$,

$$\|\boldsymbol{I} - \boldsymbol{A}_1\boldsymbol{A}_2^T\|_F,$$

where F indicates the *Frobenius norm*. See [19]. For a real matrix $\boldsymbol{B}$, this norm can be computed as follows:

$$\|\boldsymbol{B}\|_F = \sqrt{\operatorname{tr}(\boldsymbol{B}^T\boldsymbol{B})}.$$

Some algebraic manipulation shows that

$$\|\boldsymbol{I} - \boldsymbol{A}_1\boldsymbol{A}_2^T\|_F = \sqrt{2(3 - \operatorname{tr}(\boldsymbol{A}_1\boldsymbol{A}_2^T))}.$$

As such, there is the following problem:

$$\min_{\theta \in \mathbf{R}} f(\theta)$$

where $f(\theta) = 3 - \operatorname{tr}(\boldsymbol{R}_{\boldsymbol{u}_0,\theta}\boldsymbol{A}^T)$. Using the facts that $\boldsymbol{R}_{\boldsymbol{u}_0,\theta} = \boldsymbol{I} + \sin\theta\tilde{\boldsymbol{u}}_0 + (1 - \cos\theta)\tilde{\boldsymbol{u}}_0^2$ and $\tilde{\boldsymbol{u}}_0$ is skew symmetric together with some properties of the trace operator,

$$f(\theta) = 3 - \operatorname{tr}(\boldsymbol{A}) + \sin\theta \operatorname{tr}(\boldsymbol{A}\tilde{\boldsymbol{u}}_0) - (1 - \cos\theta)\operatorname{tr}(\boldsymbol{A}\tilde{\boldsymbol{u}}_0^2).$$

As such, the derivative of $f(\theta)$ with respect to θ is

$$\frac{df}{d\theta} = \cos\theta \operatorname{tr}(\boldsymbol{A}\tilde{\boldsymbol{u}}_0) - \sin\theta \operatorname{tr}(\boldsymbol{A}\tilde{\boldsymbol{u}}_0^2),$$

giving a critical point of

$$\theta = \arctan\left(\frac{\operatorname{tr}(\boldsymbol{A}\tilde{\boldsymbol{u}}_0)}{\operatorname{tr}(\boldsymbol{A}\tilde{\boldsymbol{u}}_0^2)}\right).$$

In practice it can be verified if this is a minimum via the first derivative test.

Now consider displacement d. In this case, there is the following problem:

$$\min_{d \in \mathbf{R}} g(d)$$

where

$$g(d) = |(\boldsymbol{I} - \boldsymbol{R}_{\boldsymbol{u}_0,\theta})\boldsymbol{x}_0 + d\boldsymbol{u}_0 - \boldsymbol{b}|^2.$$

Let $\boldsymbol{a} := (\boldsymbol{I} - \boldsymbol{R}_{\boldsymbol{u}_0,\theta})\boldsymbol{x}_0 - \boldsymbol{b}$. Then

$$\frac{dg}{dd} = 2\boldsymbol{a} \cdot \boldsymbol{u}_0 + 2d$$

giving a critical point of

$$d = -\boldsymbol{a} \cdot \boldsymbol{u}_0.$$

Again, whether or not this is a local minimum can be verified in practice.

With solutions for θ and d, the general wheel motion given by $\boldsymbol{A} \in SO(3)$ and $\boldsymbol{b} \in \mathbf{R}^3$ can now be replaced with the one closest to it that is compatible with the C joint:

$$\begin{aligned} \boldsymbol{A}^{(C)} &:= \boldsymbol{R}_{\boldsymbol{u}_0,\theta} \\ \boldsymbol{b}^{(C)} &:= (\boldsymbol{I} - \boldsymbol{R}_{\boldsymbol{u}_0,\theta})\boldsymbol{x}_0 + d\boldsymbol{u}_0 \end{aligned}$$

What can be done now is synthesize an S-S link for design position velocity, a jounce position, and a rebound position, as done in the S-S link chapter:

$$\begin{pmatrix} (\boldsymbol{\omega}_1 \times \boldsymbol{x}_1 + \boldsymbol{v}_1)^T \\ \left(\boldsymbol{b}_2^{(C)} - (\boldsymbol{I} - \boldsymbol{A}_2^{(C)})\boldsymbol{x}_1\right)^T \\ \left(\boldsymbol{b}_3^{(C)} - (\boldsymbol{I} - \boldsymbol{A}_3^{(C)})\boldsymbol{x}_1\right)^T \end{pmatrix} \boldsymbol{x}_0^{(2)} = \begin{pmatrix} (\boldsymbol{\omega}_1 \times \boldsymbol{x}_1 + \boldsymbol{v}_1)^T \boldsymbol{x}_1 \\ (\boldsymbol{b}_2^{(C)})^T(\boldsymbol{A}_2^{(C)}\boldsymbol{x}_1 + \boldsymbol{b}_2^{(C)}/2) \\ (\boldsymbol{b}_3^{(C)})^T(\boldsymbol{A}_3^{(C)}\boldsymbol{x}_1 + \boldsymbol{b}_3^{(C)}/2) \end{pmatrix}.$$

The key is that the extra wheel positions honor the C joint geometry!

7.4 C(S-S) Example

To construct an example C(S-S) the C joint solution can be combined with a suitable S-S link. The S-S link synthesis method described above is used. Positions 2 and 3 are chosen as $z = 25$ mm and $z = -25$ mm, respectively, as for the five link suspension. These result in $\theta_2 = 0.0167$, $d_2 = 4.54$ mm and $\theta_3 = -0.0157$, $d_3 = -3.30$ mm (all printed to three significant figures). The same packaging cube as the five link suspension is employed, letting $\boldsymbol{x}_1$ take values according to a discretization with a one millimeter step size in all directions. Unfortunately, none of the link solutions fit inside the cube. Instead the shortest of the link solutions is selected, which has

$$\boldsymbol{x}_1 = \begin{pmatrix} 300 \\ 600 \\ 218 \end{pmatrix} \text{ [mm]}$$

and, to three significant figures,

$$\boldsymbol{x}_0^{(2)} = \begin{pmatrix} 1380 \\ 1210 \\ 225 \end{pmatrix} \text{ [mm].}$$

The solution is plotted in Figure 7.3. The fixed, body-side point is plotted with the triangular marker.

Analysis of the C(S-S) example requires the kinematic constraint equations $\boldsymbol{f}(\boldsymbol{q}) = \boldsymbol{0}$ as in the previous chapters. To produce four independent equations from the six C joint position equations, construct and utilize a right-handed, orthonormal basis

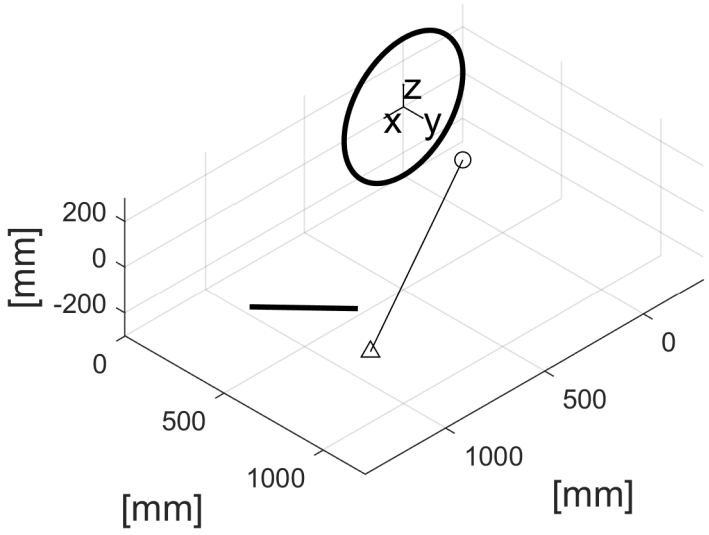

Figure 7.3. Synthesized C(S-S) suspension.

$\{\boldsymbol{u}_0, \boldsymbol{u}_1, \boldsymbol{u}_2\}$ as done for the R joint. As such,

$$\boldsymbol{f} = \begin{pmatrix} \boldsymbol{A}\boldsymbol{u}_1 \cdot \boldsymbol{u}_0 \\ \boldsymbol{A}\boldsymbol{u}_2 \cdot \boldsymbol{u}_0 \\ \boldsymbol{A}\boldsymbol{u}_1 \cdot (\boldsymbol{A}\boldsymbol{x}_0 + \boldsymbol{b} - \boldsymbol{x}_0) \\ \boldsymbol{A}\boldsymbol{u}_2 \cdot (\boldsymbol{A}\boldsymbol{x}_0 + \boldsymbol{b} - \boldsymbol{x}_0) \\ \boldsymbol{x}_1^T(\boldsymbol{I} - \boldsymbol{A}^T)\boldsymbol{x}_0^{(2)} + \boldsymbol{b}^T\boldsymbol{A}\boldsymbol{x}_1 - \boldsymbol{b}^T\boldsymbol{x}_0^{(2)} + \boldsymbol{b}^T\boldsymbol{b}/2 \end{pmatrix}.$$

Camber results are shown in Figure 7.4. The camber change appears constant, not progressive as desired. Toe results, Figure 7.5. The toe curve is slightly nonlinear. Wheel-travel angle, Figure 7.6, is achieved at design and changes very little in jounce. Wheel-travel angle mainly matters in jounce, for driven wheels, corresponding to squatting of the rear end under acceleration. The fact that changes in wheel-travel angle are small in this jounce region is good. Support angle is shown in Figure 7.7. Negative support angle for an outboard-braked rear wheel indicates reduced lifting of the rear end when braking. Here, as the rear end lifts (or the wheel moves down with respect to the vehicle body), support angle becomes less negative, indicating decreasing anti-rise behavior. This is is not ideal. For roll center height results, see Figure 7.8. The roll center height changes more quickly than desired, especially in

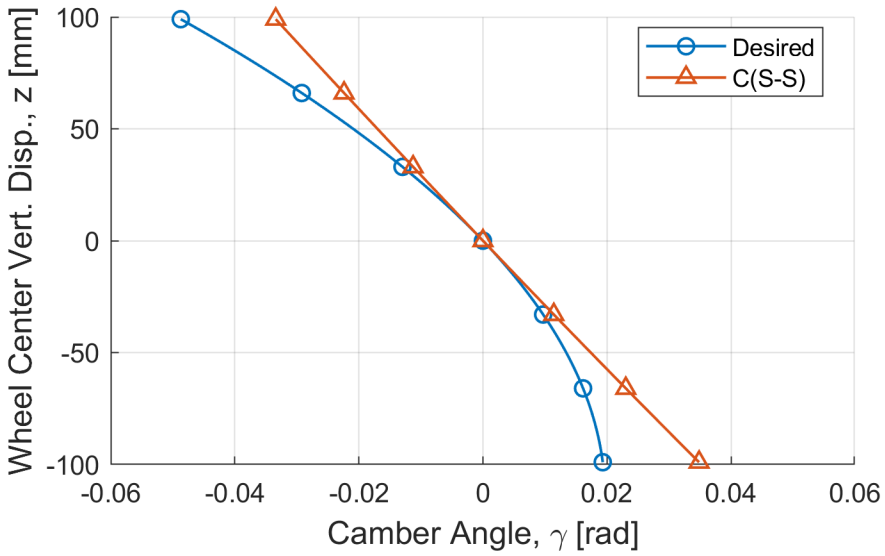

Figure 7.4. Camber curve for the synthesized C(S-S) suspension.

rebound.

A commercial example of the C(S-S) is the 1981–1987 BMW 5 Series (E28) rear suspension. Matschinsky discusses this application in [26]. The C(S-S) is appealing as an alternative to the R joint semi-trailing arm suspension, as it allows a full design position velocity to be achieved and is not much more complicated. Unfortunately, the C joint geometry itself is fully determined by the design position velocity, so wheel kinematics must be compromised if the joint does not fit in the available package space. The example here, which is 1300 mm ahead of the wheel center, is unlikely to package in practice. The corresponding S-S link is also impractical, space-wise.

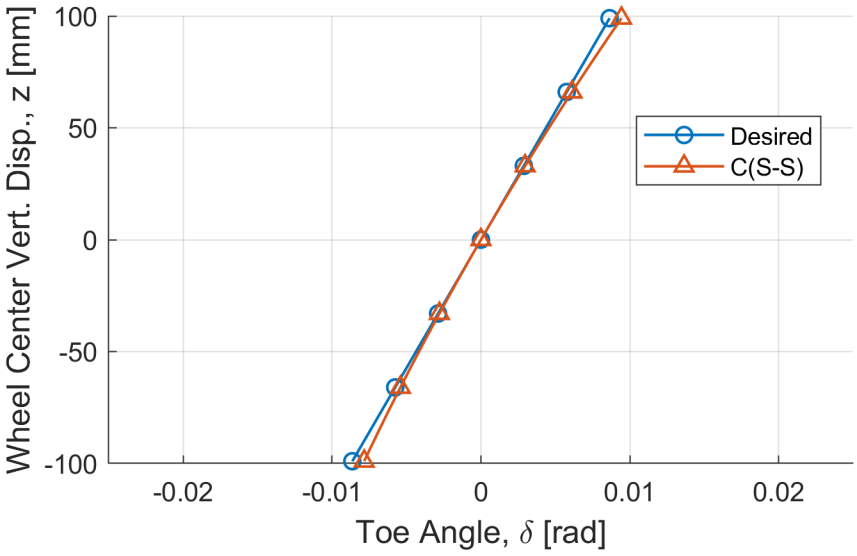

Figure 7.5. Toe curve for the synthesized C(S-S) suspension.

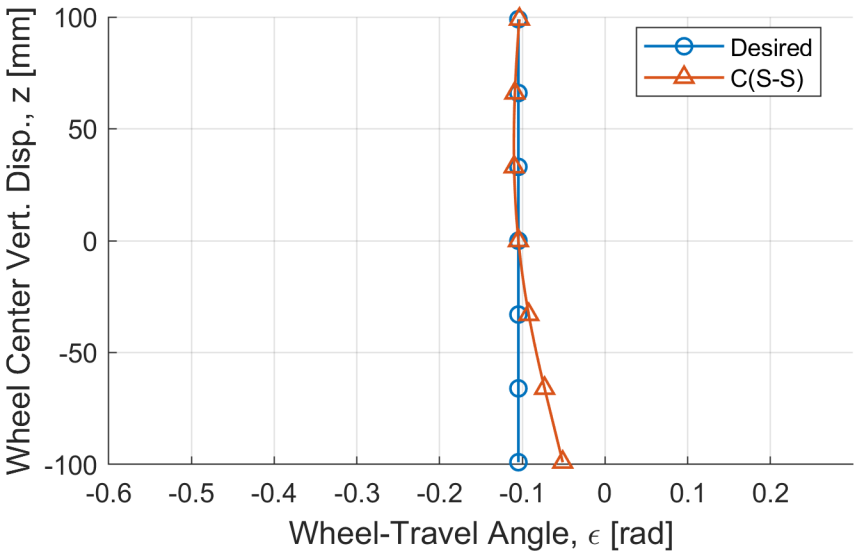

Figure 7.6. Wheel-travel angle curve for the synthesized C(S-S) suspension.

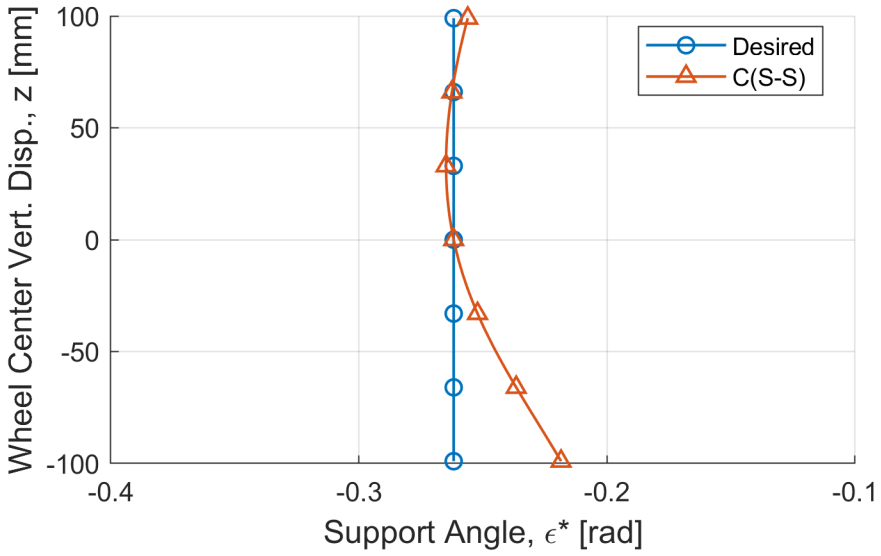

Figure 7.7. Support angle curve for the synthesized C(S-S) suspension.

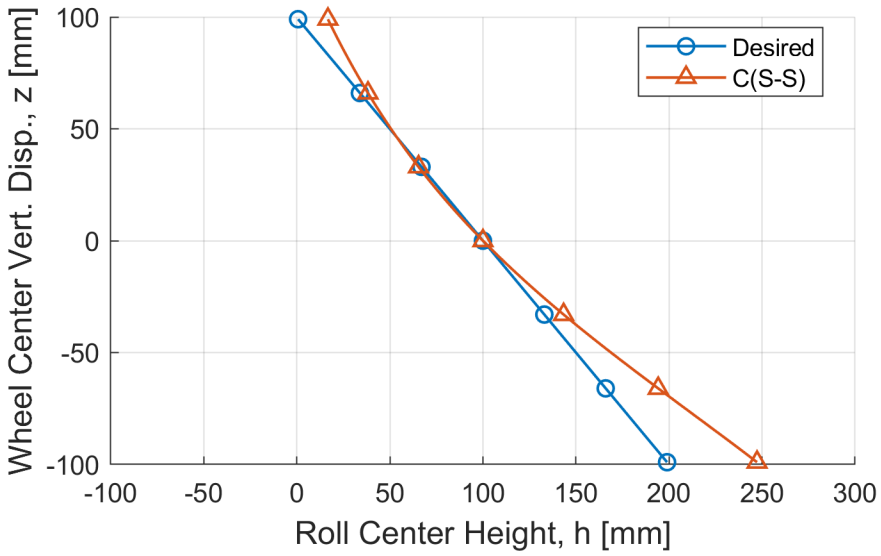

Figure 7.8. Roll center height curve for the synthesized C(S-S) suspension.

Chapter 8

The S Joint

8.1 Synthesis

The spherical (S) joint, Figure 8.1, directly connects the wheel to the vehicle body. Dimensional synthesis amounts to finding the coordinates $\boldsymbol{x} \in \mathbf{R}^3$ of the joint. For a wheel motion from design given by $\boldsymbol{A} \in SO(3)$ and $\boldsymbol{b} \in \mathbf{R}^3$, the point $\boldsymbol{x}$ must remain invariant:

$$\boldsymbol{A}\boldsymbol{x} + \boldsymbol{b} = \boldsymbol{x}.$$

With three independent design variables and these three equations, there is only one wheel position other than design that is specifiable. Design position velocity can be specified instead. Differentiation results in the velocity equation

$$\boldsymbol{\omega} \times \boldsymbol{x} + \boldsymbol{v} = \mathbf{0}.$$

That is, the velocity of the S joint coordinate must be zero at all times. Recall that $\boldsymbol{\omega} \in \mathbf{R}^3$ is the angular velocity of the wheel while $\boldsymbol{v} \in \mathbf{R}^3$ is the velocity of the point on the wheel currently passing through the origin.

For design position velocity synthesis $\boldsymbol{\omega} \times \boldsymbol{x} = -\boldsymbol{v}$ is solved for $\boldsymbol{x}$. Since the left-hand side is perpendicular to $\boldsymbol{\omega}$ the right-hand side must be as well, giving the requirement $\boldsymbol{v} \cdot \boldsymbol{\omega} = 0$ familiar from the R joint. In general, any connection having a

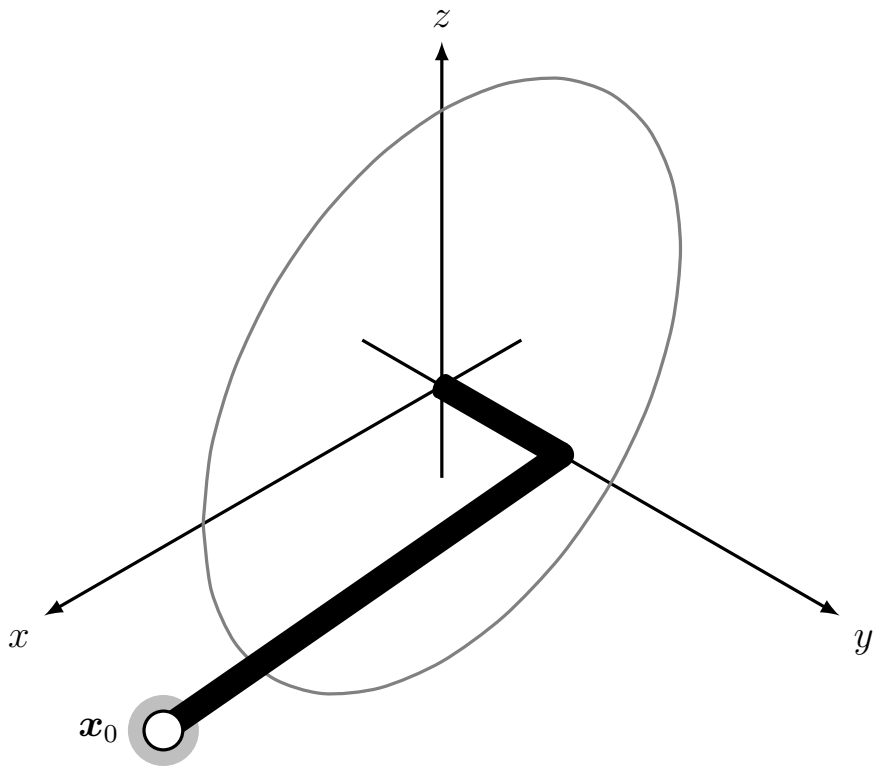

Figure 8.1. Depiction of an S joint.

fixed point requires this. Crossing both sides of the velocity design equation with $\boldsymbol{\omega}$ and using the triple product expansion results in

$$(\boldsymbol{\omega} \cdot \boldsymbol{x})\boldsymbol{\omega} - (\boldsymbol{\omega} \cdot \boldsymbol{\omega})\boldsymbol{x} = -\boldsymbol{\omega} \times \boldsymbol{v}.$$

There is not a unique solution for $\boldsymbol{x}$. The solution closest to the origin is perpendicular to $\boldsymbol{\omega}$, giving

$$\boldsymbol{x}_\perp = \frac{\boldsymbol{\omega} \times \boldsymbol{v}}{\boldsymbol{\omega} \cdot \boldsymbol{\omega}}.$$

Other solutions can be found by adding $\lambda \boldsymbol{u}$ to this shortest solution, where $\lambda \in \mathbf{R}$ and $\boldsymbol{u} = \boldsymbol{\omega}/|\boldsymbol{\omega}|$. As such, the line of solutions is $\boldsymbol{x}_\perp + \lambda \boldsymbol{u}$.

8.2 Synthesis Example

The motion specification used for the R joint example can be re-used here. The solution for $\boldsymbol{x}_\perp$ is, to three significant figures,

$$\boldsymbol{x}_\perp = \begin{pmatrix} 740 \\ 208 \\ -72.1 \end{pmatrix} \text{ [mm]},$$

while the direction of the line of solutions is

$$\boldsymbol{u} = \begin{pmatrix} -0.263 \\ 0.962 \\ 0.0669 \end{pmatrix}.$$

It should be no surprise that these are identical to the solutions of the R joint example. The advantage is that one only has to package one point on the axis, rather than a segment of it. For example, suppose a designer wants the y-coordinate of the S joint to be 100 mm. Then

$$\lambda = \frac{100 - \boldsymbol{x}_0 \cdot \boldsymbol{j}}{\boldsymbol{u}_0 \cdot \boldsymbol{j}} = -112.$$

This gives the solution of Figure 8.2, where, to three significant figures,

$$\boldsymbol{x} = \begin{pmatrix} 770 \\ 100 \\ -79.6 \end{pmatrix} \text{ [mm]}.$$

The disadvantage of the S joint versus the R joint is that it removes only three DOFs and is thus not a complete suspension linkage; it must be completed with additional connection(s) that remove the other two freedoms. In number synthesis, several possible architectures using the S joint were found. Here, the focus is on the most typical, which is the S(S-S)^2 architecture. This requires the synthesis of two S-S links with the same compromised motion specification, something not considered yet.

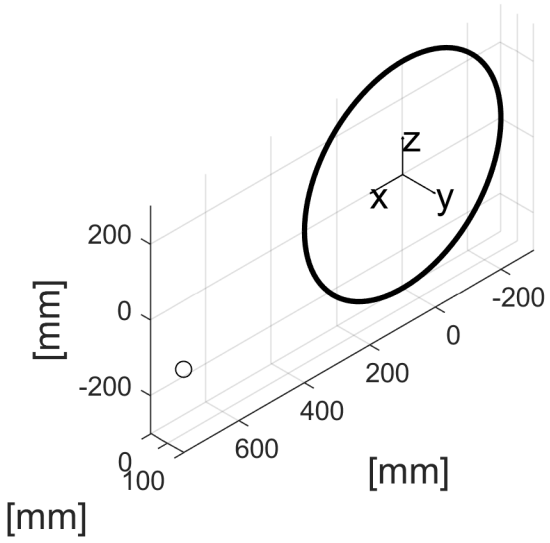

Figure 8.2. Synthesized S joint.

8.3 S-S Links for Spherical Linkages

Let $\boldsymbol{x}_1 \in \mathbf{R}^3$ be the wheel-side S joint and $\boldsymbol{x}_0 \in \mathbf{R}^3$ be the body-side S joint. If $\boldsymbol{\omega} \in \mathbf{R}^3$ and $\boldsymbol{v} \in \mathbf{R}^3$ give the desired design position wheel velocity, then

$$(\boldsymbol{\omega} \times \boldsymbol{x}_1 + \boldsymbol{v}) \cdot (\boldsymbol{x}_1 - \boldsymbol{x}_0) = 0$$

ensures that this velocity is achieved by the S-S link. This velocity requirement leaves the S-S link quite underdetermined. A useful strategy here is to specify $\boldsymbol{x}_1$ and the plan view angle α; recall that

$$\alpha = \arctan \frac{(\boldsymbol{x}_0 - \boldsymbol{x}_1) \cdot \boldsymbol{i}}{(\boldsymbol{x}_0 - \boldsymbol{x}_1) \cdot \boldsymbol{j}}.$$

This is equivalent to

$$(\boldsymbol{i} - \tan \alpha \boldsymbol{j}) \cdot (\boldsymbol{x}_1 - \boldsymbol{x}_0) = 0.$$

As such,

$$\boldsymbol{x}_1 - \boldsymbol{x}_0 = \ell \boldsymbol{e},$$

where

$$\boldsymbol{e} = \pm \frac{(\boldsymbol{\omega} \times \boldsymbol{x}_1 + \boldsymbol{v}) \times (\boldsymbol{i} - \tan\alpha \boldsymbol{j})}{|(\boldsymbol{\omega} \times \boldsymbol{x}_1 + \boldsymbol{v}) \times (\boldsymbol{i} - \tan\alpha \boldsymbol{j})|},$$

and ℓ is the link length. The expectation is, for reasonable values of α, that the y-component of $\boldsymbol{x}_1 - \boldsymbol{x}_0$ be negative. In other words, the body-side joint is expected to be closer to the vehicle body than the wheel-side joint. This fact can be used to select plus or minus for $\boldsymbol{e}$. What remains is choosing ℓ. Once this is set,

$$\boldsymbol{x}_0 = \boldsymbol{x}_1 - \ell \boldsymbol{e}.$$

One strategy is to choose ℓ based on the link length necessary for $\boldsymbol{x}_1$ to reach another point $\boldsymbol{x}_2$. This won't guarantee that $\boldsymbol{x}_1$ reaches $\boldsymbol{x}_2$ when the wheel moves, but it is better than nothing. Following this approach,

$$\begin{aligned} |\boldsymbol{x}_2 - \boldsymbol{x}_0|^2 &= \ell^2 \\ |\boldsymbol{x}_2 - \boldsymbol{x}_1 + \ell \boldsymbol{e}|^2 &= \ell^2 \\ (\boldsymbol{x}_2 - \boldsymbol{x}_1 + \ell \boldsymbol{e}) \cdot (\boldsymbol{x}_2 - \boldsymbol{x}_1 + \ell \boldsymbol{e}) &= \ell^2 \\ (\boldsymbol{x}_2 - \boldsymbol{x}_1) \cdot (\boldsymbol{x}_2 - \boldsymbol{x}_1) + 2\ell \boldsymbol{e} \cdot (\boldsymbol{x}_2 - \boldsymbol{x}_1) &= 0. \end{aligned}$$

As such,

$$\ell = -\frac{(\boldsymbol{x}_2 - \boldsymbol{x}_1) \cdot (\boldsymbol{x}_2 - \boldsymbol{x}_1)}{2\boldsymbol{e} \cdot (\boldsymbol{x}_2 - \boldsymbol{x}_1)}.$$

The point $\boldsymbol{x}_2$ can be specified as, for example, $\boldsymbol{x}_2 = \boldsymbol{A}_2 \boldsymbol{x}_1 + \boldsymbol{b}_2$, where $\boldsymbol{A}_2 \in SO(3)$ and $\boldsymbol{b}_2 \in \mathbf{R}^3$ give a second wheel position one would like to match if possible.

It would have been nice to specify two additional wheel positions, compatible with the S joint geometry, as done with the C joint. The problem is that the only S-S link solution for design position velocity and two additional, spherical wheel positions will have its fixed joint at the same location as the preexisting S joint.

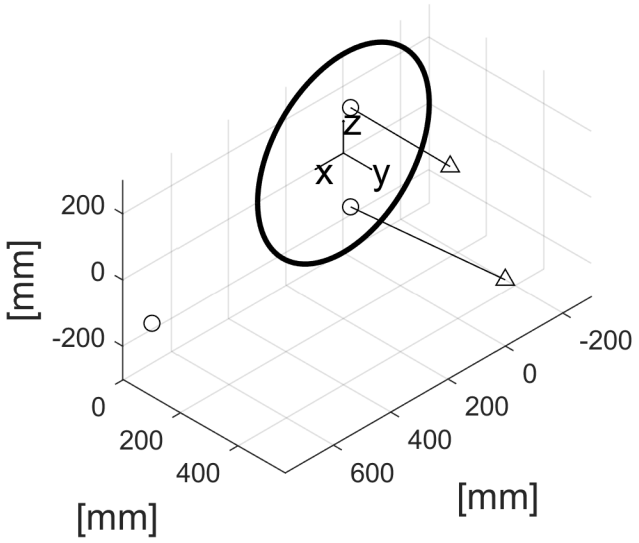

Figure 8.3. Synthesized S(S-S)^2 suspension linkage.

8.4 S(S-S)^2 Example

Here the example solution $\boldsymbol{x}$ for the S joint is combined with two S-S links. The synthesis method described above is used. The first link is synthesized from

- $\boldsymbol{x}_1 = (0, 25, 150)^T$ mm,
- $\alpha = 0$,
- $\boldsymbol{A}_2$ and $\boldsymbol{b}_2$ corresponding to $z = 25$ mm on the standard example trajectory.

This yields, to the usual three significant figures, $\boldsymbol{x}_0 = (0, 373, 146)^T$ mm. A second S-S link is found by specifying $\boldsymbol{x}_1^{(2)} = (0, 25, -150)^T$ mm and the parameters otherwise identical, yielding $\boldsymbol{x}_0^{(2)} = (0, 566, -100)^T$ mm. See Figure 8.3. The layout here is typical to isolate fore/aft compliance to the S joint, which can have a large, soft bushing. Adequate lateral stiffness is ensured by the two lateral links having relatively stiffer bushings.

Kinematic analysis uses the constraint equations

$$\boldsymbol{f}(\boldsymbol{q}) = \begin{pmatrix} \boldsymbol{x}_1^T(\boldsymbol{I} - \boldsymbol{A}^T)\boldsymbol{x}_0 + \boldsymbol{b}^T\boldsymbol{A}\boldsymbol{x}_1 - \boldsymbol{b}^T\boldsymbol{x}_0 + \boldsymbol{b}^T\boldsymbol{b}/2 \\ \left(\boldsymbol{x}_1^{(2)}\right)^T(\boldsymbol{I} - \boldsymbol{A}^T)\boldsymbol{x}_0^{(2)} + \boldsymbol{b}^T\boldsymbol{A}\boldsymbol{x}_1^{(2)} - \boldsymbol{b}^T\boldsymbol{x}_0^{(2)} + \boldsymbol{b}^T\boldsymbol{b}/2 \\ \boldsymbol{A}\boldsymbol{x} + \boldsymbol{b} - \boldsymbol{x} \end{pmatrix}.$$

Camber results are shown in Figure 8.4. Camber is qualitatively as desired. Toe, Figure 8.5, is probably the biggest issue. Toe change rate is nonconstant, resulting in a decidedly nonlinear toe curve. For wheel-travel angle, see Figure 8.6. As this is a linkage with a fixed wheel point, one velocity characteristic had to be sacrificed to ensure that $\boldsymbol{v} \cdot \boldsymbol{\omega} = 0$. Here, it was wheel-travel angle, which is not a concern if this wheel is non-driven. Support angle is shown in Figure 8.7. Only the design position value is achieved. For roll center height results, see Figure 8.8. The roll center height curve looks surprisingly good, all things considered.

The S(S-S)^2 suspension is relatively simple, but offers more elasto-kinematic tuning capability than the related R joint. On the other hand, kinematic performance is inherently compromised, due to the same problem of the wheel having a point fixed on the vehicle body. Nevertheless, this is a commercially-relevant linkage. A great example is the rear suspension on the 1990–2000 BMW 3 Series (E36 chassis code). Called the *Z-axle*, this replaced the R joint (semi-trailing arm) suspension used by the previous 3 Series (E30).

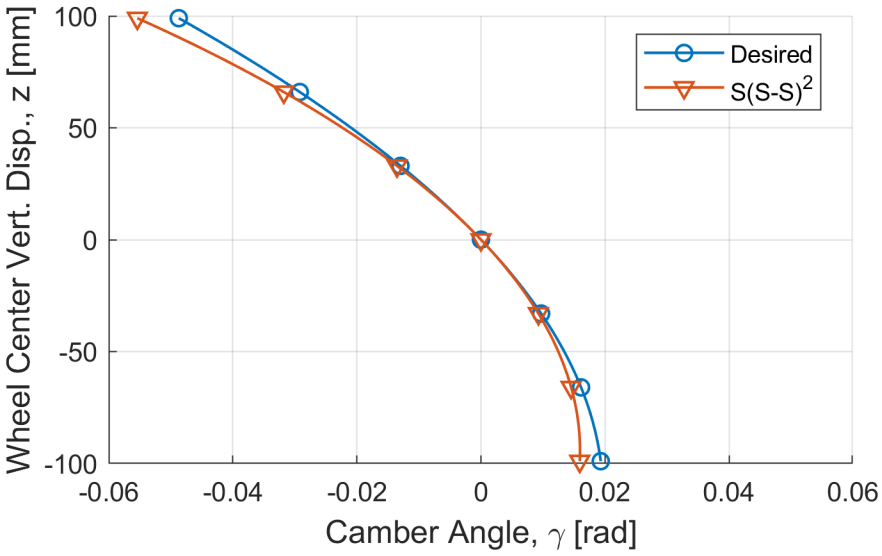

Figure 8.4. Camber curve for the synthesized S(S-S)^2 suspension.

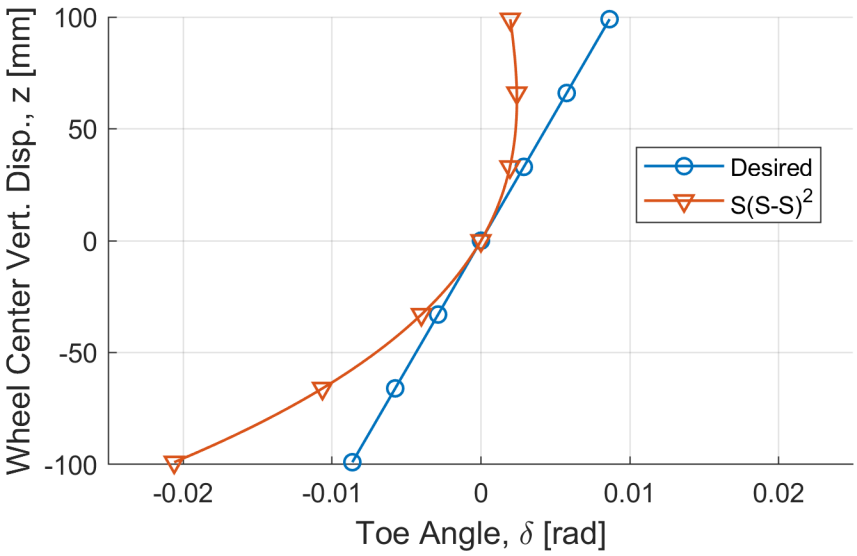

Figure 8.5. Toe curve for the synthesized S(S-S)^2 suspension.

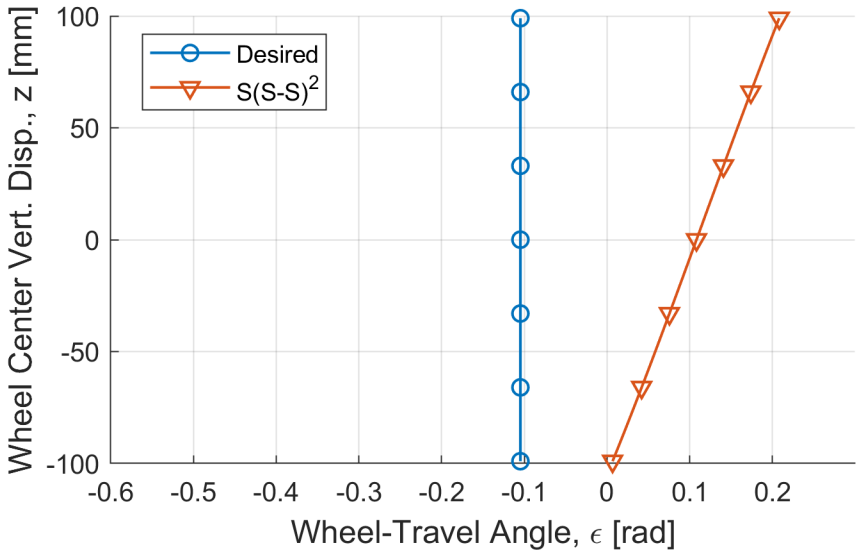

Figure 8.6. Wheel-travel angle curve for the synthesized S(S-S)^2 suspension.

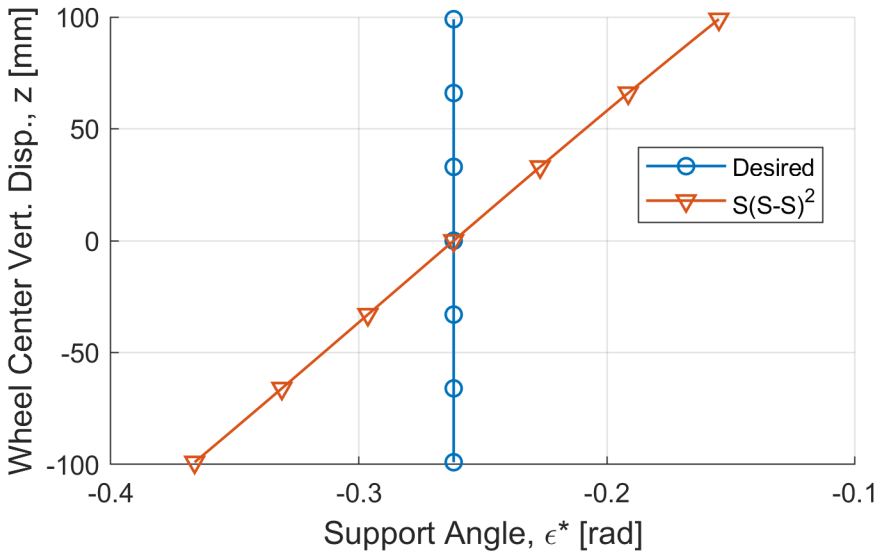

Figure 8.7. Support angle curve for the synthesized S(S-S)^2 suspension.

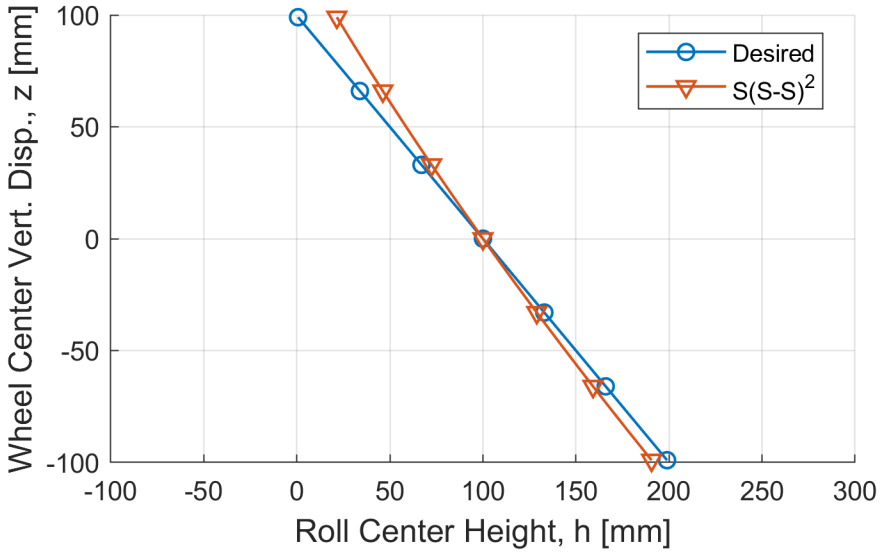

Figure 8.8. Roll center height curve for the synthesized S(S-S)^2 suspension.

Chapter 9

The R-S Link

9.1 Design Equations

The R-S link indirectly connects the wheel carrier to the vehicle body. The R joint is located on the body-side and can be given by a coordinate vector $\boldsymbol{x}_0 \in \mathbf{R}^3$ and a column vector $\boldsymbol{u}_0 \in \mathbf{R}^3$. The S joint attaches to the wheel and has geometry given by a coordinate vector $\boldsymbol{x}_1 \in \mathbf{R}^3$. See Figure 9.1. The line defining the R joint does not have the six independent design variables suggested by column vector $\boldsymbol{u}_0 \in \mathbf{R}^3$ and coordinate vector $\boldsymbol{x}_0 \in \mathbf{R}^3$. One way to see this is to note that $\boldsymbol{u}_0$ can be a unit vector,

$$\boldsymbol{u}_0 \cdot \boldsymbol{u}_0 = 1, \tag{9.1}$$

and that $\boldsymbol{x}_0$ can be the point on the R joint axis that is closest to $\boldsymbol{x}_1$, meaning that

$$(\boldsymbol{x}_1 - \boldsymbol{x}_0) \cdot \boldsymbol{u}_0 = 0. \tag{9.2}$$

When the wheel is moved from Position 1 (design) to Position i by an isometry given by $\boldsymbol{A}_i \in SO(3)$ and $\boldsymbol{b}_i \in \mathbf{R}^3$, the distance between $\boldsymbol{x}_i := \boldsymbol{A}_i\boldsymbol{x}_1 + \boldsymbol{b}_i$ and $\boldsymbol{x}_0$ must remain equal to the initial distance between $\boldsymbol{x}_1$ and $\boldsymbol{x}_0$. Additionally, if the vector between $\boldsymbol{x}_1$ and $\boldsymbol{x}_0$ is initially perpendicular to $\boldsymbol{u}_0$ then the vector between $\boldsymbol{x}_i$ and $\boldsymbol{x}_0$

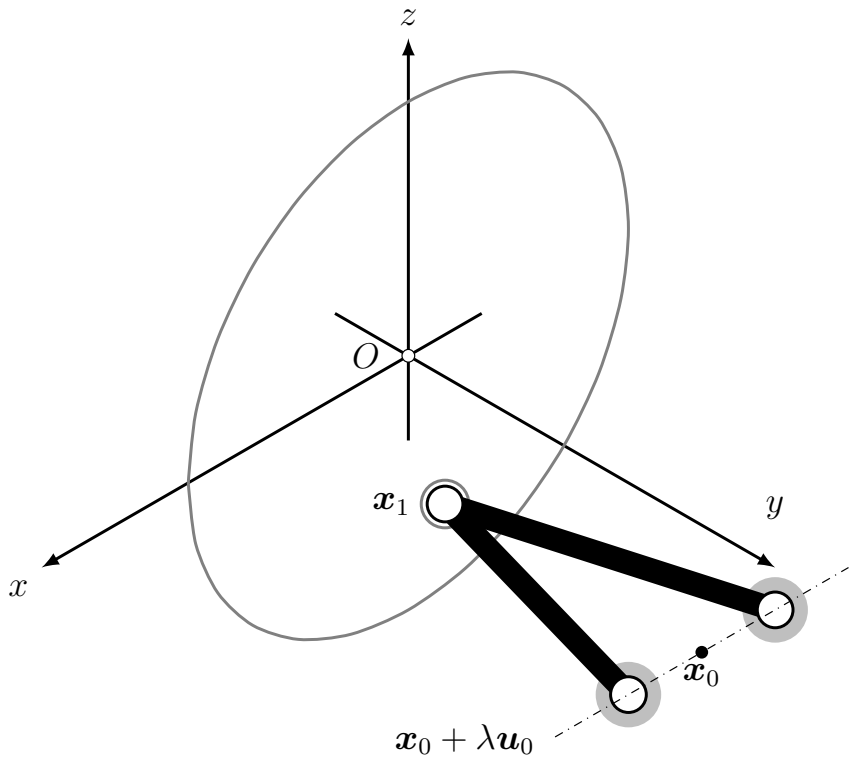

Figure 9.1. Geometry of the R-S link.

must be as well. Consequently, Position i must satisfy the following:

$$(\boldsymbol{x}_i - \boldsymbol{x}_0) \cdot (\boldsymbol{x}_i - \boldsymbol{x}_0) = (\boldsymbol{x}_1 - \boldsymbol{x}_0) \cdot (\boldsymbol{x}_1 - \boldsymbol{x}_0) \tag{9.3}$$

$$(\boldsymbol{x}_i - \boldsymbol{x}_0) \cdot \boldsymbol{u}_0 = 0. \tag{9.4}$$

When designing a suspension the designer must, at the very least, guarantee a certain design position wheel velocity. Consequently, consider the derivatives of (9.3) and (9.4), assuming that $\boldsymbol{A}_i$ and $\boldsymbol{b}_i$ are functions of wheel center vertical displacement z. Recall that these derivatives are denoted with the prime mark, so that the corresponding derivatives are

$$\boldsymbol{x}_i' \cdot (\boldsymbol{x}_i - \boldsymbol{x}_0) = 0$$

$$\boldsymbol{x}_i' \cdot \boldsymbol{u}_0 = 0.$$

As such, the design position velocity requirements are

$$\boldsymbol{x}_1' \cdot (\boldsymbol{x}_1 - \boldsymbol{x}_0) = 0$$
$$\boldsymbol{x}_1' \cdot \boldsymbol{u}_0 = 0.$$

These, together with (9.1) and (9.2), are the basic design equations. The velocity $\boldsymbol{x}_1'$ can be written as $\boldsymbol{\omega}_1 \times \boldsymbol{x}_1 + \boldsymbol{v}_1$, where $\boldsymbol{\omega}_1$ is the angular velocity at Position 1 and $\boldsymbol{v}_1$ is the velocity of the point on the wheel that is passing through the origin at Position 1. There are nine design variables given by $\boldsymbol{u}_0$, $\boldsymbol{x}_0$, and $\boldsymbol{x}_1$. There are four basic design equations. This leaves five design variables freely specifiable and so there is room to specify more wheel positions. In particular, up to two more wheel positions, 2 and 3, may be specified, using two copies of the equations (9.3) and (9.4). These additional four design equations leave just one free design variable.

R-S links are typically used in applications where a steering axis is needed. In this case, the S joint should be placed along the desired steering axis. This is not possible if only one component of $\boldsymbol{x}_1$ is specifiable. Hence, for the desired kingpin geometry to be possible, Position 3 must be sacrificed. The removal of the two equations associated with Position 3 leaves three free design variables, enough to completely specify S joint location $\boldsymbol{x}_1$ and thus satisfy the desired kingpin geometry. In this case, the complete set of design equations for the R-S link are

$$\boldsymbol{u}_0 \cdot \boldsymbol{u}_0 = 1; \tag{9.5}$$
$$(\boldsymbol{x}_i - \boldsymbol{x}_0) \cdot \boldsymbol{u}_0 = 0, \ i = 1, 2; \tag{9.6}$$
$$(\boldsymbol{x}_2 - \boldsymbol{x}_0) \cdot (\boldsymbol{x}_2 - \boldsymbol{x}_0) = (\boldsymbol{x}_1 - \boldsymbol{x}_0) \cdot (\boldsymbol{x}_1 - \boldsymbol{x}_0); \tag{9.7}$$
$$\boldsymbol{x}_1' \cdot (\boldsymbol{x}_1 - \boldsymbol{x}_0) = 0; \tag{9.8}$$
$$\boldsymbol{x}_1' \cdot \boldsymbol{u}_0 = 0. \tag{9.9}$$

The solution of these equations is discussed in the next section.

9.2 Solving the Design Equations

Equations (9.5) through (9.9) are a set of six polynomial equations in nine variables. Solution is greatly simplified by specifying $\boldsymbol{x}_1$. This is handy for ensuring a specific ball joint location or, more generally, locating the ball joint on a desired kingpin axis. As such, assume that $\boldsymbol{x}_1$ is known. Consequently, $\boldsymbol{x}_2$ and $\boldsymbol{x}_1'$ are known as well. Notice that equations (9.6) imply that

$$(\boldsymbol{x}_2 - \boldsymbol{x}_1) \cdot \boldsymbol{u}_0 = 0.$$

This result, together with (9.5) and (9.9), means that $\boldsymbol{u}_0$ is a unit vector perpendicular to both $(\boldsymbol{x}_2 - \boldsymbol{x}_1)$ and $\boldsymbol{x}_1'$. As such,

$$\boldsymbol{u}_0 = \pm \frac{\boldsymbol{x}_1' \times (\boldsymbol{x}_2 - \boldsymbol{x}_1)}{|\boldsymbol{x}_1' \times (\boldsymbol{x}_2 - \boldsymbol{x}_1)|}.$$

The sign of the solution is not meaningful. To be consistent, the plus is always taken here. With $\boldsymbol{u}_0$ known, $\boldsymbol{x}_0$ is easily determined. Notice that (9.7) can be rewritten as

$$(\boldsymbol{x}_1 - \boldsymbol{x}_2) \cdot \boldsymbol{x}_0 = (\boldsymbol{x}_1 \cdot \boldsymbol{x}_1 - \boldsymbol{x}_2 \cdot \boldsymbol{x}_2)/2.$$

This form of (9.7), together with (9.8) and the first of (9.6), allows the construction of the linear system of equations

$$\begin{pmatrix} \boldsymbol{u}_0^T \\ (\boldsymbol{x}_1 - \boldsymbol{x}_2)^T \\ (\boldsymbol{x}_1')^T \end{pmatrix} \boldsymbol{x}_0 = \begin{pmatrix} \boldsymbol{x}_1 \cdot \boldsymbol{u}_0 \\ (\boldsymbol{x}_1 \cdot \boldsymbol{x}_1 - \boldsymbol{x}_2 \cdot \boldsymbol{x}_2)/2 \\ \boldsymbol{x}_1' \cdot \boldsymbol{x}_1 \end{pmatrix},$$

which may be readily solved for $\boldsymbol{x}_0$.

As an example, the relevant wheel motion and kingpin specifications used in the S-S link chapter may be used to solve for R-S links that lie along the kingpin. Figure 9.2 shows seven such R-S link solutions. The prototypical suspension employing the R-S link is the *short-long arms (SLA)*, also known as the double-wishbone. In terms of

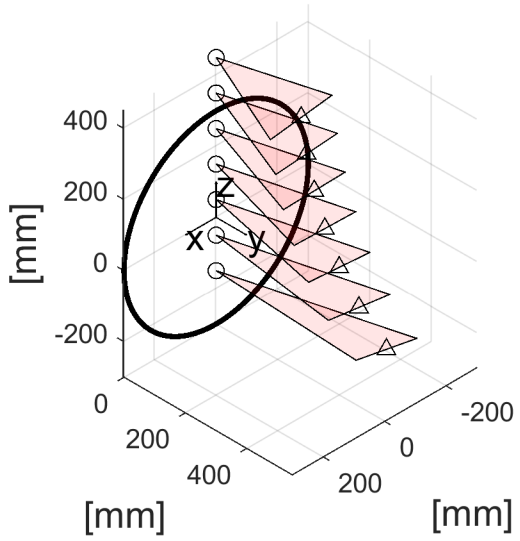

Figure 9.2. Various R-S links satisfying a design position velocity, a jounce position, and a kingpin geometry.

this dissertation's notation for suspension linkage types, this is the $(\text{R-S})^2$(S-S). The SLA name arises because a long, lower R-S link is paired with a short, upper R-S link. Another look at Figure 9.2 shows that these link lengths are the natural result of a proper wheel motion specification. As with the previous chapters, a complete example is considered next; of course, the SLA is chosen. As such, methods for generating S-S links with the correct properties must be introduced. The S-S link in these types of suspensions is called a *tie rod*, or track rod, and its geometry is dictated both by wheel kinematics and steering system requirements. Methods appropriate for these conditions are introduced in the next section.

9.3 Tie Rod Synthesis

A *tie rod* is a special type of S-S link that is actuated by the steering system, allowing rotation of the wheel about its kingpin axis. Here, actuation is presumed to be provided by a rack-and-pinion having attachment points on each end of the rack. In this section, $\boldsymbol{x}_0$ refers to the body-side tie-rod S joint while $\boldsymbol{x}_1$ refers to the wheel-side tie-rod S joint. To be compatible with the R-S links synthesized previously, the design

equations

$$(\boldsymbol{x}_2 - \boldsymbol{x}_0) \cdot (\boldsymbol{x}_2 - \boldsymbol{x}_0) = (\boldsymbol{x}_1 - \boldsymbol{x}_0) \cdot (\boldsymbol{x}_1 - \boldsymbol{x}_0)$$
$$\boldsymbol{x}_1' \cdot (\boldsymbol{x}_1 - \boldsymbol{x}_0) = 0$$

are employed, where $\boldsymbol{x}_2 = \boldsymbol{A}_2\boldsymbol{x}_1 + \boldsymbol{b}_2$ and $\boldsymbol{x}_1' = \boldsymbol{\omega}_1 \times \boldsymbol{x}_1 + \boldsymbol{v}_1$. A method for generating packageable tie rods is as follows. First, recognize that the y-component y_0 of the body-side point $\boldsymbol{x}_0$ is fixed by a given choice of steering rack width. In particular, if s is the design position track width and w is the steering rack width, then $y_0 = s/2 - w/2$. Using this fact, for a given choice of $\boldsymbol{x}_1$, wheel-side point $\boldsymbol{x}_0$ can be found by solving the linear equations

$$\begin{pmatrix} (\boldsymbol{x}_1 - \boldsymbol{x}_2)^T \\ (\boldsymbol{x}_1')^T \\ \boldsymbol{j}^T \end{pmatrix} \boldsymbol{x}_0 = \begin{pmatrix} (\boldsymbol{x}_1 \cdot \boldsymbol{x}_1 - \boldsymbol{x}_2 \cdot \boldsymbol{x}_2)/2 \\ \boldsymbol{x}_1' \cdot \boldsymbol{x}_1 \\ (s - w)/2 \end{pmatrix}.$$

A package space can by suitably discretized and filled with tie rod solutions that fit. As an example, consider a rack having width $w = 650$ mm and the package space (cube) of the earlier S-S link chapter, discretized into points spaced 10 mm apart. This results in 3286 link solutions that fit. Requiring that they fit inside the same rim as the earlier S-S link example reduces the number of solutions to 106, as seen in Figure 9.3. Choosing among the various candidate solutions is made easier by considering a steering system criterion associated with the Ackermann steering geometry.

Ackermann steering geometry has all four wheels trace circles around a common center point, Figure 9.4. This geometry reduces the amount of tire slip that occurs when maneuvering at low speeds. At its essence, this means that the inside front wheel steers more than the outside front wheel, with the actual difference in steer angle not strictly set by achieving perfect Ackermann geometry. This is because Ackermann geometry is not particularly relevant at high speeds where the tire slip angles are unavoidably large. In [41, Figure 3.92], a difference of 3° when the inside

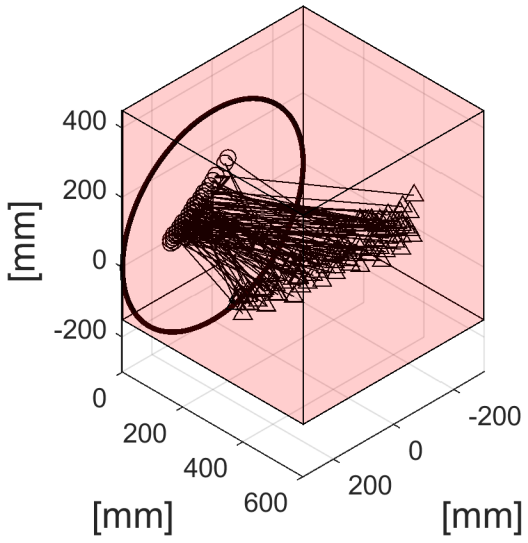

Figure 9.3. Packageable tie rods satisfying a design position velocity, a jounce position, and a steering rack width.

wheel is at 20° of steer is given as an example tolerance for Ackermann behavior. This means that the outside wheel is at 17° when the inside wheel is at 20°. The approach here for reducing the number of tie rod solutions is to filter them based on their closeness to a desired Ackermann tolerance. This requires knowing how much the wheel turns for a given rack displacement, or vice versa.

For the wheel to achieve a steer angle, it must rotate by an angle θ about the kingpin axis. Here the kingpin axis is given by the point $\boldsymbol{d} = (n, r_s, -r)^T$ and the unit vector

$$\boldsymbol{e} = \frac{(-\tan\tau, \tan\sigma, 1)^T}{|(-\tan\tau, \tan\sigma, 1)^T|}.$$

Recall that r is wheel radius, n is caster offset, r_s is scrub radius, τ is caster angle, and σ is kingpin inclination angle. A rotation by θ about this axis maps outer tie rod point $\boldsymbol{x}_1$ to

$$\boldsymbol{x}_3 := \boldsymbol{R}_{\boldsymbol{e},\theta}(\boldsymbol{x}_1 - \boldsymbol{d}) + \boldsymbol{d}.$$

To achieve this Position 3, the inner tie rod point $\boldsymbol{x}_0$ must have been translated by some rack displacement d_r in the y-direction. As such, Position 3 must satisfy

$$(\boldsymbol{x}_3 - (\boldsymbol{x}_0 + d_r\boldsymbol{j})) \cdot (\boldsymbol{x}_3 - (\boldsymbol{x}_0 + d_r\boldsymbol{j})) = (\boldsymbol{x}_1 - \boldsymbol{x}_0) \cdot (\boldsymbol{x}_1 - \boldsymbol{x}_0).$$

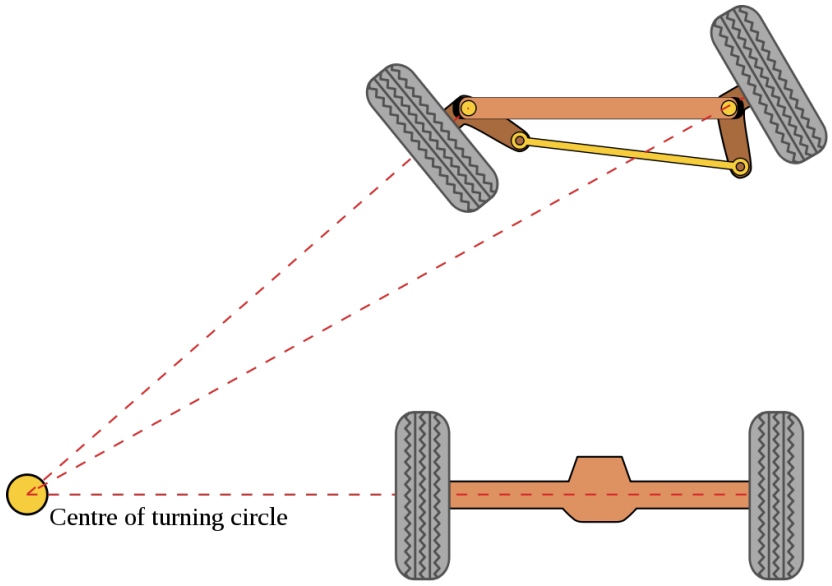

Figure 9.4. Illustration of the Ackermann steering geometry [53].

Consequently, for a desired θ, necessary rack displacement d_r may be computed. For a right-hand rear wheel considered here, a positive θ means steering to the left and so this is outside wheel of the turn. The angle of the inside wheel may be found by computing θ^* for opposite and equal displacement $-d_r$. When reflected across the vehicle, this wheel will be steered to the left by $-\theta^*$. Consequently, the difference in kingpin rotation angle will be $\Delta\theta := -\theta^* - \theta$. The tie rod closest to this desired difference can then be selected. For example, suppose $2^\circ \leq \Delta\theta \leq 4^\circ$ is wanted when $\theta = 20^\circ$. Searching the 106 tie rod solutions that package inside the wheel results in 17 solutions meeting this criterion, Figure 9.5.

9.4 The SLA Suspension

With a set of R-S links and tie rods now generated, a complete SLA suspension may assembled and analyzed, beginning with the R-S links. There are 601 solutions that fit in the packaging cube when considering S joints every millimeter along the kingpin. Of these, 299 fit inside the wheel. Suspension designers typically want the distance between the S joints along the kingpin to be as large as possible; select two R-S links according to this heuristic. The tie rod is easier to package around, for example, a

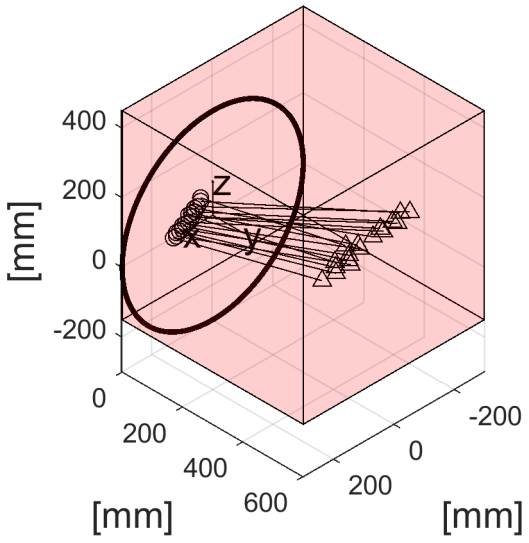

Figure 9.5. The 17 tie rod solutions that meet the example Ackermann criterion.

Table 9.1. Coordinates of the SLA example (three significant figures).

	Lower R-S	Upper R-S	Tie Rod
u_0	-0.983	-1.00	—
v_0	0.00350	0.00140	—
w_0	-0.183	-0.0248	—
x_0	-7.12	0.593	12.2
y_0	547	355	375
z_0	-101	144	5.61
x_1	0.00	0.00	140
y_1	0.00	0.00	10
z_1	-150	148	10

rear-drive half-shaft, if it has a plan view angle closer to zero and lies fully to one side of the wheel center (x-direction) in plan view. Applied here this amounts to choosing the tie rod in Figure 9.5 that has inner point $\boldsymbol{x}_0$ closest to the viewer. Of course, other methods could be employed to choose among the final solutions, such as minimizing reaction loads in the links for any load cases of interest, as done for the five S-S link suspension. The coordinates of the complete SLA example are presented in Table 9.1; for a plot, see Figure 9.6.

As with the previous examples, the synthesized suspension linkage must be analyzed to assess its ability to meet the idealized wheel trajectory. Here, the kinematic

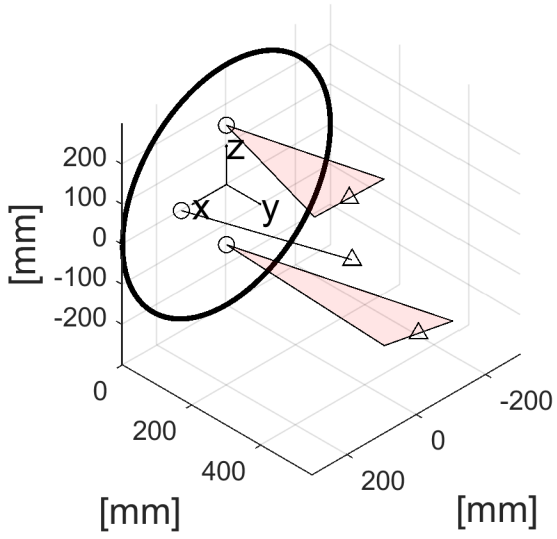

Figure 9.6. Plot of the assembled SLA suspension.

constraint equations

$$\boldsymbol{f}(\boldsymbol{q}) = \begin{pmatrix} \left(\boldsymbol{x}_1^{(1)}\right)^T (\boldsymbol{I} - \boldsymbol{A}^T)\boldsymbol{x}_0^{(1)} + \boldsymbol{b}^T\boldsymbol{A}\boldsymbol{x}_1^{(1)} - \boldsymbol{b}^T\boldsymbol{x}_0^{(1)} + \boldsymbol{b}^T\boldsymbol{b}/2 \\ \left(\boldsymbol{A}\boldsymbol{x}_1^{(1)} + \boldsymbol{b} - \boldsymbol{x}_0^{(1)}\right) \cdot \boldsymbol{u}_0^{(1)} \\ \left(\boldsymbol{x}_1^{(2)}\right)^T (\boldsymbol{I} - \boldsymbol{A}^T)\boldsymbol{x}_0^{(2)} + \boldsymbol{b}^T\boldsymbol{A}\boldsymbol{x}_1^{(2)} - \boldsymbol{b}^T\boldsymbol{x}_0^{(2)} + \boldsymbol{b}^T\boldsymbol{b}/2 \\ \left(\boldsymbol{A}\boldsymbol{x}_1^{(2)} + \boldsymbol{b} - \boldsymbol{x}_0^{(2)}\right) \cdot \boldsymbol{u}_0^{(2)} \\ \left(\boldsymbol{x}_1^{(3)}\right)^T (\boldsymbol{I} - \boldsymbol{A}^T)\boldsymbol{x}_0^{(3)} + \boldsymbol{b}^T\boldsymbol{A}\boldsymbol{x}_1^{(3)} - \boldsymbol{b}^T\boldsymbol{x}_0^{(3)} + \boldsymbol{b}^T\boldsymbol{b}/2 \end{pmatrix}$$

are used, where superscript (1) is the lower R-S link, superscript (2) is the upper R-S link, and superscript (3) is the tie rod. Camber results are shown in Figure 9.7. Toe results, Figure 9.8. For wheel-travel angle, see Figure 9.9. Support angle is shown in Figure 9.10. For roll center height results, see Figure 9.11. Despite specifying only design position velocity and one jounce position ($z = 25$ mm), the wheel-travel curves closely match the specification. Not only that, but a kingpin axis and an Ackermann criterion have been achieved. Due to its excellent kinematics and relative simplicity versus the five link suspension, the SLA has long been associated with performance and racing cars.

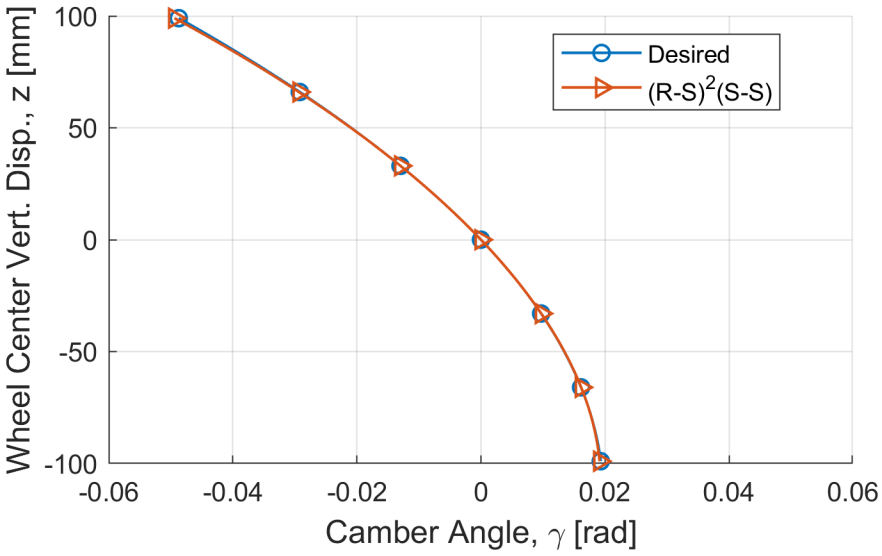

Figure 9.7. Camber curve for the synthesized SLA suspension.

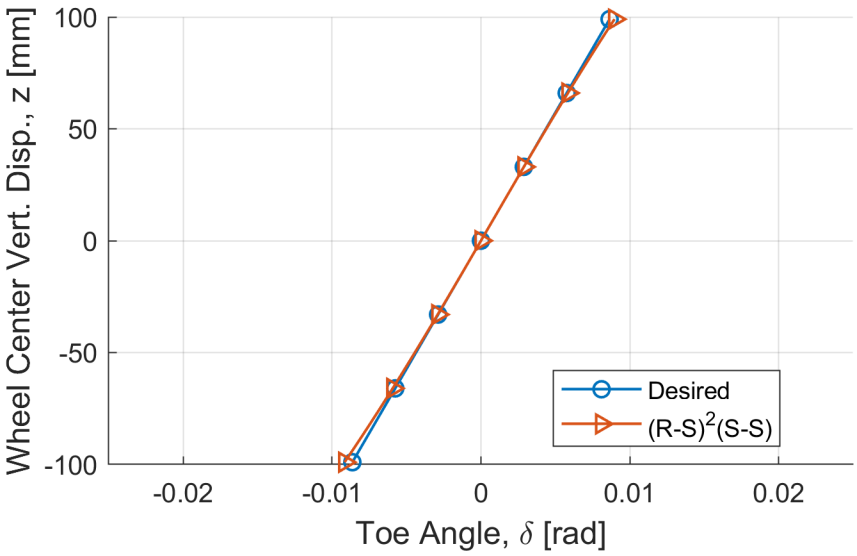

Figure 9.8. Toe curve for the synthesized SLA suspension.

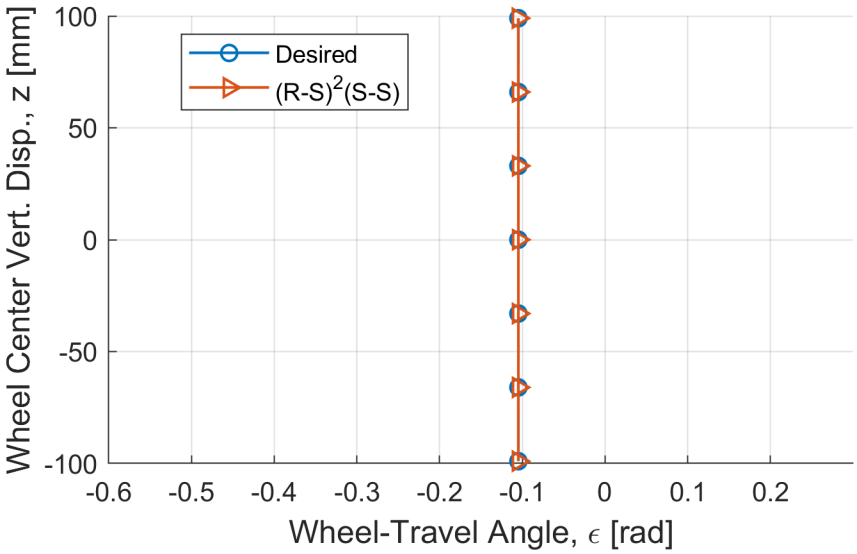

Figure 9.9. Wheel-travel angle curve for the synthesized SLA suspension.

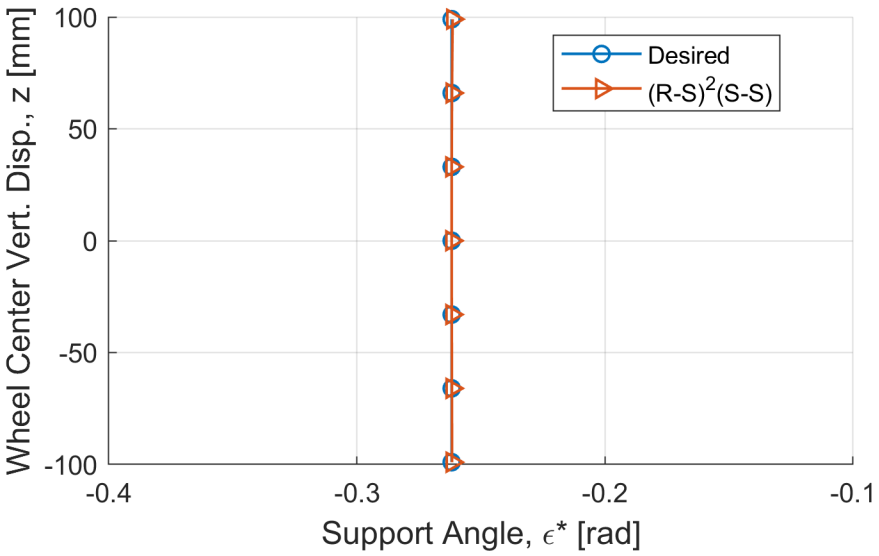

Figure 9.10. Support angle curve for the synthesized SLA suspension.

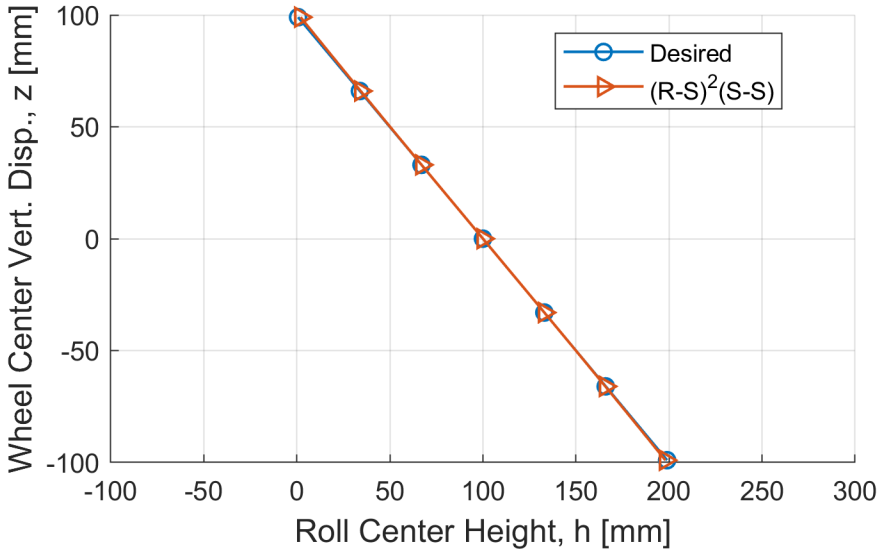

Figure 9.11. Roll center height curve for the synthesized SLA suspension.

Chapter 10

The S-R Link

10.1 Design Equations

The S-R link indirectly connects the wheel carrier to the vehicle body, Figure 10.1. The body-side S joint is given by coordinate vector $\boldsymbol{x}_0$, while the wheel-side R joint is given by column vector $\boldsymbol{u}_1$ and coordinate vector $\boldsymbol{x}_1$. These line coordinates must satisfy

$$\boldsymbol{u}_1 \cdot \boldsymbol{u}_1 = 1$$
$$(\boldsymbol{x}_1 - \boldsymbol{x}_0) \cdot \boldsymbol{u}_1 = 0.$$

When the wheel is moved from Position 1, the design position, to Position i by an isometry having $\boldsymbol{A}_i \in SO(3)$ and $\boldsymbol{b}_i \in \mathbf{R}^3$, the new location of the point on the R joint axis is

$$\boldsymbol{x}_i := \boldsymbol{A}_i \boldsymbol{x}_1 + \boldsymbol{b}_i,$$

while the new direction of the R joint axis is

$$\boldsymbol{u}_i := \boldsymbol{A}_i \boldsymbol{u}_1.$$

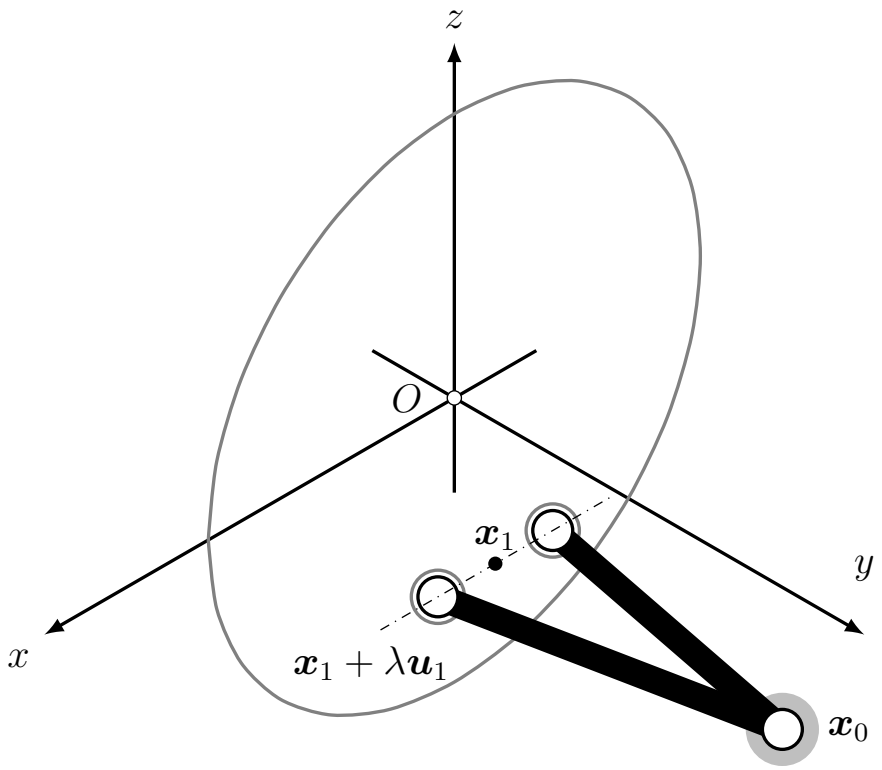

Figure 10.1. Illustration of the S-R link.

The equations that must be satisfied in this Position i are very similar to the R-S link:

$$(\boldsymbol{x}_i - \boldsymbol{x}_0) \cdot (\boldsymbol{x}_i - \boldsymbol{x}_0) = (\boldsymbol{x}_1 - \boldsymbol{x}_0) \cdot (\boldsymbol{x}_1 - \boldsymbol{x}_0)$$
$$(\boldsymbol{x}_i - \boldsymbol{x}_0) \cdot \boldsymbol{u}_i = 0.$$

Equations for velocity follow by differentiation with respect to z, where again the prime mark is used to denote these derivatives:

$$\boldsymbol{x}_i' \cdot (\boldsymbol{x}_i - \boldsymbol{x}_0) = 0$$
$$(\boldsymbol{x}_i - \boldsymbol{x}_0) \cdot \boldsymbol{u}_i' + \boldsymbol{x}_i' \cdot \boldsymbol{u}_i = 0.$$

The individual derivatives $\boldsymbol{x}_i'$ and $\boldsymbol{u}_i'$ may be written as

$$\begin{aligned}\boldsymbol{x}_i' &= \boldsymbol{\omega}_i \times \boldsymbol{x}_i + \boldsymbol{v}_i \\ \boldsymbol{u}_i' &= \boldsymbol{\omega}_i \times \boldsymbol{u}_i;\end{aligned}$$

where, at a Position i, $\boldsymbol{\omega}_i$ is the angular velocity of the wheel, and $\boldsymbol{v}_i$ is the velocity of the point on the wheel that is passing through the origin.

The complete design equations, including design position velocity and $n-1$ positions other than design, are

$$\begin{aligned}\boldsymbol{u}_1 \cdot \boldsymbol{u}_1 &= 1 \\ (\boldsymbol{x}_i - \boldsymbol{x}_0) \cdot \boldsymbol{u}_i &= 0,\ i = 1, \ldots, n. \\ (\boldsymbol{x}_i - \boldsymbol{x}_0) \cdot (\boldsymbol{x}_i - \boldsymbol{x}_0) &= (\boldsymbol{x}_1 - \boldsymbol{x}_0) \cdot (\boldsymbol{x}_1 - \boldsymbol{x}_0),\ i = 2, \ldots, n \\ \boldsymbol{x}_1' \cdot (\boldsymbol{x}_1 - \boldsymbol{x}_0) &= 0 \\ (\boldsymbol{x}_1 - \boldsymbol{x}_0) \cdot \boldsymbol{u}_1' + \boldsymbol{x}_1' \cdot \boldsymbol{u}_1 &= 0.\end{aligned}$$

When $n = 2$, there are six equations in nine design variables; when $n = 3$, there are eight equations in the nine variables. No further wheel positions may be included (unless the design position velocity requirement is dropped). In the next section, the focus is on solving these design equations in a manner that produces so-called *control blades*.

10.2 Control Blades

The *control blade* is an S-R link that has its R joint axis in the vertical direction, with the S joint connecting to the vehicle-body forward of the wheel carrier. In practice, this type of S-R link may be realized with a thin metal "blade", connecting with a rubber bushing to the vehicle body and attaching rigidly to the wheel carrier. The R joint mobility is thus provided by flexion of the control blade [26, pp. 260, 327–328]. The control blade is typically completed with three lateral S-S links, as shown in

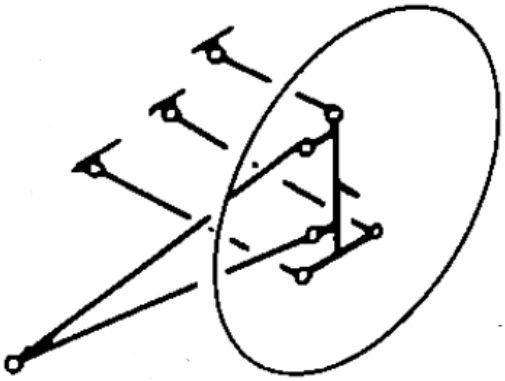

Figure 10.2. A typical control blade geometry [26].

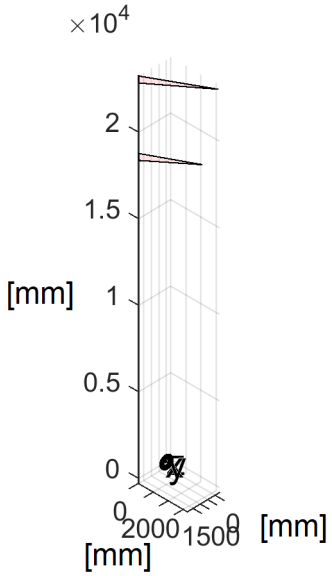

Figure 10.3. Control blade solutions unreasonably far from wheel when specifying design position velocity and $z = 25$ mm jounce position.

Figure 10.2. This suspension is commonly-used and was introduced by the 1999 Ford Focus [18, p. 404]. Its ubiquity and distinctiveness amongst other suspension types using the S-R link made it the example of choice for this chapter.

To design control blades, the R joint axis is required to be vertical. In other words, $\boldsymbol{u}_1 = \boldsymbol{k}$. What this means is that, at most, design position velocity and a Position 2 can be specified. This is because defining $\boldsymbol{u}_1$ completely removes three design variables. Unfortunately, experience has shown that synthesizing S-R links for design position velocity and a second position with $\boldsymbol{u}_1 = \boldsymbol{k}$ produces links that do not fit in a reasonable amount of space. As an example, see Figure 10.3. In this case, the

usual wheel motion specification was employed to create the six design equations in the nine design variables. The system was then squared up with the equation $\boldsymbol{u}_1 = \boldsymbol{k}$ and the solver Bertini [5] was employed to solve the resulting polynomial system. Only two solutions were found, neither of which were close to packageable.

The next step is to use design position velocity as the only wheel motion requirement. The relevant design equations are

$$\begin{aligned}(\boldsymbol{x}_1 - \boldsymbol{x}_0) \cdot \boldsymbol{u}_1 &= 0\\ \boldsymbol{x}_1' \cdot (\boldsymbol{x}_1 - \boldsymbol{x}_0) &= 0\\ (\boldsymbol{x}_1 - \boldsymbol{x}_0) \cdot \boldsymbol{u}_1' + \boldsymbol{x}_1' \cdot \boldsymbol{u}_1 &= 0.\end{aligned}$$

Here, it makes sense to specify $\boldsymbol{x}_1$ in addition to $\boldsymbol{u}_1$. Then $\boldsymbol{x}_0$ is determined by solving the linear system of equations

$$\begin{pmatrix} \boldsymbol{u}_1^T \\ (\boldsymbol{x}_1')^T \\ (\boldsymbol{u}_1')^T \end{pmatrix} \boldsymbol{x}_0 = \begin{pmatrix} \boldsymbol{x}_1 \cdot \boldsymbol{u}_1 \\ \boldsymbol{x}_1' \cdot \boldsymbol{x}_1 \\ \boldsymbol{x}_1 \cdot \boldsymbol{u}_1' + \boldsymbol{x}_1' \cdot \boldsymbol{u}_1 \end{pmatrix}. \tag{10.1}$$

To synthesize some control blades using (10.1), allow $\boldsymbol{x}_1$ to take values in the cuboid

$$\{(x, y, z)^T \in \mathbf{R}^3 : 100 \leq x \leq 300, 100 \leq y \leq 200, -150 \leq z \leq 450\},$$

which is discretized to the millimeter; the packaging cube used in prior examples is not well-suited to the expected layout of the control blade. The R joint direction vector $\boldsymbol{u}_1 = \boldsymbol{k}$ for all cases. This synthesis produces $201 \times 101 \times 601$ control blade solutions. Asking that the lateral distance between $\boldsymbol{x}_0$ and $\boldsymbol{x}_1$ be no more than 10 mm results in 25503 solutions, the shortest of which has, to three significant figures,

$$\begin{aligned}\boldsymbol{x}_0 &= (1710, 209, 225)^T\\ \boldsymbol{x}_1 &= (300, 200, 225)^T.\end{aligned}$$

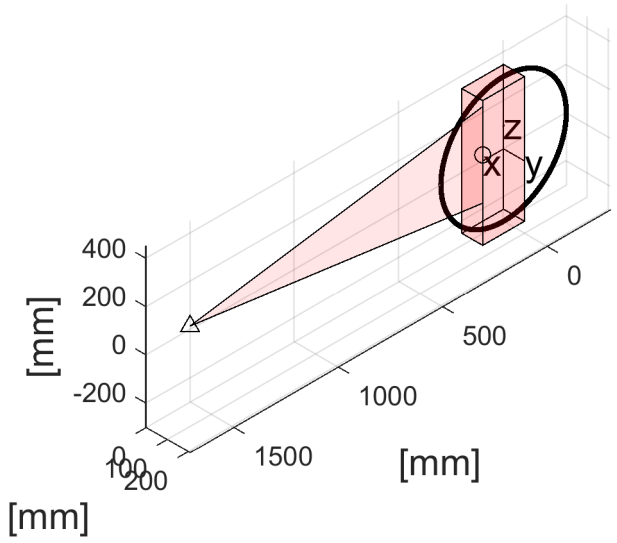

Figure 10.4. A control blade synthesized from the velocity specification.

This solution is plotted in Figure 10.4. The cuboid used for $\boldsymbol{x}_1$ is shown as well. The fixed S joint is denoted with a triangular marker while the point on the R joint axis closest to it is denoted with a circular marker. The control blade solution is quite long, meaning the body-side point would be difficult to package. Reducing required design-position wheel-travel angle ε from -6° to, say, $+6^\circ$, results in a shorter solution; to three significant figures,

$$\boldsymbol{x}_0 = (747, 207, -70)^T$$
$$\boldsymbol{x}_1 = (300, 200, -70)^T.$$

For a non-driven rear axle, wheel-travel angle is not truly necessary; as such, it is not unreasonable to sacrifice it for shorter control blades. Indeed, the Ford Focus is mostly sold as a front-wheel-drive vehicle and so this is an acceptable compromise. In order to facilitate comparison of all synthesized linkage examples, the longer solution is used moving forward. To complete this control blade example some lateral S-S links are needed.

10.3 S-S Links for the Control Blade

In this section, let $\boldsymbol{x}_0$ and $\boldsymbol{x}_1$ be the body-side and wheel-side joint coordinates for an S-S link, respectively. Previously, the design-position velocity synthesis equation

$$\boldsymbol{x}_1' \cdot (\boldsymbol{x}_1 - \boldsymbol{x}_0) = 0$$

was developed. The approach here is the same as used for the S-S links in the S joint chapter: specify $\boldsymbol{x}_1$, plan view angle α, and link length ℓ. As such,

$$\boldsymbol{x}_0 = \boldsymbol{x}_1 - \ell \boldsymbol{e},$$

where

$$\boldsymbol{e} = \pm \frac{\boldsymbol{x}_1' \times (\boldsymbol{i} - \tan\alpha \boldsymbol{j})}{|\boldsymbol{x}_1' \times (\boldsymbol{i} - \tan\alpha \boldsymbol{j})|}.$$

The choice of sign is based on which solution places the body-side point outboard of the wheel-side point. Link length ℓ is best-established by what it would need to be to hypothetically allow the wheel-side point to reach a point $\boldsymbol{x}_2 = \boldsymbol{A}_2 \boldsymbol{x}_1 + \boldsymbol{b}_2$. See the S joint chapter. This means that

$$\ell = -\frac{(\boldsymbol{x}_2 - \boldsymbol{x}_1) \cdot (\boldsymbol{x}_2 - \boldsymbol{x}_1)}{2\boldsymbol{e} \cdot (\boldsymbol{x}_2 - \boldsymbol{x}_1)}.$$

Using this method, three lateral links (plan view angle zero) are easily synthesized. As is typical for control blade suspensions, two of the three are made below the wheel center with the other up top. In particular, see Table 10.1. The link lengths were computed based on the $z = +25$ mm jounce position. The completed suspension linkage is shown in Figure 10.5.

Table 10.1. Coordinates of the three lateral S-S links used for the control blade example (three significant figures).

	Back Lower	Front Lower	Upper
x_0	-100	100	0
y_0	742	653	505
z_0	-94.9	-107	146
x_1	-100	100	0
y_1	200	200	200
z_1	-150	-150	150

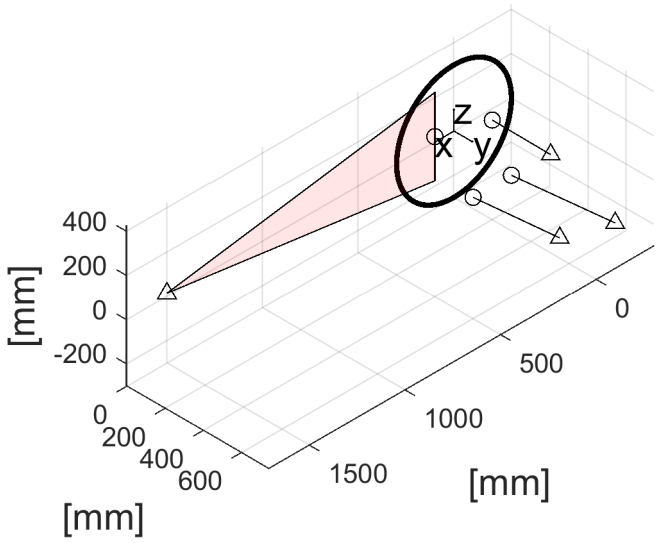

Figure 10.5. A complete control blade suspension synthesized from the velocity specification.

10.4 Analysis of the Control Blade Suspension

For this suspension,

$$\boldsymbol{f}(\boldsymbol{q}) = \begin{pmatrix} (\boldsymbol{x}_i - \boldsymbol{x}_0) \cdot (\boldsymbol{x}_i - \boldsymbol{x}_0) - (\boldsymbol{x}_1 - \boldsymbol{x}_0) \cdot (\boldsymbol{x}_1 - \boldsymbol{x}_0) \\ (\boldsymbol{x}_i - \boldsymbol{x}_0) \cdot \boldsymbol{u}_i \\ [(\boldsymbol{x}_i - \boldsymbol{x}_0) \cdot (\boldsymbol{x}_i - \boldsymbol{x}_0) - (\boldsymbol{x}_1 - \boldsymbol{x}_0) \cdot (\boldsymbol{x}_1 - \boldsymbol{x}_0)]_{\mathrm{BL}} \\ [(\boldsymbol{x}_i - \boldsymbol{x}_0) \cdot (\boldsymbol{x}_i - \boldsymbol{x}_0) - (\boldsymbol{x}_1 - \boldsymbol{x}_0) \cdot (\boldsymbol{x}_1 - \boldsymbol{x}_0)]_{\mathrm{FL}} \\ [(\boldsymbol{x}_i - \boldsymbol{x}_0) \cdot (\boldsymbol{x}_i - \boldsymbol{x}_0) - (\boldsymbol{x}_1 - \boldsymbol{x}_0) \cdot (\boldsymbol{x}_1 - \boldsymbol{x}_0)]_{\mathrm{UP}} \end{pmatrix},$$

where the first two equations are for the control blade itself and the last three equations are for the back link, front link, and upper link, respectively. These equations can be solved using the same iterative method as before.

Camber results are shown in Figure 10.6. Toe results, Figure 10.7. For wheel-travel angle, see Figure 10.8. Support angle is shown in Figure 10.9. For roll center height results, see Figure 10.10. Front-view kinematics (camber, roll center height) are quite good considering only design-position velocity was specified. The link length requirement on the lateral S-S links likely contributes to this performance. The toe curve is linear to about ± 50 mm of vertical wheel travel, another good performer considering the motion specification. The wheel-travel angle becomes increasingly positive with jounce, meaning diminished anti-squat — not ideal if this is a rear-drive vehicle. Support angle becomes increasingly negative with rebound; this is increasing anti-lift behavior. The control blade suspension is an interesting design, but its kinematic performance does not seem to justify its number of links, its packaging issues, and its inability to accommodate a kingpin axis, especially compared to the SLA suspension. Perhaps its elastokinematic performance is why it has become so popular for compact car rear suspensions.

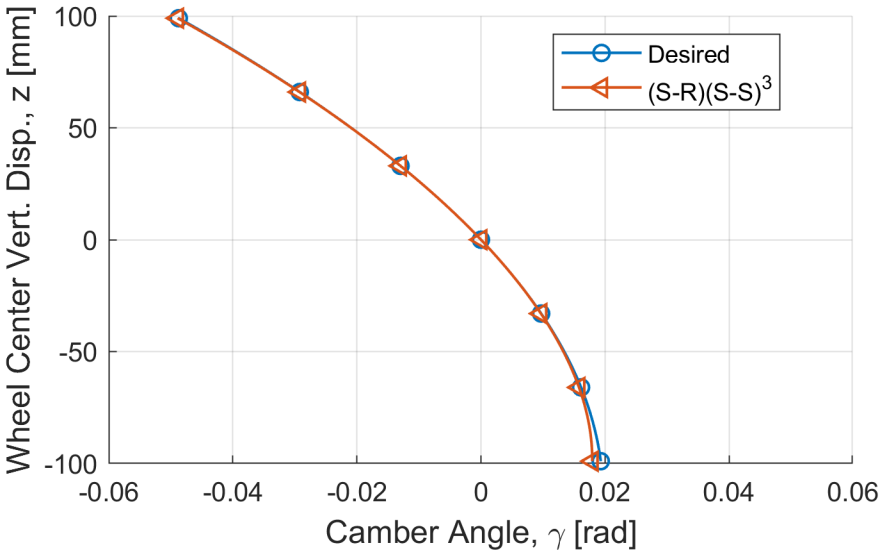

Figure 10.6. Camber curve for the synthesized control blade suspension.

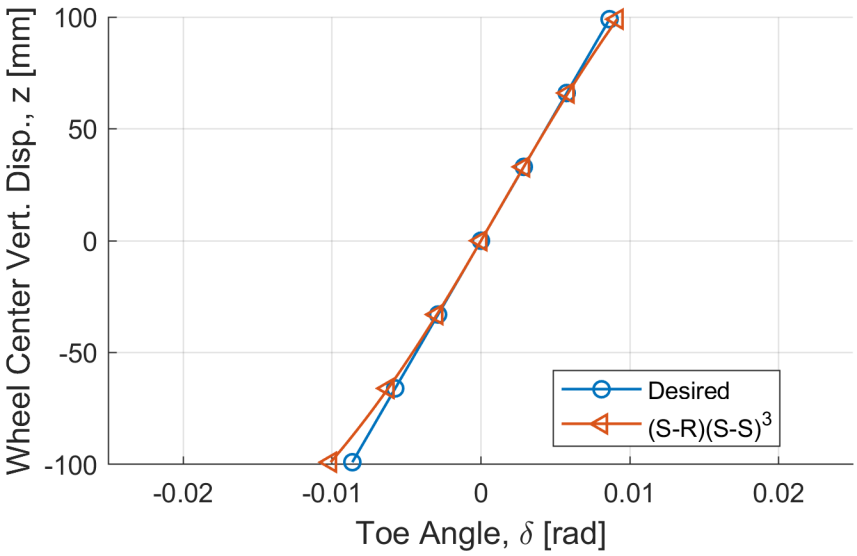

Figure 10.7. Toe curve for the synthesized control blade suspension.

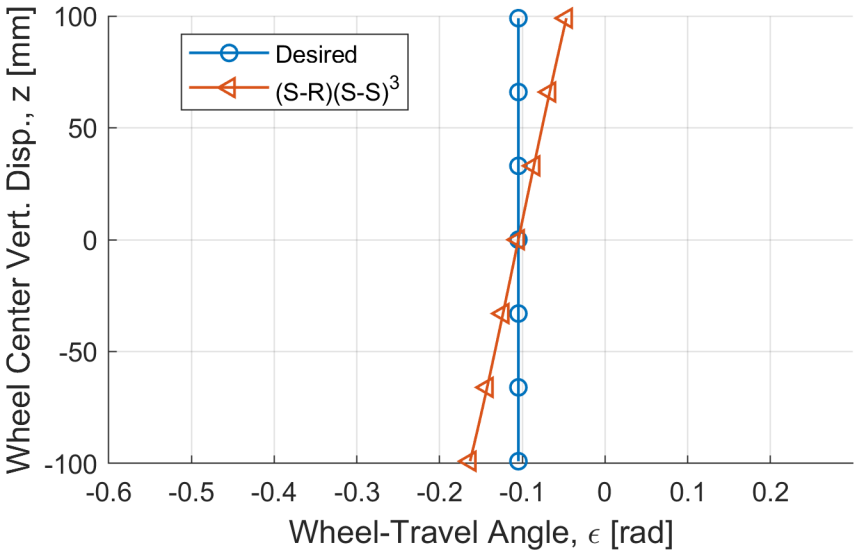

Figure 10.8. Wheel-travel angle curve for the synthesized control blade suspension.

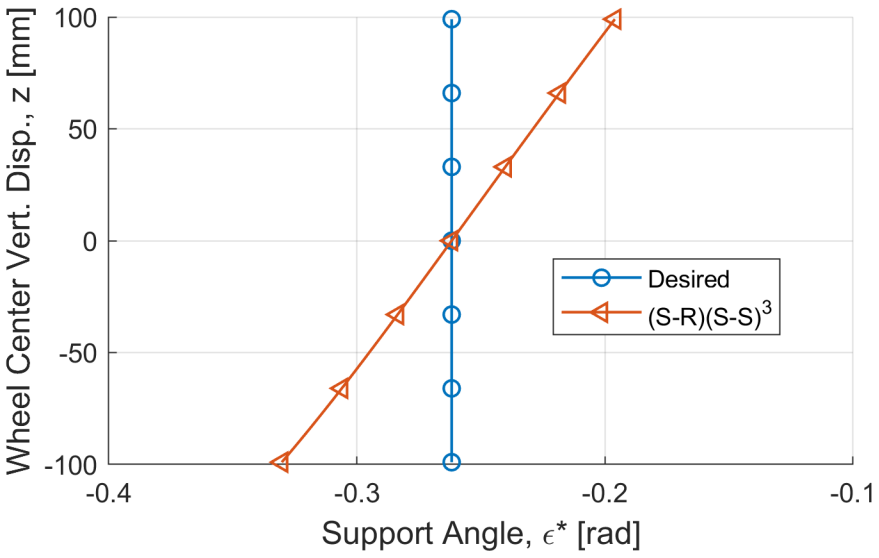

Figure 10.9. Support angle curve for the synthesized control blade suspension.

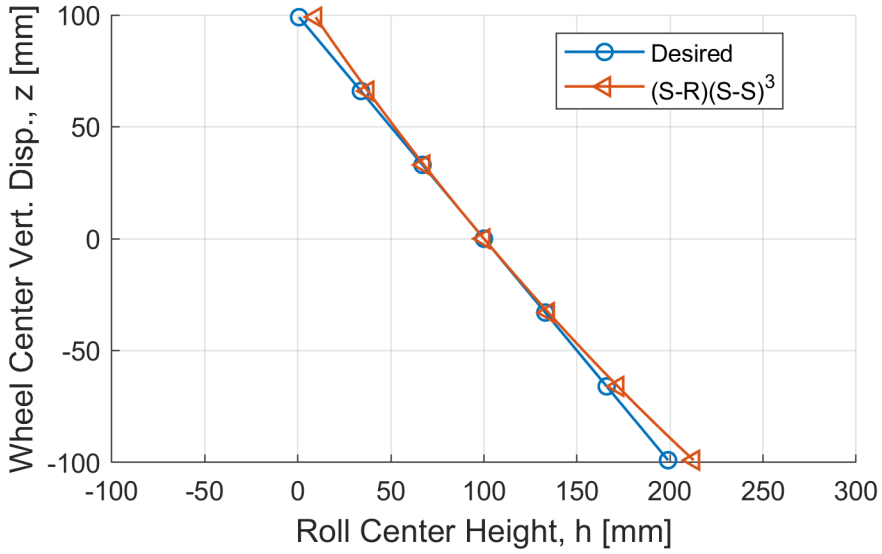

Figure 10.10. Roll center height curve for the synthesized control blade suspension.

Chapter 11

The R-R Link

11.1 Design Equations

The R-R link indirectly connects the wheel carrier to the vehicle body, as illustrated in Figure 11.1. The body-side R joint is given by column vector $\boldsymbol{u}_0$ and coordinate vector $\boldsymbol{x}_0$, which must satisfy

$$\begin{aligned} \boldsymbol{u}_0 \cdot \boldsymbol{u}_0 &= 1 \\ (\boldsymbol{x}_1 - \boldsymbol{x}_0) \cdot \boldsymbol{u}_0 &= 0, \end{aligned}$$

while the wheel-side R joint is given by column vector $\boldsymbol{u}_1$ and coordinate vector $\boldsymbol{x}_1$, which must satisfy

$$\begin{aligned} \boldsymbol{u}_1 \cdot \boldsymbol{u}_1 &= 1 \\ (\boldsymbol{x}_1 - \boldsymbol{x}_0) \cdot \boldsymbol{u}_1 &= 0. \end{aligned}$$

The R joint axes arising from synthesis are expected to be *skew*; that is, they do not intersect and are not parallel. In the former case, the wheel will rotate about the fixed point of intersection — spherical motion. In the latter case, the wheel will move in the plane normal to the shared axes' direction — planar motion. The desired wheel motion is, in general, spatial, so the expectation is to find R-R geometries with skew

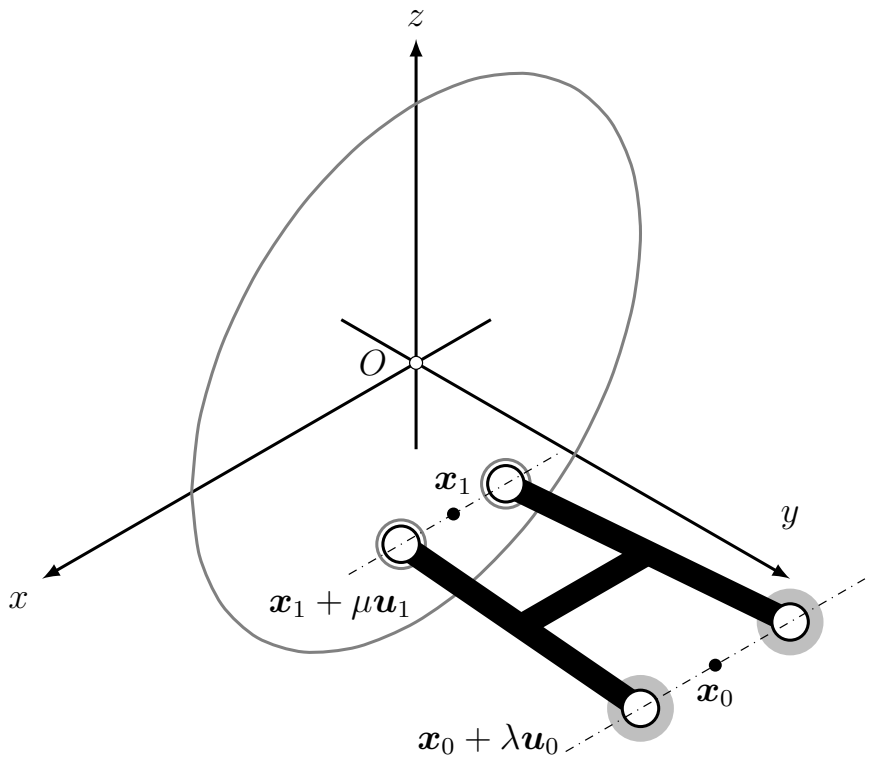

Figure 11.1. Illustration of the R-R link.

axes.

When the wheel moves from Position 1 (design) to Position i, the wheel-side R joint coordinates $\boldsymbol{x}_1$ and $\boldsymbol{u}_1$ transform to

$$\begin{aligned} \boldsymbol{x}_i &= \boldsymbol{A}_i\boldsymbol{x}_1 + \boldsymbol{b}_1 \\ \boldsymbol{u}_i &= \boldsymbol{A}_i\boldsymbol{u}_1, \end{aligned}$$

and the following equations must be satisfied [51]:

$$\begin{aligned} (\boldsymbol{x}_i - \boldsymbol{x}_0) \cdot \boldsymbol{u}_0 &= 0 \\ (\boldsymbol{x}_i - \boldsymbol{x}_0) \cdot \boldsymbol{u}_i &= 0 \\ (\boldsymbol{x}_i - \boldsymbol{x}_0) \cdot (\boldsymbol{x}_i - \boldsymbol{x}_0) &= (\boldsymbol{x}_1 - \boldsymbol{x}_0) \cdot (\boldsymbol{x}_1 - \boldsymbol{x}_0) \\ [(\boldsymbol{x}_i + \boldsymbol{u}_i) - (\boldsymbol{x}_0 + \boldsymbol{u}_0)] \cdot [(\boldsymbol{x}_i + \boldsymbol{u}_i) - (\boldsymbol{x}_0 + \boldsymbol{u}_0)] &= \\ [(\boldsymbol{x}_1 + \boldsymbol{u}_1) - (\boldsymbol{x}_0 + \boldsymbol{u}_0)] \cdot [(\boldsymbol{x}_1 + \boldsymbol{u}_1) - (\boldsymbol{x}_0 + \boldsymbol{u}_0)]&. \end{aligned}$$

The first three are the result of combining the R-S and S-R displacement equations. The last equation, which is another constant-distance constraint across the R joint axes, ensures that the wheel-side R joint cannot rotate about the axis through $\boldsymbol{x}_1$ and $\boldsymbol{x}_0$.

It should be no surprise that velocity equations for the R-R link are required. These follow from the above displacement equations:

$$\begin{aligned}
\boldsymbol{x}_i' \cdot \boldsymbol{u}_0 &= 0 \\
(\boldsymbol{x}_i - \boldsymbol{x}_0) \cdot \boldsymbol{u}_i' + \boldsymbol{x}_i' \cdot \boldsymbol{u}_i &= 0 \\
\boldsymbol{x}_i' \cdot (\boldsymbol{x}_i - \boldsymbol{x}_0) &= 0 \\
(\boldsymbol{x}_i' + \boldsymbol{u}_i') \cdot [(\boldsymbol{x}_i + \boldsymbol{u}_i) - (\boldsymbol{x}_0 + \boldsymbol{u}_0)] &= 0,
\end{aligned}$$

where

$$\begin{aligned}
\boldsymbol{x}_i' &= \boldsymbol{\omega}_i \times \boldsymbol{x}_i + \boldsymbol{v}_i \\
\boldsymbol{u}_i' &= \boldsymbol{\omega}_i \times \boldsymbol{u}_i.
\end{aligned}$$

Suppose the goal is to synthesize R-R links for design-position velocity as well as $n-1$ wheel positions other than design. In this case, the complete design equations

are

$$\begin{aligned}
\boldsymbol{u}_0 \cdot \boldsymbol{u}_0 &= 1 \\
\boldsymbol{u}_1 \cdot \boldsymbol{u}_1 &= 1 \\
(\boldsymbol{x}_i - \boldsymbol{x}_0) \cdot \boldsymbol{u}_0 &= 0,\ i = 1, \ldots, n \\
(\boldsymbol{x}_i - \boldsymbol{x}_0) \cdot \boldsymbol{u}_i &= 0,\ i = 1, \ldots, n \\
(\boldsymbol{x}_i - \boldsymbol{x}_0) \cdot (\boldsymbol{x}_i - \boldsymbol{x}_0) &= (\boldsymbol{x}_1 - \boldsymbol{x}_0) \cdot (\boldsymbol{x}_1 - \boldsymbol{x}_0),\ i = 2, \ldots, n \\
[(\boldsymbol{x}_i + \boldsymbol{u}_i) - (\boldsymbol{x}_0 + \boldsymbol{u}_0)] \cdot [(\boldsymbol{x}_i + \boldsymbol{u}_i) - (\boldsymbol{x}_0 + \boldsymbol{u}_0)] &= \\
[(\boldsymbol{x}_1 + \boldsymbol{u}_1) - (\boldsymbol{x}_0 + \boldsymbol{u}_0)] \cdot [(\boldsymbol{x}_1 + \boldsymbol{u}_1) - (\boldsymbol{x}_0 + \boldsymbol{u}_0)]&,\ i = 2, \ldots, n \\
\boldsymbol{x}_1' \cdot \boldsymbol{u}_0 &= 0 \\
(\boldsymbol{x}_1 - \boldsymbol{x}_0) \cdot \boldsymbol{u}_1' + \boldsymbol{x}_1' \cdot \boldsymbol{u}_1 &= 0 \\
\boldsymbol{x}_1' \cdot (\boldsymbol{x}_1 - \boldsymbol{x}_0) &= 0 \\
(\boldsymbol{x}_1' + \boldsymbol{u}_1') \cdot [(\boldsymbol{x}_1 + \boldsymbol{u}_1) - (\boldsymbol{x}_0 + \boldsymbol{u}_0)] &= 0.
\end{aligned}$$

When $n = 1$, there are eight design equations; when $n = 2$, there are 12 design equations. There are 12 design variables, so design-position velocity plus one additional wheel position is the most-complete wheel trajectory specification possible, with no choice of free parameter. Without free parameters, it is extremely difficult to package a linkage. Consequently, the design-position velocity synthesis, $n = 1$, will be the focus in the next section.

11.2 Synthesis Example

For design position velocity only, the R-R link design equations reduce to

$$\begin{aligned}
\boldsymbol{u}_0 \cdot \boldsymbol{u}_0 &= 1 \\
\boldsymbol{u}_1 \cdot \boldsymbol{u}_1 &= 1 \\
(\boldsymbol{x}_1 - \boldsymbol{x}_0) \cdot \boldsymbol{u}_0 &= 0 \\
(\boldsymbol{x}_1 - \boldsymbol{x}_0) \cdot \boldsymbol{u}_1 &= 0 \\
\boldsymbol{x}_1' \cdot \boldsymbol{u}_0 &= 0 \\
(\boldsymbol{x}_1 - \boldsymbol{x}_0) \cdot \boldsymbol{u}_1' + \boldsymbol{x}_1' \cdot \boldsymbol{u}_1 &= 0 \\
\boldsymbol{x}_1' \cdot (\boldsymbol{x}_1 - \boldsymbol{x}_0) &= 0 \\
(\boldsymbol{x}_1' + \boldsymbol{u}_1') \cdot [(\boldsymbol{x}_1 + \boldsymbol{u}_1) - (\boldsymbol{x}_0 + \boldsymbol{u}_0)] &= 0.
\end{aligned}$$

There are eight design equations in 12 design variables. A useful way to create a set of design equations with an equal number of variables is to specify wheel-side coordinate $\boldsymbol{x}_1$ and the minimum link length ℓ, which adds the design equation

$$(\boldsymbol{x}_1 - \boldsymbol{x}_0) \cdot (\boldsymbol{x}_1 - \boldsymbol{x}_0) = \ell^2,$$

giving nine equations in nine unknowns. This approach is convenient for packaging because it allows the wheel-side coordinate $\boldsymbol{x}_1$ to be defined, where space is at a premium. Additionally, forcing a certain minimum link length ℓ prevents the synthesis of implausibly-long links.

As an example, let $\boldsymbol{x}_1 = (0, 100, -150)^T$, with $\ell = 350$ (all units are millimeters). Synthesis proceeded by using the existing design-position velocity specification and Bertini as the polynomial-system solver. Bertini found 8 real solutions but only two were unique. The duplicates were because either sign of $\boldsymbol{u}_0$ (and $\boldsymbol{u}_1$) satisfies the design equations. Of the two unique solutions, one placed the body-side side point on the wrong side of the wheel, meaning the link would have to pass through the wheel, which is not physically possible. This leaves the solution shown in Figure 11.2, which,

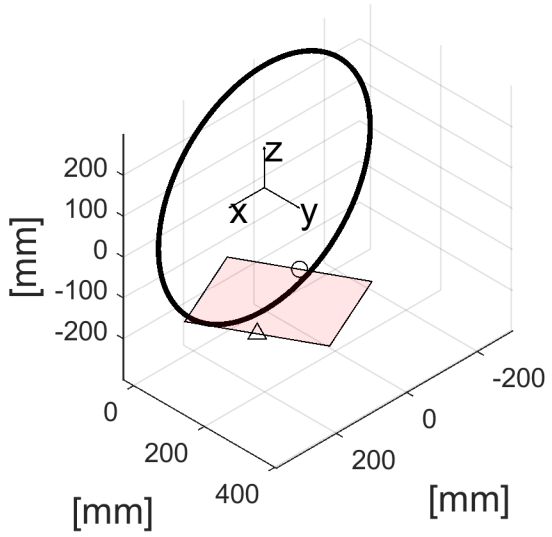

Figure 11.2. An R-R link synthesized from design-position velocity. The triangular marker denotes the fixed joint axis, while the circular marker denotes the moving joint axis.

to three significant figures, has

$$\boldsymbol{u}_0 = (-0.505, 0.863, -0.0205)^T$$
$$\boldsymbol{x}_0 = (294, 274, -74.1)^T$$
$$\boldsymbol{u}_1 = (-0.495, 0.866, -0.0664)^T$$
$$\boldsymbol{x}_1 = (0.00, 100, -150)^T.$$

Note that this solution fits inside the packaging cube used previously.

The only complete suspension linkage using the R-R link arising from the number synthesis is the (R-R)(S-S), which is often referred to as the *trapezoidal link* suspension due to the trapezoidal geometry suggested by the R-R link. Naturally, methods to generate S-S links are wanted that produce complete trapezoidal link suspensions.

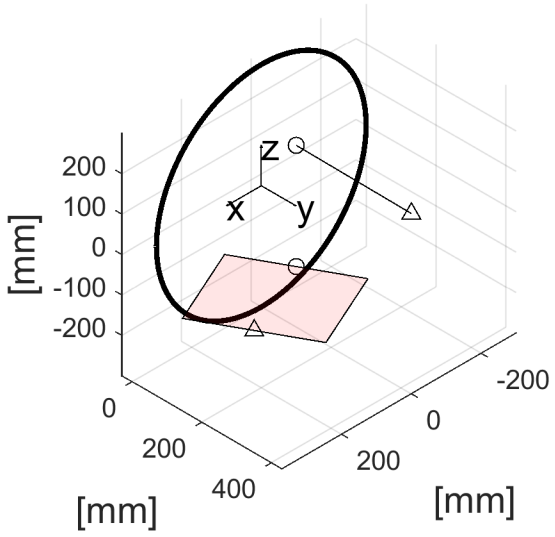

Figure 11.3. A trapezoidal link suspension synthesized from design-position velocity.

11.3 S-S Links for the Trapezoidal Link Suspension

Let $\boldsymbol{x}_1^*$ denote the wheel-side coordinate of an S-S link and $\boldsymbol{x}_0^*$ denote the body-side coordinate of an S-S link. To produce S-S links that complete a trapezoidal link suspension, the same approach as seen in the S joint and S-R link chapters is used: specify $\boldsymbol{x}_1^*$, plan view angle α^*, and link length ℓ^*. In this example, let

$$\boldsymbol{x}_1^* = (0, 100, 150)^T,$$

which is simply 300 mm above $\boldsymbol{x}_1$, the R-R link connection at the wheel. For plan view angle, let $\alpha^* = 0$, producing a true lateral link. Link length ℓ^* is based on the wheel hypothetically achieving a +25 mm jounce position. As such, to three significant figures,

$$\boldsymbol{x}_0^* = (0.00, 429, 146)^T.$$

Note that this link fits in the packaging cube first introduced in the S-S link chapter. The complete trapezoidal link suspension is shown in Figure 11.3.

11.4 Analyzing the Trapezoidal Link Suspension

The relevant equations for analysis are

$$\boldsymbol{f}(\boldsymbol{q}) = \begin{pmatrix} (\boldsymbol{x}_i - \boldsymbol{x}_0) \cdot \boldsymbol{u}_0 \\ (\boldsymbol{x}_i - \boldsymbol{x}_0) \cdot \boldsymbol{u}_i \\ (\boldsymbol{x}_i - \boldsymbol{x}_0) \cdot (\boldsymbol{x}_i - \boldsymbol{x}_0) - (\boldsymbol{x}_1 - \boldsymbol{x}_0) \cdot (\boldsymbol{x}_1 - \boldsymbol{x}_0) \\ [(\boldsymbol{x}_i + \boldsymbol{u}_i) - (\boldsymbol{x}_0 + \boldsymbol{u}_0)] \cdot [(\boldsymbol{x}_i + \boldsymbol{u}_i) - (\boldsymbol{x}_0 + \boldsymbol{u}_0)] - L^2 \\ (\boldsymbol{x}_i^* - \boldsymbol{x}_0^*) \cdot (\boldsymbol{x}_i^* - \boldsymbol{x}_0^*) - (\boldsymbol{x}_1^* - \boldsymbol{x}_0^*) \cdot (\boldsymbol{x}_1^* - \boldsymbol{x}_0^*) \end{pmatrix}$$

where

$$L^2 = [(\boldsymbol{x}_1 + \boldsymbol{u}_1) - (\boldsymbol{x}_0 + \boldsymbol{u}_0)] \cdot [(\boldsymbol{x}_1 + \boldsymbol{u}_1) - (\boldsymbol{x}_0 + \boldsymbol{u}_0)] \,.$$

Camber results are shown in Figure 11.4. Toe results, Figure 11.5. For wheel-travel angle, see Figure 11.6. Support angle is shown in Figure 11.7. For roll center height results, see Figure 11.8.

Camber and toe track well close to the design position, but eventually fall away from the desired curves. Wheel-travel angle experiences large changes; it becomes increasingly positive with jounce, producing undesirable pro-squat effects for rear drive vehicles. Support angle indicates increasing anti-lift as the rear end rises. Roll center height trends correctly but does not change as much with jounce and rebound as desired. The biggest issue is with wheel-travel angle; if this suspension was used on a non-driven rear axle this would not be as much of a concern.

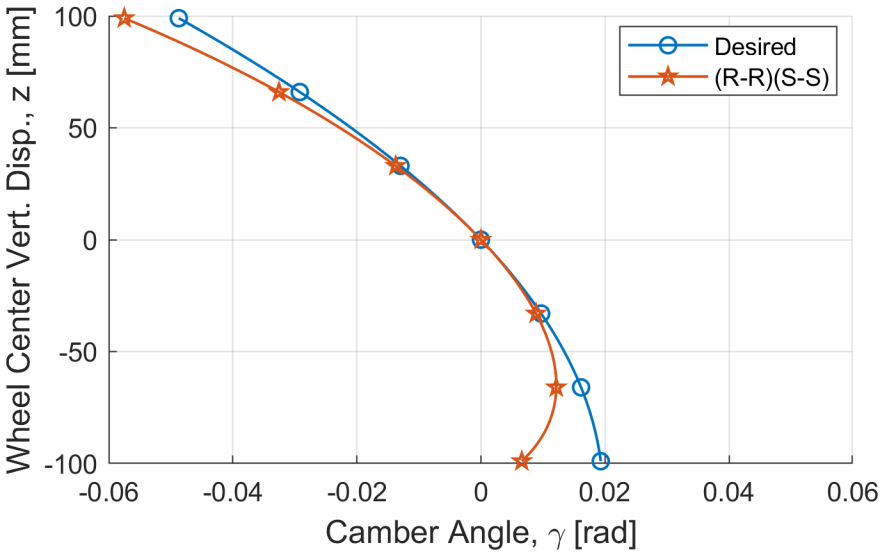

Figure 11.4. Camber curve for the synthesized trapezoidal link suspension.

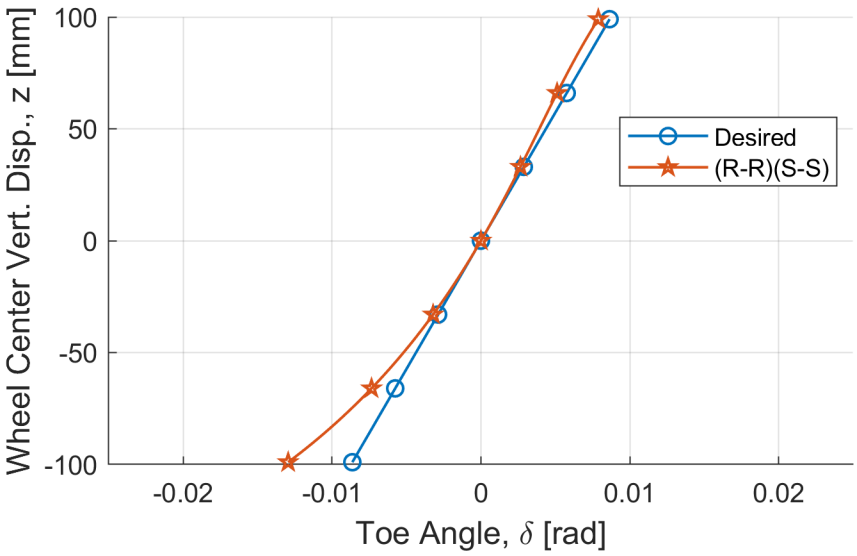

Figure 11.5. Toe curve for the synthesized trapezoidal link suspension.

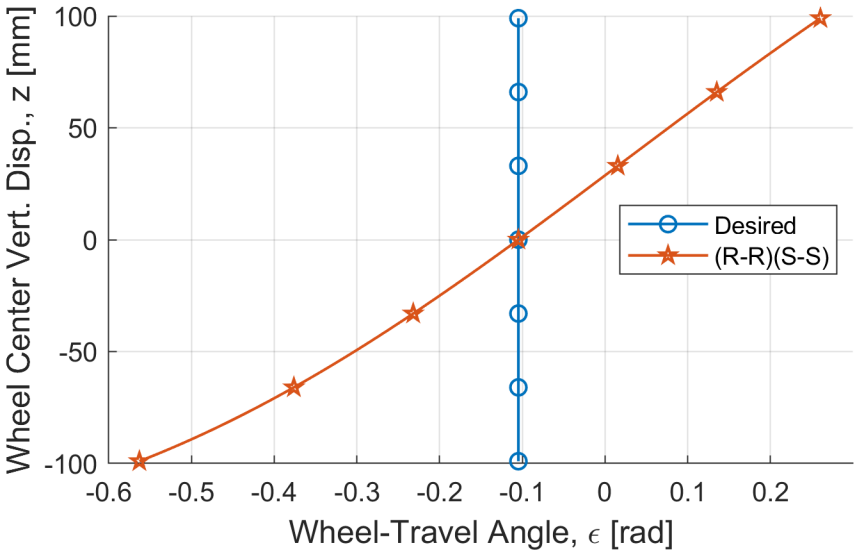

Figure 11.6. Wheel-travel angle curve for the synthesized trapezoidal link suspension.

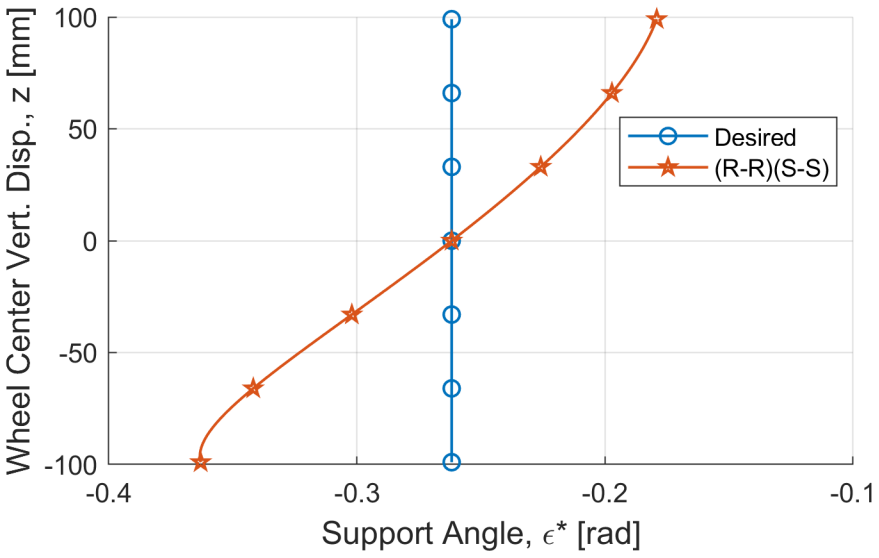

Figure 11.7. Support angle curve for the synthesized trapezoidal link suspension.

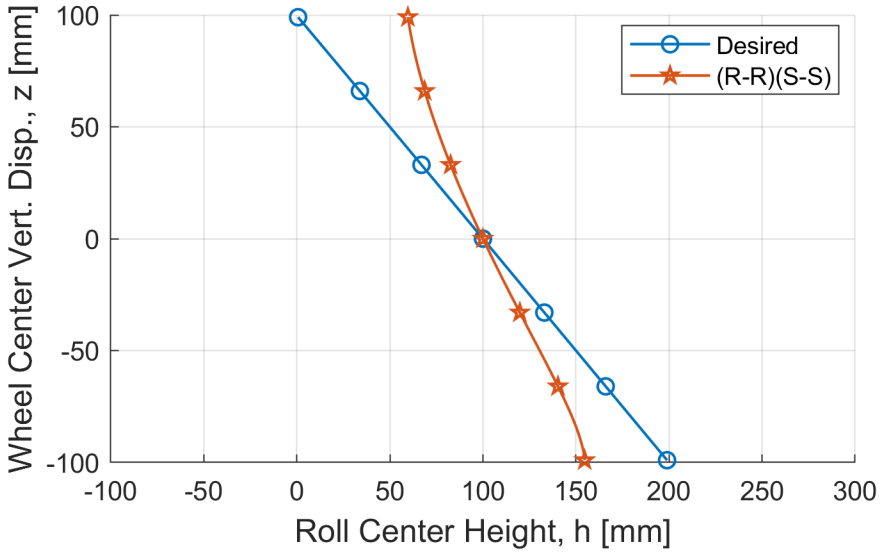

Figure 11.8. Roll center height curve for the synthesized trapezoidal link suspension.

Chapter 12

The S-C Link

12.1 Design Equations

The S-C link is depicted in Figure 12.1. It creates an indirect connection between the wheel carrier and the vehicle body. The S joint is located on the body-side by coordinate vector $\boldsymbol{x}_0$. The C joint is assumed to pass through the S joint, so only a column vector $\boldsymbol{u}_1$ that gives its direction is needed. The reason it is assumed that the C joint passes through the S joint is that this is how S-C links are encountered in practice as *damper struts*, which provide both kinematic constraint and damping in one unit. In some cases, these additionally accommodate coil springs, resulting in the so-called *coil-over strut*. From a wheel-kinematics point-of-view the damper strut and coil-over strut are equivalent. Since the S-C link is encountered as one of these struts, assume (really, *require*) that the column vector $\boldsymbol{u}_1$ has a nonzero component in the vertical direction. After all, the strut should damp vertical motion of the wheel. Consequently, rather than require that $\boldsymbol{u}_1$ be a unit vector, instead assign it design variables u_1 and v_1 such that

$$\boldsymbol{u}_1 = (u_1, v_1, 1)^T.$$

When the wheel is moved from Position 1 (design) to Position i, the point $\boldsymbol{x}_1 := \boldsymbol{x}_0$

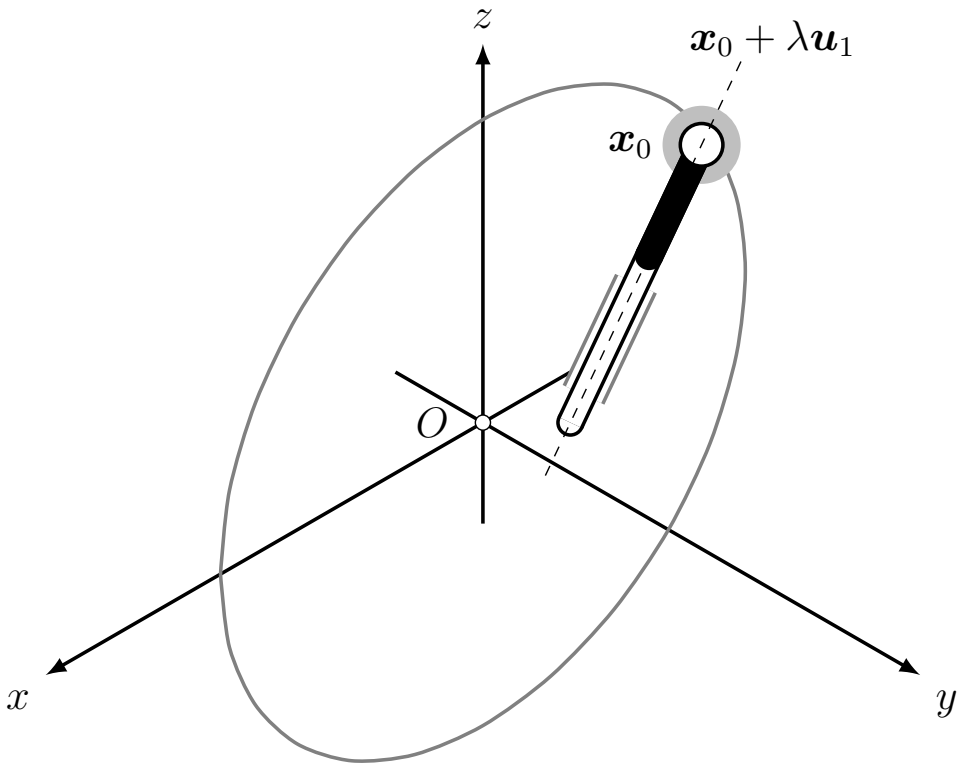

Figure 12.1. Illustration of the S-C link.

on the strut axis is mapped to

$$\boldsymbol{x}_i = \boldsymbol{A}_i \boldsymbol{x}_1 + \boldsymbol{b}_i,$$

while the strut direction vector $\boldsymbol{u}_1$ is mapped to

$$\boldsymbol{u}_i = \boldsymbol{A}_i \boldsymbol{u}_1.$$

The strut requires that the line through $\boldsymbol{x}_i$ with direction $\boldsymbol{u}_i$ always pass through fixed point $\boldsymbol{x}_0$. In other words, for some $t \in \mathbf{R}$,

$$\boldsymbol{x}_i + t\boldsymbol{u}_i = \boldsymbol{x}_0.$$

The next step is to eliminate t, as follows. Some substitution and manipulation results

in

$$t \begin{pmatrix} u_1 \\ v_1 \\ 1 \end{pmatrix} = \boldsymbol{A}_i^T(\boldsymbol{x}_0 - \boldsymbol{x}_i),$$

so that $t = \boldsymbol{k}^T \boldsymbol{A}_i^T(\boldsymbol{x}_0 - \boldsymbol{x}_i)$, reducing the three equations to the two equations

$$u_1 \boldsymbol{k}^T \boldsymbol{A}_i^T(\boldsymbol{x}_0 - \boldsymbol{x}_i) = \boldsymbol{i}^T \boldsymbol{A}_i^T(\boldsymbol{x}_0 - \boldsymbol{x}_i)$$
$$v_1 \boldsymbol{k}^T \boldsymbol{A}_i^T(\boldsymbol{x}_0 - \boldsymbol{x}_i) = \boldsymbol{j}^T \boldsymbol{A}_i^T(\boldsymbol{x}_0 - \boldsymbol{x}_i).$$

These two may be rewritten as

$$\left[\boldsymbol{A}_i(u_1 \boldsymbol{k} - \boldsymbol{i})\right]^T (\boldsymbol{x}_i - \boldsymbol{x}_0) = 0 \tag{12.1}$$
$$\left[\boldsymbol{A}_i(v_1 \boldsymbol{k} - \boldsymbol{j})\right]^T (\boldsymbol{x}_i - \boldsymbol{x}_0) = 0. \tag{12.2}$$

The vector $\boldsymbol{f}_1 := u_1 \boldsymbol{k} - \boldsymbol{i}$ is perpendicular to $\boldsymbol{u}_1$, as is the vector $\boldsymbol{g}_1 := v_1 \boldsymbol{k} - \boldsymbol{j}$. Hence, these displacement equations require that $\boldsymbol{f}_i = \boldsymbol{A}_i \boldsymbol{f}_1$ and $\boldsymbol{g}_i = \boldsymbol{A}_i \boldsymbol{g}_1$ be perpendicular to the displacement vector $\boldsymbol{x}_i - \boldsymbol{x}_0$. In other words, $\boldsymbol{u}_i$ should be parallel to $\boldsymbol{x}_i - \boldsymbol{x}_0$. This could be ensured with $\boldsymbol{u}_i \times (\boldsymbol{x}_i - \boldsymbol{x}_0) = \boldsymbol{0}$, but this introduces three equations when only two are truly necessary. (In fact, (12.1) and (12.2) are equivalent to two of the cross product equations.) Naturally, there is interest in the derivatives of (12.1) and (12.2). These are simply

$$\boldsymbol{f}_i \cdot \boldsymbol{x}_i' + \boldsymbol{f}_i' \cdot (\boldsymbol{x}_i - \boldsymbol{x}_0) = 0$$
$$\boldsymbol{g}_i \cdot \boldsymbol{x}_i' + \boldsymbol{g}_i' \cdot (\boldsymbol{x}_i - \boldsymbol{x}_0) = 0.$$

In the design position,

$$\boldsymbol{f}_1 \cdot \boldsymbol{x}_1' + \boldsymbol{f}_1' \cdot (\boldsymbol{x}_1 - \boldsymbol{x}_0) = 0$$
$$\boldsymbol{g}_1 \cdot \boldsymbol{x}_1' + \boldsymbol{g}_1' \cdot (\boldsymbol{x}_1 - \boldsymbol{x}_0) = 0,$$

which simplify to

$$\boldsymbol{f}_1 \cdot \boldsymbol{x}_1' = 0$$
$$\boldsymbol{g}_1 \cdot \boldsymbol{x}_1' = 0$$

since $\boldsymbol{x}_1 = \boldsymbol{x}_0$.

Overall, the design equations for an S-C link achieving design position velocity as well as $n-1$ positions other than design are

$$\boldsymbol{f}_1 \cdot \boldsymbol{x}_1' = 0$$
$$\boldsymbol{g}_1 \cdot \boldsymbol{x}_1' = 0$$
$$\boldsymbol{f}_i \cdot (\boldsymbol{x}_i - \boldsymbol{x}_0) = 0;\ i = 2, \ldots, n$$
$$\boldsymbol{g}_i \cdot (\boldsymbol{x}_i - \boldsymbol{x}_0) = 0;\ i = 2, \ldots, n.$$

When $n = 2$, there are four design equations in the five design variables u_1, v_1, and $\boldsymbol{x}_0$. When $n = 3$, there are six design equations, so this number of wheel positions is not possible (unless design-position velocity is sacrificed). When $n = 1$, there are just two design equations, so, for example, body-side coordinate $\boldsymbol{x}_0$ may be freely specified. This is helpful if the strut is to help establish a kingpin axis; the point $\boldsymbol{x}_0$ must lie on the desired axis. Considering that most struts are used to establish a steering axis, synthesis methods for this scenario are developed in the next section.

12.2 Synthesis Methods

For a desired kingpin axis with the S-C (strut) link, the designer is limited to specifying wheel velocity at the design position. The design equations reduce to

$$\boldsymbol{f}_1 \cdot \boldsymbol{x}_1' = 0$$
$$\boldsymbol{g}_1 \cdot \boldsymbol{x}_1' = 0.$$

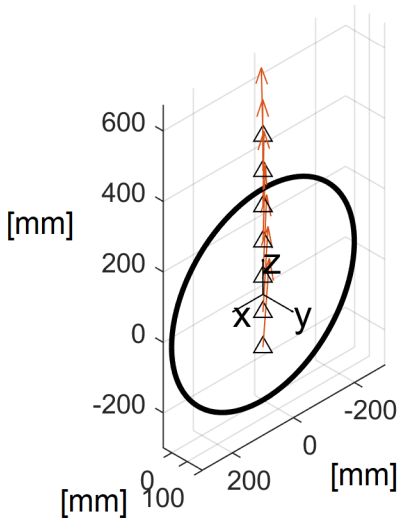

Figure 12.2. S-C link solutions along a simple kingpin geometry. Triangular markers denote $\boldsymbol{x}_0$, while arrows indicate the direction of each corresponding solution for $\boldsymbol{u}_1$.

For a desired kingpin axis, it must be possible to freely choose $\boldsymbol{x}_0$. Since $\boldsymbol{x}_1 = \boldsymbol{x}_0$, this means that only u_1 and v_1 are to be determined. Here $\boldsymbol{f}_1 = u_1\boldsymbol{k} - \boldsymbol{i}$ and $\boldsymbol{g}_1 = v_1\boldsymbol{k} - \boldsymbol{j}$. Consequently,

$$u_1 = \frac{\boldsymbol{i} \cdot \boldsymbol{x}_1'}{\boldsymbol{k} \cdot \boldsymbol{x}_1'}$$
$$v_1 = \frac{\boldsymbol{j} \cdot \boldsymbol{x}_1'}{\boldsymbol{k} \cdot \boldsymbol{x}_1'}.$$

If the desired kingpin axis is given by $\boldsymbol{d} + t\boldsymbol{e}$, where $\boldsymbol{d}$ is a point on the axis, $\boldsymbol{e}$ is a direction vector of the axis, and $t \in \mathbf{R}$, then the necessary strut direction vector $\boldsymbol{u}_1 = (u_1, v_1, 1)^T$ may be easily computed for every point $\boldsymbol{x}_0$ along the axis. For example, consider the typical design-position wheel velocity with the previously-used vertical kingpin passing through the wheel center, Figure 12.2. These solutions show the difficulty in packaging a strut that achieves a desired kingpin and the desired wheel kinematics; in this case, it would clearly be difficult to locate body-side point $\boldsymbol{x}_0$ this close to the wheel since the strut would then pass through the tire. These issues emphasize the need for additional compromise.

In particular, the following approach may be taken. First, define a set of acceptable

Table 12.1. Example S-C solution (three significant figures).

x_0	y_0	z_0	u_1	v_1	w_1	n	r_s	τ	σ
-105	179	450	0.124	0.106	1.00	0.00	20.0	8°	12°

kingpins by establishing intervals for caster offset n, scrub radius r_s, caster angle τ, and kingpin inclination angle σ. Second, choose a desired height for the wheel-side point $\boldsymbol{x}_0$; that is, select z_0. Then, a set of acceptable S joint points may be generated according to

$$\boldsymbol{x}_0 = \begin{pmatrix} n \\ r_s \\ -r \end{pmatrix} + (r + z_0) \begin{pmatrix} -\tan\tau \\ \tan\sigma \\ 1 \end{pmatrix}.$$

This follows from $(n, r_s, -r)^T$, where r is wheel radius, being a point on the kingpin axis, $(-\tan\tau, \tan\sigma, 1)^T$ being kingpin direction, and $(r + z_0)$ being the line parameter such that the desired S joint height is achieved. (Refer back to the S-S link chapter for initial kingpin geometry discussion.) With this set of acceptable points generated, strut direction vector $\boldsymbol{u}_1$ may be readily-computed for each. Then, the solution with minimum inclination angle between $\boldsymbol{u}_1$ and the vertical may be selected. This is simply a heuristic on the idea that vertical wheel motion should correlate well to strut extension/compression. For example, let

$$\begin{aligned} n, r_s &\in \{0, 5, 10, 15, 20\} \\ \tau &\in \{4^\circ, 5^\circ, 6^\circ, 7^\circ, 8^\circ\} \\ \sigma &\in \{8^\circ, 9^\circ, 10^\circ, 11^\circ, 12^\circ\}, \end{aligned}$$

with $z_0 = 450$. From these $5^4 = 625$ solutions are produced for $\boldsymbol{u}_1$. The one that is closest to vertical is shown in Figure 12.3, with details shown in Table 12.1. In this case, the 625 solutions' inclination angles varied only between 9.27° and 9.92° degrees, with the former being that of the selected solution. Notice that the final solution for $\boldsymbol{x}_0$ is within the packaging cube used in various prior examples.

One of the most common independent suspensions uses the S-C link, an R-S link,

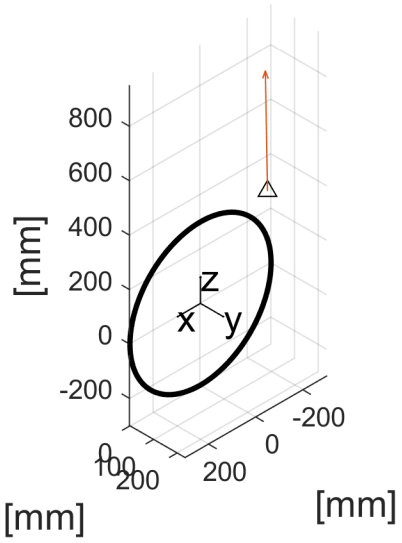

Figure 12.3. S-C link solution that is the most vertical of those generated from a set of kingpin geometries.

and an S-S link — the garden-variety *MacPherson strut* suspension. Next, methods for synthesizing compatible R-S and S-S links are presented.

12.3 Compatible R-S & S-S Links

In this case, R-S links must be synthesized solely from design position velocity, requiring a slightly different approach than encountered previously. In this section, let $\boldsymbol{u}_0$ and $\boldsymbol{x}_0$ define the direction and location of the body-side R joint, respectively, and let $\boldsymbol{x}_1$ locate the wheel-side S joint. For design position velocity only, the R-S link design equations reduce to

$$\begin{aligned} \boldsymbol{u}_0 \cdot \boldsymbol{u}_0 &= 1 \\ (\boldsymbol{x}_1 - \boldsymbol{x}_0) \cdot \boldsymbol{u}_0 &= 0 \\ \boldsymbol{x}_1' \cdot (\boldsymbol{x}_1 - \boldsymbol{x}_0) &= 0 \\ \boldsymbol{x}_1' \cdot \boldsymbol{u}_0 &= 0. \end{aligned}$$

As such, there are nine design variables in four design equations. To ensure compatibility of the R-S link with the desired kingpin axis, $\boldsymbol{x}_1$ must be satisfied. For example, it can be where the kingpin of Table 12.1 intersects the floor of the packaging cube, giving, to three significant figures,

$$\boldsymbol{x}_1 = (-21.1, 51.9, -150)^T.$$

This leaves two free design variables. To aid in packaging the linkage, the minimum length between $\boldsymbol{x}_1$ and $\boldsymbol{x}_0$ can be set; for example, $|\boldsymbol{x}_1 - \boldsymbol{x}_0| = 500$ mm. Additionally, if $\boldsymbol{u}_0 = (u_0, 0, w_0)^T$, then the R joint axis will be parallel to the vehicle center-line in the top view, again helping packaging. These specifications, together with the usual design position velocity requirement, result in the R-S link shown in Fig. 12.4. Solution was via Bertini. Four real solutions were found; two were duplicates while one had the body-side point outboard of the wheel and the other did not. The packageable solution was selected. Explicit coordinates for the example solution are, to three significant figures,

$$\boldsymbol{u}_0 = (0.982, 0.00, 0.189)^T$$
$$\boldsymbol{x}_0 = (-29.7, 550, -105)^T.$$

To complete the example MacPherson strut suspension, an S-S link can be generated using the link length/plan view angle approach encountered in previous chapters. In this case, wheel-side S joint is set at $(150, 0, 0)^T$, plan view angle at zero, with the $z = +25$ mm position used to compute link length. As such, body-side S joint is located at, to three significant figures, $(150, 372, 10.8)^T$. This is the S-S link shown in Fig. 12.4.

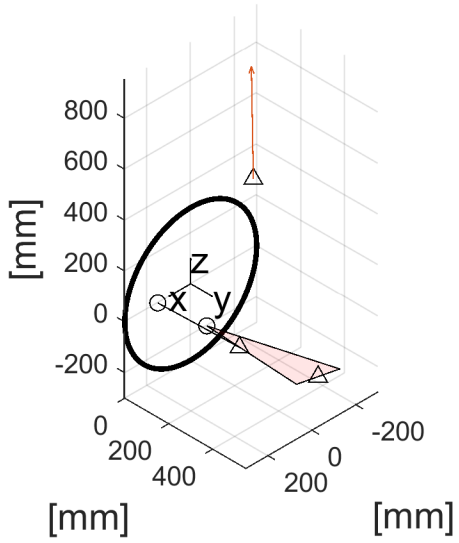

Figure 12.4. S-C link example completed with an R-S link and an S-S link.

12.4 Analyzing the MacPherson Strut Suspension

For kinematic analysis of a MacPherson strut suspension, the following kinematic constraints equations must be solved:

$$\boldsymbol{f}(\boldsymbol{q}) = \begin{pmatrix} \begin{pmatrix} \boldsymbol{f}_i \cdot (\boldsymbol{x}_i - \boldsymbol{x}_0) \\ \boldsymbol{g}_i \cdot (\boldsymbol{x}_i - \boldsymbol{x}_0) \end{pmatrix}_{\text{S-C}} \\ \begin{pmatrix} (\boldsymbol{x}_i - \boldsymbol{x}_0) \cdot \boldsymbol{u}_0 \\ (\boldsymbol{x}_i - \boldsymbol{x}_0) \cdot (\boldsymbol{x}_i - \boldsymbol{x}_0) - (\boldsymbol{x}_1 - \boldsymbol{x}_0) \cdot (\boldsymbol{x}_1 - \boldsymbol{x}_0) \end{pmatrix}_{\text{R-S}} \\ ((\boldsymbol{x}_1 - \boldsymbol{x}_0) \cdot (\boldsymbol{x}_i - \boldsymbol{x}_0) - (\boldsymbol{x}_1 - \boldsymbol{x}_0) \cdot (\boldsymbol{x}_1 - \boldsymbol{x}_0))_{\text{S-S}} \cdot \end{pmatrix}.$$

These follow from appropriate application of the S-C, R-S, and S-S displacement design equations.

Here, the example MacPherson strut suspension is analyzed. Camber results are shown in Figure 12.5. Camber performance of the suspension is poor, with the camber change rate leveling off with jounce. Figure 12.6 shows the toe curve of the synthesized MacPherson strut suspension. While acceptable at/around the design position, toe quickly deviates from the desired value; a linear toe curve is not achieved. For wheel-travel angle, Figure 12.7. If this was a rear-drive vehicle, anti-squat behavior would

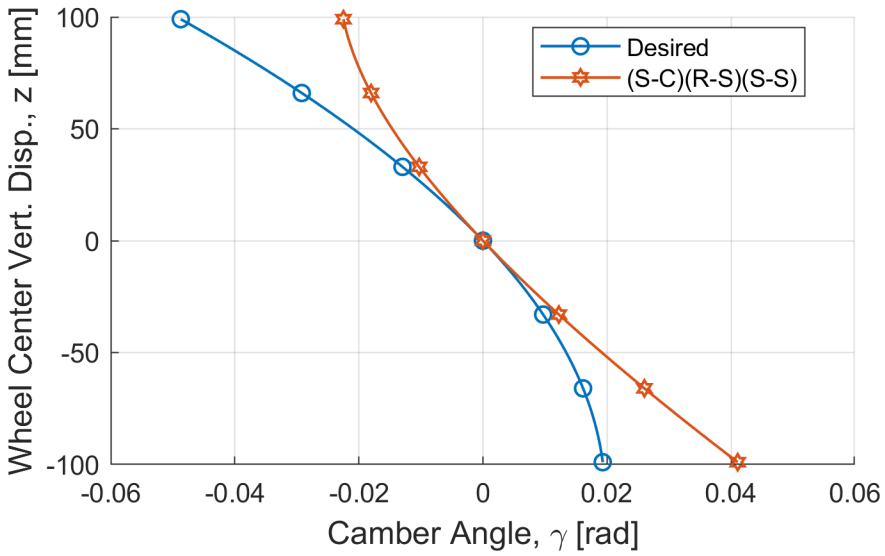

Figure 12.5. Camber curve for the synthesized MacPherson strut suspension.

be established in the design position by the negative wheel-travel angle. As the rear of the vehicle squats, jounce increases, resulting in increasingly less negative wheel-travel angle. This would correspond to a diminishing anti-squat effect. Support angle is shown in Figure 12.8. For an outboard-braked rear wheel, negative support angle in the design position establishes anti-rise behavior (reduces rising of rear end under braking). As the rear end rises, the wheel moves downward with respect to the vehicle body, resulting in slightly less negative support angle. As such, some decrease in anti-rise behavior under braking is to be expected. For roll center height results, Figure 12.9. The MacPherson strut suspension shows more roll center height change than desired; however, the trend is correct.

Most of the kinematic shortcomings are due to the strut itself — after all, the SLA, or (R-S)^2(S-S) suspension, is otherwise similar and performs significantly better when it comes to wheel-kinematics. Despite this, suspensions employing struts remain immensely popular for front axles, perhaps due to the fact that they (1) integrate the damper (and often the spring too) into a kinematic link, and (2) accommodate a steering axis. In the introduction chapter, a cited study showed about three-fourths of 2010 model-year front axles employed a MacPherson strut.

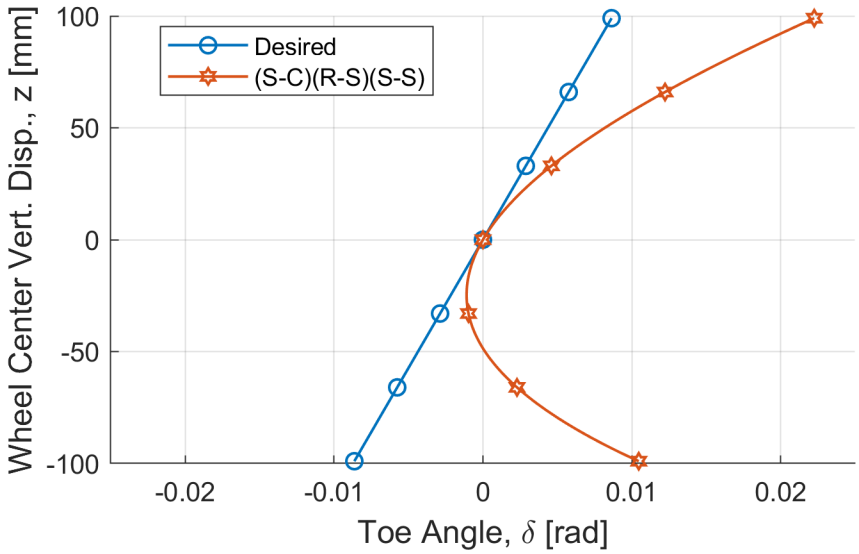

Figure 12.6. Toe curve for the synthesized MacPherson strut suspension.

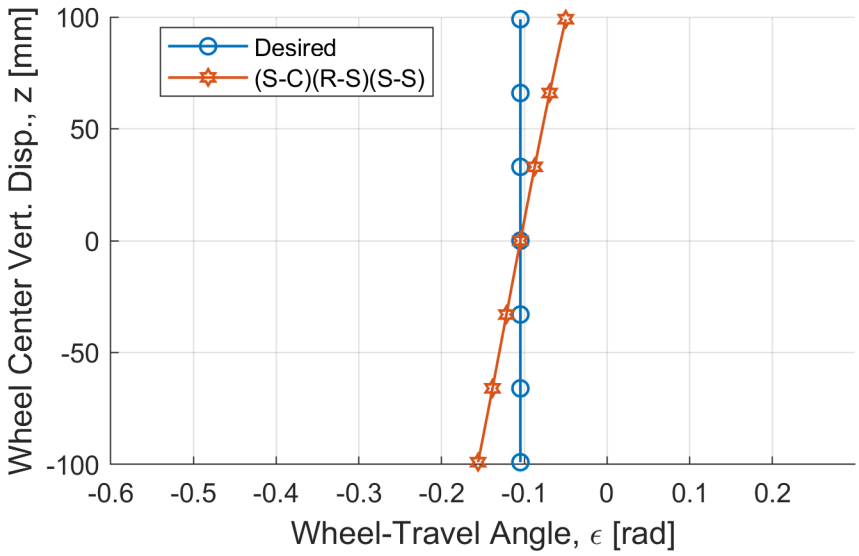

Figure 12.7. Wheel-travel angle curve for the synthesized MacPherson strut suspension.

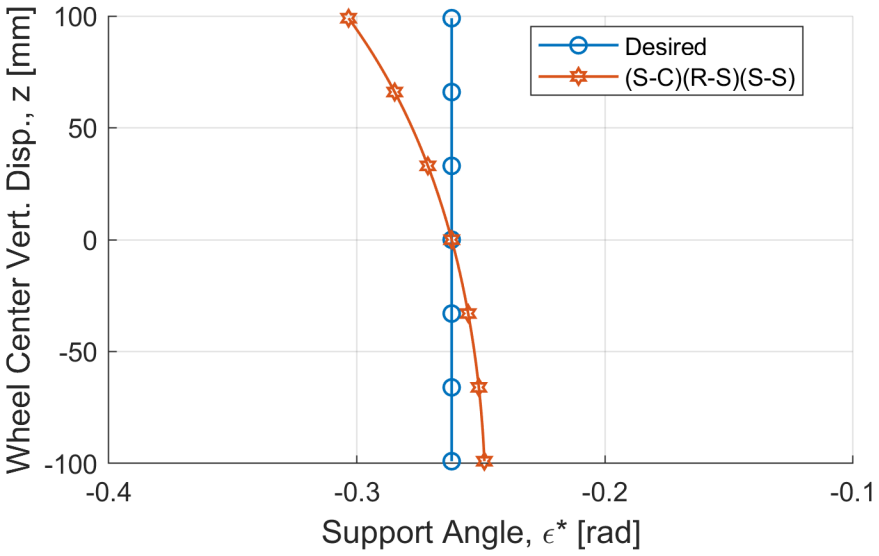

Figure 12.8. Support angle curve for the synthesized MacPherson strut suspension.

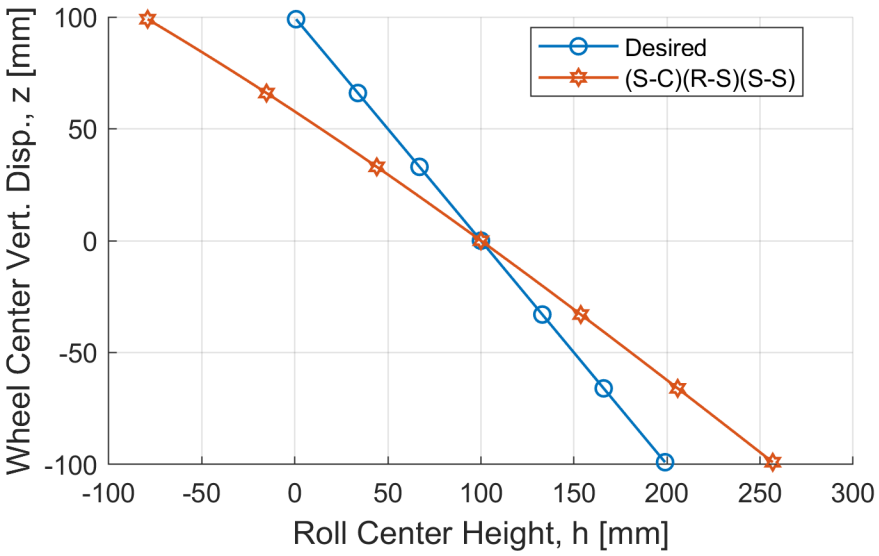

Figure 12.9. Roll center height curve for the synthesized MacPherson strut suspension.

Chapter 13

Discussion

This closing chapter begins with a *comparison of selected architectures*. After this, the focus shifts to a discussion on the *methods developed* and how these address the initial research objectives. From there, discussion segues to areas of the problem that could be addressed as *logical extensions* of this dissertation.

13.1 Comparison of Selected Architectures

In the eight body-wheel connection chapters, limited comparisons were made regarding how the different architectures performed with respect to each other. This section shows how the eight examples perform with respect to each other relative to the desired wheel trajectory of the wheel kinematics chapter. Rarely have this many spatial suspensions been generated from the same basic motion specification, making this an interesting exercise.

- *Camber angle — Figure 13.1.* Recall that the desired camber curve introduced in the wheel kinematics chapter was progressively negative with jounce. Of the eight example suspensions, three did not perform in this manner: R, C(S-S), and (S-C)(R-S)(S-S), with the last of these performing the worst.

- *Toe angle — Figure 13.2.* The desired curve is linear, giving a slight roll understeer effect; that is, the outside rear wheel when cornering should steer the

vehicle away from the turn. The biggest two outliers are S(S-S)^2 and (S-C)(R-S)(S-S), with the former giving less toe change in jounce than desired and the latter giving more toe change in jounce than desired.

- *Wheel-travel angle — Figure 13.3.* Wheel-travel angle was intended to be negative and constant, giving an approximately-constant anti-squat effect if employed on a driven rear axle. The R and S(S-S)^2 fail to meet even the design-position wheel-travel value due to their inability to provide a wheel motion without a fixed point. The suspension that shows the most wheel-travel angle change overall is the (R-R)(S-S) suspension.

- *Support angle — Figure 13.4.* Support angle was intended to be negative and constant, giving an approximately-constant anti-rise effect if employed on an outboard-braked rear wheel. Most suspensions get close to this or provide increasingly-negative support angle in rebound, giving an increasing anti-rise effect. However, two suspensions show increasingly-positive support angle in rebound: C(S-S) and (S-C)(R-S)(S-S).

- *Roll center height — Figure 13.5.* Roll center height curves for all examples are approximately linear, as desired. The (S-C)(R-S)(S-S) suspension exhibited more roll center height change than all the others, while the R suspension showed the least roll center height change.

Another way to compare the architectures is to rank them according to their deviation from the desired wheel trajectory. One way to accomplish this is to use the *root mean square error* for each of the characteristics of interest. For a given architecture, at each z value, the difference between a kinematic characteristic and its desired value may be computed. The RMS value of these differences across all z is then a scalar measure on the architecture's performance for that kinematic characteristic. These RMS errors may be computed for every relevant characteristic of every example architecture and then ranked; see Figure 13.6. To rank the example architectures overall, their average rank across the categories of Figure 13.6 is used; see Table 13.1.

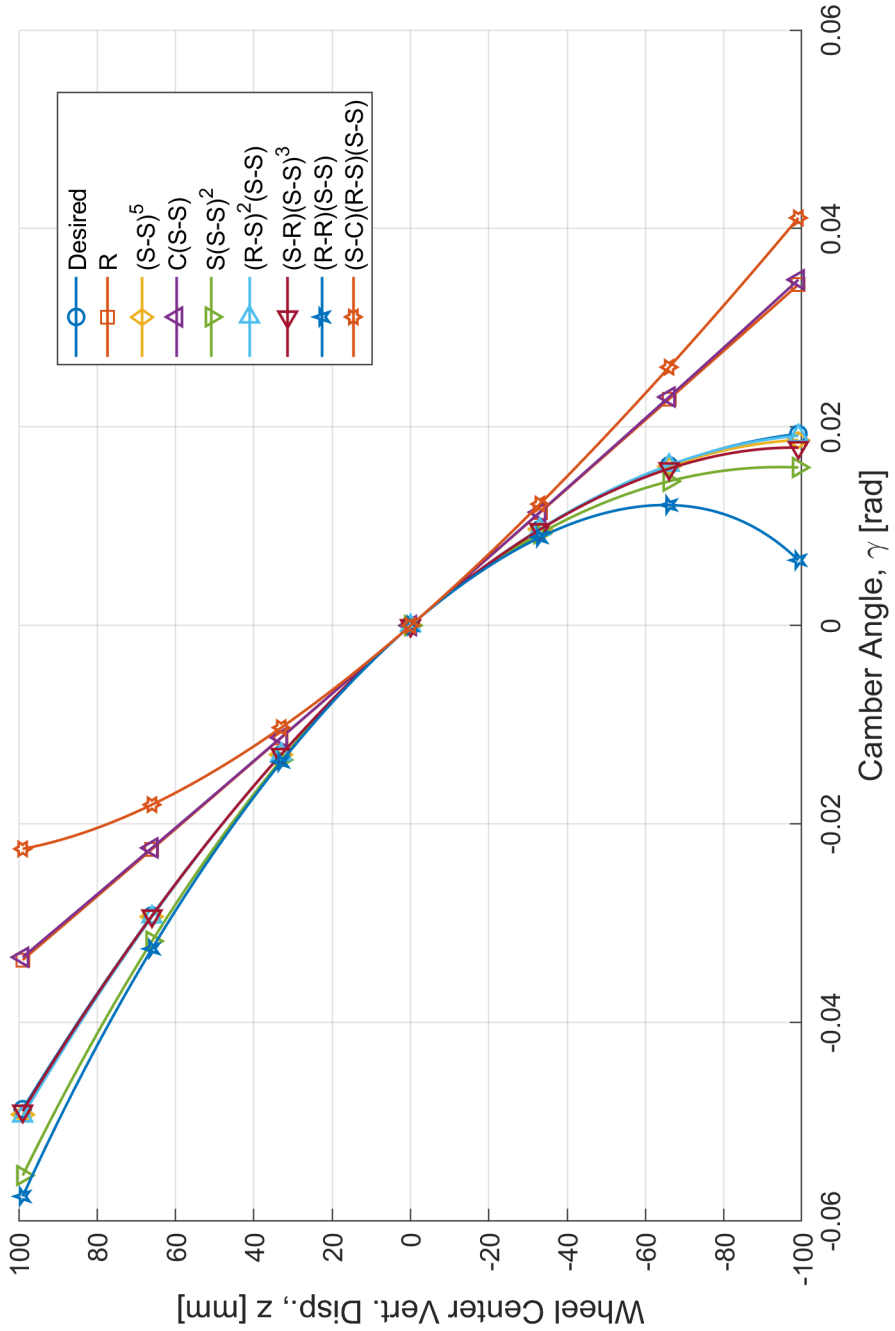

Figure 13.1. Desired camber curve compared with that of the eight synthesized examples.

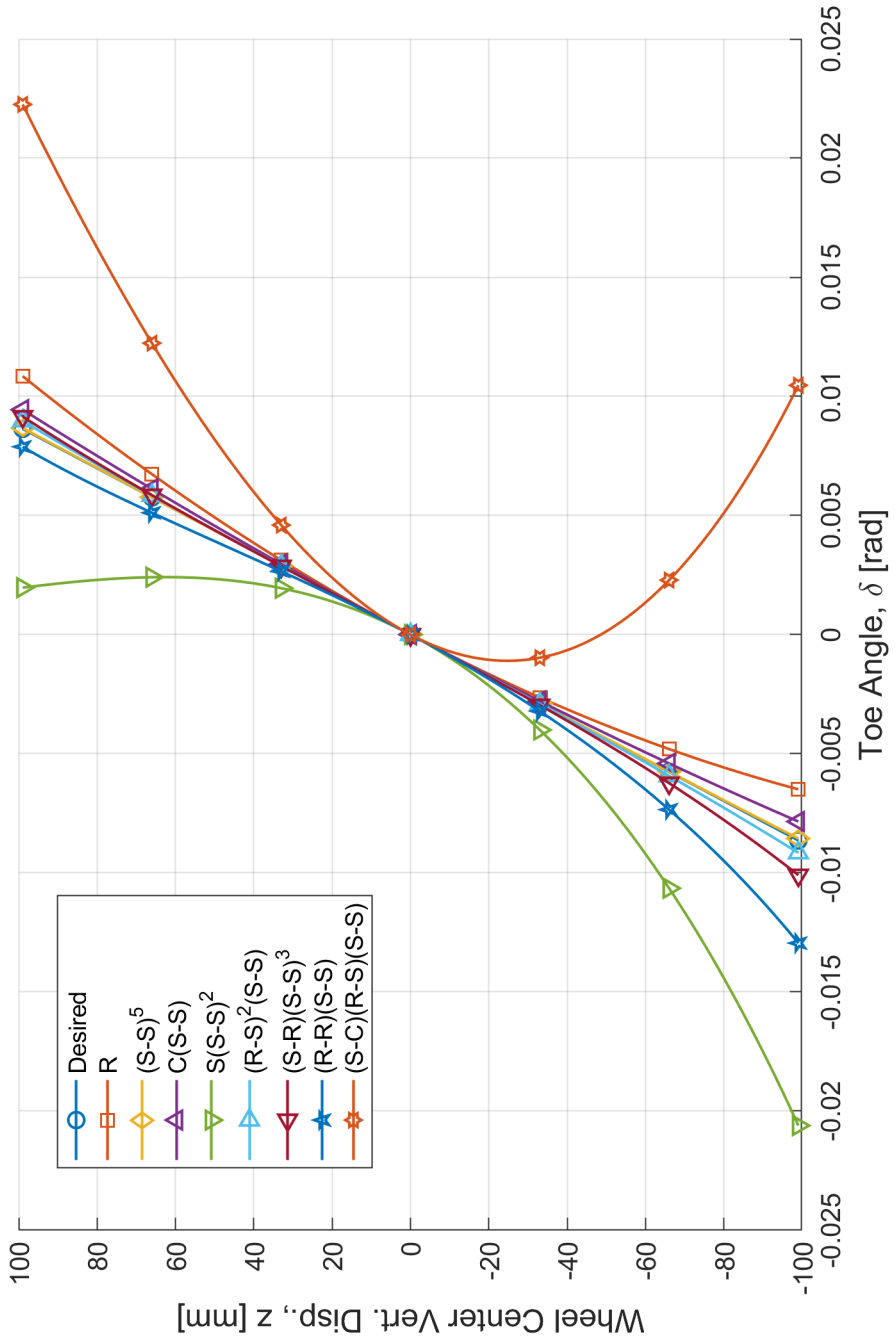

Figure 13.2. Desired toe curve compared with that of the eight synthesized examples.

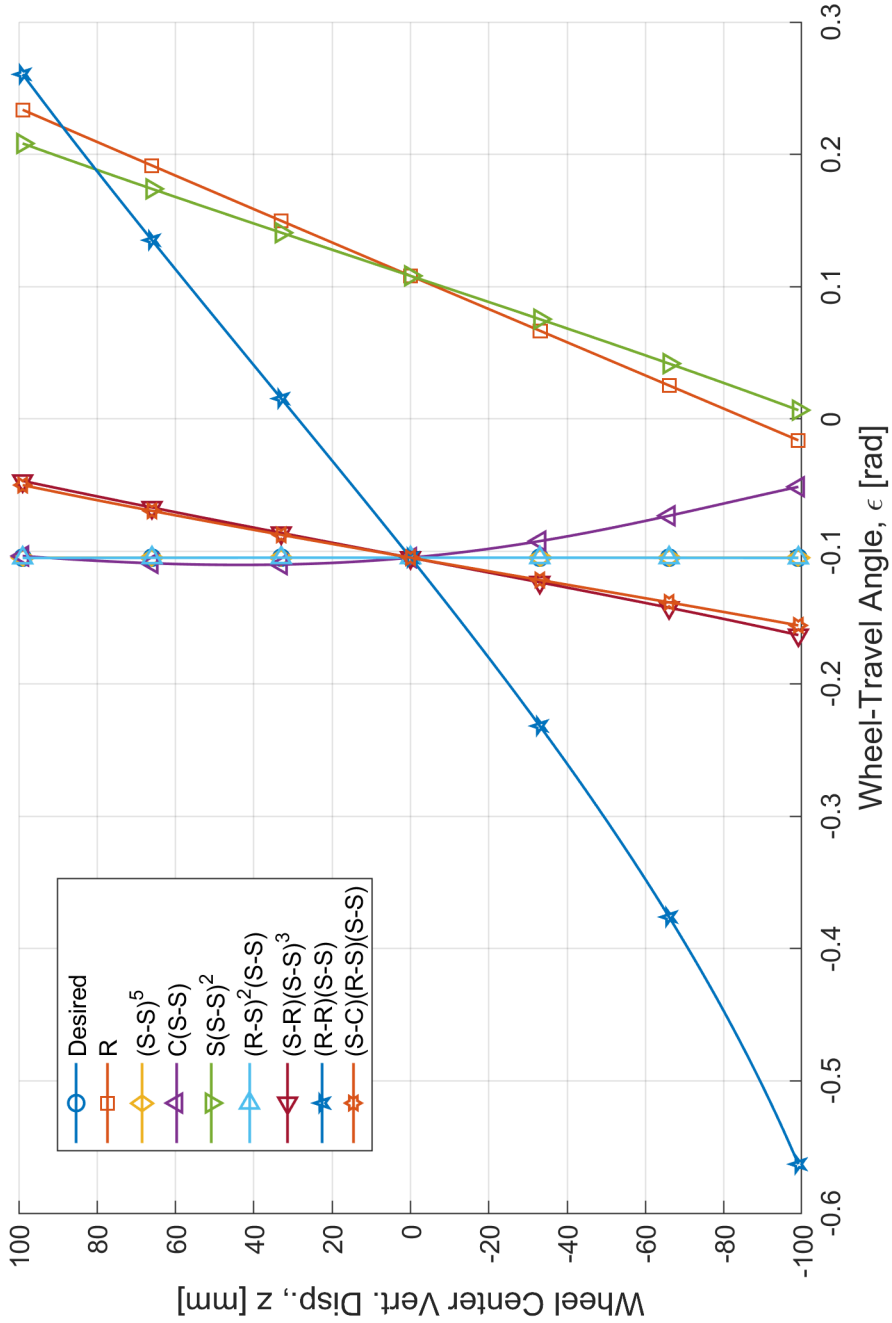

Figure 13.3. Desired wheel-travel angle curve compared with that of the eight synthesized examples.

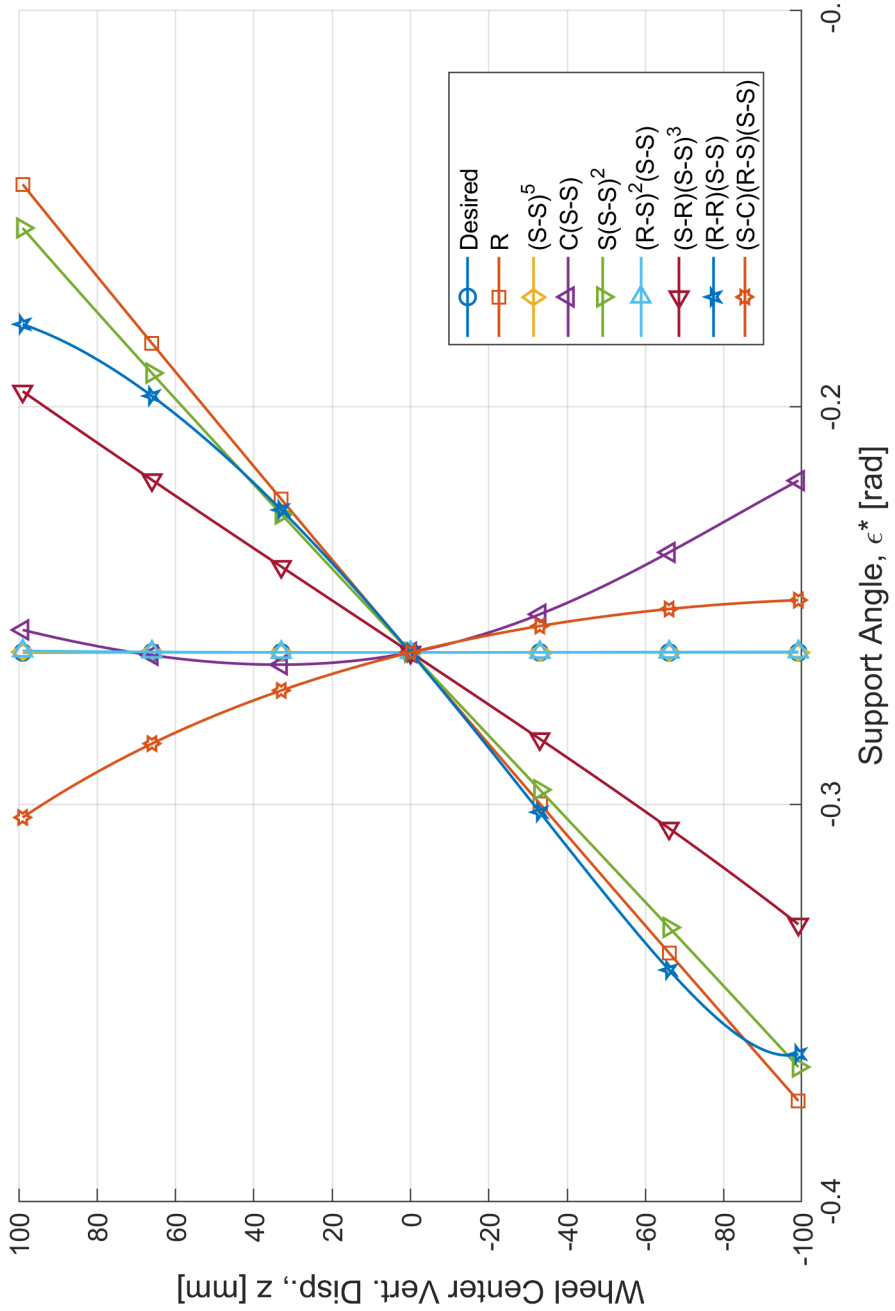

Figure 13.4. Desired support angle curve compared with that of the eight synthesized examples.

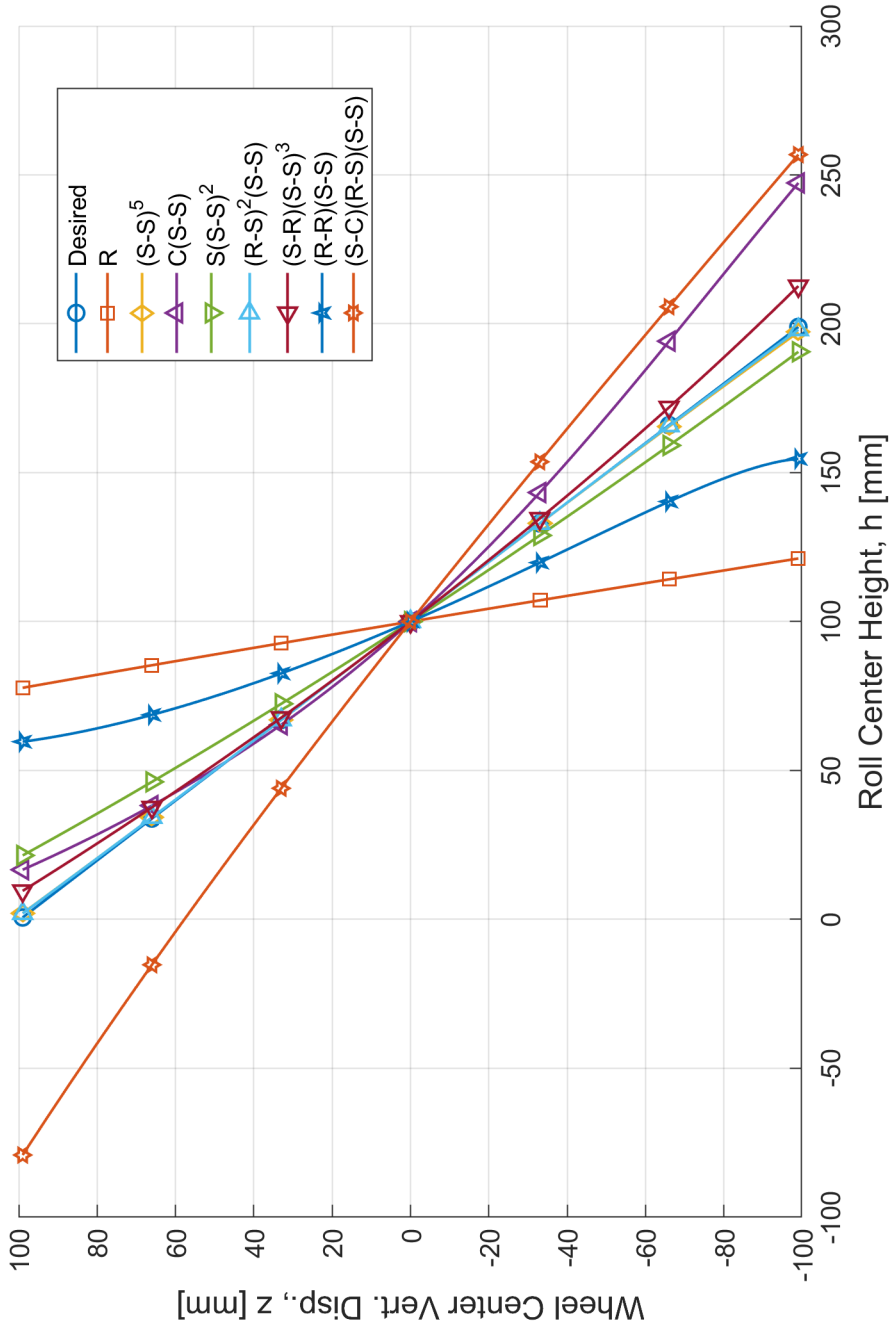

Figure 13.5. Desired roll center height curve compared with that of the eight synthesized examples.

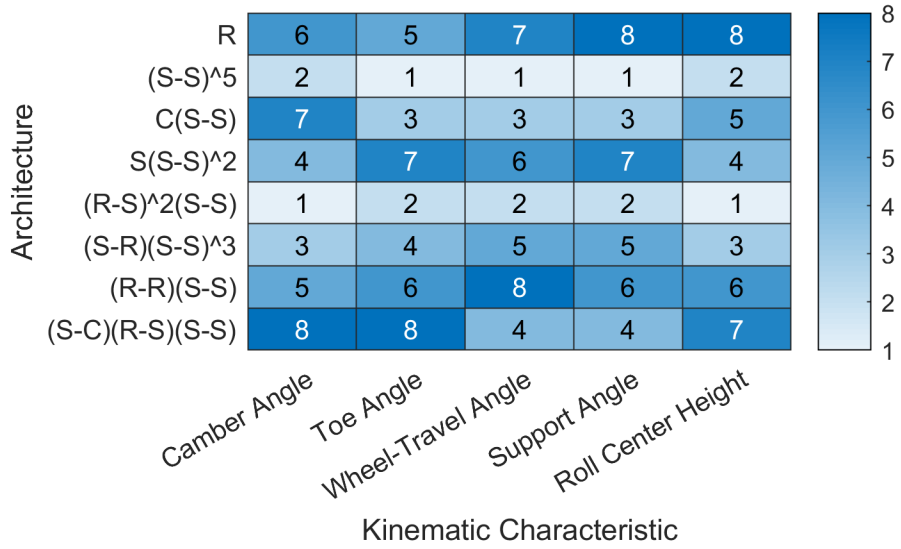

Figure 13.6. Ranking the architectures according to RMS error (1 = Best).

Table 13.1. Average and overall ranking of the example suspensions, including number of independent design variables and if steered.

Architecture	Ind. Design Variables	Steered?	Avg. Rank	Overall Rank
$(\text{S-S})^5$	$6 \times 5 = 30$	Yes	1.4	1
$(\text{R-S})^2(\text{S-S})$	$7 \times 2 + 6 = 20$	Yes	1.6	2
$(\text{S-R})(\text{S-S})^3$	$7 + 6 \times 3 = 25$	No	4.0	3
C(S-S)	$4 + 6 = 10$	No	4.2	4
$\text{S}(\text{S-S})^2$	$3 + 6 \times 2 = 15$	No	5.6	5
(S-C)(R-S)(S-S)	$5 + 7 + 6 = 18$	Yes	6.2	6*
(R-R)(S-S)	$8 + 6 = 14$	No	6.2	6*
R	4	No	6.8	8

*Tie.

The general trend is that kinematic performance improves as the number of independent design variables increases, provided these are used for wheel-kinematics considerations and not non-kinematic considerations. That luxury cars use the (S-S)^5 should be no surprise: it meets both kinematic and non-kinematic requirements with ease, taking full advantage of its 30 independent design variables. Sports and racing cars have long relied on the (R-S)^2(S-S), which nearly equals the (S-S)^5 in kinematic performance while using fewer components. The (S-R)(S-S)^3, or control blade, performs relatively well but recall its packaging difficulties. It has more independent design variables (25) than the (R-S)^2(S-S) (20), but the S-R design variables are in this case put to use achieving the vertical "control blade" configuration rather than an additional wheel position. Not far behind is the C(S-S), which does very well with its 10 design variables, but was not packageable and was not forced to accommodate any other non-kinematic requirements. The S(S-S)^2 does quite well considering it is not a truly spatial linkage (the wheel carrier always has that fixed point). In fact, the S(S-S)^2 does better than the spatial (R-R)(S-S) and (S-C)(R-S)(S-S) linkages. The kinematic performance of the (S-C)(R-S)(S-S) belies its ubiquity in passenger cars. It does, however, accommodate a steering axis — the only other examples to do so are the (S-S)^5 and the (R-S)^2(S-S). Having to accommodate a steering axis with the S-C link is why its 18 independent design variables do not place it higher up the ranking. In last place overall is the R joint suspension, unsurprising considering its simple (or crude, depending on one's point-of view) geometry.

13.2 Methods Developed

The previous ten chapters have presented a systematic treatment of suspension geometry in three dimensions. Here, the research objectives from the introduction chapter are recalled and discussion is given on how the methods developed in this dissertation address those initial objectives. From Section 1.4:

1. Develop a mathematically-complete wheel motion specification that is compatible with the existing velocity specification.

2. Enumerate all possible independent suspension architectures.

3. Formulate methods allowing all possible architectures to be dimensioned according to the motion specification.

4. Develop methods to filter suspension geometry solutions according to non-kinematic design requirements such as allotted space or desired kingpin geometry.

The wheel-motion formalism developed in Chapter 3, Wheel Kinematics, clearly and completely addresses (1). It does so by showing how velocity characteristics can be converted to position parameters and vice versa. This allows a curve in $SE(3)$, the group of spatial rigid body motions, to be defined in terms of suspension characteristics of interest such as camber angle and roll center height. The tangent of this curve at the design position corresponds to the traditional velocity specification used to design suspension linkages.

Objective (2) was addressed in Chapter 4, Number Synthesis. There, a set of practical body-wheel connections was the basis for an enumeration of independent suspension linkages. This enumeration resulted in all possible architectures *for that set of body-wheel connections*. Obviously, more connections could be considered. The chosen set of connections represents those in current use for independent suspensions and was considered sufficient to demonstrate the efficacy of the methods. For more discussion on other connections see Section 13.3. Overall, the systematic enumeration of Chapter 4 shows that potential architectures can be readily generated from a basic set of assumptions, meaning all architectures resulting from those assumptions may be included in the design process.

The third objective was addressed by giving each of the considered body-wheel connections its own chapter (Chapters 5–12). In each of these, the kinematic design equations were developed and strategies for their solution introduced. Importantly, all design equations included design-position velocity as the baseline specification, consistent with traditional suspension design practice. In some cases, it was possible to develop closed-form expressions for synthesis; in others, it was necessary to solve

Table 13.2. Synthesis cases developed in this dissertation and the chapter(s) they appear in.

Connection	Design Pos. Vel.	with Jounce Pos.	with Rebound Pos.
R	5*	†	†
S-S	7, 8*, 10–12	9	6
C	7	†	†
S	8*	†	†
R-S	12	9	□
S-R	10	□	□
R-R	11	□	†
S-C	12	□	†

*With "fixed-point" velocity. †Impossible. □ Possible, but no complete example provided.

linear or polynomial systems of equations. In all cases the dimensional synthesis methods can be easily programmed, allowing numerous suspension geometries to be generated in parallel. As a means of concisely summarizing the synthesis methods developed in this dissertation, Table 13.2 has been prepared. Using the synthesis methods developed in this dissertation, any necessary combination of connections may be generated, allowing any of the linkages enumerated in the number synthesis chapter to be produced.

Objective (4) was addressed in the body-wheel connection chapters (Chapters 5–12) in two ways. First, when possible, meaningful techniques for specifying free design variables were developed. For example, allowing one end of an S-S link to take values in a packaging cube. Second, when possible, a set-based design approach for filtering the solution families to satisfy non-kinematic design considerations was developed. For example, filtering S-S link solutions according to their ability to establish a kingpin axis or achieve a desired plan view angle. It is helpful to visualize this set-based design approach using Venn diagrams. In Figure 13.7, seven such illustrations are shown, corresponding to each of the example architectures — except for the R architecture, which had only one solution and so no set-based design process was necessary. In general, the simpler architectures (less independent design variables) did not benefit as much from the approach as, say, the $(\text{S-S})^5$. Nevertheless, using the set-based approach, packaging requirements may be met and large solution families may be

practically searched through according to other non-kinematic design requirements, thus achieving objective four.

13.3 Logical Extensions

By no means does this work demonstrate every method that could be developed for the spatial suspension geometry problem. Considering what has been demonstrated, what types of problems can the methodology be naturally extended to?

The lowest-hanging fruits are of course the blanks in Table 13.2. These were cases where additional points of the desired wheel trajectory curve could be achieved; but, for various reasons, these synthesis cases were not fully developed. For the R-S link, achieving velocity, jounce, and rebound resulted in only one free design variable, not enough to achieve a desired kingpin axis. Certainly if one wanted an R-S link without a specifiable kingpin, they could solve the design equations developed in §9.1. The S-R link could practically be synthesized for velocity and jounce; this would be similar to what was done for the R-S link. In the S-R chapter, the focus is on the control blade example; as discussed, it proved difficult to package a control blade meeting both velocity and jounce requirements. As far as synthesis of S-R links for velocity, jounce, and rebound, the necessary equations are in §10.1. With only one free parameter, packageable results will be difficult. The R-R link for velocity and jounce has no free design variables, making this an extremely impractical case. The S-C link could easily be synthesized for velocity and jounce, but in doing so would lose its ability to specify a kingpin axis. Additional possibilities not shown in the table are the S-S link for additional wheel positions. Up to six wheel positions other than design may be specified over the baseline design position velocity. These cases were investigated enough to determine that they do not produce easily-packageable results. Instead, the set-based strategy of Ch. 6 was much-preferred, allowing the free design variables of the velocity/jounce/rebound case to be put to good use to achieve packaging, plan view angle, kingpin axis, reaction load minimization, etc.

Naturally, the methods developed in this dissertation could be used to synthesize

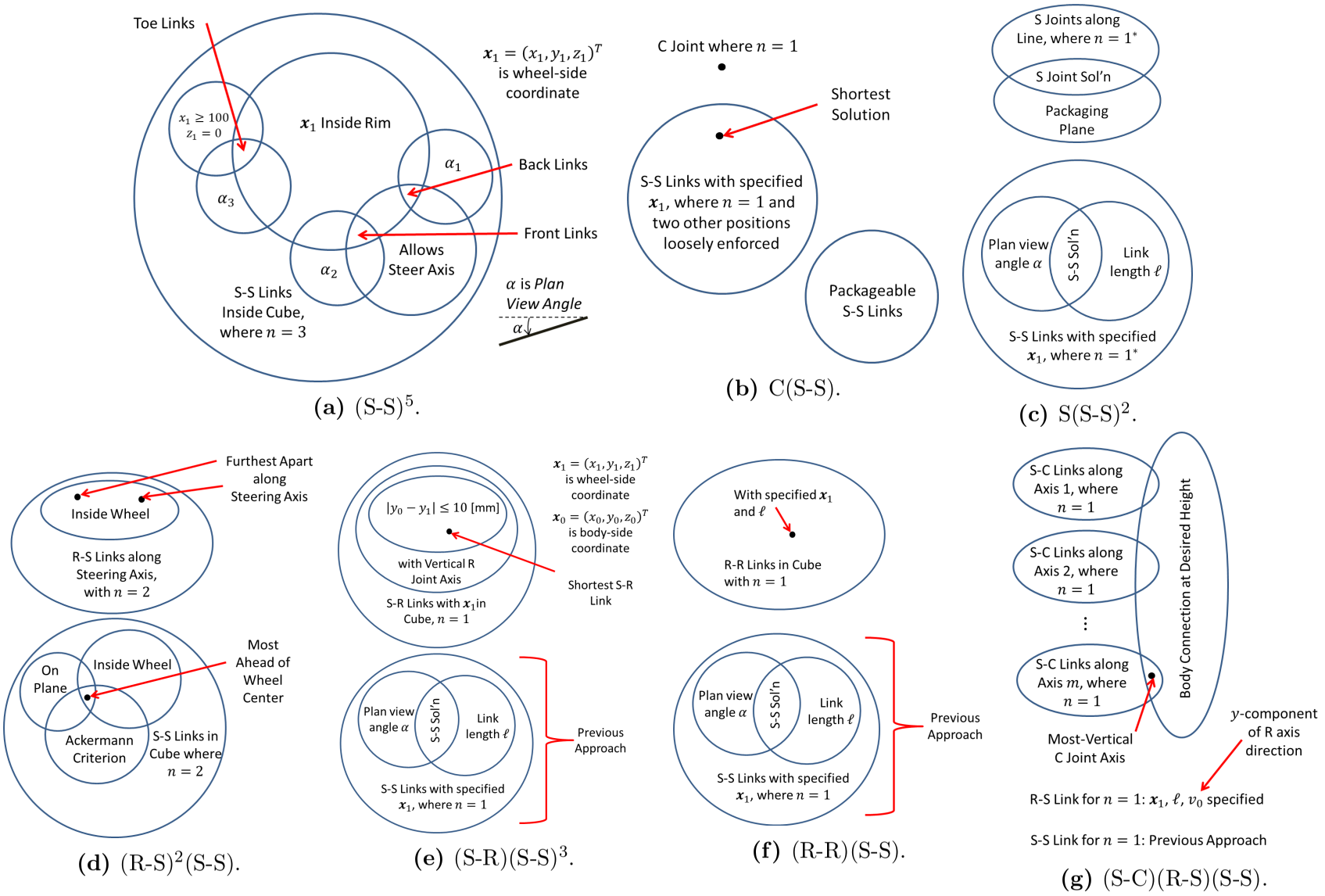

Figure 13.7. Visualizations of the set-based design process applied to each of the example architectures. (Set-based design was not necessary for the R architecture.)

examples of the suspensions from number synthesis (Ch. 4) that are missing. Of the 16 architectures deemed practical, eight were included as full examples. Since the purpose of this dissertation is to communicate the methods developed, not to design every type of suspension, the omission of these architectures — {S, R-S}, {S, S-R}, {S, S-C}, {R-S, S-R, S-S}, {S-R, S-R, S-S}, {S-R, S-C, S-S}, {R-S, S-S, S-S, S-S}, {S-C, S-S, S-S, S-S} — is of no concern.

The methods of this dissertation could easily be extended to additional body-wheel connections, provided those connections impose algebraic kinematic constraint equations. One way to build up a body-wheel connection library from a more first-principles point-of-view is to start with the lower pairs: prismatic (P), revolute (R), helical (H), cylindrical (C), planar (E), and spherical (S). Of these, only the H joint is not algebraic [66], and it is not particularly relevant for car suspensions anyway. With the basic building blocks of R, P, C, E, and S, any number of body-wheel connections may be systematically enumerated. Of course, the connections in this dissertation would arise from such an enumeration. The limited number of body-wheel connections of this dissertation reflects the reality that joints like the planar joint E are perhaps not so useful for car suspensions.

The package spaces employed in this dissertation were cuboids. More interesting volumes could be considered relatively easily — true wheelhouse geometry, inner wheel geometry with brake package geometry, etc. A related effort would be to generate, for a given geometry, the *working volume* of the wheel; that is, the space it sweeps out through its vertical stroke. This working volume could then be used to assess clearances. The clearance between the links, themselves, and the wheel are also important and should be assessed. These could be studied using the tools developed in this dissertation.

More could be done with steering. In this dissertation, the steering system was addressed in two ways. First, it was shown how to establish the kingpin axis for body-wheel connections allowing such an axis (S-S, R-S, S-C). Second, it was shown how a tie rod could be synthesized according to an Ackermann criterion (Ch. 9, for the R-S link). Not addressed more generally is how the wheel's position and orienta-

tion change as a function of steer input. Suspension designers are interested in, for example, camber angle at various steer angles. This is because camber is a concern primarily of lateral dynamics, where at least the front wheels will be steered. Additional motion requirements could be incorporated. The most general way to do this is to no longer think of the desired wheel trajectory as a curve in $SE(3)$, but rather as a surface in $SE(3)$. The question then becomes how to develop such a motion formalism and synthesis methods to take advantage of it. The intent with this dissertation was to take the traditional single-DOF suspension geometry treatment to its logical end: a truly spatial problem, respecting the challenge of understanding three-dimensional rigid body motion and of generating spatial rigid body guidance mechanisms. In some ways, a two-DOF suspension/steering linkage should be thought of more like a robotic manipulator, and perhaps that literature is where one should turn if interested in developing such a treatment. Of course, why shouldn't designers investigate suspension linkages with even more DOFs? Why restrict these to passive control of the wheel when one could independently set every position parameter for every scenario? If someone pursues these questions, and finds their way to this dissertation, this treatment of the single-DOF suspension problem provides a good foundation to build upon. To understand surfaces, one must first understand curves.

Since many linkages do not incorporate a strut, separate springs and dampers must be placed to complete the suspension. Anti-roll bars (another type of spring, establishing roll stiffness) are usually desired as well. Designers are interested in the so-called installation ratios of these components. These ratios relate spring or damper motion to vertical wheel travel. One could, for example, search for a spring attachment point along a link so that the desired installation ratio is achieved. Clearance issues associated with adding these components may also be assessed in the geometry stage.

Another consideration in the wheel-kinematics stage of the design process is *adjustability*. Manufacturing tolerances in the vehicle body and suspension assembly can result in a wheel that is not necessarily in the desired design position. This can occur when a vehicle is first assembled or when parts are replaced in the field. To

compensate for these realities, suspensions must be adjustable. Most critical are camber and toe angle adjustments. For steered axles, it is also nice to be able to adjust caster angle. Some sports and racing cars can even adjust roll center height, wheel-travel angle, etc. in the pursuit of improved performance. Whatever the reason may be, suspension adjustability is a critical requirement that must be addressed shortly after the draft suspension geometry is synthesized. In most cases, adjustment is incorporated in one of three ways: adjustable-length links, eccentric bolts, and shims. For example, tie rods may be threaded in reversed directions on each end, allowing a rotation of the link to shorten or extend to rotate the wheel about the kingpin axis and adjust toe angle. An upper R-S link may be mounted to the vehicle body with an eccentric bolt, so that when the bolt is spun in the mounting holes, it pulls the R joint inboard/outboard, ultimately adjusting camber angle. In racing, mechanics can shim the outer S joint of a lower R-S link up/down to adjust roll center height. Such adjustments modify not only the design position characteristics, but also how the wheel-kinematics change with vertical wheel travel. In some cases, large adjustments can cause the linkage to bind up (lose mobility) at some point in its travel. Various adjustment strategies may be investigated for the linkage at hand. Common adjustment types may be mathematically-modeled and linkages may be analyzed across the intended range of adjustment. This process will ensure a properly-adjustable suspension linkage for the intended application, and such developments could be considered a logical extension of this work.

A concept related to adjustability is the *robustness* of the suspension geometry. What is meant here is how variation in the geometry affects the resultant wheel-kinematics, recognizing that variation will occur when these mechanisms are physically realized and that it is not always possible to design in enough (or any) adjustment. Is the suspension geometry so sensitive that even small changes in a geometry point greatly affect, for example, toe angle behavior? Could various link solutions be filtered according to sensitivities of interest, so that in cases where adjustment is not possible, the most robust geometries are selected? A proper sensitivity study would also suggest ways to efficiently design the adjustment capabilities of a suspension

— for example, is the variation of one particular geometry point well-correlated to changes in the camber curve? A common desire among designers is that the adjustment of, say, the camber curve does not affect anything else, such as the roll center height curve. As such, a sensitivity study could show how to design adjustment into the geometry in the best possible way, so that wheel-kinematic characteristics such as camber angle, toe angle, wheel-travel angle, support angle, and roll center height can be tuned independently. Further, rather than presuming eccentric bolts, threaded rods, etc., one could instead use a sensitivity study to figure out *how* the geometry should adjust in an abstract sense, then figure out how to implement that adjustability physically. Such an approach is both in the spirit of and a logical extension of this dissertation.

The methods developed in this dissertation are at the subsystem level: generating architectures and geometries according to wheel-kinematic requirements. The treatment included only one wheel in isolation, rather than trying to model a whole vehicle. The next step along these lines is to study and improve the methods used to achieve elastokinematic requirements. Recall that suspension designers are interested in how the wheel moves under load: for example, longitudinal compliance under impact (mm/kN), toe change under braking (deg/kN). These requirements are often stated for the wheel's design position, in the form of a stiffness or compliance matrix relating net force/moment and wheel position/orientation. Since there is now a wheel motion formalism allowing designers to specify kinematic characteristics throughout the wheel's travel, why not specify a compliance matrix at every point? What methods could be developed to achieve these results?

An important step is locating bushings. For example, an R joint is, in practice, achieved with two cylindrical rubber bushings spaced some distance apart. Coming from kinematic synthesis, the R joint axis is known but not the bushing spacing. It is also not known how the bushings should be oriented with respect to the axis. Should they be parallel? Slightly off? Should the bushing be mounted to the vehicle body or wheel carrier in single or double shear? Bushing location is an important design variable when designing for elastokinematics. What methods could be developed to

best locate bushings along existing axes? Bushing stiffness of course plays a role here and would need to be modeled as well. With bushings located and specified, it is possible in this stage to start to develop some fairly reasonable values for the loads the links must carry. With these, structural design (shaping the cross section of each link) may proceed. With a better understanding of space requirements, clearances may be assessed with greater fidelity than before.

Some potential starting points for research into elastokinematics: [21, 22, 13, 7, 24, 32]. Gerrard's approach to elastokinematic design [13], in particular, is a great starting point, because his approach to suspension geometry was very much an inspiration for this dissertation. It is one thing to produce a mechanism or machine that works, or to even make said mechanism or machine work slightly better; it is another thing entirely to state clearly what is desired in the abstract and generate design solutions directly. For the independent suspension problem, engineers are fortunate that so much of what matters is modeled well by elementary geometry and mechanics. This fact makes better design methods possible, beyond even what has been developed in this dissertation.

References

[1] R. Ackermann. *Observations on Ackermann's Patent Moveable Axles: For Four Wheeled Carriages, Containing Engraved Elevations of Carriages, with Plans and Sections, Conveying Accurate Ideas of this Superior Improvement*. R. Ackermann, 1819. URL: https://books.google.com/books?id=Kbg5AQAAMAAJ.

[2] The Autocar Technical Staff. *The Autocar Handbook*. 13th ed. Iliffe & Sons Ltd., 1935. URL: http://commons.wikimedia.org/wiki/Category:Scans_from_%27Autocar_Handbook%27,_Thirteenth_edition.

[3] P. Barak. *Magic Numbers in Design of Suspensions for Passenger Cars*. Tech. rep. 911921. Society of Automotive Engineers, Inc., 1991.

[4] D. Bates, A. Newell, and M. Niemerg. "BertiniLab: A MATLAB interface for solving systems of polynomial equations". In: *Numerical Algorithms* 71 (2016), pp. 229–244.

[5] D. J. Bates et al. *Bertini: Software for Numerical Algebraic Geometry*. 2013. URL: https://bertini.nd.edu/.

[6] D. J. Bates et al. *Numerically Solving Polynomial Systems with Bertini*. Society for Industrial and Applied Mathematics, 2013.

[7] M. J. Burgess et al. *A Tool for Rapid Vehicle Suspension Design*. Tech. rep. 2004-01-3543. Society of Automotive Engineers, Inc., 2004.

[8] Ford Motor Company. *Ford Manual for Owners and Operators of Ford Cars*. Ford Motor Company, 1915. URL: https://books.google.com/books?id=NdDhAAAAMAAJ.

[9] J. Dixon. *The Shock Absorber Handbook*. Wiley-Professional engineering publishing series. Wiley, 2008. ISBN: 9780470516423. URL: https://books.google.com/books?id=0RDTBQAAQBAJ.

[10] D. Edmunds. *2012 Ford Focus Titanium: Suspension Walkaround*. Edmunds.com. 2011. URL: https://www.edmunds.com/car-reviews/track-tests/2012-ford-focus-titanium-suspension-walkaround.html.

[11] S. P. Fuja, H. A. Schmid, and J. P. Ryan. *Synthesis of Chassis Parameters for Ride and Handling on the 1997 Chevrolet Corvette*. Tech. rep. 970097. Society of Automotive Engineers, Inc., 1997.

[12] M. B. Gerrard. *Kinematic Suspension Linkages - A Model for Their Behaviour and a Procedure for Their Design*. Tech. rep. 2002-01-0281. Society of Automotive Engineers, Inc., 2002.

[13] M. B. Gerrard. *The Equivalent Elastic Mechanism: A Tool for the Analysis and Design of Compliant Suspension Linkages*. Tech. rep. 2005-01-1719. Society of Automotive Engineers, Inc., 2005.

[14] K. Gläser, W. Christophliemke, and D. Etzold. *Twist-beam axle for motor vehicles*. US Patent 6,523,841. 2003. URL: http://www.google.com/patents/US6523841.

[15] Robert Bosch GmbH. *Automotive Handbook: 8th Edition*. Translated from the German. Robert Bosch GmbH, 2011.

[16] R. S. Hartenberg and J. Denavit. *Kinematic Synthesis of Linkages*. McGraw-Hill, 1964.

[17] J. D. Hauenstein and A. J. Sommese. "What is numerical algebraic geometry?" In: *Journal of Symbolic Computation* 79 (2017), pp. 499–507.

[18] B. Heißing and M. Ersoy. *Chassis Handbook*. Vieweg+Teibner Verlag, 2011.

[19] D. Q. Huynh. "Metrics for 3D Rotations: Comparison and Analysis". In: *Journal of Mathematical Imaging and Vision* 35 (2009), pp. 155–164.

[20] H. Y. Kang and C. H. Suh. "Synthesis and Analysis of Spherical-Cylindrical (SC) Link in the MacPherson Strut Suspension Mechanism". In: *Journal of Mechanical Design* 116 (1994), pp. 599–606.

[21] J. S. Kang et al. *Elastokinematic Analysis and Optimization of Suspension Compliance Characteristics*. Tech. rep. 970104. Society of Automotive Engineers, Inc., 1997.

[22] J. Knapczyk and M. Maniowski. "Stiffness synthesis of a five-rod suspension for given load-displacement characteristics". In: *Proceedings of the Institution of Mechanical Engineers, Part D: Journal of Automobile Engineering* 110 (2006), pp. 879–889.

[23] A. Leykin and R. Krone. *NAG4M2 – Numerical Algebraic Geometry*. 2011. URL: http://people.math.gatech.edu/~aleykin3/NAG4M2/index.html.

[24] L. Li et al. *Optimization of Suspension Elastomeric Bushing Compliance Under Constraints of Handling, Ride, and Durability*. Tech. rep. 2010-01-0721. Society of Automotive Engineers, Inc., 2010.

[25] T.-Y. Li et al. *Hom4PS-3*. 2013. URL: http://www.hom4ps3.org/store/c1/Featured_Products.html.

[26] W. Matschinsky. *Road Vehicle Suspensions*. Translated from the German. Professional Engineering Publishing, 2000.

[27] J. M. McCarthy and G. S. Soh. *Geometric Design of Linkages*. Springer, Second Edition, 2011.

[28] E. McCausland. *AM General Considering Selling Build-Your-Own Humvee Kits*. 2012. URL: http://www.automobilemag.com/news/report-am-general-may-soon-sell-build-your-own-humvee-kits-161171/.

[29] W. Milliken and D. Milliken. *Chassis Design: Principles and Analysis*. Society of Automotive Engineers, Inc., 2002.

[30] W. Milliken and D. Milliken. *Race Car Vehicle Dynamics*. Society of Automotive Engineers, Inc., 1995.

[31] M. W. Neal and M. A. Dona. *Ride and Handling Development of the 1997 Chevrolet Corvette*. Tech. rep. 970098. Society of Automotive Engineers, Inc., 1997.

[32] A. L. Nedley and W. J. Wilson. *A New Laboratory Facility for Measuring Vehicle Parameters Affecting Understeer and Brake Steer*. Tech. rep. 720473. Society of Automotive Engineers, Inc., 1972.

[33] M. von der Ohe. *Front and Rear Suspension of the New Mercedes Model W201*. Tech. rep. 831045. Society of Automotive Engineers, Inc., 1983.

[34] M. M. Plecnik and J. M. McCarthy. "Vehicle Suspension Design Based on a Six-Bar Linkage". In: *International Design Engineering Technical Conferences and Computers and Information in Engineering Conference*. ASME, 2014, Volume 5A: 38th Mechanisms and Robotics Conference.

[35] M. Raghavan. *An Atlas of Linkages for Independent Suspensions*. Tech. rep. 911925. Society of Automotive Engineers, Inc., 1991.

[36] M. Raghavan. "Number and Dimensional Synthesis of Independent Suspension Mechanisms". In: *Mechanism and Machine Theory* 31 (1996), pp. 1141–1153.

[37] M. Raghavan. "Suspension Design for Linear Toe Curves: A Case Study in Mechanism Synthesis". In: *Journal of Mechanical Design* 126 (2004), pp. 279–282.

[38] M. Raghavan. "Suspension Synthesis for N:1 Roll Center Motion". In: *Journal of Mechanical Design* 127 (2005), pp. 673–678.

[39] M. Raghavan and B. Roth. "Solving Polynomial Systems for the Kinematic Analysis and Synthesis of Mechanisms and Robotic Manipulators". In: *Journal of Mechanical Design* 117 (1995), pp. 71–79.

[40] D. Redmond. *Steering System*. Image is a scan from either a 1956 or 1965 manual from Willys. 2009. URL: `http://cj3b.info/Parts.html`.

[41] J. Reimpell, H. Stoll, and J. W. Betzler. *The Automotive Chassis: Engineering Principles*. Translated from the German. Butterworth-Heinemann, 2001.

[42] J. Roe. *Elementary Geometry*. Oxford Science Publications, 1993.

[43] J. P. Ryan, S. P. Fuja, and H. A. Schmid. *Objective Ride and Handling Goals for the 1997 Chevrolet Corvette*. Tech. rep. 970091. Society of Automotive Engineers, Inc., 1997.

[44] R. Sancibrian et al. "Kinematic design of double-wishbone suspension systems using a multiobjective optimisation approach". In: *Vehicle System Dynamics: International Journal of Vehicle Mechanics and Mobility* 48 (7 2010), pp. 793–813.

[45] H. A. Schmid, S. P. Fuja, and J. P. Ryan. *Design Synthesis of Suspension Architecture for the 1997 Chevrolet Corvette*. Tech. rep. 970092. Society of Automotive Engineers, Inc., 1997.

[46] Porsche Engineering Services. *Ultra Light Steel Auto Body: Phase 2 Findings*. Tech. rep. Ultra Light Steel Auto Body Consortium, 1998.

[47] P. A. Simionescu and D. Beale. "Synthesis and Analysis of the Five-Link Rear Suspension System Used in Automobiles". In: *Mechanism and Machine Theory* 37 (2002), pp. 815–832.

[48] J. Simister and A. Morgan. *VW Golf 2.0 FSI*. 2003. URL: `https://web.archive.org/web/20070927000516/http://www.evo.co.uk/carreviews/evocarreviews/41365/vw_golf_20_fsi.html`.

[49] A. J. Sommese and C. W. Wampler. *The Numerical Solution of Systems of Polynomials Arising in Engineering and Science*. World Scientific, 2005.

[50] C. H. Suh. *Synthesis and Analysis of Suspension Mechanisms with Use of Displacement Matrices*. Tech. rep. 890098. Society of Automotive Engineers, Inc., 1989.

[51] C. H. Suh and C. W. Radcliffe. *Kinematics and Mechanisms Design*. Wiley, 1978.

[52] L.-W. Tsai and A. P. Morgan. "Solving the Kinematics of the Most General Six- and Five-Degree-of-Freedom Manipulators by Continuation Methods". In: *Journal of Mechanisms, Transmissions, and Automation in Design* 107 (1985), pp. 189–200.

[53] User:Bromskloss. *Illustration of Ackermann steering geometry*. Wikimedia Commons. 2010. URL: https://commons.wikimedia.org/wiki/File:Ackermann_turning.svg.

[54] User:CapriRacer. *Colorized tire footprint pressure distribution*. Wikimedia Commons. 2009. URL: https://commons.wikimedia.org/wiki/File:Tirefootprint.jpg.

[55] User:Casito. *MacPherson strut suspension*. Wikimedia Commons. 2005. URL: https://commons.wikimedia.org/wiki/File:Mcpherson_strut.jpg.

[56] User:Cav. *Fiat 500R bushing*. Wikimedia Commons. 2008. URL: https://commons.wikimedia.org/wiki/File:Silentblock_500_1.jpg.

[57] User:GRAHAMUK. *Camber angle*. Wikimedia Commons. 2009. URL: https://commons.wikimedia.org/wiki/File:Cambe_angle.svg.

[58] User:LaurensvanLieshout. *Rack and pinion steering system*. Wikimedia Commons. 2010. URL: https://commons.wikimedia.org/wiki/File:Steer_system.jpg.

[59] User:RB30DE. *Double wishbone suspension*. Wikimedia Commons. 2008. URL: https://commons.wikimedia.org/wiki/File:Double_wishbone_suspension.jpg.

[60] User:Silverxxx. *Ball joint cross section*. Wikimedia Commons. 2009. URL: https://commons.wikimedia.org/wiki/File:Ball_joint_cross_section_(from_English_Wikipedia_to_be_used_in_other_languages).jpg.

[61] User:Silverxxx. *Image of front toe angle...* Wikimedia Commons. 2013. URL: https://commons.wikimedia.org/wiki/File:Toe-in_example_5_degrees_positive.png.

[62] User:Simiprof. *Mercedes-Benz C111 suspension*. Wikimedia Commons. 2014. URL: http://commons.wikimedia.org/wiki/File:Mercedes-Benz_C111_suspension.PNG.

[63] User:Truthdowser. *Wheelbase and track*. Wikimedia Commons. 2007. URL: https://commons.wikimedia.org/wiki/File:Wheelbase_and_Track.png.

[64] J. Verschelde. *PHCpack: a general-purpose solver for polynomial systems by homotopy continuation*. 1999. URL: http://homepages.math.uic.edu/~jan/PHCpack/phcpack.html.

[65] C. W. Wampler, A. P. Morgan, and A. J. Sommese. "Numerical Continuation Methods for Solving Polynomial Systems Arising in Kinematics". In: *Journal of Mechanical Design* 112 (1990), pp. 59–68.

[66] C. W. Wampler and A. J. Sommese. "Numerical algebraic geometry and algebraic kinematics". In: *Acta Numerica* 20 (2011), pp. 469–567.

[67] J. S. Zhao et al. "Synthesis of a Rear Wheel Suspension Mechanism with Pure Rectilinear Motion". In: *Journal of Mechanical Design* 131 (2009), pp. 101007–1–101007–9.